



Universiteit  
Leiden  
The Netherlands

## Fluorescence correlation spectroscopy on electron transfer reactions : probing inter- and intramolecular redox processes

Sen, S.

### Citation

Sen, S. (2016, June 30). *Fluorescence correlation spectroscopy on electron transfer reactions : probing inter- and intramolecular redox processes. Casimir PhD Series*. Retrieved from <https://hdl.handle.net/1887/40761>

Version: Not Applicable (or Unknown)

License: [Licence agreement concerning inclusion of doctoral thesis in the Institutional Repository of the University of Leiden](#)

Downloaded from: <https://hdl.handle.net/1887/40761>

**Note:** To cite this publication please use the final published version (if applicable).

Cover Page



Universiteit Leiden



The handle <http://hdl.handle.net/1887/40761> holds various files of this Leiden University dissertation.

**Author:** Sen, S.

**Title:** Fluorescence correlation spectroscopy on electron transfer reactions : probing inter- and intramolecular redox processes

**Issue Date:** 2016-06-30

# **Fluorescence Correlation Spectroscopy on Electron Transfer Reactions**

**Probing Inter- and Intramolecular Redox Processes**

Proefschrift

ter verkrijging van  
de graad van Doctor aan de Universiteit Leiden,  
op gezag van Rector Magnificus prof.mr. C.J.J.M. Stolker,  
volgens besluit van het College voor Promoties  
te verdedigen op donderdag 30 juni 2016  
klokke 13:45 uur

door

Saptaswa Sen

geboren te Kolkata, India  
in 1984

Promotoren: Prof. dr. G. W. Canters (Universiteit Leiden)  
Prof. dr. T. J. Aartsma (Universiteit Leiden)

Promotiecommissie: Prof. dr. E. R. Eliel (Universiteit Leiden)  
Prof. dr. E. J. J. Groenen (Universiteit Leiden)  
Prof. dr. A. Rowan (Universiteit Nijmegen)  
Dr. M. Huber (Universiteit Leiden)  
Dr. L. Jeuken (Leeds University)

Casimir PhD Series, Delft-Leiden 2016-17

ISBN: 978-90-8593-258-1

The research described in this thesis was financially supported by NWO (Netherlands Organization for Scientific Research).



# Contents

<b>Prologue</b>	<b>1</b>
<b>1. Introduction</b>	<b>2</b>
1.1 Introduction.....	3
1.2 Copper proteins .....	5
1.3 Fluorophore .....	8
1.4 Fluorescence resonance energy transfer (FRET) .....	9
1.5 Single molecule techniques.....	12
1.6 Electron transfer theory .....	17
1.7 Scope of this thesis.....	21
References.....	22
<b>2. Calibration of experimental setup, biomolecular reactions and photoinduced electron-transfer reaction</b>	<b>29</b>
2.1 Introduction.....	31
2.2 Materials and methods.....	32
2.3 Fluorescence correlation spectroscopy calibration: Results and discussion.....	37
2.4 Diffusion, bimolecular interactions and their dependency on viscosity.....	46
2.5 Photobleaching and blinking of fluorophore.....	50
2.6 Photoinduced electron transfer (PET).....	52
References.....	55
<b>3. Fluorescence correlation spectroscopic studies on labeled Zinc Azurin: Direct observation of intermolecular electron-transfer reactions between label and redox agents</b>	<b>63</b>
3.1 Introduction.....	65
3.2 Materials and methods.....	66
3.3 Results.....	71
3.4 Discussion.....	85
3.5 Concluding remarks.....	92
References.....	93
<b>4. Observation of intramolecular electrons-transfer reactions by fluorescence correlation spectroscopy: Photoinduced electron-transfer between the label and the copper center</b>	<b>96</b>
4.1 Introduction.....	98
4.2 Materials and methods.....	99
4.3 Results and discussion.....	105
4.4 Concluding remarks.....	124
References.....	127
Appendix .....	132

<b>5. Labeling and fluorescence correlation spectroscopic studies on Lys122Ser and Lys122Gln mutants of Copper Azurin</b>	<b>134</b>
5.1 Introduction.....	136
5.2 Materials and methods.....	137
5.3 Results and discussion.....	142
5.4 Comparison of fluorescence resonance energy transfer (FRET) and photoinduced electron transfer (PET) reaction in Copper Azurin-ATTO655.....	158
5.5 Future plans and concluding remarks.....	162
References.....	163
<b>6. Outlook</b>	<b>167</b>
Summary	174
Samenvatting	177
Curriculum Vitae	182
List of publications	184
Acknowledgement	186



## *Prologue*

This is where it all started. I was a research-fellow in Prof. Dr. Shyamalava Mazumdar's group at the department of chemistry, Tata Institute of Fundamental Research (TIFR), Mumbai, India. This group had a very long history of studying metal-containing proteins e.g. cytochrome  $c_{552}$ , thermostable cytochrome P450,  $Cu_A$  from cytochrome c oxidase and so on. A special focus was on cytochrome P450<sub>cam</sub>, a bacterial mono-oxygenase containing iron in the active site of the protein, the crucial model of my project. The main task was to engineer mutations in the active site of the cytochrome P450 protein, which in turn, could help in the catalytic degradation of pesticides and also of flavonoid compounds. My approach was first to scan available literature to create a full list of plausible mutants. Some of the candidates were removed from the list as they were judged to affect the active site structure of the protein too severely. Then, the rest were evaluated by energy minimization or docking procedures. In the end, I identified a few single and double mutants, which were considered capable of performing catalyzed degradation. Working with something as fragile and complex as a protein really kindled my interest in protein structure-function relationships, enzyme mechanisms and redox chemistry of proteins. I wanted to follow this interest to understand, think and research better. After the completion of the research project on cytochrome P450 enzyme in TIFR, I was lucky to be able to pursue my interests further by becoming a graduate student in Prof. Dr. Gerard W. Canters' group in the department of molecular biophysics at Leiden University, The Netherlands.

# Chapter 1

## Introduction

This chapter is a general introduction to the work presented in this thesis. A brief overview of the protein investigated, as well as the techniques used is presented. At the end, a short synopsis of each of the following chapters is provided.

## 1.1 Introduction

Redox reactions are the foundation of life. They encompass a variety of oxidation and reduction processes such as photosynthesis, redox homeostasis, cellular respiration, water oxidation and metabolism. Most importantly, enzymes are needed to make those redox reactions effective and to control them. Some of the most demanding reactions such as nitrogen fixation and photosynthesis are driven by redox active metalloproteins, enzymes that generally use small, inorganic or organic cofactors to execute those reactions. Metals such as vanadium, manganese, iron, cobalt, nickel, copper, zinc, magnesium and calcium have been found to play essential roles in the structure and function of metalloproteins(1)(2) (See Fig.1.1 for a few examples). In this thesis, the spotlight is on a redox active bacterial copper protein, azurin, which is mostly involved in the shuttling of electrons, i.e., electron transfer (ET) processes with other proteins or molecules in the cell. This feature of the protein has been exploited in many studies of protein-protein interactions, ET processes or catalysis. They have opened up new possibilities for applications in biotechnology and biosensors.

One way of monitoring ET or redox reactions is by electrochemistry such as cyclic voltammetry and protein film voltammetry. These techniques often require the surface confinement of an enzyme on an appropriately modified electrode. Since the redox cofactors or the prosthetic groups usually lay deeply buried inside the protein matrix(3)(4) and since there is limited control of the protein orientation, this may cause pathway uncertainties and heterogeneity of the ET rates.

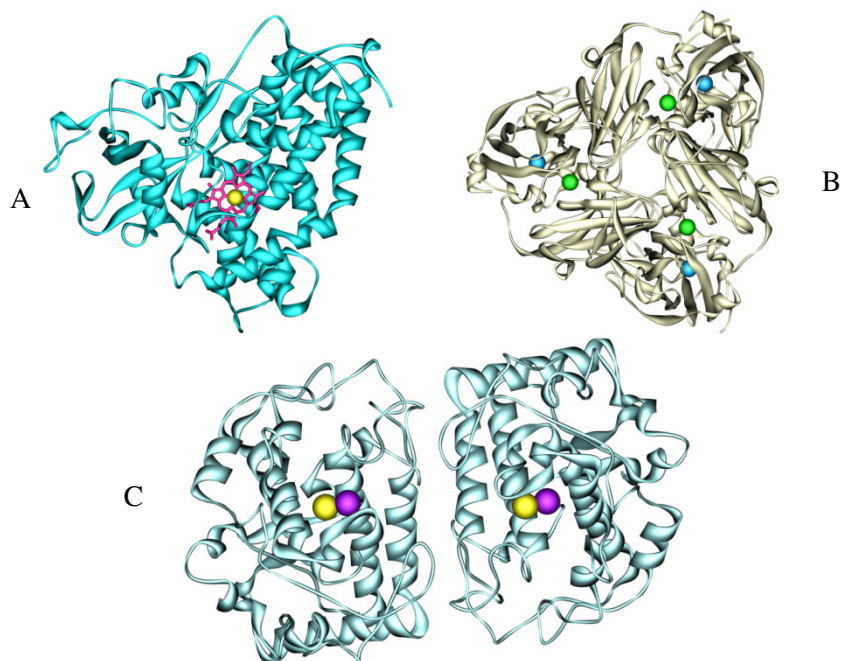


**Figure 1.1:** Crystal structures of metalloproteins. (A) 1DZ4\*: Cytochrome P450cam from *Pseudomonas putida*, a heme mono-oxygenase that catalyses the reaction of hydrocarbons with molecular oxygen at ambient temperature; the porphyrin group is shown in pink stick, and the iron ion is shown as a yellow sphere, (B) 2PP9\*: Nitrite reductase from *Alcaligenes faecalis* S-6, a copper-containing protein that catalyses the production of nitric oxide from nitrite; the green spheres show the Type II copper centers and the blue spheres represent the Type I centers in the active sites, (C) 4P6R\*: Tyrosinase from *Bacillus megaterium*, responsible for the conversion of tyrosine to melanine; copper centers are shown as yellow and violet spheres.

\*: The codes refer to the PDB accession numbers in the protein data bank ( [www.rcsb.org](http://www.rcsb.org) and H.M. Berman, J. Westbrook, Z. Feng, G. Gilliland, T.N. Bhat, H. Weissig, I.N. Shindyalov, P.E. Bourne (2000) *The Protein Data Bank, Nucleic Acids Research*, 28: 235-242.)

Singlemolecule techniques have provided direct access to the behavior of an individual molecule in solution. Single-molecule studies often make use of fluorescence imaging techniques. With this approach, the behavior of a single protein molecule, or of short-lived intermediates in a reaction can be monitored in time(5)(6)(7)(8)(9)(10). Reaction mechanisms can be investigated in detail, and the possible individual variations in a population of molecules can be accessed. The objective of the research described in this thesis is to obtain information on the heterogeneity of the activity of a redox protein via a single-molecule approach.

## 1.2 Copper proteins

Copper is an essential element for living organisms. It occurs in a variety of metalloproteins, many of which are involved in oxygen binding, blood coagulation and electron transfer and redox reactions based on the Cu(I)/Cu(II) couple. Examples are plastocyanin, rusticyanin, laccase, terminal oxidase, oxygenase, superoxide dismutase, and ceruloplasmin. The properties and activities of these copper proteins are well documented(11)(12)(13)(14). Cu(I) is a soft acid while Cu(II) is a borderline case. Thus, the copper binding sites are ligated by side chains with soft or borderline ligands e.g. nitrogen donor atoms from histidine and sulfur atoms from cysteine/methionine. These ligands are preferred over hydroxyl and carboxyl groups or primary amine-side chains, as found in serine and tyrosine, aspartate and glutamate, and asparagine, glutamine, and arginine residues, respectively. Three main types of copper centers have been documented in the literature. (a) Type I copper proteins have a beautiful blue color, far more intense than the color of synthetic copper complexes in solution, but similar in hue. They are also called cupredoxins and have a strong absorption around 600 nm. In general, their Cu-coordination sphere is based on two histidines and one cysteine. The coordination sphere may be completed by a methionine or a leucine. Type I proteins are characterized by EPR spectra exhibiting small copper hyperfine couplings and small g-anisotropy; e.g. azurin, plastocyanin and nitrite reductase(1), (b) Type II Cu, occurring in "non-blue" copper proteins, has an essentially planar coordination sphere with 2-3 histidines and oxygen from a carboxylic group. A water molecule or hydroxide ion is often found as additional coordinating ligand. These proteins have a weak absorption in the visible region, and EPR spectra with axial symmetry; e.g. galactose oxidase, amine oxidase, dopamine mono oxidase carry a Type II active site(15), (c) Type III proteins contain a dinuclear copper center with a Cu-Cu distance of ~ 350 pm; after oxygen uptake, they show absorptions at 350 nm and 600 nm, e.g. haemocyanin and tyrosinase. These proteins are EPR silent as the copper centers are anti-ferromagnetically coupled(16)(17).

There are also other types of copper proteins. They can be summarized as follows: (a) Multi-Copper Oxidases: These enzymes contain Type I, II and III centers in various stoichiometric ratios such as L-ascorbate oxidase, laccase and ceruloplasmin(11)(18). Ascorbate oxidase and laccase catalyze the reduction of oxygen to water. But ceruloplasmin is an ancient multicopper oxidase that has ferroxidase activity and functions as an antioxidant(18). (b) Copper centers in cytochrome c-oxidase and nitrous oxide reductase: the copper centers appear to be



unique in these cases. In addition to a Type II copper site, these proteins contain a Cu<sub>A</sub> center that consists of two copper ions connected by two bridging cysteine thiolates. The Cu<sub>A</sub> site has very distinct EPR and UV/Vis spectra(19)(20). There is evidence that the copper ions form a mixed valence copper pair having 1.5+ charge per Cu(21). A recent addition to the copper protein typology is the “Type zero” protein by Gray *et al.* They built a novel Cu(II) binding site by incorporating new amino acid residues at Cys112 position in *Pseudomonas aeruginosa* azurin. This mutant does not resemble any of the existing types mentioned above. X-ray crystallographic analysis has shown that this copper site adopts a distorted tetrahedral geometry with an unusually short Cu–O bond with the carbonyl of Gly45. Type zero proteins also have a relatively weak absorption near 800 nm and a narrow parallel hyperfine splitting in their EPR spectra(22).

### **1.2.1 Azurin: Central protein of this research**

Azurin is found in several gram-negative bacteria e.g. *Pseudomonas aeruginosa*, *P. aureofaciens*, *P. chlorophis*, *P. fluorescens*, *P. putida*, *Alcaligenes denitrificans*, *A. xylooxidans*, *A. faecalis*, *Bordetella bronchiseptica* and *Streptomyces thioluteus* (23). The present studies have been performed on azurin from *Pseudomonas aeruginosa*. The azurin gene encodes a signal peptide-containing protein consistent with a periplasmic location of the mature protein. Azurin is excreted to the periplasmic space, where the signal peptide is cleaved off during translocation by a signal peptidase. There is strong evidence that the protein fulfills a role in the oxidative stress-induced response in its parent host organism(24). Recently, azurin from the bacteria *Pseudomonas aeruginosa* has been reported to induce and trigger apoptosis in human cancer cells(25)(26). One of the recent biosensing-applications for azurin is the detection of superoxide species *in vitro*(27)(24)(28)(29).

Azurin is a small soluble Type I blue copper protein with molecular weight of 13,998 kDa. A large number of three-dimensional structures have been solved by X-ray crystallography or NMR(23)(30)(31). The copper ligands are His46, Cys112, and His117. Two weaker axial ligands are provided by Met121 and the carbonyl oxygen of Gly45 (Fig. 1.2). The active site shows a slightly distorted trigonal bipyramidal geometry in which the copper ion is only 0.1 Å out of the N<sub>2</sub>S plane (32). In the so-called "northern region" of the protein, the copper ion is buried at 0.7 nm distance from the surface. Azurin is composed of 128 amino acids with eight β-

strands forming two  $\beta$ -sheets in a Greek-key motif. These are connected by a  $\alpha$ -helix. This produces considerable rigidity of the polypeptide matrix. (33)(34)(35). On the opposite side of Cu-center, in the so-called southern corner of the protein, close to the N-terminus, the presence of a disulfide bond between Cys3 and Cys26 contributes to the stability of the protein. Upon removal of the copper, the protein is significantly destabilized(36)(37)(38). It has a typical UV/Vis absorption around 595-630 nm originating from a  $\pi$ - $\pi^*$  transition in the molecular orbital scheme of the oxidized copper site(39)(40) (Fig. 1.2). This transition mainly involves the  $d_{x^2-y^2}$ -orbital on the copper and the 3p-orbital of the Cys112-sulfur (41)(42). Upon reduction, the strong blue color disappears due to the  $d^{10}$  electronic configuration of copper. This change in absorption spectrum allows us to monitor the oxidation state of the protein by optical techniques(43)(44). There is only one single tryptophan residue at position 48 in azurin which is buried inside the hydrophobic core of the protein. The absorption and fluorescence maxima of the tryptophan occur at 291 nm and 309 nm, respectively (Fig. 1.3). One of the Cu ligands, His117, protrudes through the surface of the protein, and it connects the copper ion with the surroundings of the protein. The so-called hydrophobic patch around His117 consists of a number of apolar amino acid residues which facilitate the formation of electron-transfer (ET) complexes(45). The redox properties of azurin are dictated by the copper site. The redox potential of Cu-azurin depends on pH, and amounts to 310 mV (vs. NHE) at pH 7.0(46)(47)(48). The copper ion in azurin can also be reconstituted with  $Zn^{2+}$ . The resulting zinc-azurin is redox inactive and is often used for control experiments.

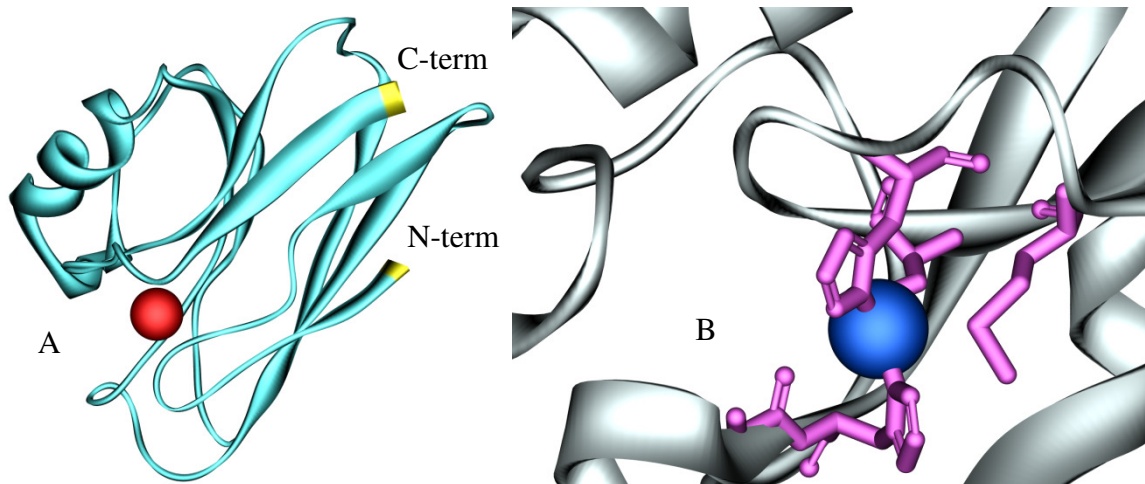


**Figure 1.2:** Ribbon presentation of azurin from *Pseudomonas aeruginosa*. The copper ion is shown as a red sphere. C-terminus and the N-terminus have been marked in yellow. (B) Close-up of the active site. Copper is shown as a blue sphere. The pink ball and sticks display the active site ligands of the copper (His117, His46, Cys112, Met121, and Gly45).

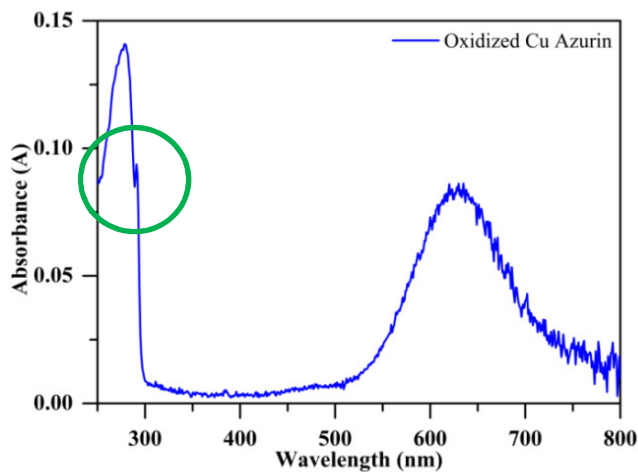


**Figure 1.3:** UV-vis spectrum of 14  $\mu\text{M}$  azurin from *P. aeruginosa* in 20 mM HEPES, pH 7.0 in the oxidized form. The shoulder at 291 nm is marked by a green circle and is due to the presence of single tryptophan residue in azurin.

### 1.3 Fluorophores

The key fluorophores used in fluorescence based biochemical assays are categorized into three groups(49)(50)(51)(52)(53)(54) (See Fig. 1.4 for example). The first group corresponds to the natural fluorophores such as flavins, the indole ring of tryptophan, tyrosines, nicotinamide

adenine dinucleotide (NADH) and chlorophyll(50). The second group comprises fluorescent molecules whose optical properties are sensitive to the presence of a particular molecule or ion e.g.  $\text{Na}^+$ ,  $\text{Ca}^{2+}$ ,  $\text{Mg}^{2+}$ ,  $\text{Cl}^-$ (50). Finally, in cases, where the molecule of interest is non-fluorescent, or its intrinsic fluorescence is too low or in the wrong wavelength region, one can label or fuse it with an external probe. This external probe can be either an intrinsically fluorescent protein such as a green fluorescent protein (GFP), a chimeric fused protein or a small organic compound(50). A recent addition to the collection of fluorescent labels refers to nanometer sized quantum dots(55). Their emission depends on the size of the particle but all quantum dots can be excited with near UV light.

In the present thesis, we used small organic fluorophores (extrinsic) to label azurin(56)(57)(58)(59)(60). These extrinsic chromophores were attached covalently for example by a maleimide for sulfhydryl labeling, or a succinimidyl ester for the labeling of primary amines(54)(56)(58). The labeling reactions can be controlled by the pH of the solution. Lysine-derived amines and the N-terminus of the protein are the primary targets for the labeling reactions by succinimidyl esters. They are good nucleophiles, and lysines are more reactive than the N-terminus above pH 8.0 ( $pK_a = 9.18$ )(58). (61)(62)(63). Thiols are reactive at neutral pH allowing the selective coupling to fluorophores even in the presence of amines.

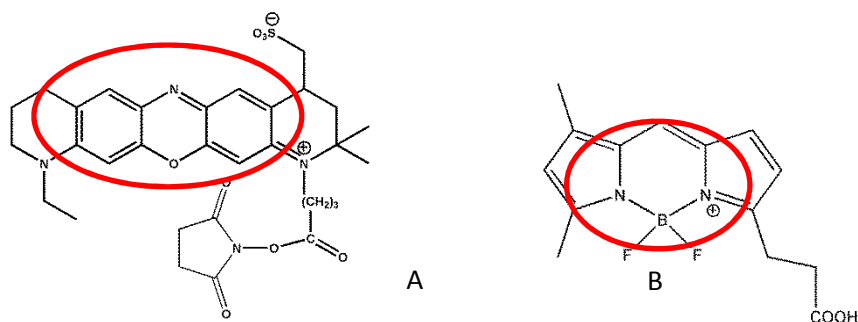


**Figure 1.4:** Chemical structures of two commonly used fluorophores: (A) ATTO655 NHS (group 1) and (B) BODIPY FL carboxy (group 2). The red circled regions display the chromophoric zones of the dyes.

#### 1.4 Fluorescence and Förster Resonance Energy Transfer (FRET)

The origin of fluorescence phenomenon can be illustrated with a simple three electronic-state diagram as proposed by Alexander Jablonski (See Fig. 1.5)(50). The diagram shows the ground state ( $S_0$ ), the first excited singlet state ( $S_1$ ), 2<sup>nd</sup> excited singlet state ( $S_2$ ) and triplet state ( $T_1$ ) respectively. Each of them carries a series of vibrational states. Molecules are excited by an

external source, e.g. an incandescent lamp or a laser, and they relax back to the ground state ( $S_0$ ) thereby emitting fluorescence (red arrow) on a timescale of nanoseconds. The orange dotted line represents the fast internal conversion from  $S_2$  to  $S_1$ . The molecules in the  $S_1$  state can also undergo a transition to  $T_1$ , which is called inter-system crossing (blue arrow). As the transition-probability from  $T_1$  to  $S_0$  is low, long-lived phosphorescence (dotted red arrow) often occurs on a millisecond to second time scale. Fluorescence resonance energy transfer (FRET) is an energy transfer between two molecules by which a donor molecule transfers its excitation energy to an acceptor molecule without emission of a photon(64)(49)(65)(66). Förster, Stryer, and Haugland described how the FRET efficiency,  $E$ , depends on the donor-acceptor separation between two atoms or molecules(49). According to Eqn. 1.1

$$E = R_0^6 / (R_0^6 + r^6) \quad (1.1)$$

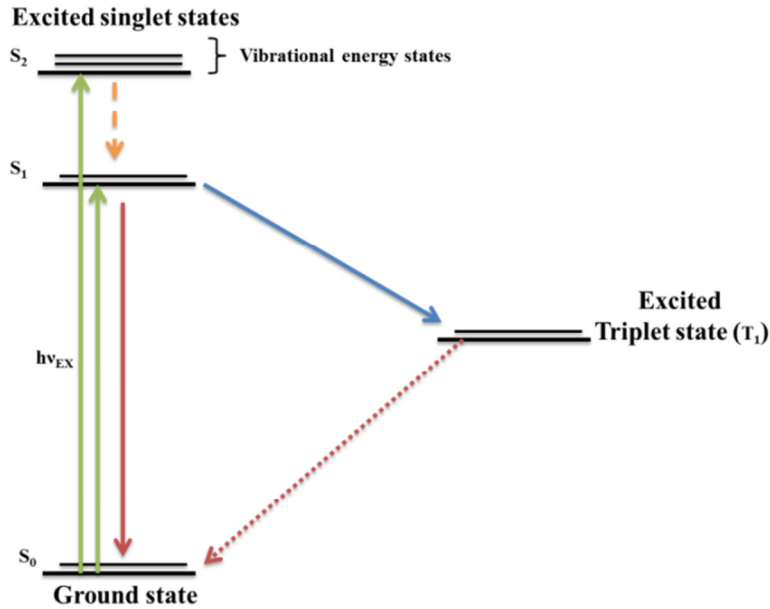


**Figure 1.5:** A Jablonski diagram depicting the electronic states involved in the processes of excitation and emission.  $S_0$  represents the electronic ground state of the molecule;  $S_1$  and  $S_2$  are the 1<sup>st</sup> and 2<sup>nd</sup> excited singlet states. Each state contains vibrational levels, a few of which are indicated in the diagram.  $T_1$  is the lowest triplet state. Green arrows: excitation; red arrow: emission; blue arrow:  $S_1$  to  $T_1$  transition.

where  $r$  represents the distance between the donor and the acceptor, and  $R_0$  is the Förster radius.  $R_0$  is the distance at which the energy transfer efficiency is 50%. The Förster radius depends on the spectral features of the donor and acceptor as follows:

$$R_0 = 0.211[\kappa^2 \eta^{-4} Q_D J(\lambda)]^{1/6} \quad (1.2)$$

where  $\kappa$  is the dipole orientation factor,  $\eta$  is the refractive index of the medium,  $Q_D$  is the quantum yield of the donor, and  $J(\lambda)$  is the overlap integral defined as

$$J(\lambda) = \int_0^\infty I_D(\lambda) \epsilon_A(\lambda) \lambda^4 d\lambda / \int_0^\infty I_D(\lambda) d\lambda \quad (1.3)$$

where  $I_D(\lambda)$  is termed the fluorescence intensity of the donor and  $\epsilon_A(\lambda)$  is the extinction coefficient of the acceptor molecule at the wavelength  $\lambda$ . The energy transfer efficiency,  $E$ , is given by

$$E = 1 - (\tau_{DA}^f / \tau_D^f) = 1 - (F_{DA} / F_D) \quad (1.4)$$

where  $\tau_D^f$  and  $\tau_{DA}^f$  are fluorescence lifetimes of the donor in the absence and in the presence of the acceptor, respectively, and  $F_D$  and  $F_{DA}$  stand for the fluorescence intensities of the donor in the absence and the presence of the acceptor, respectively.

FRET-based applications can be found in the fields of biosensor design, single molecule imaging of cells, molecular motors, DNA mechanical movements, etc.

#### 1.4.1 The FluRedox principle: FRET as a reporter of the redox state of the proteins

The FRET-based FluRedox technique monitors the redox state of a metalloprotein via fluorescence detection (Fig. 1.6). The emission of a covalently attached fluorophore (donor) reflects the changes in the absorbance of the prosthetic group (FRET acceptor). Cu-azurin, exploited in the current thesis, in its oxidized form shows an absorbance maximum at 628 nm which overlaps with the fluorescence emission of ATTO655 dye (Fig. 1.7). The energy transfer, i.e. the FRET, is high in this form, and the fluorescence of the dye is quenched. However, FRET is low when the copper azurin is reduced since the 628 nm absorption disappears upon the reduction of the proteins. Successful applications of this principle have been reported(6)(44)(67)(68)(69).

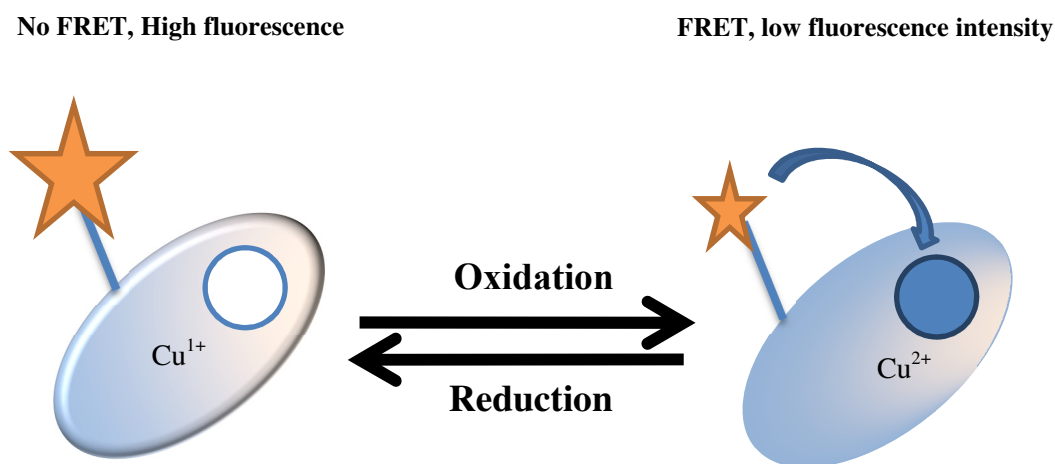


**Figure 1.6:** Illustration of the FluRedox principle. On the left-hand side, the fluorescence of the label is high, and no FRET occurs due to the reduction of the cofactor in the active site of the protein; at the right side, the fluorescence of the label is quenched due to FRET between the label and the cofactor of the protein and fluorescence is low. The label is shown as an orange star.

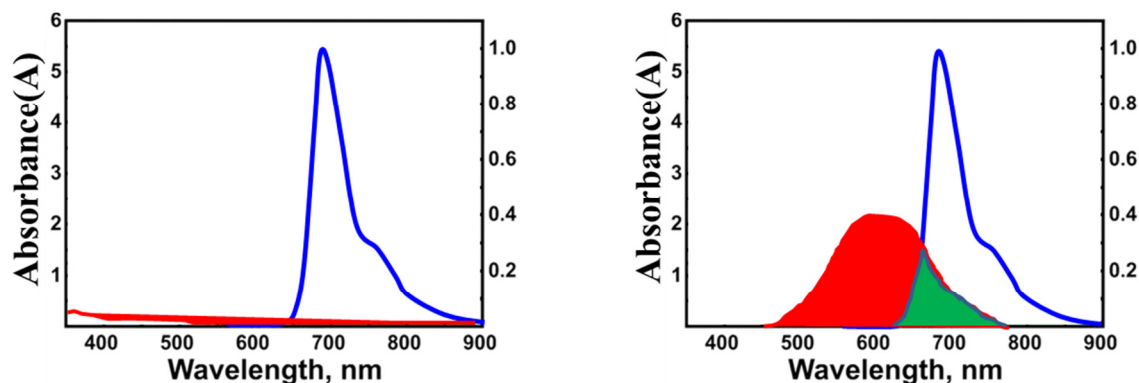


**Figure 1.7:** Example of spectral overlap between the absorption spectra of a cupredoxin and the emission of a dye. In the left panel, the red line displays the absorption spectrum of the reduced form of the protein and the right panel shows the spectrum of the oxidized form. The green area is the overlap with the emission spectrum (blue line) of the dye.

## 1.5 Single-Molecule Techniques

Single-molecule fluorescence techniques such as Fluorescence correlation spectroscopy (FCS), Fluorescence lifetime imaging (FLIM), Photobleaching FRET, Light Sheet Microscopy provide new and detailed information about (70)(8)(9)(10)(71)(72)(73)(74)(75)(76) enzyme mechanisms, protein-protein interactions, conformational changes of a molecule, molecular reaction dynamics, etc., at single molecule level. For exhaustive reviews of these achievements see(76)(77)(78). Here an introduction to the methodologies used in the present thesis is presented.

### 1.5.1 Fluorescence Correlation Spectroscopy

In a simple fluorescence correlation spectroscopy (FCS) setup (Fig. 1.8) the fluorescent sample is kept on a stage, and a laser of a particular wavelength is focused in the sample through an objective lens with high numerical aperture (Fig.1.9). The emitted light passes through the same objective and a pinhole of micrometer size and is subsequently detected with a photo diode. The small pinhole helps to eliminate out-of-focus fluorescence from the image plane of the objective. Thus, a high signal to noise ratio is obtained from a fluorescent sample. The optical setup (Fig. 1.8) produces a tiny observation or detection volume which is in the order of femtoliters and the fluorescent signals from diffusing molecules can be collected and analyzed. If the number of molecules in the detection volume is small, we can observe single molecular events from the labeled molecules in the form of signal fluctuations (79)(80)(81)(82)(83)(84).



The observation time of the fluorescently labeled molecule is limited by the residence time of that molecule inside the detection volume.

FCS makes use of the autocorrelation function  $G(\tau)$ . First, the signal from the sample is recorded as a fluorescence trace,  $F(t)$ . The autocorrelation function is then defined as

$$G(\tau) = \langle \delta F(t) \times \delta F(t+\tau) \rangle / \langle F(t) \rangle^2 \quad (1.6)$$

where brackets “ $\langle \rangle$ ” denote averaging over time  $t$ ,  $\delta F(t) = F(t) - \langle F(t) \rangle$  and  $\tau$  is a variable interval. This function therefore, computes its self-similarity after a lag time  $\tau$ . It contains information about equilibrium concentrations, reaction kinetics and diffusion rates of molecules in the sample of interest. For example, if a labeled molecule moves in and out of the detection volume, the autocorrelation curve may look as depicted in Fig. 1.10.

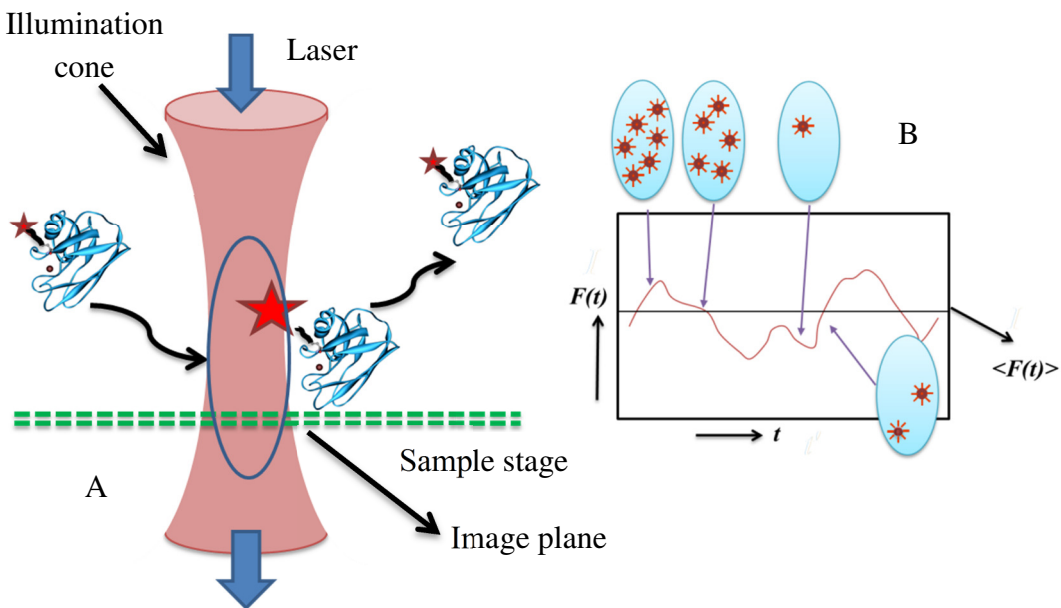


**Figure 1.8:** (A) Zoomed view of the detection volume (blue ellipsoid): the red illumination cone represents the laser beam and a labeled protein moves in and out of the focus; (B) the recorded fluorescence intensity signal (red line) fluctuates.

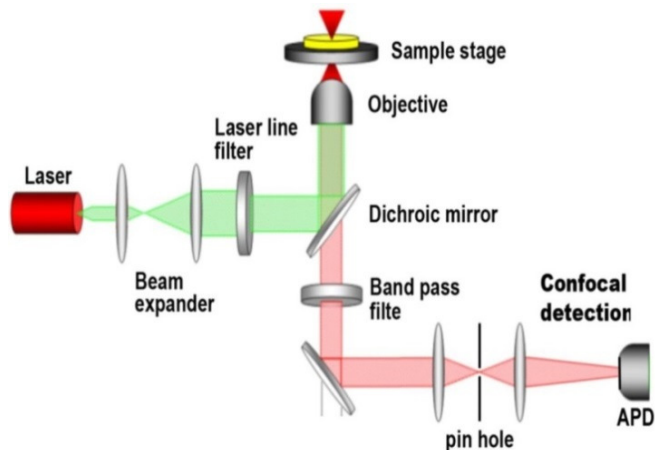


**Figure 1.9:** A simplified diagram of the FCS setup. The instrumentation for FCS will be discussed in Chapter 2. The fluorescent sample is kept on a sample stage (gray) and a laser beam (green) of a particular wavelength is focused in the sample through filters, a dichroic mirror and an objective lens. Then, the emitted light or fluorescence (red) is passed through the same objective, dichroic mirror, and a micron size pinhole. The fluorescence is detected at an avalanche photodiode (APD) (gray).

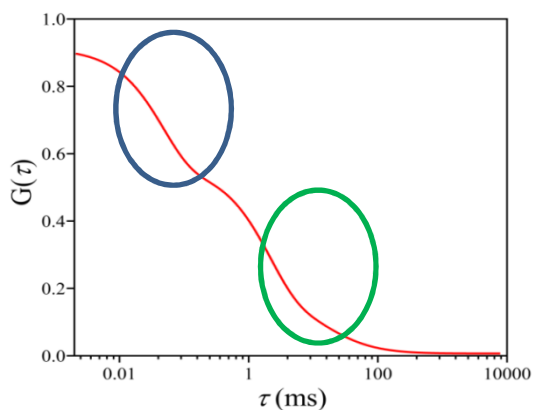


**Figure 1.10:** Example of an autocorrelation curve (red). The green circled region corresponds with the diffusion of the particle, the blue circled region corresponds with a reaction that is faster than diffusion.

The calculation of the autocorrelation function is based on the assumption that the light intensity in the detection volume has approximately a three-dimensional Gaussian profile. This results in(85)

$$\begin{aligned}
G(\tau) &= G(0) \cdot \left(1 + \frac{4D\tau}{r_0^2}\right)^{-1} \cdot \left(1 + \frac{4D\tau}{z_0^2}\right)^{-1/2} \\
&= G(0) \cdot \left(1 + \frac{\tau}{\tau_D}\right)^{-1} \cdot \left(1 + \left(\frac{r_0}{z_0}\right)^2 \frac{\tau}{\tau_D}\right)^{-1/2} \\
&= G(0) \cdot \left(1 + \frac{\tau}{\tau_D}\right)^{-1} \cdot \left(1 + \frac{\tau}{k^2 \tau_D}\right)^{-1/2}
\end{aligned} \tag{1.7}$$

where  $\tau_D = \frac{r_0^2}{4D}$ ,

and  $k = \frac{z_0}{r_0}$ .

$D$  is the diffusion coefficient of the molecule of interest,  $\tau_D$  is the residence time of the molecule in the detection volume and  $r_0$  and  $z_0$  denote the distances from the center of the observation volume to the point where the intensity has dropped by a factor of  $1/e^2$  in the radial and axial direction, respectively.

$G(0)$  is given by

$$G(0) = \frac{1}{\langle N \rangle} = \frac{1}{c \cdot V_{eff} \cdot N_A} \tag{1.8}$$

where,  $\langle N \rangle$  corresponds to the average number of particles in the detection volume,  $c$  is the sample concentration of the molecule of interest,  $V_{eff}$  is the effective detection volume, and  $N_A$  is Avogadro's constant.  $V_{eff}$  is larger by a factor of  $2^{(2/3)}$  than the confocal volume, which is calculated on the basis of a Gaussian intensity profile.

Compared to classical measurements, FCS is a special technique in the sense that the molecular dynamics on different time scales can be investigated in a single measurement. Photochemical reactions can induce changes in fluorescence intensity. As the time window in

FCS ranges typically from  $10^{-12}$  sec to several seconds(86)(87)(88), those changes can be observed in the autocorrelation curve as depicted in the example of Fig. 1.10. The decay at the short time scale corresponds with a reaction that modifies the fluorescence of the molecule like triplet state blinking, FRET-induced quenching, protonation or electron transfer. From such a decay the reaction rate and the steady-state population of the molecules with the reaction can be investigated. When more than one reaction occurs, the expression for the autocorrelation functions becomes:

$$G(\tau)=G(0)G_{diff}(\tau)G_1(\tau)\dots G_n(\tau) \quad (1.9)$$

with

$$G_i(\tau) = \frac{1 - F_i + F_i e^{-\frac{\tau}{\tau_i}}}{1 - F_i} \quad (i=1,2\dots n)$$

where  $F_1, \dots, F_n$  are the fractions of fluorescent molecules associated with having relaxation times  $\tau_1, \dots, \tau_n$  respectively. In Chapters 3 and 4, equations 1.7-1.9 will be used to analyze inter- and intra-molecular ET reactions in ATTO655 labeled azurin.

### 1.6 Electron transfer (ET) theory

Redox proteins are nanoscale electronic devices. They can convert energy from one form to another(89)(90)(91) by driving electrons and protons. Copper proteins containing blue sites mostly function as electron carriers and are involved in biological energy conversions and biochemical transformations. Possessing two oxidation states and a wide range of redox potentials (200-1000 mV) are functional advantages of these proteins to mediate electrons(92)(93). Our understanding of the electronic and functional properties of copper proteins has dramatically advanced partly due to the availability of high-resolution crystal structures and model complexes. In the following paragraph, a short review of ET theory and expressions for the rates of electron transfer between a weakly coupled donor and an acceptor are given.

The investigation of ET kinetics was started over 50 years ago. (94)(95). Because electrons move much faster than nuclei, the nuclei remain fixed during ET reactions (Franck-

Condon Principle). The transition state for such a reaction must lie at a point in the nuclear-configuration space where the reactant and product states are degenerate. This means that the only instant at which an electron can shuttle between two species occurs when both have achieved the same nuclear configuration as a result of thermally induced fluctuations. Thus, the kinetics of the reaction depends on an activation barrier ( $\Delta G^\ddagger$ ) (Fig. 1.11). In general, the factors that control the rate constant of electron transfer ( $k_{ET}$ ) include the distance ( $r$ ) between donor and acceptor, the Gibbs free energy of activation, and the reorganization energy of the reaction. The rate of the electron-transfer process is given by(96)

$$k_{ET} = \frac{2\pi}{h} \frac{H_{DA}^2}{\sqrt{4\pi\lambda k_B T}} e^{-\frac{(\Delta G_{CS}^0 + \lambda)^2}{4\lambda k_B T}} \quad (1.10)$$

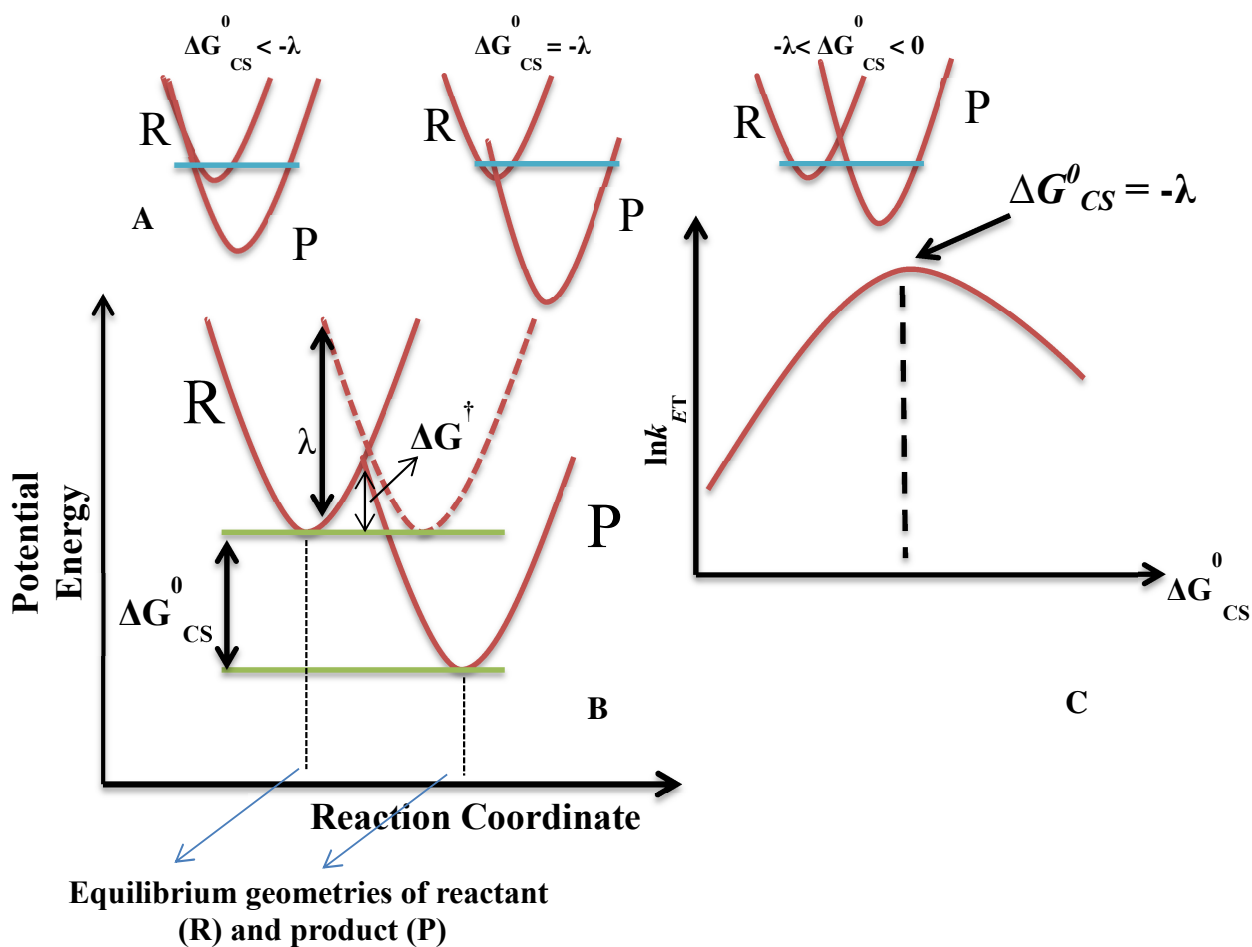


**Figure 1.11:** A schematic potential energy diagram for electron transfer. Reactant and Product are represented by R and P. Their nuclear motions are sketched as single harmonic oscillators. The activation energy of the reaction depends on the free energy of the reaction and the reorganization energy [Adapted from *Quarterly Reviews of Biophysics* 2003, 36(3), pp. 341–372]

- $H_{DA}$  determines the electronic coupling between donor and acceptor and is generally represented as

$$H_{DA}^2 = H_0^2 \exp[-\beta(r-r_0)] \quad (1.11)$$

where  $r_0$  is the distance when donor and acceptor are in direct contact,  $\beta$  is the distance-decay constant presenting the efficiency of the ET reaction in the protein medium. It can vary between  $1.4\text{\AA}^{-1}$  to  $0.7\text{\AA}^{-1}$  depending on the secondary structure of the protein (96)(97)(98)(99)(100)(101)(102).

- The activation energy,  $\Delta G^\ddagger$ , is related to the standard reaction Gibbs free energy ( $\Delta G_{CS}^0$ ) and the reorganization energy ( $\lambda$ ), and is given by (96)(103)(104)

$$\Delta G^\ddagger = \frac{(\Delta G_{CS}^0 + \lambda)^2}{4\lambda} \quad (1.12)$$

This  $\Delta G_{CS}^0$  is the free-energy change for the charge-separation and can be estimated using the Rehm-Weller approach to be described in Chapter 2.

- The ET between donor and acceptor often results in molecular rearrangement of the reactants. The energy required for this rearrangement before ET is called the reorganization energy ( $\lambda$ ). It is a combination of changes in the nuclear configuration of the redox centers (changes in bond angles and lengths) and the surrounding solvent and protein matrix during ET. For a high ET rate, the reorganization energy has to be small.  $k_B$  is the Boltzmann constant, and  $T$  is the temperature expressed in Kelvin.

A profile for the potential energy curve has been displayed schematically in Fig. 1.11. Reactant (R) is converted into the product (P) after ET. A plot of  $\ln k_{ET}$  vs.  $\Delta G^0$  has (Fig. 1.11 C) a bell-shape.(96)(105)(104). The following regimes are usually distinguished.

- a normal regime for small driving forces ( $-\lambda < \Delta G^0 < 0$ ) in which the process is thermally activated and  $\ln k_{ET}$  increases with increasing driving force;
- an activationless regime in which a change in driving force does not cause large changes in the reaction rate, and where  $-\lambda = \Delta G^0$ .
- an “inverted” regime for strongly exergonic processes ( $-\lambda > \Delta G^0$ ) in which  $\ln k_{ET}$  decreases with increasing driving force.

The plot illustrates that the ET rate will increase with  $-\Delta G^0$  until a maximum rate is observed for  $-\Delta G^0 = \lambda$  and the rate then decreases.

In essence, Marcus semi-classical theory suggests that an electron can travel from one redox center to another one over a limited distance. ET may occur through space or by hopping, or the electron can travel through covalent and hydrogen bonds to reach its destination [(96) and references therein]. The effect of parameters like distance, redox potential, and temperature on ET rates has been well established theoretically as well as experimentally(106)(107)(108).

## **1.7 Scope of this thesis**

**Chapter 2** reports the calibration of the instrumental setup required for the FCS measurements. Calibration was performed by using a commercially available organic dye, ATTO655, and recording its fluorescence intensity over time at different concentrations. The instrumental factor “*k*” obtained from the calibration measurements, has been used for the fitting of the autocorrelation curves of labeled Zn and Cu azurin samples in Chapter 3, 4 and 5. Chapter 2 also includes a general discussion of bimolecular interactions and photoinduced electron transfer reactions in proteins.

In **Chapter 3**, the species obtained from labeling of zinc azurin with ATTO655 are analyzed by using FCS. The analysis of the autocorrelation functions report on the bimolecular ET reactions between the dye and the redox chemicals [ascorbate, potassium hexacyanoferrate (II) or (III)].

**Chapter 4** reports on the photoinduced electron transfer reactions in labeled copper azurin. First, the species obtained from labeling copper azurin with ATTO655 are analyzed by using FCS. The analysis of the autocorrelation functions reports on the microsecond dynamics of the intramolecular ET reactions between the dye and redox-active center. It is shown that in oxidoreductases photoinduced intra-molecular electron-transfer (PET) between the label and active center may occur over long distances and is not restricted to situations where the label is in Van-der-Waals contact with the redox center.

**Chapter 5** describes an extensive study of Cu-Azurin variants (K122Q and K122S). We use FCS to study the ET kinetics between the dye and the copper center in copper azurin variants. Our first strategy was to label the variants with ATTO655 and characterize the products of the labeling reactions between the label ATTO655 and the blue copper azurin and then extend our investigation into the properties of a specific labeled species under redox conditions using FCS. The analysis reveals that intramolecular photoinduced electron transfer (PET) can reach the sub-millisecond time scale depending on the position of the Cu-label on the azurin surface. Finally, the distance dependences of the FRET and PET rates on the Cu-label distance are compared. At the end, a general conclusion is presented, and the perspectives are discussed.



## References

- (1) Holm, R. H.; Kennepohl, P.; Solomon, E. I. Structural and Functional Aspects of Metal Sites in Biology. *Chem. Rev.* **1996**, *96*, 2239–2314.
- (2) Thomson, A. J.; Gray, H. B. Bio-inorganic chemistry. *Curr. Opin. Chem. Biol.* **1998**, *2*, 155–158.
- (3) Gilardi, G.; Fantuzzi, a; Sadeghi, S. J. Engineering and design in the bioelectrochemistry of metalloproteins. *Curr. Opin. Struct. Biol.* **2001**, *11*, 491–9.
- (4) Zhang, J.; Chi, Q.; Hansen, A. G.; Jensen, P. S.; Salvatore, P.; Ulstrup, J. Interfacial electrochemical electron transfer in biology - towards the level of the single molecule. *FEBS Lett.* **2012**, *586*, 526–35.
- (5) Schuler, B.; Eaton, W. A. Protein folding studied by single-molecule FRET. *Curr. Opin. Struct. Biol.* **2008**, *18*, 16–26.
- (6) Kuznetsova, S.; Zauner, G.; Aartsma, T. J.; Engelkamp, H.; Hatzakis, N.; Rowan, A. E.; Nolte, R. J. M.; Christianen, P. C. M.; Canters, G. W. The enzyme mechanism of nitrite reductase studied at single-molecule level. *Proc. Natl. Acad. Sci. U. S. A.* **2008**, *105*, 3250–3255.
- (7) Elmalk, A. T.; Salverda, J. M.; Tabares, L. C.; Canters, G. W.; Aartsma, T. J. Probing redox proteins on a gold surface by single molecule fluorescence spectroscopy. *J. Chem. Phys.* **2012**, *136*, 235101.
- (8) Chen, P.; Andoy, N. M. Single-molecule fluorescence studies from a bioinorganic perspective. *Inorganica Chim. Acta* **2008**, *361*, 809–819.
- (9) Wang, Q.; Goldsmith, R. H.; Jiang, Y.; Bockenbauer, S. D.; Moerner, W. E. Probing single biomolecules in solution using the anti-Brownian electrokinetic (ABEL) trap. *Acc. Chem. Res.* **2012**, *45*, 1955–64.
- (10) Mollova, E. T. Single-molecule fluorescence of nucleic acids. *Curr. Opin. Chem. Biol.* **2002**, *6*, 823–828.
- (11) Solomon, E. I.; Sundaram, U. M.; Machonkin, T. E. Multicopper Oxidases and Oxygenases. *Chem. Rev.* **1996**, *96*, 2563–2606.
- (12) Solomon, E. I. Electronic structures of active sites in copper proteins: Contributions to reactivity. *J. Inorg. Biochem.* **1993**, *51*, 450.
- (13) Holwerda, R. a; Wherland, S.; Gray, H. B. Electron transfer reactions of copper proteins. *Annu. Rev. Biophys. Bioeng.* **1976**, *5*, 363–396.
- (14) Pérez-Henarejos SA, Alcaraz LA, D. A. Blue Copper Proteins: A rigid machine for efficient electron transfer, a flexible device for metal uptake. *Arch. Biochem. Bophysics* **2015**, *584*, 134–148.
- (15) Klinman, J. P. Mechanisms whereby mononuclear copper proteins functionalize organic substrates. *Chem. Rev.* **1996**, *96*, 2541–2562.
- (16) Lewis, E. a.; Tolman, W. B. Reactivity of Dioxygen-Copper Systems. *Chem. Rev.* **2004**,

104, 1047–1076.

- (17) Fillion, L. 3.2 A structure of the copper containing oxygen carrying protein Panulirus interruptus haemocyanine. *Nature* **1984**, *309*, 23–29.
- (18) Hellman, N. E.; Gitlin, J. D. Ceruloplasmin metabolism and function. *Annu. Rev. Nutr.* **2002**, *22*, 439–458.
- (19) Paumann, M.; Lubura, B.; Regelsberger, G.; Feichtinger, M.; Köllensberger, G.; Jakopitsch, C.; Furtmüller, P. G.; Peschek, G. A.; Obinger, C. Soluble CuA Domain of Cyanobacterial Cytochrome c Oxidase. *J. Biol. Chem.* **2004**, *279*, 10293–10303.
- (20) Lappalainen, P.; Aasa, R.; Malmström, B. G.; Saraste, M. Soluble CuA-binding domain from the Paracoccus cytochrome c oxidase. *J. Biol. Chem.* **1993**, *268*, 26416–26421.
- (21) Fee, J. a; Choc, M. G.; Findling, K. L.; Lorence, R.; Yoshida, T. Properties of a copper-containing cytochrome c<sub>1</sub>aa<sub>3</sub> complex: a terminal oxidase of the extreme thermophile *Thermus thermophilus* HB8. *Proc. Natl. Acad. Sci. U. S. A.* **1980**, *77*, 147–151.
- (22) Lancaster, K. M.; Debeer, S.; Yokoyama, K.; Richards, J. H.; Gray, H. B. Type Zero Copper proteins. *NIH Public Access* **2010**, *1*, 711–715.
- (23) Kolczak, U., Dennison, C., Messerschmidt, A., and Canters, G. W. *Handbook of Metalloproteins*; Messerschmidt, A., Huber, R., Poulos, T. L., and Wieghardt, K., Ed.; John Wiley & Sons, Ltd: Chichester, 2001.
- (24) Yang, D. S.; Miao, X. D.; Ye, Z. M.; Feng, J.; Xu, R. Z.; Huang, X.; Ge, F. F. Bacterial redox protein azurin induce apoptosis in human osteosarcoma U2OS cells. *Pharmacol. Res.* **2005**, *52*, 413–421.
- (25) Yamada, T.; Goto, M.; Punj, V.; Zaborina, O.; Chen, M. L.; Kimbara, K.; Majumdar, D.; Cunningham, E.; Das Gupta, T. K.; Chakrabarty, A. M. Bacterial redox protein azurin, tumor suppressor protein p53, and regression of cancer. *Proc. Natl. Acad. Sci. U. S. A.* **2002**, *99*, 14098–103.
- (26) Ananda M Chakrabartya Bacterial azurin in potential cancer therapy. *Cell Cycle* **2016**.
- (27) Yamada, T.; Goto, M.; Punj, V.; Zaborina, O.; Kimbara, K.; Das Gupta, T. K.; Chakrabarty, a. M. The bacterial redox protein azurin induces apoptosis in J774 macrophages through complex formation and stabilization of the tumor suppressor protein p53. *Infect. Immun.* **2002**, *70*, 7054–7062.
- (28) Yamada, T.; Hiraoka, Y.; Ikehata, M.; Kimbara, K.; Avner, B. S.; Das Gupta, T. K.; Chakrabarty, A. M. Apoptosis or growth arrest: Modulation of tumor suppressor p53's specificity by bacterial redox protein azurin. *Proc. Natl. Acad. Sci. U. S. A.* **2004**, *101*, 4770–4775.
- (29) Shleev, S.; Wetterö, J.; Magnusson, K. E.; Ruzgas, T. Electrochemical characterization and application of azurin-modified gold electrodes for detection of superoxide. *Biosens. Bioelectron.* **2006**, *22*, 213–219.
- (30) Adman, E. T. and Jensen, L. H. Structural Features of Azurin at 2.7 Å Resolution. *Isr. J. Chem.* **1981**, *21*, 8–12.

- (31) Nar, H.; Messerschmidt, a.; Van De Kamp, M.; Canters, G. W.; Huber, R. Crystal structure analysis of oxidized *Pseudomonas aeruginosa* azurin at pH 5.5 and pH 9.0. A pH-induced conformational transition involves a peptide bond flip. *J. Mol. Biol.* **1991**, *221*, 765–772.
- (32) Nar, H.; Messerschmidt, A.; Huber, R.; Van De Kamp, M.; Canters, G. W. Crystal structure analysis of oxidized *Pseudomonas aeruginosa* azurin at pH 5.5 and pH 9.0. A pH-induced conformational transition involves a peptide bond flip. *J. Mol. Biol.* **1991**, *221*, 765–772.
- (33) Engeseth, H. R.; McMillin, D. R. Studies of thermally induced denaturation of azurin and azurin derivatives by differential scanning calorimetry: evidence for copper selectivity. *Biochemistry* **1986**, *25*, 2448–2455.
- (34) Leckner, J.; Bonander, N.; Wittung-Stafshede, P.; Malmström, B. G.; Karlsson, B. G. The effect of the metal ion on the folding energetics of azurin: A comparison of the native, zinc and apoprotein. *Biochim. Biophys. Acta - Protein Struct. Mol. Enzymol.* **1997**, *1342*, 19–27.
- (35) Carmelo Rosa, Danilo Milardi, Domenico Grasso, Rita Guzzi, L. S. Thermodynamics of the thermal unfolding of azurin. *J. Phys. Chem.* **1995**, *99*, 14864–14870.
- (36) Palm-Espling, M. E.; Niemiec, M. S.; Wittung-Stafshede, P. Role of metal in folding and stability of copper proteins in vitro. *Biochim. Biophys. Acta - Mol. Cell Res.* **2012**, *1823*, 1594–1603.
- (37) Leckner, J. Folding and structure of azurin - The influence of a metal. *Thesis-Chalmers Univ. Technol.* **2001**.
- (38) Pozdnyakova, I.; Guidry, J.; Wittung-Stafshede, P. Studies of *Pseudomonas aeruginosa* azurin mutants: cavities in beta-barrel do not affect refolding speed. *Biophys. J.* **2002**, *82*, 2645–2651.
- (39) Dennison, C. Investigating the structure and function of cupredoxins. *Coord. Chem. Rev.* **2005**, *249*, 3025–3054.
- (40) Gray, H. B.; Malmström, B. G.; Williams, R. J. Copper coordination in blue proteins. *J. Biol. Inorg. Chem. JBIC a Publ. Soc. Biol. Inorg. Chem.* **2000**, *5*, 551–559.
- (41) Lowery, M.; Solomon, E. Axial ligand bonding in blue copper proteins. *Inorganica Chim. Acta* **1992**, *200*, 233–243.
- (42) Solomon, E.; Hare, J. Spectroscopic studies of stellacyanin, plastocyanin, and azurin. Electronic structure of the blue copper sites. *J. Am. Chem. Soc.* **1980**, *102*, 168–178.
- (43) Schmauder, R.; Alagaratnam, S.; Chan, C.; Schmidt, T.; Canters, G. W.; Aartsma, T. J. Sensitive detection of the redox state of copper proteins using fluorescence. *J. Biol. Inorg. Chem.* **2005**, *10*, 683–687.
- (44) Kuznetsova, S.; Zauner, G.; Schmauder, R.; Mayboroda, O. A.; Deelder, A. M.; Aartsma, T. J.; Canters, G. W. A Förster-resonance-energy transfer-based method for fluorescence detection of the protein redox state. *Anal. Biochem.* **2006**, *350*, 52–60.

- (45) Kamp, M. Van De; Floris, R. Site-directed mutagenesis reveals that the hydrophobic patch of azurin mediates electron transfer. *J. Am. Chem. Soc.* **1990**, *112*, 907–908.
- (46) Van de Kamp M1, Canters GW, Andrew CR, Sanders-Loehr J, Bender CJ, P. J. Effect of lysine ionization on the structure and electrochemical behaviour of the Met44-->Lys mutant of the blue-copper protein azurin from *Pseudomonas aeruginosa*. *Eur. J. Biochem.* **1993**, *218*, 229–238.
- (47) van de Kamp, M.; Canters, G. W.; Wijmenga, S. S.; Lommen, A.; Hilbers, C. W.; Nar, H.; Messerschmidt, A.; Huber, R. Complete sequential <sup>1</sup>H and <sup>15</sup>N nuclear magnetic resonance assignments and solution secondary structure of the blue copper protein azurin from *Pseudomonas aeruginosa*. *Biochemistry* **1992**, *31*, 10194–10207.
- (48) Farver, O.; Skov, L. K.; Van De Kamp, M.; Canters, G. W.; Pecht, I. The effect of driving force on intramolecular electron transfer in proteins. Studies on single-site mutated azurins. *Eur. J. Biochem.* **1992**, *210*, 399–403.
- (49) Stryer, L.; Haugland, R. P. Energy transfer: a spectroscopic ruler. *Proc. Natl. Acad. Sci. U. S. A.* **1967**, *58*, 719–726.
- (50) Lakowicz, J. R. *Principles of Fluorescence Spectroscopy*; 2006.
- (51) Shimomura, O., Saiga, Y., and Johnson, F. H. Fluorescence Energy transfer. *Fed. Proc.* **1962**, 401–03.
- (52) Zauner, G.; Lonardi, E.; Bubacco, L.; Aartsma, T. J.; Canters, G. W.; Tepper, A. W. J. W. Tryptophan-to-dye fluorescence energy transfer applied to oxygen sensing by using type-3 copper proteins. *Chem. - A Eur. J.* **2007**, *13*, 7085–7090.
- (53) Chalfie, M.; Tu, Y.; Euskirchen, G.; Ward, W. W.; Prasher, D. C. Green fluorescent protein as a marker for gene expression. *Science* **1994**, *263*, 802–805.
- (54) Ernst, L. a; Gupta, R. K.; Mujumdar, R. B.; Waggoner, a S. Cyanine dye labeling reagents for sulfhydryl groups. *Cytometry* **1989**, *10*, 3–10.
- (55) Ruan, G.; Winter, J. O. Alternating-color quantum dot nanocomposites for particle tracking. *Nano Lett.* **2011**, *11*, 941–945.
- (56) Panchuk-Voloshina, N.; Haugland, R. P.; Bishop-Stewart, J.; Bhalgat, M. K.; Millard, P. J.; Mao, F.; Leung, W. Y.; Haugland, R. P. Alexa dyes, a series of new fluorescent dyes that yield exceptionally bright, photostable conjugates. *J. Histochem. Cytochem.* **1999**, *47*, 1179–1188.
- (57) Sauer, M.; Han, K. T.; Müller, R.; Nord, S.; Schulz, a.; Seeger, S.; Wolfrum, J.; Arden-Jacob, J.; Deltau, G.; Marx, N. J.; Zander, C.; Drexhage, K. H. New fluorescent dyes in the red region for biodiagnostics. *J. Fluoresc.* **1995**, *5*, 247–261.
- (58) Brinkley, M. A brief survey of methods for preparing protein conjugates with dyes, haptens, and cross-linking reagents. *Bioconjug. Chem.* **1992**, *3*, 2–13.
- (59) Mujumdar, R. B.; Ernst, L. a; Mujumdar, S. R.; Lewis, C. J.; Waggoner, a S. Cyanine dye labeling reagents: sulfoindocyanine succinimidyl esters. *Bioconjug. Chem.* **1993**, *4*, 105–111.

- (60) Buschmann, V.; Weston, K. D.; Sauer, M. Spectroscopic study and evaluation of red-absorbing fluorescent dyes. *Bioconjug. Chem.* **2003**, *14*, 195–204.
- (61) Lina F. Bernal-Perez, Laszlo Prokai, Y. R. Selective N-terminal fluorescent labeling of proteins using 4-chloro-7-nitrobenzofurazan: A method to distinguish protein N-terminal acetylation. *Anal. Biochem.* **2012**, *428*, 13–15.
- (62) Chan, A. O.-Y.; Ho, C.; Chong, H.; Leung, Y.-C.; Huang, J.; Wong, M.; Che, C. Modification of N-terminal  $\alpha$ -amino groups of peptides and proteins using ketenes. *J. Am. Chem. Soc.* **2012**, *134*, 2589–98.
- (63) Williamson, D. J.; Fascione, M. A.; Webb, M. E.; Turnbull, W. B. Efficient N-Terminal Labeling of Proteins by Use of Sortase. *Angew. Chemie Int. Ed.* **2012**, *51*, 9377–9380.
- (64) Förster, T.; Energiewanderung, Z.; Von, F. Zwischenmolekulare Energiewanderung und Fluoreszenz. *Ann. Phys.* **1939**, *248*, 55–75.
- (65) Clegg, R. M. Fluorescence resonance energy transfer. *Curr. Opin. Biotechnol.* **1995**, *6*, 103–110.
- (66) Steinberg, I. Z. Long-range nonradiative transfer of electronic excitation energy in proteins and polypeptides. *Annu. Rev. Biochem.* **1971**, *40*, 83–114.
- (67) Schmauder, R.; Alagaratnam, S.; Chan, C.; Schmidt, T.; Canters, G. W.; Aartsma, T. J. Sensitive detection of the redox state of copper proteins using fluorescence. *J. Biol. Inorg. Chem.* **2005**, *10*, 683–7.
- (68) Schmauder, R.; Librizzi, F.; Canters, G. W.; Schmidt, T.; Aartsma, T. J. The oxidation state of a protein observed molecule-by-molecule. *Chemphyschem* **2005**, *6*, 1381–6.
- (69) Gustiananda, M.; Andreoni, A.; Tabares, L. C.; Tepper, A. W. J. W.; Fortunato, L.; Aartsma, T. J.; Canters, G. W. Sensitive detection of histamine using fluorescently labeled oxido-reductases. *Biosens. Bioelectron.* **2012**, *31*, 419–25.
- (70) Edman, L.; Mets, U.; Rigler, R. Conformational transitions monitored for single molecules in solution. *Proc. Natl. Acad. Sci. U. S. A.* **1996**, *93*, 6710–6715.
- (71) Xie, X. S. Single-Molecule Approach to Enzymology. *Single Mol.* **2001**, *2*, 229–236.
- (72) Eggeling, C.; Widengren, J.; Brand, L.; Schaffer, J.; Felekyan, S.; Seidel, C. A. M. Analysis of photobleaching in single-molecule multicolor excitation and Förster resonance energy transfer measurements. *J. Phys. Chem. A* **2006**, *110*, 2979–95.
- (73) Dittrich, P.; Schwille, P. Photobleaching and stabilization of fluorophores used for single-molecule analysis with one- and two-photon excitation. *Appl. Phys. B Lasers Opt.* **2001**, *73*, 829–837.
- (74) Lu, H. P.; Xie, X. S. Single-Molecule Kinetics of Interfacial Electron Transfer. **1997**, *5647*, 2753–2757.
- (75) Cordes, T.; Maiser, A.; Steinhauer, C.; Schermelleh, L.; Tinnefeld, P. Mechanisms and advancement of antifading agents for fluorescence microscopy and single-molecule spectroscopy. *Phys. Chem. Chem. Phys.* **2011**, *13*, 6699–709.

- (76) Bustamante, C. In singulo biochemistry: when less is more. *Annu. Rev. Biochem.* **2008**, *77*, 45–50.
- (77) Piehler, J. New methodologies for measuring protein interactions in vivo and in vitro. *Curr. Opin. Struct. Biol.* **2005**, *15*, 4–14.
- (78) Ha, T.; Selvin, P. R. The New Era of Biology In Singulo. *Cold Spring Harb. Lab. Press* **2008**, 1–36.
- (79) Ries, J.; Schwille, P. Fluorescence correlation spectroscopy. *BioEssays* **2012**, *34*, 361–368.
- (80) Elson, E. L. Fluorescence correlation spectroscopy: Past, present, future. *Biophys. J.* **2011**, *101*, 2855–2870.
- (81) Bacia, K.; Kim, S. A.; Schwille, P. Fluorescence cross-correlation spectroscopy in living cells. *Nat. Methods* **2006**, *3*, 83–89.
- (82) Hess, S. T.; Huang, S.; Heikal, A. A.; Webb, W. W. Biological and chemical applications of fluorescence correlation spectroscopy: A review. *Biochemistry* **2002**, *41*, 697–705.
- (83) Chiantia, S.; Ries, J.; Schwille, P. Fluorescence correlation spectroscopy in membrane structure elucidation. *Biochim. Biophys. Acta* **2009**, *1788*, 225–233.
- (84) Widengren, J.; Rigler, R.; Mets, Ü. Triplet-state monitoring by fluorescence correlation spectroscopy. *J. Fluoresc.* **1994**, *4*, 255–258.
- (85) Ries, J.; Schwille, P. Fluorescence correlation spectroscopy. *Bioessays* **2012**, *34*, 361–8.
- (86) Kapusta, P.; Wahl, M.; Benda, A.; Hof, M.; Enderlein, J. FLCS - Fluorescence lifetime correlation spectroscopy. *SymPhoTime* **2007**, *17*, 43–8.
- (87) Rüttinger, S.; Kapusta, P.; Patting, M.; Wahl, M.; Macdonald, R. On the resolution capabilities and limits of fluorescence lifetime correlation spectroscopy (FLCS) measurements. *J. Fluoresc.* **2010**, *20*, 105–14.
- (88) Kapusta, P.; Wahl, M.; Benda, A.; Hof, M.; Enderlein, J. Fluorescence lifetime correlation spectroscopy. *J. Fluoresc.* **2007**, *17*, 43–8.
- (89) Artés, J. M.; López-Martínez, M.; Díez-Pérez, I.; Sanz, F.; Gorostiza, P. Nanoscale charge transfer in redox proteins and DNA: Towards biomolecular electronics. *Electrochim. Acta* **2014**, *140*, 83–95.
- (90) Aviram, A.; Ratner, M. A. Molecular rectifiers. *Chem. Phys. Lett.* **1974**, *29*, 277–283.
- (91) Kuznetsov, a. M.; Ulstrup, J. Theory of electron transfer at electrified interfaces. *Electrochim. Acta* **2000**, *45*, 2339–2361.
- (92) Farver, O.; Pecht, I. Electron transfer in blue copper proteins. *Coord. Chem. Rev.* **2011**, *255*, 757–773.
- (93) Canters, G. W.; Gilardi, G. Engineering type 1 copper sites in proteins. *FEBS Lett* **1993**, *325*, 39–48.
- (94) Marcus, R. A.; Sutin, N. Electron transfers in chemistry and biology. *Biochim. Biophys.*

- Acta - Rev. Bioenerg.* **1985**, *811*, 265–322.
- (95) Marcus, R. A. Electron Transfer Reactions in Chemistry: Theory and Experiment. *Angew. Chemie Int. Ed.* **1993**, *32*, 1111–1121.
- (96) Winkler, J. R.; Gray, H. B. Long-range electron tunneling. *J. Am. Chem. Soc.* **2014**, *136*, 2930–2939.
- (97) C. C. Moser, C. C. Page, X. Chen, P. L. D. Biological electron tunneling through native protein media. *J. Biol. Inorg. Chem.* **1997**, *2*, 393–398.
- (98) Winkler, J. R.; Gray, H. B. Electron tunneling in proteins: Role of the intervening medium. *J. Biol. Inorg. Chem.* **1997**, *2*, 399–404.
- (99) Beratan, D. N.; Betts, J. N.; Onuchic, J. N. Protein electron transfer rates set by the bridging secondary and tertiary structure. *Science (80-. )*. **1991**, *252*, 1285–1288.
- (100) Beratan, D. N.; Onuchic, J. N.; Winkler, J. R.; Gray, H. B. Electron-tunneling pathways in proteins. *Science* **1992**, *258*, 1740–1741.
- (101) Page, C. C.; Moser, C. C.; Chen, X.; Dutton, P. L. Natural engineering principles of electron tunnelling in biological oxidation-reduction. *Nature* **1999**, *402*, 47–52.
- (102) Moser, C. C.; Keske, J. M.; Warncke, K.; Farid, R. S.; Dutton, P. L. Nature of biological electron transfer. *Nature* **1992**, *355*, 796–802.
- (103) Gray, H. B.; Winkler, J. R. Long-range electron transfer. *Proc. Natl. Acad. Sci. U. S. A.* **2005**, *102*, 3534–3539.
- (104) Paola Ceroni and Vincenzo Balzani Photoinduced Energy and Electron Transfer Processes. In *The Exploration of Supramolecular Systems and Nanostructures by Photochemical Techniques*; 2012; pp. 21–38.
- (105) Gray, H. B.; Winkler, J. R. Long-range electron transfer. *Proc. Natl. Acad. Sci. U. S. A.* **2005**, *102*, 3534–9.
- (106) Gray, H. B.; Winkler, J. R. Electron flow through metalloproteins. *Biochim. Biophys. Acta* **2010**, *1797*, 1563–72.
- (107) Chi, Q.; Zhang, J.; Jensen, P. S.; Christensen, H. E. M.; Ulstrup, J. Long-range interfacial electron transfer of metalloproteins based on molecular wiring assemblies. *Faraday Discuss.* **2006**, *131*, 181–195; discussion 205–220.
- (108) McLendon, G.; Hake, R. Interprotein electron transfer. *Chem. Rev.* **1992**, *92*, 481–490.

## **Chapter 2**

# **Calibration of experimental setup, bimolecular reactions and photoinduced electron-transfer reactions**



**Abstract**

The calibration of the instrumental setup required for fluorescence correlation measurements is reported. Calibration was performed using a commercially available organic dye ATTO655 and recording its fluorescence intensities (autocorrelation functions) over time having different concentrations. The instrumental factor “ $k$ ” obtained through the calibration measurements has been used for the fitting of the autocorrelation curves (ACF) of labeled Zinc and Copper azurin samples in Chapter 3, 4 and 5. This chapter also includes a general discussion of bimolecular interactions and photoinduced electron transfer reactions in proteins.

## 2.1 Introduction

When diffusion was first analyzed by Stokes and Einstein<sup>(1)(2)(3)</sup>, its importance soon gained recognition in the scientific world and the concept of diffusional motion found use in the fields of fluid mechanics, biophysics, soft-condensed-matter physics. Since then, a variety of experimental methods has been developed to monitor particles in solution. Fluorescence correlation spectroscopy (FCS) was introduced in the 1970s as a technique to study diffusion<sup>(4)</sup>. In the beginning, the main drawback with this method was the large observation volume and low signal to noise ratio. Later on, with the implementation of confocal microscopy and advanced hard- and software, it became a powerful technique for biological applications<sup>(5)(6)(7)(8)(9)</sup>. In recent years, this technique has been developed further, and FCS became widely applicable from biology and chemistry *in vitro* to the study of molecular motions inside the living cells.

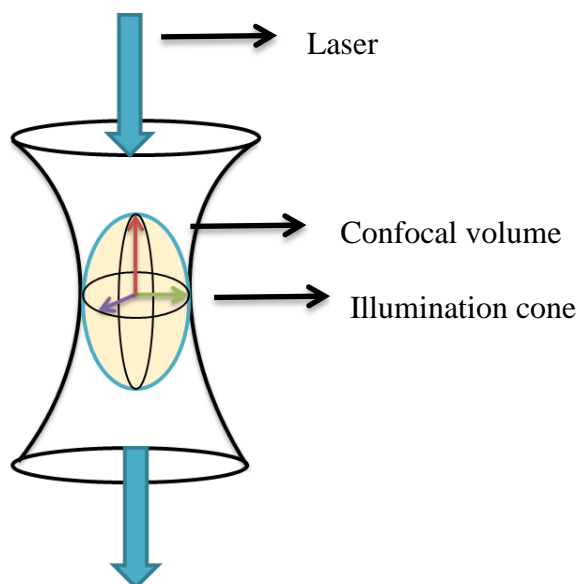


**Figure 2.1:** A cartoon depicting the confocal volume and the illumination cone generated by a tightly focused laser in solution.  $x$ -,  $y$ - and  $z$ -axis of the confocal volume have been represented by green, violet and red arrows. A three-dimensional parameter  $k$  for the instrument is expressed as the ratio of the length of  $z$ -axis to that of the axes in the  $xy$ -plane.

As discussed in the previous chapter, the principle of FCS is to measure fluorescence intensity fluctuations caused by labeled molecules diffusing in and out of the confocal volume of a fluorescence microscope. A schematic diagram of the confocal volume is displayed in Figure 2.1. Fluorescence fluctuations are correlated over time, and the autocorrelation function  $G(t)$  is

generated.  $G(t)$  decays as the molecules diffuse out of the confocal volume with a characteristic correlation time  $\tau_D$ , which is related to the diffusion coefficient  $D$  of the diffusing molecules. Accurate evaluation of the confocal volume is needed for the correct interpretation of experimental data and the design of an appropriate diffusion model. The three-dimensional parameters  $k$  and  $r_0$  (*vide infra*) describe the geometry of the volume as displayed in Figure 2.1. In a calibration procedure to be described here, a reference dye is used to measure those parameters(10)(11)(12).

ATTO655 is a dye well-suited to calibrate a confocal microscope. It has a strong absorption, high fluorescence quantum yield and high thermal and photostability. It also has good water solubility. The fluorescence excitation range of ATTO655 dye is from 640 - 660 nm. The diffusion coefficient of ATTO655 NHS ester dye has been measured to be  $425 \pm 6 \mu\text{m}^2/\text{s}$  at 295 K(11).

As the diffusion motion of dye molecules is influenced by the properties of the liquid in which the dyes are dissolved, we can observe the reaction dynamics on a time scale between picoseconds and milliseconds depending on the solvent by FCS. The lower limit is defined by the instrument response function while the residence time of the labeled molecules in the confocal volume controls the upper limit. This residence time can be varied by changing the viscosity of the solution, or by linking the molecules to bigger, and thereby slower diffusing particles. In the present thesis, sucrose has been used to increase the viscosity of the medium. In our experiments, the solution conditions were varied from pure water (viscosity  $\sim 1$  cP) to 57.0% (w/w) sucrose (viscosity  $\sim 37.5$  cP) at room temperature (22 °C). This has allowed investigation of inter- as well as intra-molecular dynamics of the azurin-dye conjugate.

We calibrated our FCS setup using pure buffer and a 57.0% (w/w) sucrose solution containing different ATTO655 dye concentrations. The main goal of this work was to precisely determine the three-dimensional parameters ( $k$  and  $r_0$ ) of the experimental setup. The results were used in our FCS measurements discussed in the next chapters.

## **2.2 Materials and Methods**

### **2.2.1 Reagents and Samples**

Unless stated otherwise, all the reagents were purchased from Sigma-Aldrich (Sigma-Aldrich Corp., St. Louis, USA) and used as received. The fluorescent label ATTO655 N-

hydroxysuccinimidyl ester (NHS-ester: Product no. AD-655-31) was purchased from ATTO-TEC GmbH (Siegen, Germany) as a powder and dissolved in water-free DMSO before use, as suggested by the supplier. Sucrose was purchased from Sigma-Aldrich (Product no. 84100-microbiology grade). Chemical structure of ATTO655 has been shown in Fig. 1.4A in Chapter 1. It has been reported that ATTO655 has a tendency to dimerize which could result in a reduction of the diffusion coefficient at high concentrations(13). Hence, most of the diffusion measurements were performed on samples in the concentration ranges of from pM to nM. Samples for the FCS calibration measurements with different ATTO655 concentrations (100 pM to 10 nM) were prepared by dissolving small amounts of the dye in 20 mM HEPES pH 7.0 buffer or in 57% (w/w) sucrose containing 0.05% Tween-20 (a detergent polysorbate) to prevent any surface adhesion or aggregation.

### **2.2.2 Preparation of sucrose solution**

A 75% (w/v) stock solution of sucrose was prepared by adding 10 ml of a 500 mM HEPES pH 7.0 buffer solution to 37.5 g of high purity (purity >99.5%) D(+)-saccharose powder. The volume was adjusted to 50 ml by adding Milli-Q water or buffer. The solution was thoroughly sonicated to achieve complete dissolution of the sucrose and degassed to avoid the presence of air bubbles. The precise concentration of the solution was checked by measuring the refractive index  $n_r$ , which was determined at 22°C with a Zeiss Abbe refractometer (Carl Zeiss, Germany). The refractive index of several preparations of the stock solution was found to be 1.445 ( $\pm 0.002$ ) corresponding with a content of 61.4% sucrose (w/w) and a viscosity of 75 cP(14). Table 2.1 shows the variation of refractive indexes of the aqueous sucrose solutions prepared for FCS measurements as a function of sucrose concentration.

Amount of sucrose stock solution ( $\mu\text{l}$ )	Amount of Buffer ( $\mu\text{l}$ )	Refractive Index ( $n_r$ )(a)	Composition (%w/w)(b)	Viscosity (cP) (c)
400	0	1.445 $\pm$ 0.002	61.4	75.0
372	28	1.435 $\pm$ 0.002	57.0	37.5
320	80	1.415 $\pm$ 0.002	47.6	12.1
267	133	1.393 $\pm$ 0.002	36.5	4.90
187	213	1.382 $\pm$ 0.002	30.5	3.25
91	309	1.367 $\pm$ 0.002	21.9	2.12
42	358	1.347 $\pm$ 0.002	9.4	1.30
0	400	1.330 $\pm$ 0.002	0	1.00

**Table 2.1:** Viscosity and refractive indexes for the sucrose solutions. (a) Data obtained using Zeiss Abbe refractometer (Carl Zeiss, Germany), (b) Composition of the sucrose solutions according to the tables in the CRC Handbook of Chemistry and Physics relating composition to refractive index (check ref(16)), (c) Viscosities of the sucrose solutions according to the tables in the CRC Handbook of Chemistry and Physics relating composition to viscosity (ref(16) for details).

### 2.2.3 Sample preparation for FCS experiments

For each measurement, a fresh sample solution was prepared by mixing 372  $\mu\text{l}$  of the sucrose stock solution (75 % w/v) with 4  $\mu\text{l}$  of bovine serum albumin (BSA) stock solution (10 mg/ml), 4  $\mu\text{l}$  of a 100 nM azurin stock solution and between 10 and 20  $\mu\text{l}$  of 2 or 20 mM freshly prepared stock solutions of ascorbate or hexacyanoferrate(II) or (III). The sample was adjusted to 400  $\mu\text{l}$  by admixture ( $\leq 20 \mu\text{l}$ ) of 100 mM HEPES buffer, pH 7.0. The precise concentration of the sample solution was checked by measuring the refractive index  $n_r$  at 22°C with a Zeiss Abbe refractometer and the sucrose content of the samples was found to be 57.0% (w/w) (i.e. 70% w/v), corresponding to a viscosity of 37.5 cP at 22°C. The final sample concentration of labeled azurin was around 0.4-0.8 nM (for azurin expression and purification, see Chapter 3 for details). For calibration measurements of the instrument, samples were prepared containing only ATTO655 dye (no azurin) without redox agents.

### 2.2.4 FCS setup

The FCS calibration measurements were carried out at room temperature on a home-built confocal setup (Fig. 2.2B) equipped with an Axiovert 100 inverted microscope (Carl Zeiss, Germany) and a high numerical aperture (NA) water immersion objective (60x water, NA 1.2,

Olympus UPLSAPO). Excitation at 639 nm was provided by a pulsed diode laser head (LDH-P-C-635-B, PicoQuant GmbH, Berlin, Germany) driven by a picosecond laser driver (LDH-800-B, PicoQuant GmbH, Berlin, Germany). The fluorescence from the sample was collected by the water objective and spatially filtered using a 50  $\mu\text{m}$  pinhole. The fluorescence from the dye was passed through an emission filter (HQ 675/50m, Chroma Technology Corp., VT, USA), and focused onto a single-photon avalanche photodiode (SPCM-AQRH 14, Perkin Elmer Inc., USA). The signal from the diode was read out by using a TimeHarp200 counting board (PicoQuant GmbH, Berlin, Germany). The power used for the calibration and for other FCS measurements amounted to 20  $\mu\text{W}$ , as measured after the objective, corresponding to a specific power of  $\sim 4.3$   $\text{kW}/\text{cm}^2$  at the sample. For both, ATTO655 in pure buffer and ATTO655 in sucrose solution, five FCS experiments were performed. The dye concentrations were 100 pM, 250 pM, 500 pM, 1 nM, 2 nM.

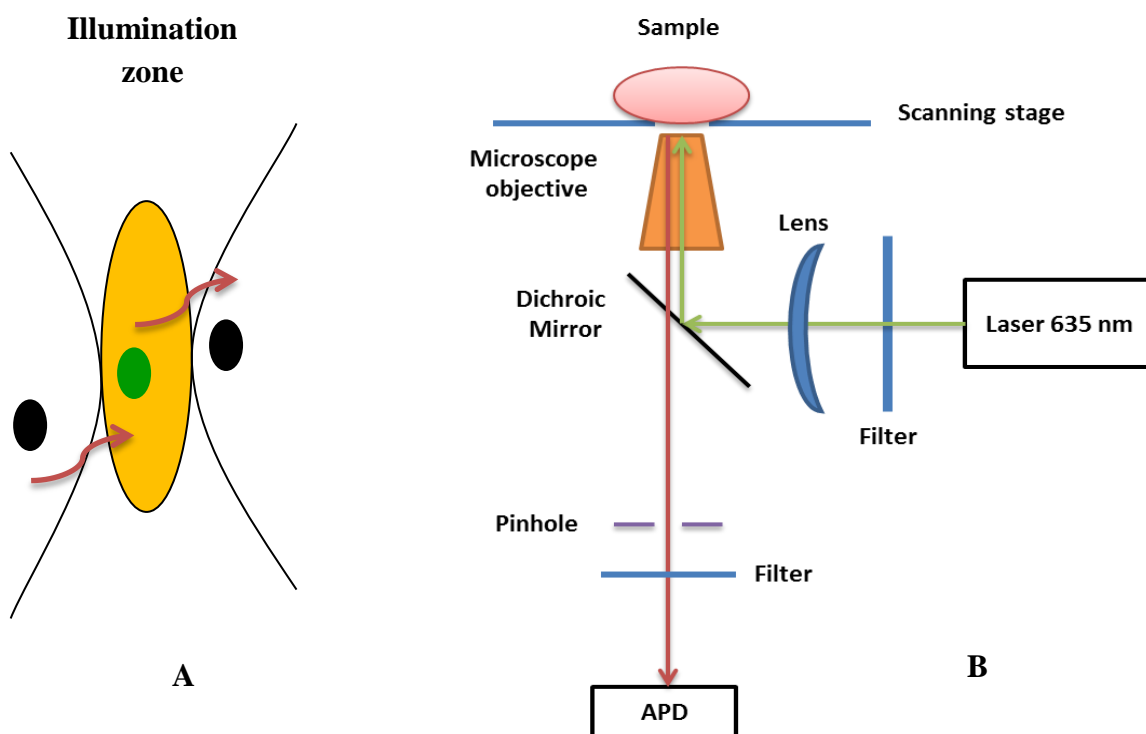


**Figure 2.2:** (A) Representation of the effective volume (yellow) where molecules move freely in the solution; the black dot represents a labeled molecule and it turns fluorescent (green) when it is in the effective volume, (B) Scheme of the confocal setup used for the measurements.

### ***2.2.5 Fluorescence Lifetime Correlation Spectroscopy (FLCS) data acquisition***

For the acquisition of FLCS data, the sample was deposited on a cleaned glass slide and covered with the cap of a polypropylene test tube to avoid evaporation of the solvent during the measurements. A new cap was used for each measurement to avoid sample cross-contamination. For each experimental condition, time traces were recorded for durations varying from 5 to 10 minutes, depending on the conditions of the experiment. The raw data were stored as time-tagged time-resolved (t3r) data files and subsequently elaborated using the SymPhoTime software package. To eliminate the detector afterpulsing and other sources of noise due to detector imperfections, the single photon arrival time data were filtered as described in reference (15). For this, the internal dedicated routine of the SymPhoTime software package was used. Briefly, after acquisition of the data, the time correlation single-photon counting (TCSPC) histogram for the measurement was built. After narrowing down the time window of the TCSPS decay, fitting was performed with an exponential function as described in ref. (16). Based on the fitted values the software automatically generated a set of filter functions. The filter functions were subsequently used by the software to select the photons for the calculation of the autocorrelation function. The autocorrelation from the single-photon counting data was calculated using the SymPhoTime software package and the data were analyzed using FCS equation as described in the section 2.3.

### ***2.2.6 Preparation of glass slides***

Round glass coverslips with 0.25 mm thickness (Marienfeld, VWR International) were used for all FCS measurements. They were first cleaned with methanol and then treated with 4.0M sodium hydroxide, each step taking 30 minutes at room temperature. Afterwards, the coverslips were rinsed several times with Milli-Q water and then sonicated in acetone for 15-20 minutes. The coverslips thus prepared were stored in Milli-Q water. A confocal image of a cleaned glass slide is presented in Fig. 2.3. For nano-rod coating, ozone cleaned glass coverslips were prepared using UVO-Cleaner Model 42-220, Jetlight Company Inc., Irvine, California, USA.

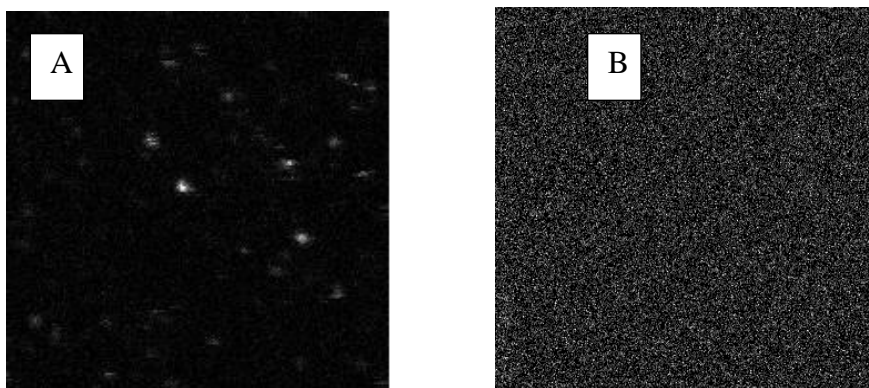


**Figure 2.3:**  $40 \times 40 \mu\text{m}^2$  images taken under confocal fluorescence microscope of a glass slide: (A) before and (B) after cleaning.

### **2.2.7 Preparation of gold nano-rods**

The gold nano-rods were first prepared with the seed-mediated growth method as described in the literature(17). A surfactant called Cetyl-trimethylammonium bromide (CTAB) was added to a suspension of gold nano-rods in the buffer. The excess amount of CTAB was washed out and the rods were dispersed into Milli-Q water. The nano-rods thus prepared, had average dimensions of  $45 \text{ nm} \times 100 \text{ nm}$ . Their longitudinal plasmon resonates around  $640 \text{ nm}$  in water. The nano-rods were spin-coated on a cleaned glass surface using a spin-coater (SpinCoater Model P6700 Series, Specialty Coating System Inc., West Minnesota, Indianapolis, USA) in two spinning steps:  $2000 \text{ rpm}$  for  $30 \text{ sec}$  and  $4000 \text{ rpm}$  for another  $30 \text{ sec}$ .

### **2.3 FCS calibration: results and discussion**

ATTO655 was chosen for labeling purposes since its properties have been thoroughly documented by Sauer, Tinnefeld and others((18)(19)(20)(21)(22) and references therein). This dye is not easily oxidized whereas the reduced form is quickly oxidized back by oxygen. Under aerobic conditions the dye is stable, shows little blinking and is not easily bleached.

#### **2.3.1 Calibration of the probe volume**

For the FCS measurements, a typical sample consists of a dilute water-based solution of fluorescently labeled molecules. A laser beam is focused in the sample with a high numerical aperture lens creating a measurement volume with a diffraction-limited spot (Fig. 2.2A). When



using a dichroic mirror, a micrometer size pinhole, lens and beam splitter, only fluorescence originating from the measurement volume is collected. A typical range of pinhole diameters is 30-100  $\mu\text{m}$ . The pinhole is used to reject the out-of-focus light. The emitted fluorescence is projected onto an avalanche photo diode (APD) and the autocorrelation function (ACF) is generated. Analysis of the ACF gives us information about the time scale of the diffusion ( $\tau_D$ ), the diffusion coefficient ( $D$ ) and the number of molecules  $\langle N \rangle$  in the effective volume.  $\tau_D$  depends on the size and shape of the measurement volume, referred to as effective volume,  $V_{\text{eff}}$  of the setup. It is necessary to know beforehand the size and shape of the effective volume. Therefore, calibration of the setup is important and it is about determining the size of  $V_{\text{eff}}$ .

For calibration of the effective volume in 20 mM HEPES pH 7.0 buffer and in 57% (w/w) sucrose, it is assumed that the light intensity in the effective volume exhibits a three dimensional Gaussian profile i.e. the intensity of the laser beam is represented by the formula:

$$I = I_0 e^{-2(x^2 + y^2 + \frac{z^2}{k^2})/r^2}$$

where  $I_0$  describes the intensity at the center of the laser beam and  $x$ ,  $y$  and  $z$  represent the three coordinates of the illuminated volume (Fig. 2.1). Thus the confocal volume is an ellipsoid where the ellipse is rotated around the long axis.

The autocorrelation function has the form:

$$G(\tau) = G(0) \cdot \left(1 + \frac{4D\tau}{r_0^2}\right)^{-1} \cdot \left(1 + \frac{4D\tau}{z_0^2}\right)^{-1/2} \quad (2.1)$$

$$= G(0) \cdot \left(1 + \frac{\tau}{\tau_D}\right)^{-1} \cdot \left(1 + \left(\frac{r_0}{z_0}\right)^2 \frac{\tau}{\tau_D}\right)^{-1/2} \quad (2.2)$$

$$= G(0) \cdot \left(1 + \frac{\tau}{\tau_D}\right)^{-1} \cdot \left(1 + \frac{\tau}{k^2 \tau_D}\right)^{-1/2} \quad (2.3)$$

where  $G(\tau)$  is the auto-correlation function,  $D$  is the diffusion coefficient of the molecule of interest,  $\tau_D$  is the residence time of the molecule in the confocal volume and  $r_0$  and  $z_0$  denote the distances from the center of the confocal volume where the intensity has dropped by a factor of  $1/e^2$  in the radial and axial direction, respectively. The diameter of the diffraction limited spot

depends on the wavelength  $\lambda$  of the probing light and the lens-numerical aperture for the measurements.

Single molecule FCS measurements possess some intrinsic limitations. One of the pitfalls is refractive index changes in solutions. It can cause distortions of the effective volume. Such distortions appear in particular polymer solvents e.g. sucrose, glycerol-solution. Creating different models with distorted volume is a hard even impossible task. For FCS analysis, we assumed an ellipsoid shape of the effective volume in 57% w/w sucrose solution similar that in buffer and determined  $V_{eff}$  in 57% w/w sucrose solution. Apart from the refractive index, slight changes in coverslip thickness, pinhole adjustments, laser beam geometry or optical saturation can lead change in the effective volume.

One way to determine the confocal parameters is by plotting  $G(0)$  as a function of the concentration of the dye (Eqn. (2.4)). If the measured signal fluctuations are only due to the diffusion, the amplitude of autocorrelation function equals to the inverse number of the fluorescence molecules present in the effective volume  $V_{eff}$  on average. Using a dilution series of labeled sample, the effective volume can be determined(11),

$$G(0) = \frac{1}{\langle N \rangle} = \frac{1}{c \cdot V_{eff} \cdot N_A} \quad (2.4)$$

where  $\langle N \rangle$  is the average number of particles in the probe volume,  $c$  is the concentration of the dye,  $V_{eff}$  is the effective probe volume, and  $N_A$  is Avogadro's constant  $6.022 \times 10^{23} \text{ mol}^{-1}$ .  $V_{eff}$  is approximated with three-dimensional Gaussian shape function and is larger than the confocal volume(23) by a factor of  $2^{(2/3)}$ .

$$V_{conf} = \left(\frac{\pi}{2}\right)^{3/2} r_0^2 z_0 = \left(\frac{1}{2}\right)^{3/2} V_{eff} \quad (2.5)$$

First the autocorrelation amplitudes of a dilution series of ATTO655 in buffer and sucrose were determined experimentally. Two datasets for FCS curves for buffer and 57% (w/w) sucrose solution have been presented in Fig. 2.4 and Fig. 2.5. The concentrations of dye used were: 2.0, 1.0, 0.5, 0.25, and 0.1 nM. A plot of  $\langle N \rangle$  values versus the dye concentration was obtained (Fig. 2.6). The slope of a linear fit of the data corresponds to  $V_{eff} N_A$  from which the size of the effective volume was calculated (Fig. 2.6). In buffer,  $V_{eff}$  was  $2.3 \pm 0.2 \text{ fL}$  and in 57%

(w/w) sucrose solution it was  $2.9 \pm 0.1$  fL. This approach is model free: it makes no assumptions about the geometry of  $V_{eff}$  or the diffusion model. It only measures the correlation amplitude of a series of samples with known concentrations.

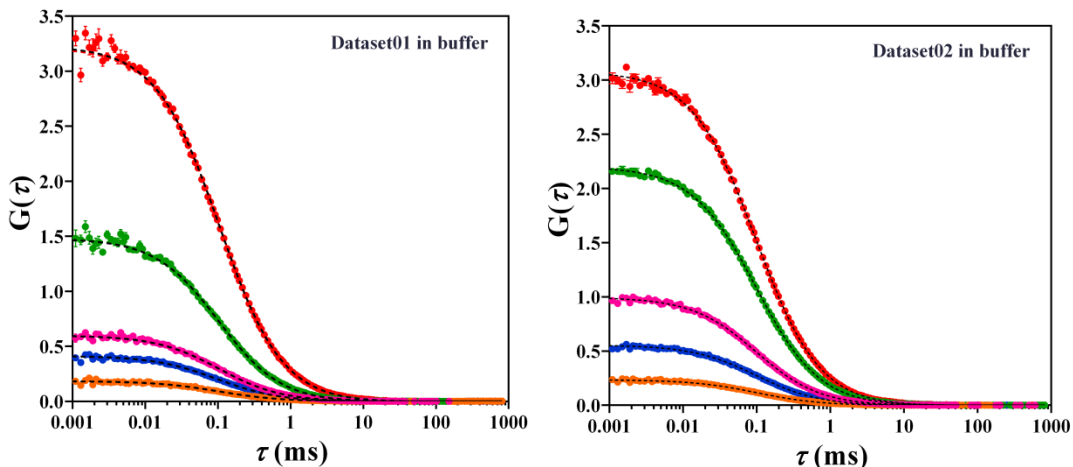


**Figure 2.4:** FCS traces of ATTO655 obtained in the buffer. Two datasets are shown here. The buffer used was 20 mM HEPES pH 7.0 and the concentration of the dye was 2.0 (orange), 1.0 (blue), 0.5 (pink), 0.25 (green), and 0.1 (red) nM. The dots are experimental data points and dashed lines are fits of the data. Error bars denote the standard errors as obtained from the fitting procedure.

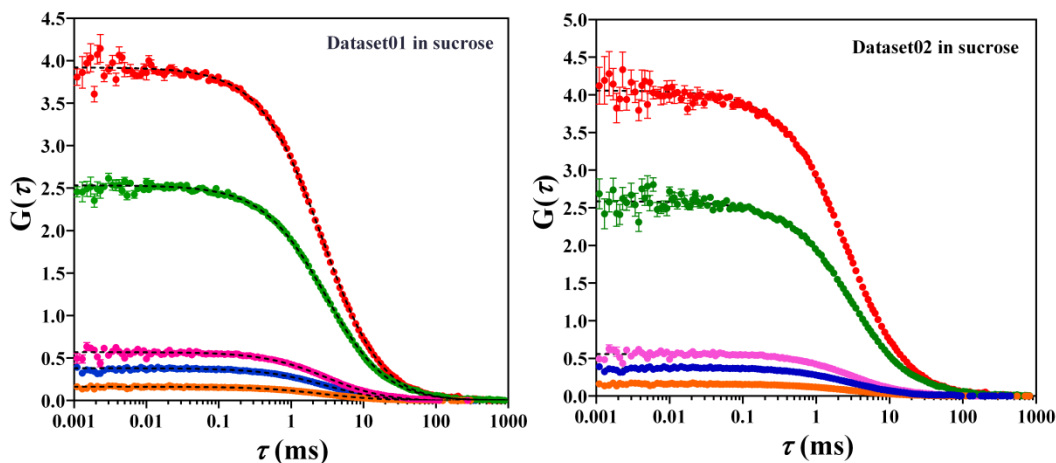


**Figure 2.5:** FCS traces of ATTO655 obtained in 57% (w/w) sucrose solution. Two datasets are shown here. The buffer used was 20 mM HEPES pH 7.0. The concentration of the dye was 2.0 (orange), 1.0 (blue), 0.5 (pink), 0.25 (green), and 0.1 (red) nM. The dots are experimental data points and dashed lines are fits of the data. Error bars denote the standard errors as obtained from the fitting procedure.

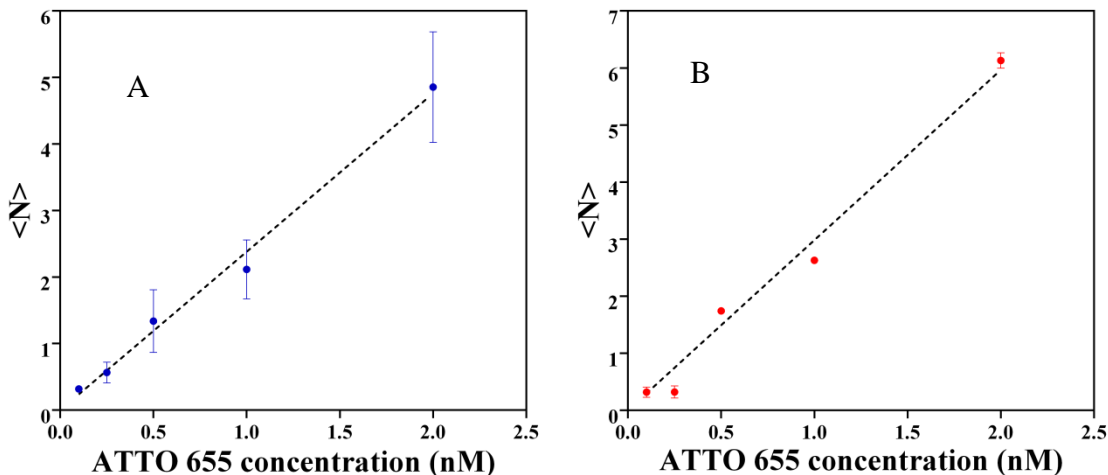


**Figure 2.6:** Plots of  $\langle N \rangle$  as a function of the ATTO655 concentrations in: (A) 20 mM HEPES buffer pH 7.0 and (B) 57% (w/w) sucrose solution. In both, the black dashed lines are linear fits of the data. (Average values of  $\langle N \rangle$  from two datasets for buffer and 57% (w/w) sucrose solution (See Figs. 2.4 and 2.5) have been used to plot)

The other way to determine the probe volume is by fitting the autocorrelation data (Fig. 2.4 and 2.5) with Eqn. 2.3 using a weighted least-square Levenberg-Marquardt method, where the variance of each data point is used as a weighting factor. First, with known diffusion coefficient of ATTO655 in water ( $426\mu\text{m}^2\text{ s}^{-1}$ ), the diffusion coefficient of ATTO655 in 57% w/w sucrose solution was estimated according to the Stokes-Einstein law (see 2.4 section). The diffusion coefficient was found to be  $11.0\mu\text{m}^2\text{ s}^{-1}$ . Next, GraphPad Prism 5 and 6 (GraphPad Inc. USA) was used as the fit program for fitting the autocorrelation data. After fitting the autocorrelation curves obtained from a dilution series of ATTO655 in the pure buffer, the resulting parameters were  $386\pm 1$  nm and  $6.5\pm 0.2$  for  $r_0$  and  $k$  respectively (Fig. 2.7). The effective volume was calculated by  $V_{\text{eff}} = \sqrt{\pi^3 k r_0^3}$  (see Eqn. 2.5) giving  $V_{\text{eff}} = 2.1\pm 0.5$  fL. Then, the same procedure was applied to calibrate  $V_{\text{eff}}$  for the 57% (w/w) sucrose stock solution resulting in  $r_0 = 389\pm 2$  nm,  $k = 3.8\pm 0.4$ , and  $V_{\text{eff}} = 1.3\pm 0.2$  fL, respectively. The experimentally obtained “ $k$ ” value in 57% (w/w) sucrose solution was used for the fitting of the ACFs of labeled azurin samples (Chapter 3, 4 and 5).

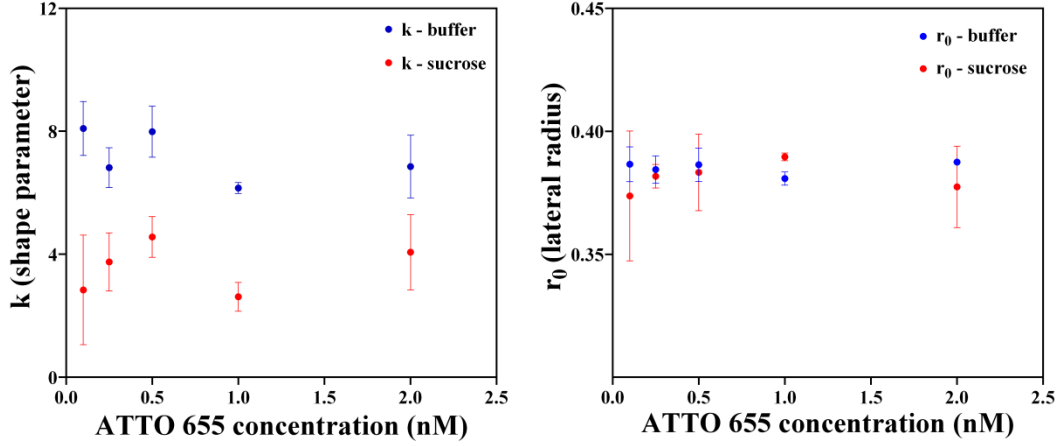


**Figure 2.7:** Experimentally obtained parameters ( $k$ ,  $r_0$ ) for dilution series of ATTO655 in (A) buffer and (B) 57% (w/w) aqueous sucrose solution.

From the fits of the ACFs also  $\tau_D$  was determined (See Fig. 2.4 and 2.5). The average diffusion times for the dye as obtained from the fits amounted to  $0.102 \pm 0.01$  ms (water) and  $2.9 \pm 0.3$  ms (57% w/w sucrose solution) (Fig. 2.8). On the basis of the known diffusion coefficient of ATTO655 in water ( $D = 383 \mu\text{m}^2\text{s}^{-1}$ ) and  $r_0 = 385$  nm a value of 0.097 ms is calculated for  $\tau_D$  (Eqn. 2.7), in good agreement with the experimentally determined value. Diffusion coefficient depends on the viscosity of the solution (see section 2.4, Eqn. 2.11). In the present case, as the viscosity increases by a factor of 40 going from 0% sucrose solution to 57% (w/w) sucrose solution, the increase of the diffusion time is by a factor of 29 (Fig. 2.8).

$$\tau_D = \frac{r_0^2}{4D} \quad (2.7)$$

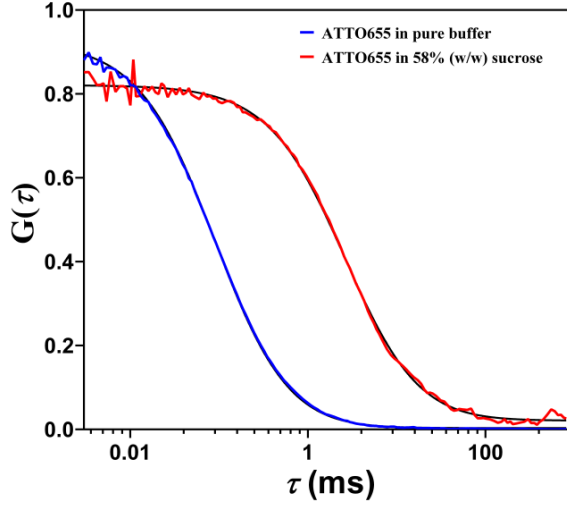


**Figure 2.8:** Experimentally obtained ACFs for ATTO655 in buffer (red) and 57% (w/w) sucrose (blue) solution. The black lines are the fits according to the Eqn.  $G(\tau) = G(0)G_{diff}(\tau)$ , with  $\tau_D = 0.102$  ms in pure buffer and  $\tau_D = 2.9$  ms for the 57% (w/w) sucrose solution.

### 2.3.2 Determination of confocal volume by nano-rod scanning

It was an additional interest for us to determine the effective volume based on the imaging of gold nano-rods. Besides laser excitation power, the measurement conditions were kept similar as mentioned for previous FCS calibration measurements (see Section 2.3.1 for details). The nano rods are treated as point sources and can be used in order to scan the volume.

Sample medium	$x$ ( $r_0$ ) ( $\mu\text{m}$ )	$y$ ( $\mu\text{m}$ )	$z$ (axial $z_0$ ) ( $\mu\text{m}$ )	$k$	$V_{eff}$ (fL)
Air	0.424	0.419	1.953	4.6	1.9
Buffer	0.380	0.455	1.579	4.2	1.2
70% (w/v) sucrose	0.520	0.590	1.895	3.6	2.8

**Table 2.2:** Experimentally obtained dimensions of the effective volume in micrometers determined from Gaussian fits of the sections shown in Fig. 2.9. Mean values are shown here.

For effective volume determination, the MicroTime 200 system equipped with an axial piezo positioner was used to scan the nano-rod coated glass substrate. It can scan in the lateral xy-as well as in the axial xz-plane. The scanner accuracy is  $\pm 3.0$  nm and can be disregarded as a source

of uncertainty. Approximately 200  $\mu\text{l}$  of buffer or sucrose solution was added on the surface of the nano-rod deposited glass slides and then the imaging was performed. First, an overview image was taken from which bright spots were selected for further analysis. Then, from those bright spots, sectional scans were recorded in a plane, e.g.  $xy$ -scan. Then, they were fitted with a two-dimensional Gaussian distribution as described in the application note of PicoQuant(11). In the present work, three scanning measurements were performed under air, water and in 57% (w/w) aqueous sucrose solution respectively. Fig. 2.9 shows the images of 2D sections for the effective volumes in air, buffer and sucrose solution. The experimentally obtained effective volume under different conditions with the lateral radius ( $r_0$ ) and the eccentricity ( $k$ ) have been summarized in Table 2.2. Using the lateral and axial dimensions, extracted from the different sections of the volume,  $V_{eff}$  is calculated according to Eqn. 2.8 as described in ref.(11):

$$V_{eff} = \pi^{(3/2)} \cdot x \cdot y \cdot z \text{ (fL)} \quad (2.8)$$

Although the imaging method resulted in slightly different values for  $V_{eff}$ , the calculated volume was found to be similar to the values (1-2 fL) reported in See section 2.3.1.

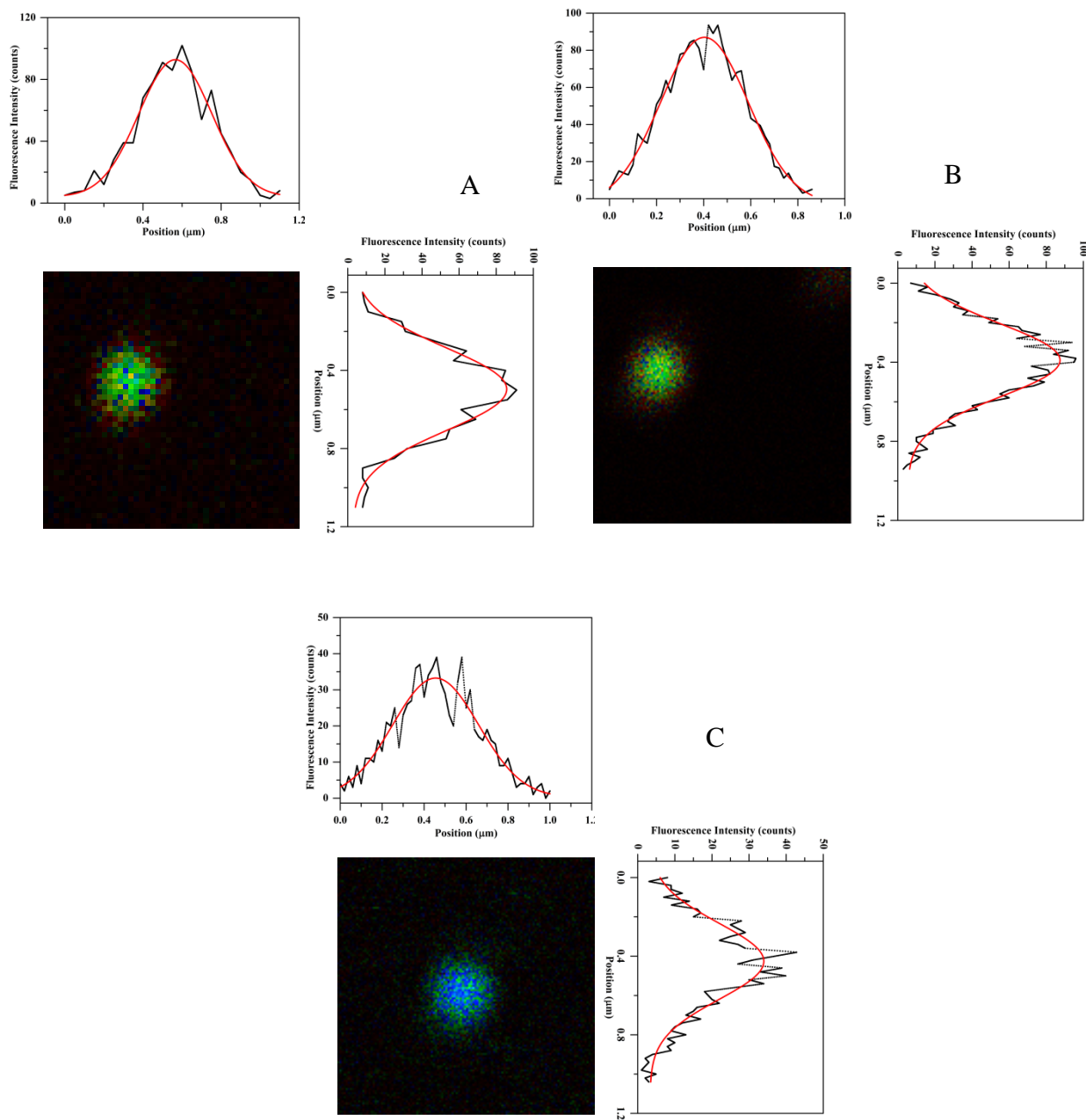


**Figure 2.9:** *xy* sections of the effective volumes, measured with  $45 \text{ nm} \times 100 \text{ nm}$  gold-nano rods in (A) air (B) buffer and (C) 57% (w/w) sucrose solution ( $z$  is along the optical axis). Along with the 2D sections line profiles through the center positions are shown. Experimental data are shown in black whereas line sections of the 2D Gaussian fits are represented by red.



## ***2.4 Diffusion, bimolecular interactions and their dependency on viscosity***

In the present thesis, we have investigated short-time-scale dynamics such as photoinduced electron transfer reactions in azurin-dye constructs or the blinking of the dye in the presence of redox agents by fluorescence correlation spectroscopy. We need to consider reactions of the label with a) chemicals in solution (intermolecular reactions) and b) the metal center in the protein (intramolecular reactions). The intermolecular reactions between the label (ATTO 655) and the redox agents (ascorbate, potassium hexacyanoferrate (III)) depend on the diffusion times of those molecules. To assess this, we look into the diffusion time scales of labeled proteins and into the rates of the bimolecular reaction between the labeled azurin and redox agents. What are the association rates and how do they vary as a function of viscosity?

When reactions between molecules occur at every collision, the reaction is diffusion controlled. Association rates in solution are determined by the time it takes to bring reactive partners together by diffusion. Such association reactions, in general, have very small activation barriers and diffusion controlled reactions have rates of  $k_d = 10^9$ - $10^{10} \text{ M}^{-1}\text{s}^{-1}$  in aqueous solution at room temperature(24)(25). In the present work, the reaction between the redox chemicals and the dye is diffusion controlled (See Chapter 3 for details). After the redox reaction, the dye enters into a dark state. To be observable by FCS, the reaction between the redox agent and the label has to take place within the time it takes for the labeled protein to cross the effective volume.

As mentioned earlier, the diffusion can be varied by varying the viscosity ( $\eta$ ) of the solution. A rough estimate of the diffusion time of azurin in a sucrose solution can be obtained from the rule of thumb that  $\tau_D$  is proportional to the cube root of the molecular weight(26). With a molecular weight 13998 for azurin and 887 for ATTO655 and a diffusion time of 2.9 ms for ATTO 655 in 57% (w/w) sucrose solution (See page 13), the estimated diffusion correlation time for azurin in 57% (w/w) sucrose solution would amount to 7 ms. Single molecule FCS measurements on labeled zinc azurin samples in pure buffer showed that the diffusion time amounted to 200  $\mu\text{sec}$ , which shifted to the millisecond range when a 57% (w/w) sucrose solution was used. The average diffusion time was found to be  $12 \pm 2$  ms (Fig. 2.10) in agreement with expectation.

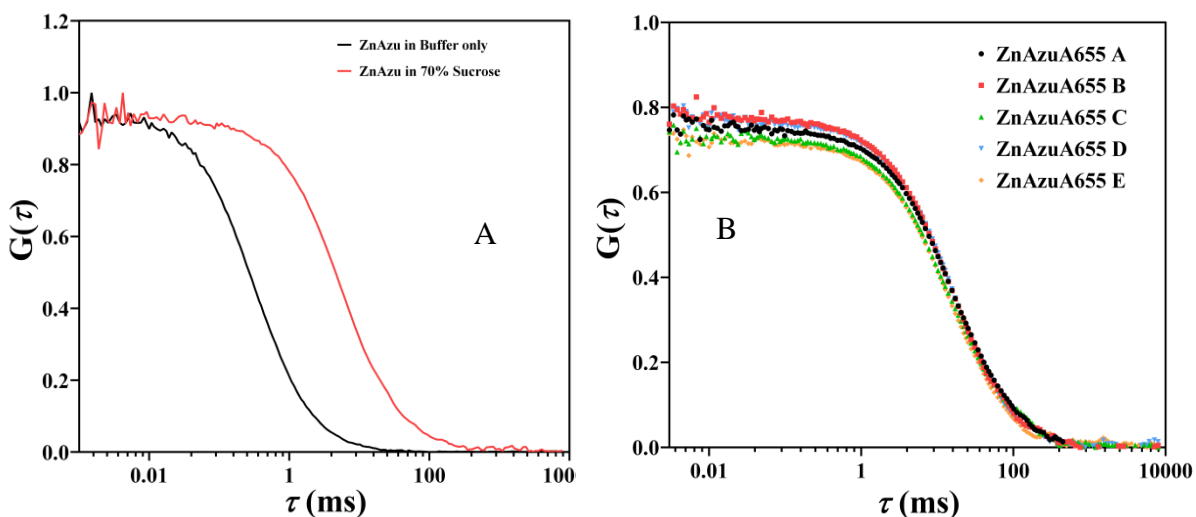


**Figure 2.10:** (A) Experimentally obtained ACFs for ATTO655 labeled Zn azurin in buffer and 57% (w/w) aqueous sucrose solution without redox agents. (B) ACFs of ATTO655 labeled ZnAzu prepared in 57% (w/w) sucrose solution without redox chemicals for five sets of experiments.

Within the sucrose concentration range from 70 % (w/v) to 60 % (w/v), the diffusion correlation time of labeled azurin changes from 12 to 3 ms. This range is preferred for FCS measurements if we want to study any microsecond dynamics (blinking, electron transfer, conformational changes etc.) in the sample. Our next interest was to estimate the bimolecular rate constants between the label and the redox agents. How is it assessed?

The diffusion controlled bimolecular reaction rate  $k_d$  can be estimated from Smoluchowski's principle(27)(28)(29)

$$k_d = 4\pi(D_A + D_B)(r_A + r_B) = 4\pi D_{AB} R_{AB} \quad (2.9)$$

where  $D_A$  and  $D_B$  are the diffusion constants (in  $\text{cm}^2\text{s}^{-1}$ ) and  $r_A$  and  $r_B$  are the hydrodynamic radii (in cm) of the reacting spherical molecules, respectively. The unit of  $k_d$  is  $\text{M}^{-1}\text{s}^{-1}$ .  $R_{AB} = (r_A + r_B)$  is the minimal distance between the centers of the two molecules. The diffusion constant for their relative motion is represented by  $D_{AB} = D_A + D_B$ . In the present case, we are dealing with molecules of different size (e.g. hexacyanoferrate (III), ATTO655, azurin). The diffusion of redox agents, e.g., sodium ascorbate is rapid in the solution compared to that of large azurin protein ( $\sim 3$  nm). The labeled azurin and the redox chemicals are assumed to be spherical in shape with  $r_A \gg r_B$ . If  $D_{AB}$  is in the order of  $10^{-7}\text{ cm}^2\text{s}^{-1}$  for small proteins(30)(31) and  $R_{AB}$  is close

to 1 Å, the bimolecular rate constant amounts to  $\sim 7 \times 10^8 \text{ M}^{-1}\text{s}^{-1}$  at ambient temperature using Eqn. 2.9. For small molecules with  $D$  in the order of  $10^{-5} \text{ cm}^2\text{s}^{-1}$ , this rate constant can reach  $\sim 10^{10} \text{ M}^{-1}\text{s}^{-1}$  in aqueous solution(32)(33)(34). This is the maximum diffusion controlled bimolecular rate, known as Smoluchowski's limit.

Another aspect is that ATTO655 labeled azurin is not reactive over its entire surface. For a labeled species, the dye is attached to a particular position on the protein surface. The oxidant or reductant will have productive associations with only a fraction of the total surface area of azurin. The reaction rate will depend on the fraction of the reactive configurations of labeled molecules in solution. For this, we consider the molecules to be spherical: molecule A (labeled protein) and molecule B (redox agent). The labeled protein A of radius  $r_A$  is chosen at the origin of a spherical polar coordinate system  $(r, \theta)$ . B molecules are uniformly reactive over their entire surfaces. The surface of the labeled protein is reactive only over the axially symmetric range  $0 < \theta < \theta_0$ . A reactive encounter may only occur if the redox agent is located within the reaction radius  $R_{AB}$  and within the range  $0 < \theta < \theta_0$  over the protein surface (Fig. 2.10). It has been calculated(35) that

$$k_d = 4\pi D_{AB} R_{AB} \sin(\theta_0/2) \quad (2.10)$$

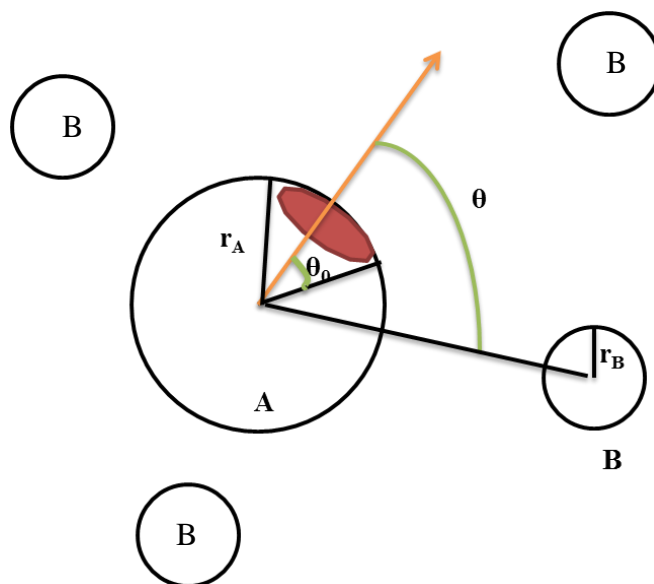


**Figure 2.11:** Schematic diagram of the reactive-patch geometry of the association complex [molecule A with reactive surface patch (red)]. As discussed in the text, an association is assumed to take place only after the two molecules have come into contact. The red area shows the reactive patch for the labeled protein. The redox agents (B) are spherical and assumed to have homogeneous reactivity over their entire surface. (Adapted from *Biophysical Journal*, 1981, volume 36, pp. 697-714)

If there are severe steric constraints,  $\theta_0$  may become very small, which will reduce the maximum diffusion controlled bimolecular rate considerably. There are many other factors which can affect the association rate constants e.g. short range forces, the presence of receptors on the molecular surface, coupling of the diffusion processes(27)(28)(29)(36).

As mentioned previously (see section 2.3), according to the Stokes-Einstein law, the diffusion coefficient depends on the viscosity of the solution as well as the temperature:

$$D = k_B T / 6\pi\eta r \quad (2.11)$$

It predicts that the application of a high viscosity liquid such as a sucrose solution or glycerol can slow down the diffusion processes as  $k_d \propto 1/\eta$ . In glycerol (viscosity 950 cP),  $k_d$  may reach values of  $10^6 \text{ M}^{-1} \text{ s}^{-1}$ . As a consequence, the reactions between the label and redox agent will be slowed down. A flurry of experiments have been performed to understand the variation of association rates as a function of diffusion coefficients and

viscosities(29)(37)(36)(38)(39)(40)(41)(42)(43)(44). In our work, the use of 57% (w/w) sucrose has increased the viscosity by a factor of 40 (Table 1), which suggests that  $k_d$  can reach  $10^7$ - $10^8$   $M^{-1}s^{-1}$  in 57% (w/w) sucrose solution compared to  $10^9$ - $10^{10}$   $M^{-1}s^{-1}$  in buffer. Using labeled ZnAzu, the rates of reaction between the redox agents and the labeled protein have been experimentally obtained from single molecule FCS measurements and will be discussed in Chapter 3.

## **2.5 Photobleaching and blinking of fluorophore**

The use of organic fluorophores and fluorescent proteins in biochemical and biophysical applications of single-molecule spectroscopy is a common practice now-a-days(45)(46)(47)(48)(49). It is important to choose the appropriate fluorescent probe in order to be able to interpret the results for each experiment. For this it becomes essential to understand the photochemical and photophysical processes of the dyes. We briefly discuss the photophysical processes in this section. Photoinduced processes of a dye can be observed in various ways (Fig. 2.12). After photoexcitation, either the excited molecules return directly to the ground state via fluorescence (radiative process) or non-radiative decay or the molecules decay to triplet states via intersystem crossing. Since the rate of conversion of a triplet state to the ground state is slow due to spin conversion, the molecules stay in the triplet state for a long time. In solution, when such deactivation processes are not too fast, i.e., when the lifetime is sufficiently long, a molecule in the triplet state has a chance to react with other molecules in the surrounding medium. For example, dissolved oxygen, which has a triplet ground state, can react with fluorophores in the triplet state, leading to free radicals that are toxic to cells. On the other hand, during photobleaching, a fluorophore permanently loses the ability to fluoresce due to photon-induced chemical damage or covalent modification. Fluorophores in the excited singlet or triplet state also can react with other small molecules or biomolecules. For fluorophores in solution, redox blinking can be easily induced by the presence of oxidants such as oxygen, methylviologen or by reductants such as ascorbate, DTT, potassium hexacyanoferrate (II) etc. For example, Vogelsang *et al.* in 2008 showed that the blinking process can be altered by changing the ratio of reducing agents and oxygen in the solution(50). Molecules containing heavy atoms, such as the halogens and transition metals, often facilitate intersystem crossing resulting in blinking. Therefore, photobleaching and blinking of fluorescent dyes must be controlled carefully, especially for single molecule analysis. Single-molecule measurements have

been carried out to understand the blinking properties of the conventional dyes(50)(51)(52)(53)(54)(55). Mainly, the excitation conditions and local environment have been varied to determine the various causes for the blinking.

Studies also have been performed to understand photoinduced electron-transfer reactions involving fluorescent labels attached to the proteins(22)(50)(53)(56)(57)(58)(59)(60)(61)(62)(63). To a lesser extent, the propensity of the label to engage in redox reactions with protein residues and protein cofactors has been studied for some fluorescent labels. In case of proteins, tryptophan was not the only moiety to show redox activity towards the fluorescent probes, metal cofactors, NADH, FAD, porphyrins and tyrosines also can show such activities.

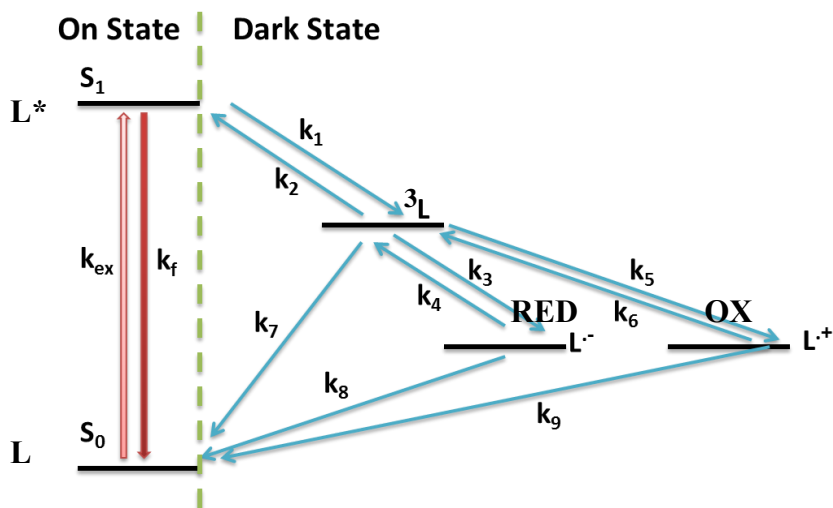


**Figure 2.12:** A “Jablonski diagram” of a fluorophore. The fluorophore ( $L$ ) is excited from its ground state ( $S_0$ ) to the first excited state ( $S_1$ ) with an excitation rate  $k_{ex}$  and it fluoresces with the rate  $k_f$  with a lifetime of a few nanoseconds. Competing processes are non-radiative decay to  $S_0$  and intersystem crossing to the triplet state ( $^3L$ ) ( $k_1, k_2$ ). If an oxidant or a reductant is added, the triplet state may be depopulated quickly and radical cations ( $L\cdot+$ ) or anions ( $L\cdot-$ ) ( $k_3, k_4, k_5, k_6$ ) are formed, respectively. The triplet state can also return to  $S_0$  ( $k_7$ ) by a radiative process (phosphorescence). Depending on the redox potentials, these dark states ( $L\cdot+, L\cdot-$ ) are comparatively stable but can be returned to  $S_0$  by the complementary process in a buffer containing a reducing as well as an oxidizing compound ( $k_8, k_9$ ).

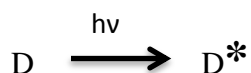
In the present thesis, blinking of the fluorophore and photoinduced electron transfer in a labeled azurin have been investigated in detail. It is shown how single molecule FCS can be utilized to analyze diffusion, blinking and PET in a labeled sample.

## 2.6 Photoinduced electron transfer (PET)

We have discussed in chapter 1 the electron transfer between a donor and an acceptor. This reaction can be thermally or photochemically induced. In recent years, photoinduced electron transfer reactions (PET) have been studied (64)(65)(66)(67)(68)(69). Photoinduced intramolecular and intermolecular electron-transfer reactions are of special interest due to their importance in photosynthesis, photochemical reactions, photoimaging, solar energy conversion and many other applications(70)(71)(72)(73)(74). For bimolecular electron transfer between two species in their ground states, the standard free energy change is given by

$$\Delta G_{CS}^0 = IP_D - EA_A \quad (2.12)$$

where,  $IP_D$  is the ionization potential of the donor and  $EA_A$  is the electron affinity of the acceptor. These quantities are estimated from the energies of the highest occupied molecular orbital (HOMO) and lowest unoccupied molecular orbital (LUMO) orbitals of the donor and the acceptor, respectively. The PET reaction takes place when a short pulse of light activates an electron-rich molecule, and an electron is transferred from the HOMO to the LUMO of the donor and from there to the LUMO orbital of the electron deficient acceptor. When the donor absorbs light and gets excited, it changes the redox properties of the donor.



Then, it interacts with the acceptor, and there is formation of a short-lived intermediate called the encounter complex. If we consider the PET reactions in solution, the lifetimes of these complexes are of the order of nanoseconds, and the quenching occurs by the acceptor i.e. it accepts the electron from the donor.



Now,  $(IP_D - EA_A)$  decides the feasibility of electron transfer between donor and acceptor in the ground state. According to Rehm and Weller(75), for photoinduced electron transfer between an a donor ( $D$ ) and the acceptor ( $A$ ) (either one of them may be the electronically excited molecular entity), the change in standard Gibbs free energy can be approximated as

$$\Delta G = eE_{D^+/D} - eE_{A^-/A} - \Delta G_{0,0} + (n_A - n_D - 1) \frac{e^2}{\epsilon d} \quad (2.13)$$

which describes the driving force  $\Delta G$  for the ET by a donor ( $D$ ) to an acceptor ( $A$ ) with  $E_{D^+/D}$  and  $E_{A^-/A}$  denoting the midpoint potentials of donor and acceptor, respectively. Here, either the donor or the acceptor is optically excited with  $\Delta G_{0,0}$  denoting the energy of the corresponding optical  $0-0$  transition,  $e$  denotes the electronic charge,  $d$  the distance between donor and acceptor,  $\epsilon$  the dielectric constant and  $n_A$  and  $n_D$  the charges of acceptor and donor in units of  $|e|$ , respectively. Eqn. 2.13 has been used to calculate the driving forces of the PET reactions in Cu azurin-ATTO655 bioconjugate (See chapter 4). In addition to PET, various other processes may occur e.g. formation of chemical products, radiative and non-radiative decay, intersystem crossing.

A number of studies have been reported to determine the distance and medium dependence of the electronic coupling in proteins ((76)(77)(78)(79)(80) and references therein). Motivated mostly by the reaction mechanism of respiratory electron-transport chains and electron-transfer reactions in redox enzymes, various experiments have been performed for a precise understanding of PET rates in relation to reorganization energies of the proteins, dependence on redox potentials of donor and acceptor etc. For reviews of these achievements the reader is referred to the literature (81)(82)(83)(84)(85). Gray and coworkers, made major contributions in understanding PET reactions in metalloproteins like azurin. They explored the distance dependence of ET tunneling through the folded organic framework of the protein by employing surface-attached coordination compounds(83).

Ruthenium and osmium compounds were attached at several locations in the  $\beta$ -strand structure of azurin and the driving-force dependence of ET between reduced Cu(I) and oxidized Ru(III) or Os(III) was examined by laser-flash quench studies. The distance between the redox centers was varied from 16 to 26 Å depending on the position of the label on the strand. The ET times were found to increase exponentially from microseconds to milliseconds with increase in the distance between the donor and acceptor. Close van der Waals contact (3 Å) between two redox centers results in a  $10^{13} \text{ s}^{-1}$  ET rate. The results basically show that beyond this distance (26 Å) multiple tunneling steps are required for efficient ET reaction. Analysis of labeled azurin



with Ru(III) or Os(III) metal complexes provided the driving forces and reorganization energies for ET reaction between the two redox centers allowing for the calculation of the electronic coupling matrix element and the decay constant ( $\beta$ ). In all cases, the reorganization energies and the decay constants were found to be  $0.7\pm 0.1$  eV and  $1.0\pm 0.3$  Å<sup>-1</sup> respectively. Similar ET rates in solution and crystal forms of Ru(III) or Os(III)-complexes suggested that bulk water played a minor role in ET reaction and the intervening protein backbone is necessary for electron-transfer. Gray also found that if Cu(I) is replaced by Zn(II) in Ru-azurin complex, the photogenerated holes remained localized on the Ru center. The ET rates from Cu(I) to Ru(III) did not decrease upon lowering the temperature(86)(87)(88). All these data proved that there was no hopping mechanism operational in photogenerated Ru-azurin complexes.

Onuchic proposed a pathway model which supported Gray's work on ET reaction. The pathway model elaborates the issue of disparate contributions to ET from different pathways connecting the redox centers. Later, it was modified to take into account the anisotropic covalency of the copper site. Other supporting experimental data were provided by Farver and co-workers ((89) and references therein). They developed their own scheme for studying long range ET reactions. Their techniques did not require any modifications in azurin. Farver and coworkers investigated the long-range intramolecular electron transfer reactions in azurin by using pulse radiolytically generated CO<sub>2</sub><sup>-</sup> radicals to observe the ET reaction between the Cys3-Cys26 bridge (SS') in azurin and the oxidized copper ion similar to Ru-complexes(89)(90)(91)(92). Similar experiments were performed to understand ET pathways in TUPS-modified (thiouredopyrene-3,6,8-trisulfonate) proteins, where TUPS moieties are attached to surface lysine and cysteine residues(93)(94)(95)(96)(97)(98). Later on, the influence of Trp48 on the ET kinetics was probed by working on azurin variants, where the tryptophan residue was substituted by Ala, Phe, Ser, Tyr, Leu and Met amino acids. Farver and coworkers demonstrated the occurrence of ET by a radical/hopping mechanism through aromatic residues, as demonstrated in Rhenium-azurin complexes. Gray and coworkers also examined multistep tunneling in Re-azurin where Trp is located between Re and the copper center. Cu(I) oxidation was inhibited by the replacement of Trp by Tyr or Phe(99)(100)(101). The effects of solvent dynamics along the ET pathways are also under investigation(102). They also have constructed Ru-complexes-azurin systems in which proton-coupled electron hopping mechanism has been demonstrated(103)(104).

A recent development has been the application of electrochemistry to the study of biological ET reactions. Ulstrup and coworkers have investigated electrode-mediated ET(105)(106)(107)(108). Electron microscopic and XPS (X-ray photoelectron spectroscopy) studies of monolayers of azurin adsorbed on gold revealed that azurin is linked via sulphur linkages from the Cys3-Cys26 disulphide bridge to the gold. The measured ET rate of  $30 \text{ sec}^{-1}$  agreed with the Farver/Petch measurements ( $44 \text{ s}^{-1}$ ) compatible with ET from the disulphide interface to the copper center. The low reorganization energy ( $\lambda$ ) demonstrated that azurin can retain its activity even with disrupted disulphide bonds and when packed into monolayers on an electrode surface.

The crucial role of the protein framework in determining the electronic coupling still remains a subject of debate. Various calculations have shown that the helix and beta sheet content of a protein and its tertiary structure can influence the distance dependence of ET coupling(109). All investigations suggest that the rate of ET in proteins rapidly decreases with distance. Electrons can travel up to  $15 \text{ \AA}$  between the redox centers through the protein medium and an electron can travel much longer distances along a chain of co-factors.

## References

- (1) Einstein A. von. Über die von der molekularkinetischen Theorie der Wärme geforderte Bewegung von in ruhenden Flüssigkeiten suspendierten Teilchen. *Ann. Phys.* **1905**, 322, 549–560.
- (2) Edward, J. T. Molecular volumes and the Stokes-Einstein equation. *J. Chem. Educ.* **1970**, 47, 261.
- (3) Mason, T. G. Estimating the viscoelastic moduli of complex fluids using the generalized Stokes-Einstein equation. *Rheol. Acta* **2000**, 39, 371–378.
- (4) Magde, D.; Elson, E.; Webb, W. W. Thermodynamic fluctuations in a reacting system measurement by fluorescence correlation spectroscopy. *Phys. Rev. Lett.* **1972**, 29, 705–708.
- (5) Digman, M. A.; Gratton, E. Fluorescence correlation spectroscopy and fluorescence cross-correlation spectroscopy. *Wiley Interdiscip. Rev. Syst. Biol. Med.* **2009**, 1, 273–282.
- (6) Michalet, X.; Weiss, S.; Jäger, M. Single-molecule fluorescence studies of protein folding and conformational dynamics. *Chem. Rev.* **2006**, 106, 1785–1813.
- (7) Chiantia, S.; Ries, J.; Schwille, P. Fluorescence correlation spectroscopy in membrane

- structure elucidation. *Biochim. Biophys. Acta* **2009**, *1788*, 225–233.
- (8) Widengren, J.; Mets, U.; Rigler, R. Fluorescence correlation spectroscopy of triplet states in solution: a theoretical and experimental study. *J. Phys. Chem.* **1995**, *99*, 13368–13379.
  - (9) Ha, T. Single-molecule fluorescence resonance energy transfer. *Methods* **2001**, *25*, 78–86.
  - (10) Majer, G.; Melchior, J. P. Characterization of the fluorescence correlation spectroscopy (FCS) standard Rhodamine 6G and calibration of its diffusion coefficient in aqueous solutions. *J. Chem. Phys.* **2014**, *140*, 6–12.
  - (11) Rüttinger, S.; Buschmann, V.; Krämer, B.; Erdmann, R.; MacDonald, R.; Koberling, F. Comparison and accuracy of methods to determine the confocal volume for quantitative fluorescence correlation spectroscopy. *J. Microsc.* **2008**, *232*, 343–352.
  - (12) Hess, S. T.; Webb, W. W. Focal volume optics and experimental artifacts in confocal fluorescence correlation spectroscopy. *Biophys. J.* **2002**, *83*, 2300–17.
  - (13) Gilani, A. G.; Moghadam, M.; Hosseini, S. E.; Zakerhamidi, M. S. A comparative study on the aggregate formation of two oxazine dyes in aqueous and aqueous urea solutions. *Spectrochim. Acta, Part A* **2011**, *83*, 100–105.
  - (14) Robert C. Weast, M. J. A. *CRC Handbook of Chemistry and Physics*; CRC Press, Inc, Boca Raton, Florida.
  - (15) Kapusta, P.; Wahl, M.; Benda, A.; Hof, M.; Enderlein, J. Fluorescence lifetime correlation spectroscopy. *J. Fluoresc.* **2007**, *17*, 43–8.
  - (16) Kapusta, P.; Macháň, R.; Benda, A.; Hof, M. Fluorescence lifetime correlation spectroscopy (FLCS): Concepts, applications and outlook. *Int. J. Mol. Sci.* **2012**, *13*, 12890–12910.
  - (17) Nikoobakht, B.; El-Sayed, M. a. Preparation and growth mechanism of gold nanorods (NRs) using seed-mediated growth method. *Chem. Mater.* **2003**, *15*, 1957–1962.
  - (18) Vogelsang, J.; Cordes, T.; Forthmann, C.; Steinhauer, C.; Tinnefeld, P. Controlling the fluorescence of ordinary oxazine dyes for single-molecule switching and superresolution microscopy. *Proc. Natl. Acad. Sci. U. S. A.* **2009**, *106*, 8107–8112.
  - (19) Ha, T.; Tinnefeld, P. Photophysics of Fluorescent Probes for Single-Molecule Biophysics and Super-Resolution Imaging. *Annu. Rev. Phys. Chem.* **2012**, *63*, 595–617.
  - (20) Doose, S.; Neuweiler, H.; Sauer, M. Fluorescence quenching by photoinduced electron transfer: a reporter for conformational dynamics of macromolecules. *Chemphyschem A Eur. J. Chem. Phys. Phys. Chem.* **2009**, *10*, 1389–1398.
  - (21) Doose, S.; Neuweiler, H.; Sauer, M. Fluorescence quenching by photoinduced electron transfer: A reporter for conformational dynamics of macromolecules. *ChemPhysChem* **2009**, *10*, 1389–1398.
  - (22) Rasnik, I.; McKinney, S. A.; Ha, T. Nonblinking and long-lasting single-molecule fluorescence imaging. *Nat. Methods* **2006**, *3*, 891–893.
  - (23) Rüttinger, S.; Buschmann, V.; Krämer, B.; Erdmann, R.; Macdonald, R.; Koberling, F.

- Comparison and accuracy of methods to determine the confocal volume for quantitative fluorescence correlation spectroscopy. *J. Microsc.* **2008**, *232*, 343–352.
- (24) Wilemski, G. General theory of diffusion-controlled reactions. *J. Chem. Phys.* **1973**, *58*, 4009–4019.
- (25) Alberty, R.; Hammes, G. G. Application of the theory of diffusion-controlled reactions to enzyme kinetics. *J. Phys. Chem.* **1958**, *62*, 154–159.
- (26) A. Polson, D. V. D. R. Relationship between the diffusion constant and molecular weight. *Biochim. Biophys. Acta* **1950**, *5*, 358–360.
- (27) Berg, O. G.; Vonhippel, P. H. Diffusion-controlled Macromolecular Interactions. *Annu. Rev. Biophys. Biophys. Chem.* **1985**, *14*, 131–160.
- (28) Strickland, S.; Palmer, G.; Massey, Vi. Determination of Dissociation Constants and Specific Constants of Enzyme-Substrate (or Protein-Ligand) Interactions from Rapid Reaction Kinetic Data. *J. Biol. Chem.* **1975**, *250*, 4048–4052.
- (29) Shoup, D.; Lipari, G.; Szabo, A. Diffusion-controlled bimolecular reaction rates. The effect of rotational diffusion and orientation constraints. *Biophys. J.* **1981**, *36*, 697–714.
- (30) Young, M. E.; Carroad, P. A.; Bell, R. L. Estimation of diffusion coefficients of proteins. *Biotechnol. Bioeng.* **1980**, *22*, 947–955.
- (31) Tyn, M. T.; Gusek, T. W. Prediction of diffusion coefficients of proteins. *Biotechnol. Bioeng.* **1990**, *35*, 327–338.
- (32) Collins, F. C.; Kimball, G. E. Diffusion-controlled reaction rates. *J. Colloid Sci.* **1949**, *4*, 425–437.
- (33) Hazel, J. R.; Sidell, B. D. A method for the determination of diffusion coefficients for small molecules in aqueous solution. *Anal. Biochem.* **1987**, *166*, 335–41.
- (34) Karlsson, O. .; Stubbs, J. .; Karlsson, L. .; Sundberg, D. . Estimating diffusion coefficients for small molecules in polymers and polymer solutions. *Polymer (Guildf)*. **2001**, *42*, 4915–4923.
- (35) Berg, O. G. Orientation constraints in diffusion-limited macromolecular association. The role of surface diffusion as a rate-enhancing mechanism. *Biophys. J.* **1985**, *47*, 1–14.
- (36) Diffusion, R.; Particles, F. Rates of Diffusion-Controlled Relative Diffusion of two Free Particles. *Reactions* 113–118.
- (37) Hasinoff BB, Dreher R, D. J. The association reaction of yeast alcohol dehydrogenase with coenzyme is partly diffusion-controlled in solvents of increased viscosity. *Biochim. Biophys. Acta* **1987**, *911*, 53–58.
- (38) Andres F. Olea, J. K. T. Rate constants for reactions in viscous media: correlation between the viscosity of the solvent and the rate constant of the diffusion-controlled reactions. *J. Am. Chem. Soc.* **1988**, *110*, 4494–4502.
- (39) Feng, C.; Kedia, R. V.; Hazzard, J. T.; Hurley, J. K.; Tollin, G.; Enemark, J. H. Effect of Solution Viscosity on Intramolecular Electron Transfer in Sulfite Oxidase. *Biochemistry*

- 2002**, *41*, 5816–5821.
- (40) Kang, S. a; Crane, B. R. Effects of interface mutations on association modes and electron-transfer rates between proteins. *Proc. Natl. Acad. Sci. U. S. A.* **2005**, *102*, 15465–70.
- (41) Wenbing Li, Weihong Fan, Bradley O. Elmore, and C. F. Effect of solution viscosity on intraprotein electron transfer between the FMN and heme domains in inducible nitric oxide synthase. **2012**, *585*, 2622–2626.
- (42) Ivković-Jensen MM, K. N. Effects of viscosity and temperature on the kinetics of the electron-transfer reaction between the triplet state of zinc cytochrome c and cupriplastocyanin. *Biochemkstry* **1997**, *36*, 8135–8144.
- (43) X. Zhang, Johna Leddy, and A. J. B. Dependence of rate constants of heterogeneous electron transfer reactions on viscosity. *J. Am. Chem. Soc.* **1985**, *107*, 3719–3721.
- (44) Renat R. Nazmutdinova, Galina A. Tsirlinab, Ibragim R. Manyurova, Michael D. Bronshteina, Nina V. Titovab, Z. V. K. Misleading aspects of the viscosity effect on the heterogeneous electron transfer reactions. *J. Chem. Phys.* **2006**, *326*, 123–137.
- (45) Zheng, Q.; Juette, M. F.; Jockusch, S.; Wasserman, M. R.; Zhou, Z.; Altman, R. B.; Blanchard, S. C. Ultra-stable organic fluorophores for single-molecule research. *Chem. Soc. Rev.* **2014**, *43*, 1044–56.
- (46) Vogelsang, J. Advancing Single-Molecule Fluorescence Spectroscopy and Super-Resolution Microscopy with Organic Fluorophores. *Physics (College. Park. Md).* **2009**, 1–91.
- (47) Yuste, R. Fluorescence microscopy today. *Nat. Methods* **2005**, *2*, 902–904.
- (48) Ha, T.; Tinnefeld, P. Photophysics of Fluorescence Probes for Single Molecule Biophysics and Super-Resolution Imaging. *Annu Rev Phys Chem* **2012**, *63*, 595–617.
- (49) Willets, K. a.; Ostroverkhova, O.; He, M.; Twieg, R. J.; Moerner, W. E. Novel fluorophores for single-molecule imaging. *J. Am. Chem. Soc.* **2003**, *125*, 1174–1175.
- (50) Vogelsang, J.; Kasper, R.; Steinhauer, C.; Person, B.; Heilemann, M.; Sauer, M.; Tinnefeld, P. A reducing and oxidizing system minimizes photobleaching and blinking of fluorescent dyes. *Angew. Chemie Int. Ed.* **2008**, *47*, 5465–5469.
- (51) Zondervan, R.; Kulzer, F.; Orlinskii, S. B.; Orrit, M. Photoblinking of rhodamine 6G in poly(vinyl alcohol): Radical dark state formed through the triplet. *J. Phys. Chem. A* **2003**, *107*, 6770–6776.
- (52) Christ, Thomas, Florian Kulzer, P. B. Watching the photo-oxidation of a single aromatic. *Angew Chem Int Ed Engl.* **2001**, *40*, 4192–4195.
- (53) Heilemann, M.; Margeat, E.; Kasper, R.; Sauer, M.; Tinnefeld, P. Carbocyanine dyes as efficient reversible single-molecule optical switch. *J. Am. Chem. Soc.* **2005**, *127*, 3801–3806.
- (54) Vosch, T.; Cotlet, M.; Hofkens, J.; Van Der Biest, K.; Lor, M.; Weston, K.; Tinnefeld, P.; Sauer, M.; Latterini, L.; Müllen, K.; De Schryver, F. C. Probing Förster Type Energy Pathways in a First Generation Rigid Dendrimer Bearing Two Perylene Imide

- Chromophores. *J. Phys. Chem. A* **2003**, *107*, 6920–6931.
- (55) Orrit, M. Chemical and physical aspects of charge transfer in the fluorescence intermittency of single molecules and quantum dots. *Photochem. Photobiol. Sci.* **2010**, *9*, 637–642.
- (56) Dittrich, P.; Schwille, P. Photobleaching and stabilization of fluorophores used for single-molecule analysis with one- and two-photon excitation. *Appl. Phys. B: Lasers Opt.* **2001**, *73*, 829–837.
- (57) Widengren, J.; Chmyrov, A.; Eggeling, C.; Löfdahl, P.-A.; Seidel, C. A. M. Strategies to improve photostabilities in ultrasensitive fluorescence spectroscopy. *J. Phys. Chem. A* **2007**, *111*, 429–440.
- (58) Hinkeldey, B.; Schmitt, A.; Jung, G. Comparative photostability studies of BODIPY and fluorescein dyes by using fluorescence correlation spectroscopy. *Chemphyschem A Eur. J. Chem. Phys. Phys. Chem.* **2008**, *9*, 2019–2027.
- (59) Stennett, E. M. S.; Ciuba, M. a; Levitus, M. Photophysical processes in single molecule organic fluorescent probes. *Chem. Soc. Rev.* **2014**, *43*, 1057–75.
- (60) Cordes, T.; Vogelsang, J.; Tinnefeld, P. On the mechanism of Trolox as antiblinking and antibleaching reagent. *J. Am. Chem. Soc.* **2009**, *131*, 5018–5019.
- (61) Cordes, T.; Maiser, A.; Steinhauer, C.; Schermelleh, L.; Tinnefeld, P. Mechanisms and advancement of antifading agents for fluorescence microscopy and single-molecule spectroscopy. *Phys. Chem. Chem. Phys.* **2011**, *13*, 6699–709.
- (62) Di Fiori, N.; Meller, A. The Effect of dye-dye interactions on the spatial resolution of single-molecule FRET measurements in nucleic acids. *Biophys. J.* **2010**, *98*, 2265–72.
- (63) Chung, H. S.; Louis, J. M.; Eaton, W. Distinguishing between protein dynamics and dye photophysics in single-molecule FRET experiments. *Biophys. J.* **2010**, *98*, 696–706.
- (64) Lindstrom, C. D.; Zhu, X. Y. Photoinduced electron transfer at molecule-metal interfaces. *Chem. Rev.* **2006**, *106*, 4281–4300.
- (65) Fukui, K.; Tanaka, K. Distance dependence of photoinduced electron transfer in DNA. *Angew. Chemie, Int. Ed.* **1998**, *37*, 158–161.
- (66) de Silva, a P.; Moody, T. S.; Wright, G. D. Fluorescent PET (photoinduced electron transfer) sensors as potent analytical tools. *Analyst* **2009**, *134*, 2385–2393.
- (67) Bissell, R.; Prasanna de Silva, A.; Nimal Gunaratne, H. Q.; Mark Lynch, P. L.; Maguire, G. M.; McCoy, C.; Samankumara Sandanayake, K. R. A. Fluorescent PET (photoinduced electron transfer) sensors. In *Photoinduced Electron Transfer*; 1993; Vol. 168, pp. 223–264.
- (68) Piotrowiak, P. Photoinduced electron transfer in molecular systems: recent developments. *Chem. Soc. Rev.* **1999**, *28*, 143–150.
- (69) Tobin, P. H.; Wilson, C. J. Examining photoinduced energy transfer in pseudomonas aeruginosa azurin. *J. Am. Chem. Soc.* **2014**, *136*, 1793–1802.

- (70) Jin, Qusheng, C. M. B. Kinetics of Electron Transfer through the Respiratory Chain. *Biophys. J.* **2002**, *83*, 1797–1808.
- (71) Schertl P, B. H. Respiratory electron transfer pathways in plant mitochondria. *Front. Plant Sci.* **2014**, *5*, 1–11.
- (72) G.F. Moore, G. W. B. Energy Conversion in Photosynthesis: A Paragim for Solar Fuel Production. *Annu. Rev. Condens. Matter Phys.* **2011**, *2*, 303–327.
- (73) B.E. Ramirez, H. B. G. The currents of life: the terminal electron-transfer complex of respiration. *Proc. Natl. Acad. Sci. U. S. A.* **1995**, *92*, 11949–11954.
- (74) Jonkheijm P, Weinrich D, Schröder H, Niemeyer CM, W. H. Chemical strategies for generating protein biochips. *Angew Chem Int Ed Engl.* **2008**, *47*, 9618–47.
- (75) Rehm, D.; Weller, A. Kinetics of fluorescence quenching by electron and hydrogen-atom transfer. *Isr. J. Chem.* **1970**, *8*, 259–271.
- (76) Stuchebrukhov, A. Long-distance electron tunneling in proteins. *Theor. Chem. Acc.* **2003**, *110*, 291–306.
- (77) Gray, H. B.; Winkler, J. R. Long-range electron transfer. *Proc. Natl. Acad. Sci. U. S. A.* **2005**, *102*, 3534–9.
- (78) Winkler, J. R. J. R. Electron tunneling pathways in proteins. *Curr. Opin. Chem. Biol.* **2000**, *4*, 192–198.
- (79) Wenger, O. S. Barrier heights in long-range electron tunneling. *Inorganica Chim. Acta* **2011**, *374*, 3–9.
- (80) Jochen Blumberger Recent Advances in the Theory and Molecular Simulation of Biological Electron Transfer Reactions. *Chem. Rev.* **2015**, *115*, 11191–11238.
- (81) Steinberg, I. Z. Long-range nonradiative transfer of electronic excitation energy in proteins and polypeptides. *Annu. Rev. Biochem.* **1971**, *40*, 83–114.
- (82) Gray, H. B.; Winkler, J. R. Long-range electron transfer. *Proc. Natl. Acad. Sci. U. S. A.* **2005**, *102*, 3534–3539.
- (83) Winkler, J. R.; Gray, H. B. Long-range electron tunneling. *J. Am. Chem. Soc.* **2014**, *136*, 2930–2939.
- (84) Voityuk, A. a. Long-range electron transfer in biomolecules. Tunneling or hopping? *J. Phys. Chem. B* **2011**, *115*, 12202–12207.
- (85) Kriegl, J. M.; Nienhaus, G. U. Structural, dynamic, and energetic aspects of long-range electron transfer in photosynthetic reaction centers. *Proc. Natl. Acad. Sci. U. S. A.* **2004**, *101*, 123–8.
- (86) Schlag EW, Sheu SY, Yang DY, Selzle HL, L. S. Distal charge transport in peptides. *Angew Chem Int Ed Engl.* **2007**, *46*, 3196–3210.
- (87) Crane BR, Di Bilio AJ, Winkler JR, G. H. Electron tunneling in single crystals of *Pseudomonas aeruginosa* azurins. *J. Am. Chem. Soc.* **2001**, *123*, 11623–11631.

- (88) Chang I J, Gray H B, W. J. R. High-driving-force electron transfer in metalloproteins: intramolecular oxidation of ferrocycytochrome c by Ru(2,2'-bpy)<sub>2</sub>(im)(his-33)<sub>3</sub><sup>+</sup>. *J. Am. Chem. Soc.* **1991**, *113*, 7056–7057.
- (89) Farver, O.; Pecht, I. Long-range intramolecular electron transfer in azurins. *Proc. Natl. Acad. Sci. U. S. A.* **1989**, *86*, 6968–72.
- (90) Farver, O.; Jeuken, L. J. C.; Canters, G. W.; Pecht, I. Role of ligand substitution on long-range electron transfer in azurins. *Eur. J. Biochem.* **2000**, *267*, 3123–3129.
- (91) Farver, O.; Skov, L. K.; Van De Kamp, M.; Canters, G. W.; Pecht, I. The effect of driving force on intramolecular electron transfer in proteins. Studies on single-site mutated azurins. *Eur. J. Biochem.* **1992**, *210*, 399–403.
- (92) Farver, O.; Skov, L. K.; Pascher, T.; Karlsson, B. G.; Nordling, M.; Lundberg, L. G.; Vänngård, T.; Pecht, I. Intramolecular electron transfer in single-site-mutated azurins. *Biochemistry* **1993**, *32*, 7317–7322.
- (93) Istvan Szundi , Jenny A. Cappuccio , Natalia Borovok, A. B. K. Photoinduced Electron Transfer in the Cytochrome c/Cytochrome c Oxidase Complex Using Thiouredopyrenetrisulfonate-Labeled Cytochrome c. Optical Multichannel Detection. *Biochemistry* **2001**, *40*, 2186–2193.
- (94) Alexander B. Kotlyar , Natalia Borovok, M. H. Photoinduced Electron Transfer in Singly Labeled Thiouredopyrenetrisulfonate Cytochrome c Derivatives. *Biochemistry* **1997**, *36*, 15828–15833.
- (95) Kotlyar, A.; Borovok, N.; Hazani, M.; Szundi, I.; Einarsdóttir, Ó. Photoinduced intracomplex electron transfer between cytochrome c oxidase and TUPS-modified cytochrome c. *Eur. J. Biochem.* **2000**, *267*, 5805–5809.
- (96) Alagaratnam, S.; Meeuwenoord, N. J.; Navarro, J.; Hervás, M.; De la Rosa, M.; Hoffmann, M.; Einsle, O.; Ubbink, M.; Canters, G. W. Probing the reactivity of different forms of azurin by flavin photoreduction. *FEBS J.* **2011**, *278*, 1506–21.
- (97) Martínez-Junza, V.; Rizzi, A. C.; Alagaratnam, S.; Bell, T. D. M.; Canters, G. W.; Braslavsky, S. E. Flavodoxin relaxes in microseconds upon excitation of the flavin chromophore: detection of a UV-visible silent intermediate by laser photocalorimetry. *Photochem. Photobiol.* **2009**, *85*, 107–10.
- (98) Alagaratnam, S. *Electron Transfer in Flavodoxin-based Redox Maquettes*; Institute of Chemistry, Faculty of Mathematics & Natural Sciences, Leiden University, 2005.
- (99) Crystal Shih, Anna Katrine Museth, Malin Abrahamsson, Ana Maria Blanco-Rodriguez, Angel J. Di Bilio, Jawahar Sudhamsu, Brian R. Crane, Kate L. Ronayne, Mike Towrie, Antonín Vlček Jr., John H. Richards, Jay R. Winkler, and H. B. G. Tryptophan-Accelerated Electron Flow Through Proteins. *Science (80- )*. **2008**, *320*, 1760–1762.
- (100) Warren, J. J.; Herrera, N.; Hill, M. G.; Winkler, J. R.; Gray, H. B. Electron flow through nitrotyrosinate in *Pseudomonas aeruginosa* azurin. *J. Am. Chem. Soc.* **2013**, *135*, 11151–11158.
- (101) Winkler JR, G. H. Could tyrosine and tryptophan serve multiple roles in biological redox



- processes? *Philos. Trans. A Math. Phys. Eng. Sci.* **2015**, *373*, 2037.
- (102) Farver, O.; Zhang, J.; Chi, Q.; Pecht, I.; Ulstrup, J. Deuterium isotope effect on the intramolecular electron transfer in *Pseudomonas aeruginosa* azurin. *Proc. Natl. Acad. Sci. U. S. A.* **2001**, *98*, 4426–4430.
- (103) Warren JJ, Shafaat OS, Winkler JR, G. H. Proton-coupled electron hopping in Ru-modified *P. aeruginosa* azurin. *J. Biol. Inorg. Chem.* **2016**, *21*, 113–119.
- (104) Winkler JR, G. H. Electron flow through biological molecules: does hole hopping protect proteins from oxidative damage? *Q. Rev. Biophys.* **2015**, *48*, 411–420.
- (105) Jensen, P. S.; Chi, Q.; Zhang, J.; Ulstrup, J. Long-Range interfacial electrochemical electron transfer of *Pseudomonas aeruginosa* azurin-gold nanoparticle hybrid systems. *J. Phys. Chem. C* **2009**, *113*, 13993–14000.
- (106) Chin, Q.; Zhang, J.; Nielsen, J. U.; Friis, E. P.; Chorkendorff, I.; Canters, G. W.; Andersen, J. E. T.; Ulstrup, J. Molecular monolayers and interfacial electron transfer of *Pseudomonas aeruginosa* azurin on Au(111). *J. Am. Chem. Soc.* **2000**, *122*, 4047–4055.
- (107) Chi, Q.; Zhang, J.; Andersen, J. E. T.; Ulstrup, J. Ordered assembly and controlled electron transfer of the blue copper protein azurin at gold (111) single-crystal substrates. *J. Phys. Chem. B* **2001**, *105*, 4669–4679.
- (108) Friis, E. P.; Andersen, J. E. T.; Madsen, L. L.; Møller, P.; Ulstrup, J. In situ STM and AFM of the copper protein *Pseudomonas aeruginosa* azurin. *J. Electroanal. Chem.* **1997**, *431*, 35–38.
- (109) Beratan, D.; Betts, J.; Onuchic, J. Protein electron transfer rates set by the bridging secondary and tertiary structure. *Science (80-. )*. **1991**, *252*, 1285–1288.

## **Chapter 3**

### **Fluorescence correlation spectroscopic studies on labeled Zinc Azurin: Direct observation of intermolecular electron-transfer reactions between label and redox agents**

## **Abstract**

A detailed investigation of the products of the labeling reaction of Zinc-azurin variants with the fluorescent dye ATTO655 has been performed. Fluorescence correlation spectroscopy was performed to investigate the behavior of the labeled products under redox conditions, especially the blinking time scales and the amplitudes of non-fluorescent states of ATTO655 in labeled azurin. In this work, we have tried to understand the photoinduced electron-transfer reaction using two species: one labeled at the N-terminus and another one labeled at Lys122 position. Intermolecular electron-transfer reactions were observed between the label and the redox chemicals. Oxidizing agents had no effect on the autocorrelation functions of labeled Zn-azurin whereas the reducing agents ascorbate, hexacyanoferrate (II) caused blinking of the dye. Bimolecular reaction rates were calculated to understand the behavior of the labeled species under reducing conditions.

### 3.1 Introduction

In recent years it has been shown that fluorescent labeling can be used to monitor the working of oxido-reductases in detail at the single molecule level(1)(2)(3)(4)(5)(6). The only requirements are that the absorption spectrum of the protein changes with the redox state of the active center, and that the fluorescence of the dye overlaps with an absorption band of the active center so that Förster resonance energy transfer (FRET) may occur. An alternation of the redox state is then reflected in an alternation of the fluorescence intensity, as well as the fluorescence lifetime(7)(8)(9)(10)(11). Thus, the fluorescence time trace provides a direct record of the enzyme's activity.

The technique chosen to study the time dependence of the label emission is fluorescence correlation spectroscopy (FCS), a single-molecule technique that can be used to monitor diffusing fluorescent particles in dilute solutions. Probing small numbers of molecules at a time by FCS and statistical analysis of the data reveals dynamics otherwise obscured by ensemble averaging(12)(13)(14). When combined with modern hard- and software, FCS allows a time resolution in the picosecond range. In fluorescence correlation spectroscopy (FCS), the intensity fluctuations of fluorescent molecules excited by a Gaussian laser beam are studied. The fluctuations provide the autocorrelation functions, and the molecular diffusion time can easily be determined. By the introduction of extremely small detection volumes and modern hard- and software, the sensitivity of FCS has been increased tremendously. Thus, not only diffusion, but a range of dynamic processes, can be studied e.g. translational and rotational motions, chemical reactions and binding interactions. This, in turn, provides information on the phenomenon of blinking and the photophysics of a fluorophore. Blinking is commonly described by a three-state model: a ground state and the first excited singlet state,  $S_0$ , and  $S_1$  respectively, and the lowest triplet state  $T_1$ . Owing to its longer lifetime,  $T_1$  is considered to be the photochemically most reactive state of the dye. The presence of this state allows the fluorophore to react with other molecules and to switch between bright and dark states, i.e., to undergo blinking. This behavior of the fluorophore is responsible for intensity fluctuations. They can be analyzed by constructing the autocorrelation function (ACF) of the fluorescence-time trace. The presence of oxidizing or reducing agents in the solution can also generate blinking (15)(16)(17).

As a model system, the blue copper protein azurin from *Pseudomonas aeruginosa*, labeled with ATTO655, was chosen to investigate ET reactions. Azurin is a small protein (14

kDa) that is found in a variety of microorganisms and fulfills a putative role in oxidative stress-induced responses(18)(19). The metal ion can be substituted with  $Zn^{2+}$ , which changes the optical and mechanistic properties of the construct as  $Zn^{2+}$  is redox inactive. This chapter deals with the study of Zn Azurin (ZnAzu).

The zinc azurin originally is a by-product of heterologous expression azurin from *E. coli*. Zinc is probably incorporated into the protein during its expression and it is transported into the periplasm. The purified ZnAzu had been characterized by chemical analysis as well as by electrospray ionization mass spectrometry, and the structure was determined by X-ray crystallography previously(20). The overall structure of azurin was not perturbed by the metal exchange. However, the polypeptide structure surrounding zinc-binding site went through a small change in comparison to that in wild-type copper azurin(20)(21). Zinc azurin can also be reconstituted from copper azurin by chemical methods(22).

It is helpful to obtain an idea about the reactions that might contribute to the FCS signal in the case of ZnAzu. Neither FRET nor electron-transfer processes involving the metal center are expected to occur. Only intermolecular reaction between the redox chemicals and the label happens leading to redox induced blinking of the label. In the present study, it is shown that under specific redox conditions, a distortion is detected in the correlation curves, and this distortion can be attributed to the blinking of the labeled molecules under investigation (Fig. 3.1). Furthermore, by fitting the autocorrelation curves accurately, information on the rates of intermolecular ET reaction between the label and the added redox agents can be extracted. In this chapter, the prototype molecule ZnAzu, a diamagnetically blank species has been used to scrutinize the effects of redox chemicals and intermolecular ET reactions on the autocorrelation functions (ACF).

## **3.2 Materials and methods**

### **3.2.1 Azurin expression and purification**

Wild-type azurin (*Pseudomonas aeruginosa*) was expressed in *E.coli* and purified as previously described(20). Cells from *E.coli* JM109 were transformed using a pGK22 plasmid containing the azurin gene followed by a signal peptide for periplasmic translocation. After culturing in 6 liter luria broth (LB) medium till  $OD_{600\text{ nm}}$  reached 0.8 (with 0.5 mM isopropyl  $\beta$ -

D-1- thiogalactopyranoside, IPTG), cells were harvested and resuspended in a 20% (w/v) sucrose solution in 30 mM Tris pH 8.0 containing 1 mM EDTA for 30 min at room temperature. Thereafter the solution was centrifuged at 8000 rpm for 15 min and the supernatant-sucrose fraction was collected. Then, the cells were resuspended in Milli-Q water at 4 °C, stirred for 30 min and centrifuged again at 8000 rpm for 15 min. Subsequently the supernatant obtained from the centrifugation process was added to the previously stored sucrose fraction while the pellet was discarded. When expressed in *E. coli*, azurin usually comes as a mixture of apo- and Zn-azurin. Therefore, after the cells were lysed, copper nitrate [Cu(NO<sub>3</sub>)<sub>2</sub>] was slowly added to the medium in order to incorporate copper in the polypeptide matrix. The final concentration of Cu was kept at ~ 1 mM. Potassium hexacyanoferrate(III) was added to the solution to a final concentration of 100 μM to produce an oxidizing environment. A stepwise precipitation was performed by lowering the pH of the solution to pH 4.0 by adding concentrated acetic acid. The precipitated protein was then removed by centrifugation at 8000 rpm for 30 min.

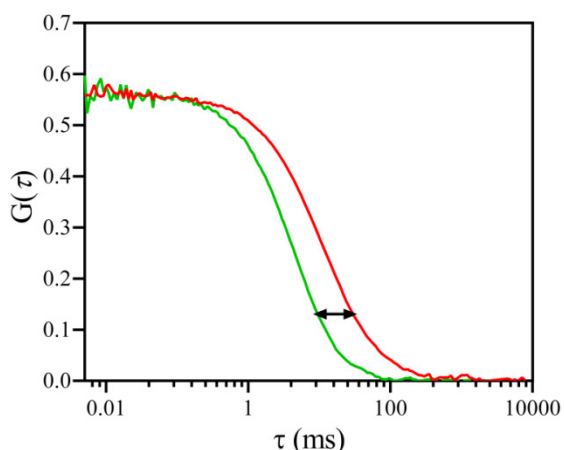


**Figure 3.1:** Example of autocorrelation curves under different conditions. The red curve belongs to the FCS data of a freely diffusing labeled molecule under oxidizing conditions (500 μM potassium hexacyanoferrate (III)) and the green curve represents the same under reducing condition (500 μM potassium hexacyanoferrate (II)).

The resulting clear supernatant solution contained azurin. It was loaded on a home packed CM Sepharose Fast Flow (GE Amersham Biosciences) column pre-equilibrated with 50 mM ammonium acetate buffer pH 4.0. Then the elution was performed using a pH gradient from pH 4.0 to pH 6.9, 50 mM ammonium acetate. Then, the fractions containing azurin were collected, pooled and the buffer was exchanged to 5 mM Tris pH 8.5. The solution was reduced

with sodium dithionite and loaded onto a home packed DEAE Sepharose Fast Flow (GE Amersham Biosciences) column. A salt gradient from 0 to 50 mM of NaCl in 5 mM Tris pH 8.0 was implemented to elute the azurin fractions. In this step, copper and zinc fractions were separated under the salt gradient. The purity of Zn azurin fractions was checked on sodium dodecyl sulphate (SDS)-polyacrylamide gel electrophoresis (PAGE) and by means of UV/Vis spectroscopy (Cary 50 spectrophotometer, Varian Inc., Agilent Technologies, USA). The buffer of Zn azurin fractions was exchanged to 20 mM HEPES, pH 7.0 and stored at -80 °C.

Subsequently, the copper fractions were pooled, the buffer was exchanged to 20 mM HEPES, pH 7.0 and the protein was oxidized by adding potassium hexacyanoferrate(III) upto 1.0 mM. The purity of the protein fractions was checked again on sodium dodecyl sulphate (SDS)-polyacrylamide gel electrophoresis (PAGE) and by means of UV/Vis spectroscopy. If necessary, the copper azurin containing fractions were further purified with a 5 ml HiTrap SP column (GE Healthcare) in 50 mM ammonium acetate and a pH gradient from pH 4.0 to pH 6.9 to avoid contamination of zinc azurin. All the chromatographic procedures were carried out on ÄKTA Purifier system (GE Healthcare). After the last column the final product appeared as a single band on SDS-PAGE gel with an apparent mass of ~14 kDa and showed an UV/Vis spectrum with  $Abs_{628\text{ nm}}/Abs_{280\text{ nm}}$  ratio of ~0.57 which indicated full loading of the copper site(20). Labeling and FCS experiments on Cu azurin will be discussed in Chapter 4.

### ***3.2.2 Characterization and labeling of Zinc-Azurin***

Unless stated otherwise, chemicals were purchased from Sigma-Aldrich (Sigma-Aldrich Corp., St. Louis, USA) and used as received. Labeling experiments on ZnAzu with stoichiometric concentrations of the active form of ATTO655 dye was performed as previously described (4)(23). The labeling reactions produced a sample containing a variety of products in which the label is attached to the surface exposed Lysines as well as to the N-terminus.

### ***3.2.3 Purification of labeled species and characterization***

To obtain a homogeneous 100% singly labeled sample from the labeling solution, ion exchange chromatography (IEC) of the labeled protein was performed following the protocol mentioned earlier(24). Fig. 3.2A shows a chromatogram of the products of the labeling reaction of ZnAzu with ATTO655 dye, where each peak corresponds to a different species. The

chromatogram shows a similar elution profile as CuAzu (Chapter 4, Fig. 4.1). By analogy with CuAz (See Chapter 4), the peaks were analyzed as follows. Peak 1 corresponds with ZnAzu and the peaks 2-4 can be assigned to singly labeled species where peak 2 is N-terminally labeled ZnAzu (Nt-ZnAzu) and peak 3 corresponds to the protein labeled at Lysine122 position (K122-ZnAzu). The *protein:label* stoichiometry for each peak was determined from the extinction coefficients  $\epsilon_{\text{Azurin}}^{280} = 9.8 \text{ mM}^{-1}\text{cm}^{-1}$  and  $\epsilon_{\text{dye}}^{663} = 125 \text{ mM}^{-1}\text{cm}^{-1}$  by UV/Vis spectrometry. Peak 2-4 were found to be singly labeled species. Fig. 3.2B represents Zn azurin labeled with ATTO655 at the N-terminus. The absorption spectrum of a labeled ZnAzu has been displayed in Fig. 3.3A. To verify the switching behavior of the labeled molecules, fluorescence time courses were measured in the bulk following the methods described in Chapter 2. ZnAzu is diamagnetic and redox inactive. Consequently, when it was labeled with the ATTO655 dye, the samples didn't show any fluorescence switching upon addition of oxidant and reductant (Fig. 3.3B).

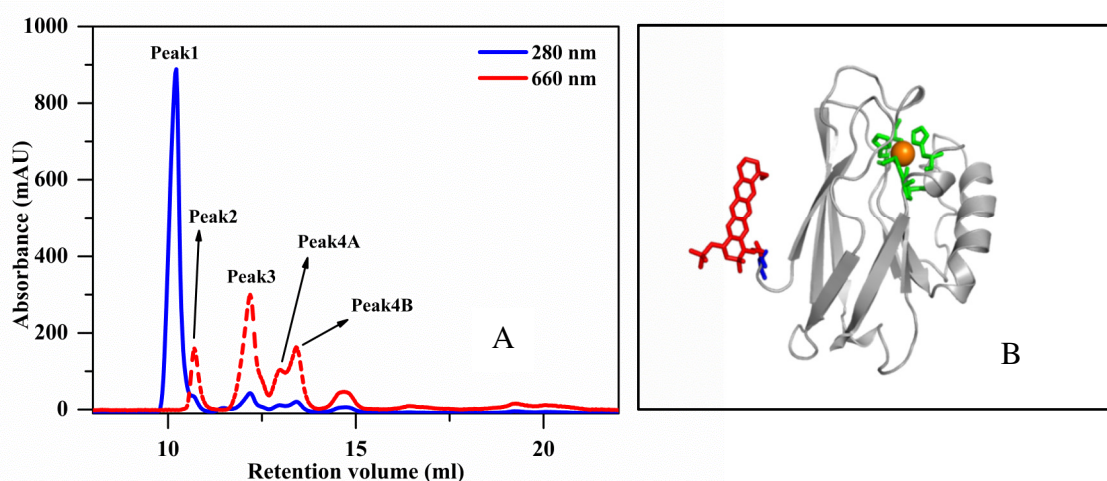


**Figure 3.2:** (A) Ion exchange chromatography of the mixture obtained after labeling ZnAzu with ATTO655. The chromatogram shows the elution pattern with monitoring two wavelengths: 280 nm (blue line), characteristic absorption of the protein; and 660 nm (red line), characteristic absorption of the label. This elution is performed in 5 mM Tris, pH 8.5 with a salt gradient of 0-80 mM. The peaks have been assigned to identify the corresponding species throughout the text. (B) Schematic representation of azurin labeled with ATTO655 at the N-terminus (Nt-ZnAzu).



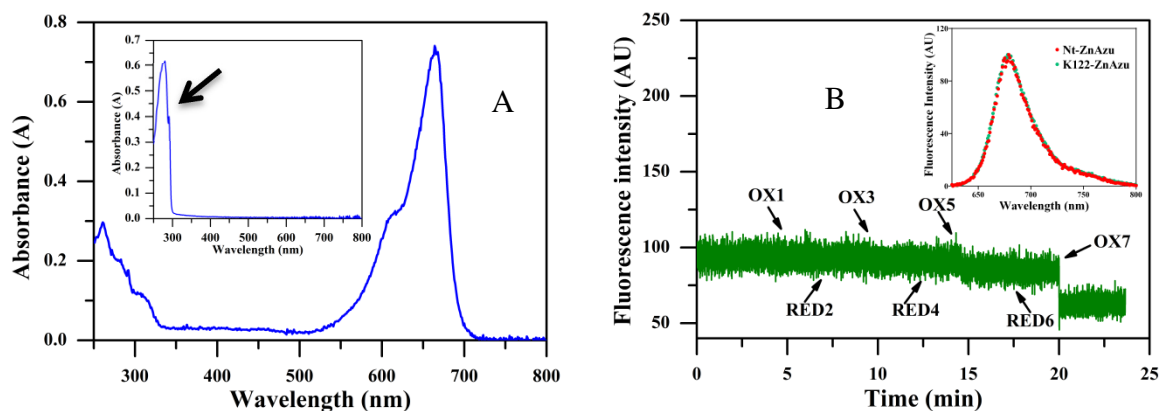


**Figure 3.3:** (A) The blue curve presents the optical absorption spectrum of 6  $\mu\text{M}$  solution of K122-ZnAzu labeled with ATTO655 in 20 mM HEPES pH 7.0 at room temperature. The UV/Vis spectrum of a 60  $\mu\text{M}$  solution of ZnAzu in 20 mM HEPES pH 7.0 has been presented in the inset. A shoulder (black arrow) at 291 nm is the signature of the single tryptophan in azurin. (B) Fluorescence switching experiment performed on 50 nM solution of ATTO655 labeled K122-ZnAzu in 20 mM HEPES pH 7.0 at room temperature. The green trace shows the fluorescence emission at 684 nm, upon excitation at 663 nm. The arrows indicate when the chemicals were added: OX stands for the addition of oxidizing agent [Hexacyanoferrate (III)], and RED stands for the addition of reductant (Ascorbate). The OX1, OX3, OX5 and OX7 correspond to the addition of 0.05, 1, 6, and 18 mM (final concentrations) of potassium hexacyanoferrate (III) to the sample, respectively. The time points RED2, RED4, and RED 6 correspond to the addition of 0.25, 1.5, and 4.5 mM of sodium ascorbate (final concentrations) respectively. No switching was observed as expected (See text). The fluorescence trace drops after the last addition of oxidant: this is due to the dilution effect. Fluorescence spectra of 50 nM solution of Nt-ZnAzu and of K122-ZnAzu are presented in the inset of Panel B.

### 3.2.4 Sample preparation for FCS experiments

FCS measurements on labeled azurin samples were performed in aqueous sucrose solution. The preparation of stock sucrose solution (75 % w/v) has been described in Chapter 2. For each measurement, a fresh sample solution was prepared by mixing 372  $\mu\text{l}$  of the sucrose stock solution with 4  $\mu\text{l}$  of bovine serum albumin (BSA) stock solution (10 mg/ml), 4  $\mu\text{l}$  of a 100 nM azurin stock solution and between 10 and 20  $\mu\text{l}$  of 2 or 20 mM freshly prepared stock solutions of ascorbate or hexacyanoferrate(II) or (III) as redox agents. The sample was adjusted to 400  $\mu\text{l}$  by admixture ( $\leq 20 \mu\text{l}$ ) of 100 mM HEPES buffer, pH 7.0. The calculated sucrose content of the samples was 57% (w/w), corresponding to a viscosity of 37.5 cP at 22°C. The final sample concentration of labeled protein was around 0.4-0.8 nM. The aqueous sucrose

solutions mentioned in Table 3.1 (8, 17, 35, 50, 60 % w/v) were prepared by using 320, 267, 187, 91, 43  $\mu\text{l}$  of stock sucrose solution (75% w/v) respectively. Then the solutions were adjusted to 400  $\mu\text{l}$  by admixture of BSA, azurin and 100 mM HEPES buffer pH 7.0 as described previously.

In the absence of BSA, the amplitude of the FCS curve [ $G(0)$ ] varied strongly depending on the added amount of chemicals like ascorbate or hexacyanoferrate. We suspect that azurin adsorbed at the glass surface (partly) desorbed upon changing the ionic strength or the redox conditions of the solution. This incident was not further investigated. The admixture of BSA reduced the effect presumably because the BSA covered the glass surface thus preventing adsorption of the azurin. An example of the effect of BSA on the FCS measurements is shown in Fig. 3.4. The amount of sample used for each measurement was 80  $\mu\text{l}$ .

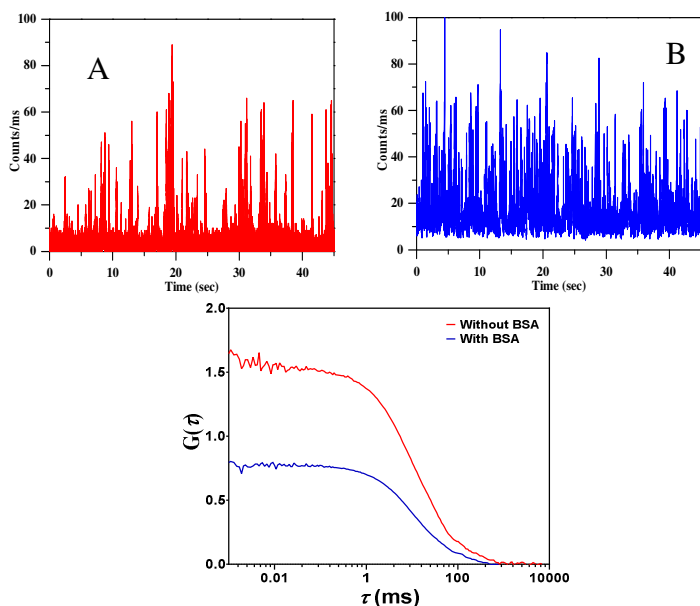


**Figure 3.4:** Illustration of the effect of addition of BSA on the FCS of a 10 nM solution of azurin labeled at position K122 by ATTO655 in 57% (w/w) sucrose solution. The upper panels show the count rate as a function of time in the absence (A) and in the presence (B) of 10 mg/ml BSA. The lower panel shows the effect on the autocorrelation function: in the absence of BSA the value of  $G(0)$ , which is inversely proportional to the concentration of the labeled protein, is greater than in the presence of BSA.

### 3.3 Results

#### 3.3.1 Diffusion of labeled Zinc-Azurin in sucrose solutions

To investigate the effects viscosity on the molecular diffusion, the translational diffusion times were determined by FCS for labeled ZnAzu at different sucrose concentrations in the absence of any redox chemicals. N-terminally labeled ZnAzu was chosen for this measurement, and the concentration of the labeled protein was kept at 1 nM. Seven different sucrose concentrations were used: 0, 8, 17, 35, 50, 60, 70% (w/v). For each measurement, 6 to 10 minutes of data acquisition time were required depending on the conditions of the experiments, and all the measurements were performed at room temperature (295 K).

Fig. 3.5 displays the autocorrelation function of a labeled sample in 57% w/v (70% w/v) sucrose solutions. The experiment was repeated for various sucrose concentrations. The results show that the diffusion time became longer with increase in sucrose concentrations from 0%w/w to 57% w/w. The diffusion times were found to be 200  $\mu$ s and 12 $\pm$ 2 ms in 0% w/v and 12 $\pm$ 2 ms in 57% w/w sucrose solution respectively. We fitted the measured correlation functions with the following FCS equations (For details, see also Chapter 1)

$$G(\tau) = G(0) * G_{diff}(\tau) \quad (3.1)$$

$$G(0) = \frac{1}{\langle N \rangle} = \frac{1}{c \cdot V_{eff} \cdot N_A} \quad (3.2)$$

$$G_{diff}(\tau) = \left(1 + \frac{\tau}{\tau_D}\right)^{-1} \cdot \left(1 + \frac{\tau}{k^2 \tau_D}\right)^{-1/2} \quad (3.3)$$

The instrument parameter  $k = 3.5$  obtained from the calibration experiments in Chapter 2 was used to fit all the autocorrelation curves (See Chapter 2). The fitting was performed in GraphPad Prism 5 (GraphPad Inc. USA) using a weighted least-square Levenberg-Marquardt method. The experimentally obtained diffusion times (Table 3.1) of labeled ZnAzu at various sucrose solutions have been used as a reference for the analysis of correlation curves for labeled CuAzu under redox conditions as a function of sucrose concentrations.

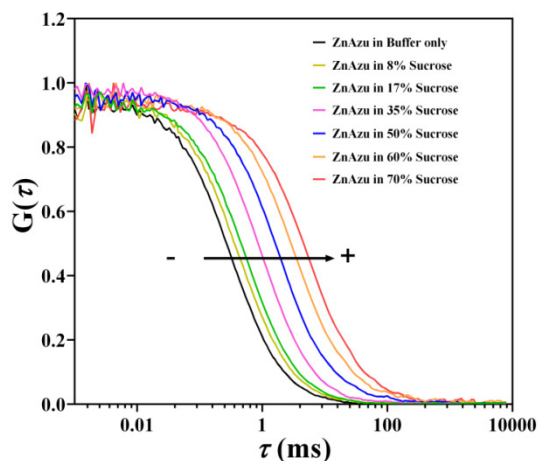


**Figure 3.5:** The autocorrelation curves for N-terminally labeled ZnAzu in buffer solutions with sucrose concentration (0, 8, 17, 35, 50, 60, 70% w/v). The black arrow indicates the increase in sucrose concentrations.

Sucrose concentration (% w/v)	Sucrose composition (% w/w)(b)	Diffusion time ( $\tau_D$ ), ms
0	0	0.2±0.01
8	9.4	0.4±0.03
17	21.9	0.6±0.03
35	30.5	1.0±0.03
50	36.5	2.0±0.12
60	47.6	3.1±0.20
70	57.0	12±2.00

**Table 3.1:** Experimentally obtained diffusion times ( $\tau_D$ ) for N-terminally labeled ZnAzu in the absence of any redox chemicals. (b) Composition of the sucrose solutions according to the tables in the CRC Handbook of Chemistry and Physics relating composition to refractive index (ref(16) and “Chapter 2, Page 38”).

### 3.3.2 FCS experiments under redox conditions

Single-molecule FCS experiments were performed at room temperature (295 K) in 100 mM HEPES buffer pH 7.0. Redox conditions were controlled by the addition of potassium hexacyanoferrate(III) and hexacyanoferrate(II) or sodium ascorbate as oxidant and reductant respectively.

#### 3.3.2.1 N-terminally labeled ZnAzu (Nt-ZnAzu)

**Oxidizing conditions:** Fluorescence time traces were recorded of 0.5-1 nM solutions of N-terminally ATTO655 labeled ZnAz in 57% w/w (70% w/v) sucrose in the presence of varying amounts (0-500  $\mu\text{M}$ ) of the oxidant potassium hexacyanoferrate(III). For each time trace the autocorrelation function was calculated. An example is shown for 50  $\mu\text{M}$  hexacyanoferrate(III) in Fig. 3.6. It appears that application of Eqn. 3.1 provides excellent fits of the data. The diffusion correlation time  $\tau_D$  obtained from the fitting of all FCS curves (0-500  $\mu\text{M}$ ) is found to be independent of the  $\text{K}_3\text{Fe}(\text{CN})_6$  concentration (inset of Fig. 3.6).

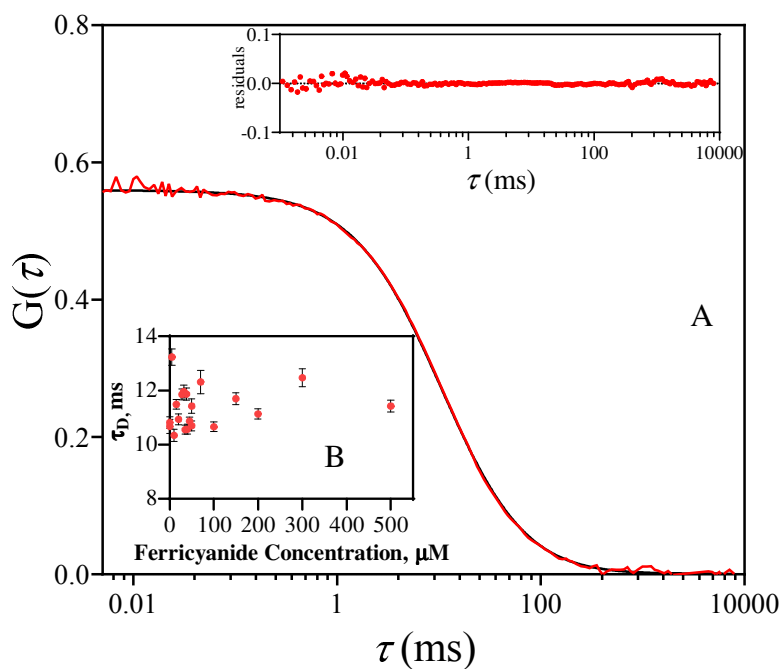


**Figure 3.6:** (A) Experimentally observed ACF of 1 nM ZnAzu labeled at the N-terminus with ATTO655 in 70 % (w/v) aqueous sucrose solution of 20 mM HEPES pH 7.0 at room temperature. The sample contained 50  $\mu\text{M}$  potassium hexacyanoferrate(III). The black line is a fit according to Eqn. 3.1 with  $G(\tau) = G(0) G_{\text{diff}}(\tau)$ . The inset on top shows the residuals of the fit. (B) Diffusion times observed at various concentrations of hexacyanoferrate(III) in 70 % (w/v) aqueous sucrose solution. Vertical bars denote 95% confidence intervals.

**Reducing conditions:** The observations are different when reducing conditions apply. Focusing on Nt-ZnAzu, the data obtained in the presence of freshly prepared potassium hexacyanoferrate(II) was fit with Eqn. 3.1 (only accounting for diffusion) (Fig. 3.7) and the residuals exhibited a noticeable non-random component and more importantly,  $\tau_D$  varied strongly with hexacyanoferrate(II) from 12 ms at 0  $\mu\text{M}$  hexacyanoferrate(II) to 2 ms at 500  $\mu\text{M}$  hexacyanoferrate(II) (Fig. 3.7 D). Since this observation physically makes no sense, the ACFs were fit with an equation containing a diffusion term and a single blinking term ( $G(\tau) = G(0) G_{diff}(\tau) G_I(\tau)$ ) (Eqn. 3.4) with the diffusion correlation time fixed at  $\tau_D = 12$  ms,

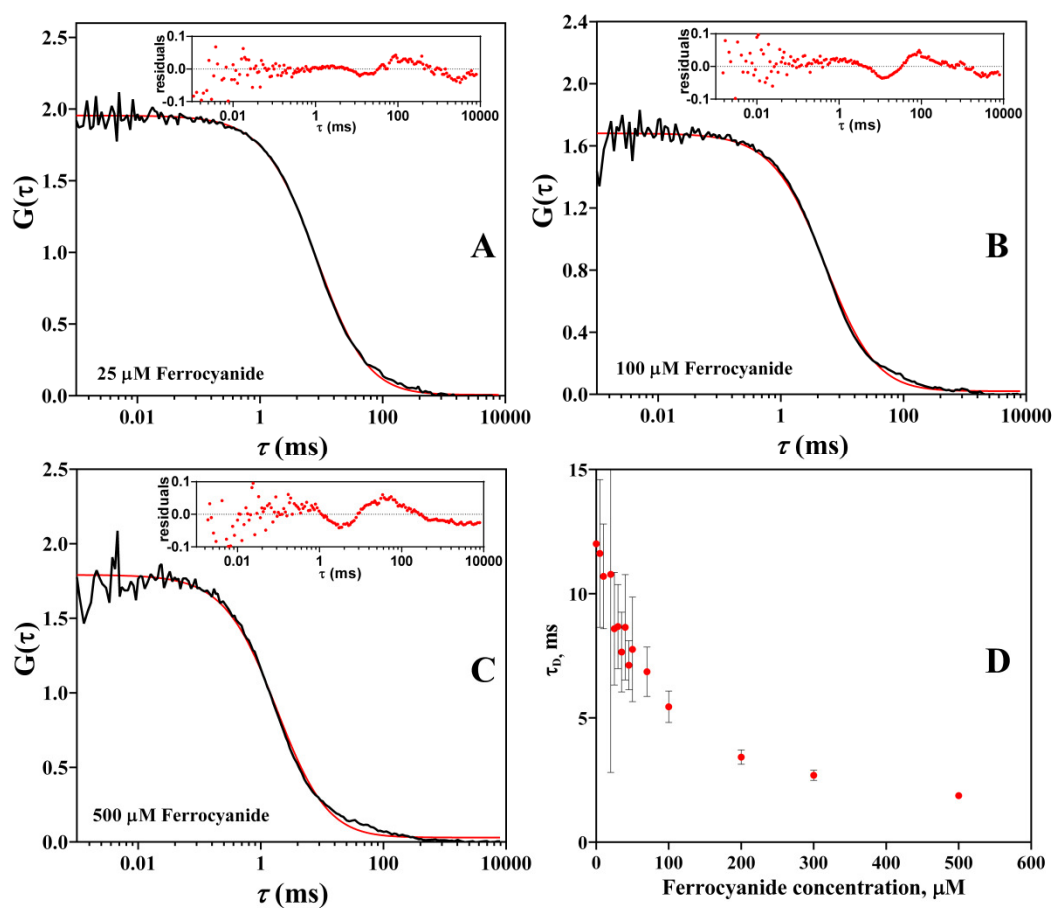


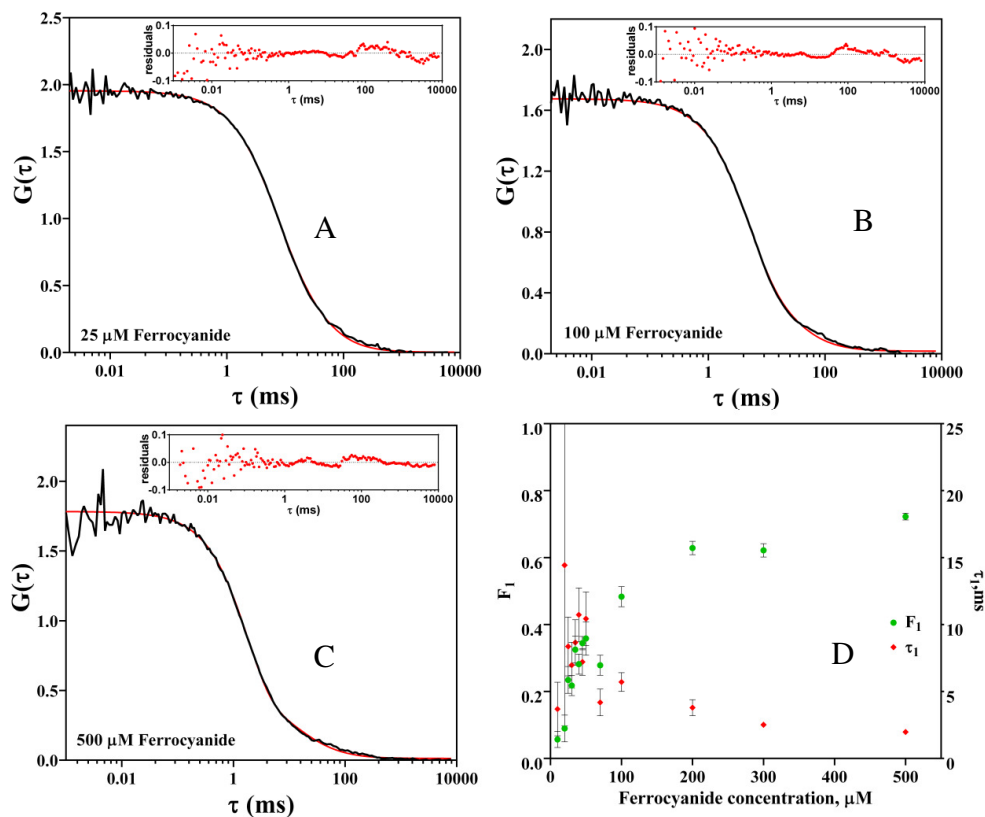
**Figure 3.7:** Experimentally observed ACFs of Zn azurin labeled at the N-terminus with ATTO655 for samples containing 25 (A), 100 (B) and 500  $\mu\text{M}$  (C) potassium hexacyanoferrate(II) (top to bottom). The red lines are fits according to Eqn. 3.1 with  $G(\tau) = G(0) G_{diff}(\tau)$ . The insets show the residuals of the fits. (D) Diffusion time derived from the fits for various concentrations of hexacyanoferrate(II).

where  $G_I(\tau)$  relates to zero-order reactions such as fluorophore blinking or a deprotonation

reaction;  $F_I$  is the fraction of molecules associated with such process, and  $\tau_I$  is the relaxation time required for that reaction. Satisfactory fits were obtained now and  $\tau_I$  and  $F_I$  can be extracted from the fitting of the FCS curves. These parameters were found to vary with reductant concentration. Fig. 3.8 displays the fitting and the residuals of FCS curves under 25, 100 and 500  $\mu\text{M}$  hexacyanoferrate (II) using the FCS equation containing a blinking term as follows

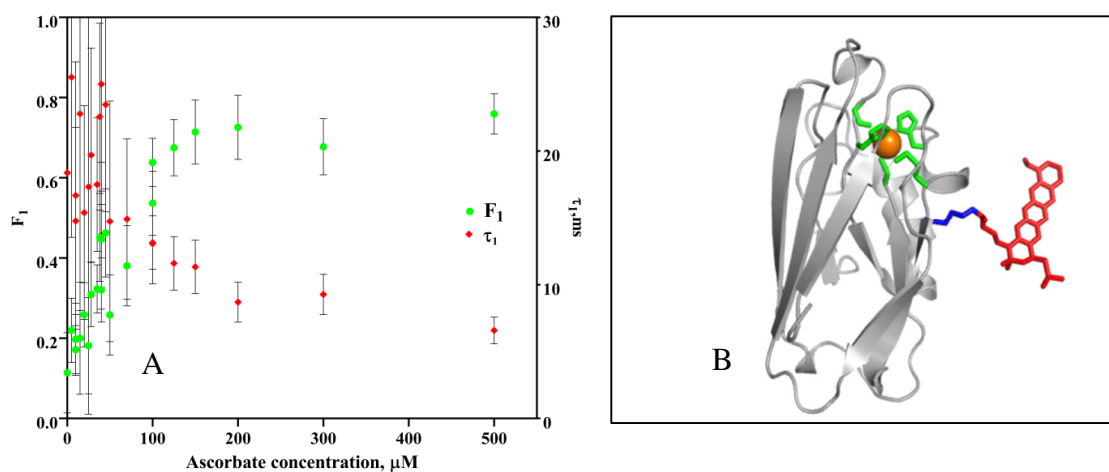
$$G(\tau) = G(0)G_{diff}(\tau)G_I(\tau) \quad (3.4)$$

$$G_I(\tau) = \frac{(1 - F_I + F_I e^{-\tau/\tau_I})}{(1 - F_I)} \quad (3.5)$$



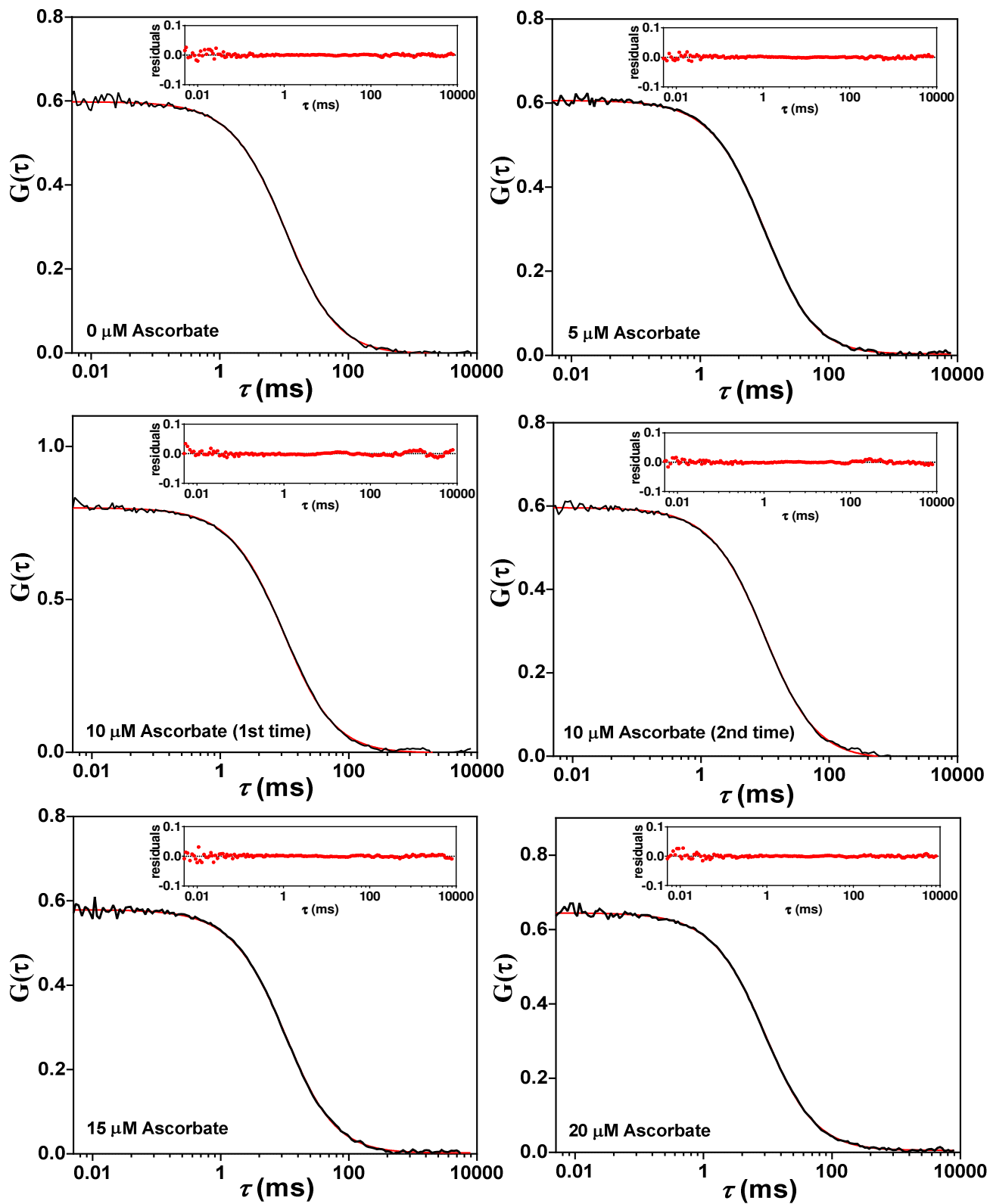
**Figure 3.8:** Experimentally observed ACFs of Zn azurin labeled at the N-terminus with ATTO655 for samples containing 25 (A), 100 (B) and 500 (C)  $\mu\text{M}$  potassium hexacyanoferrate(II). The red lines are fits according to Eqn. 3.4 with  $G(\tau) = G(0) G_{diff}(\tau) G_I(\tau)$  and  $\tau_D = 12$  ms. The insets show the residuals of the fits. (D) Parameters obtained from the fits. The red squares and green circles show the values for  $\tau_I$  and  $F_I$ , and correspond with the left and right y-axis, respectively. Vertical bars denote confidence intervals.

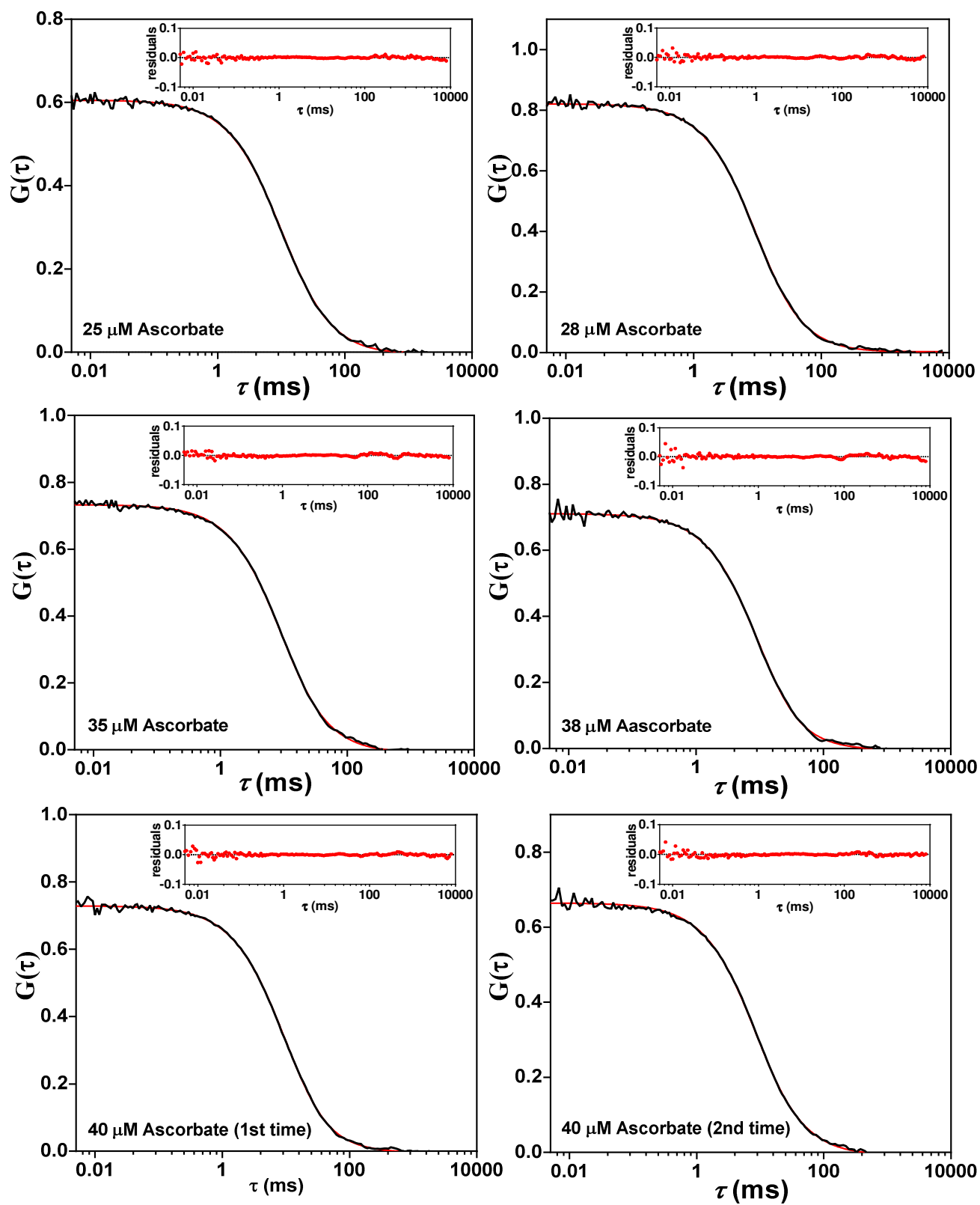
Similar experiments were performed with ascorbate as a reductant instead of potassium hexacyanoferrate(II). Again,  $\tau_1$  and  $F_1$  showed a significant variation when plotted against various ascorbate concentrations (Fig. 3.9). The confidence intervals displayed in Fig. 3.9 show that in the lower reductant concentration range (0-50  $\mu\text{M}$ ) the experimental uncertainty is considerable, which is a general observation for almost all data sets acquired in this study. Fitting of the ACFs and their residual plots for Nt-ZnAzu under reducing conditions (0-500  $\mu\text{M}$  ascorbate) are shown in Fig. 3.10.

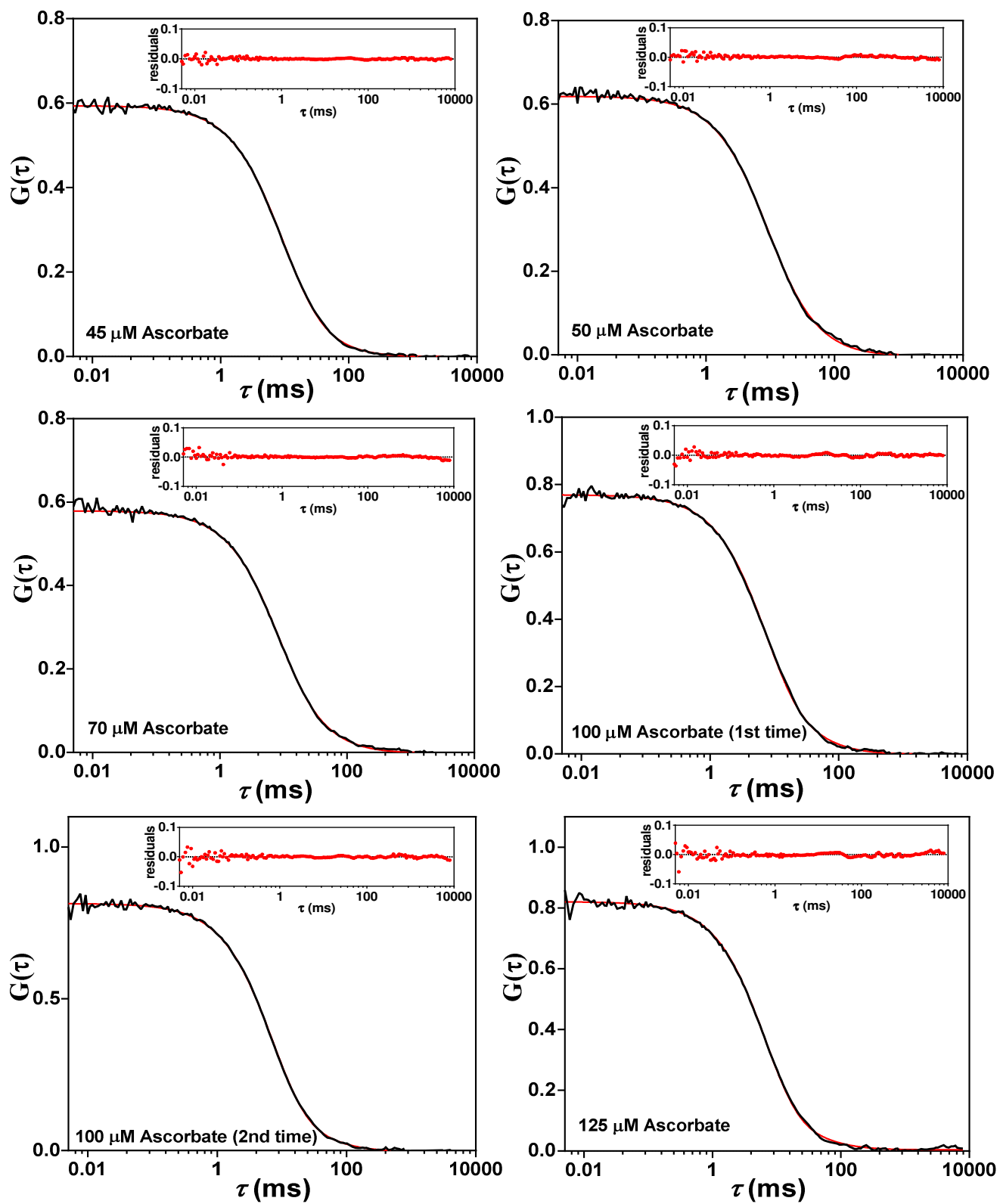


**Figure 3.9:** (A) Parameters obtained from the fits from the ACFs of Zn azurin labeled at the N-terminus with ATTO655 under 0-500  $\mu\text{M}$  ascorbate. The red squares and green circles show the values for  $\tau_1$  and  $F_1$ , and correspond with the left and right y-axis, respectively. Vertical bars denote confidence intervals. (B) A model representing azurin labeled with ATTO655 at position K122.









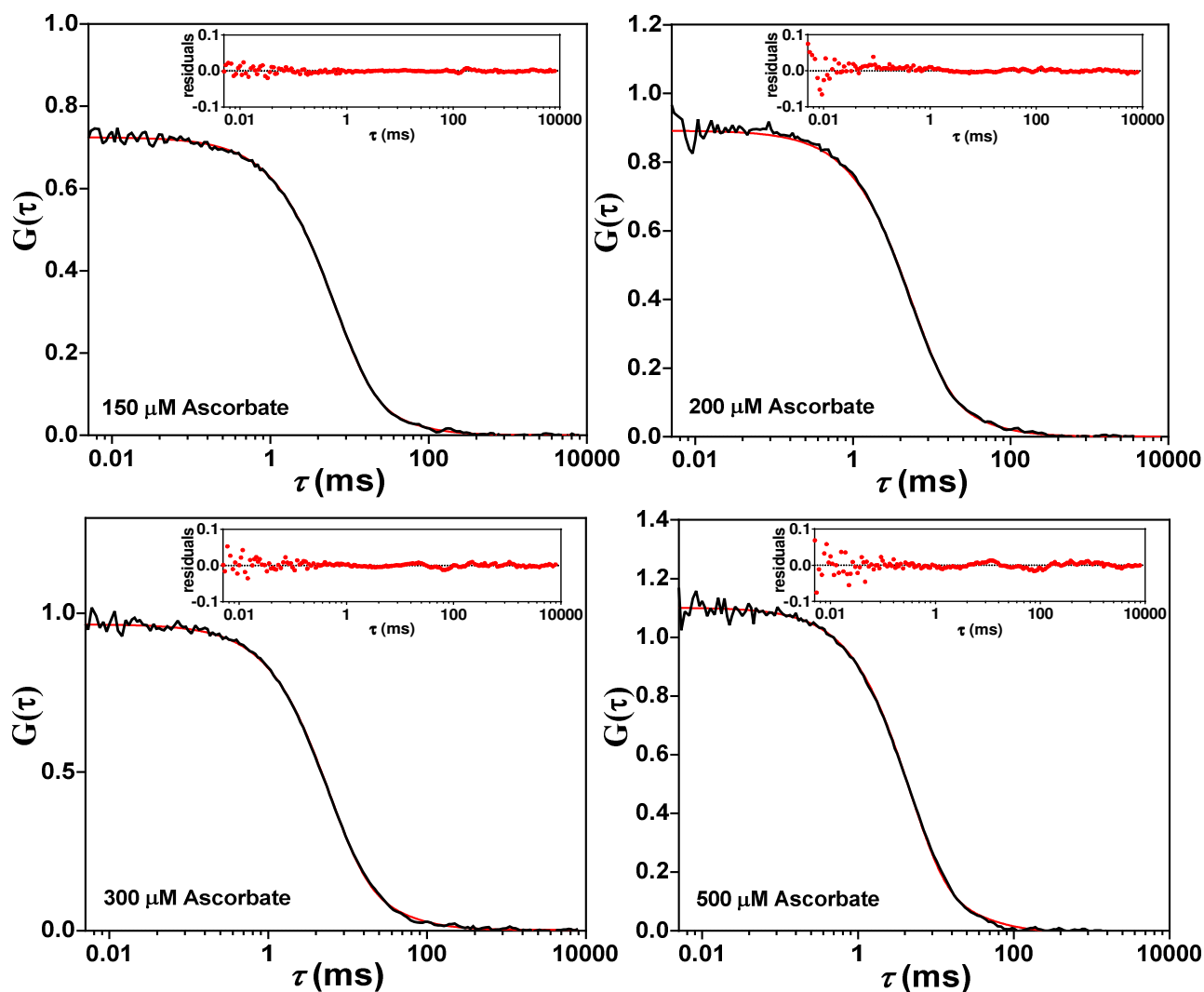
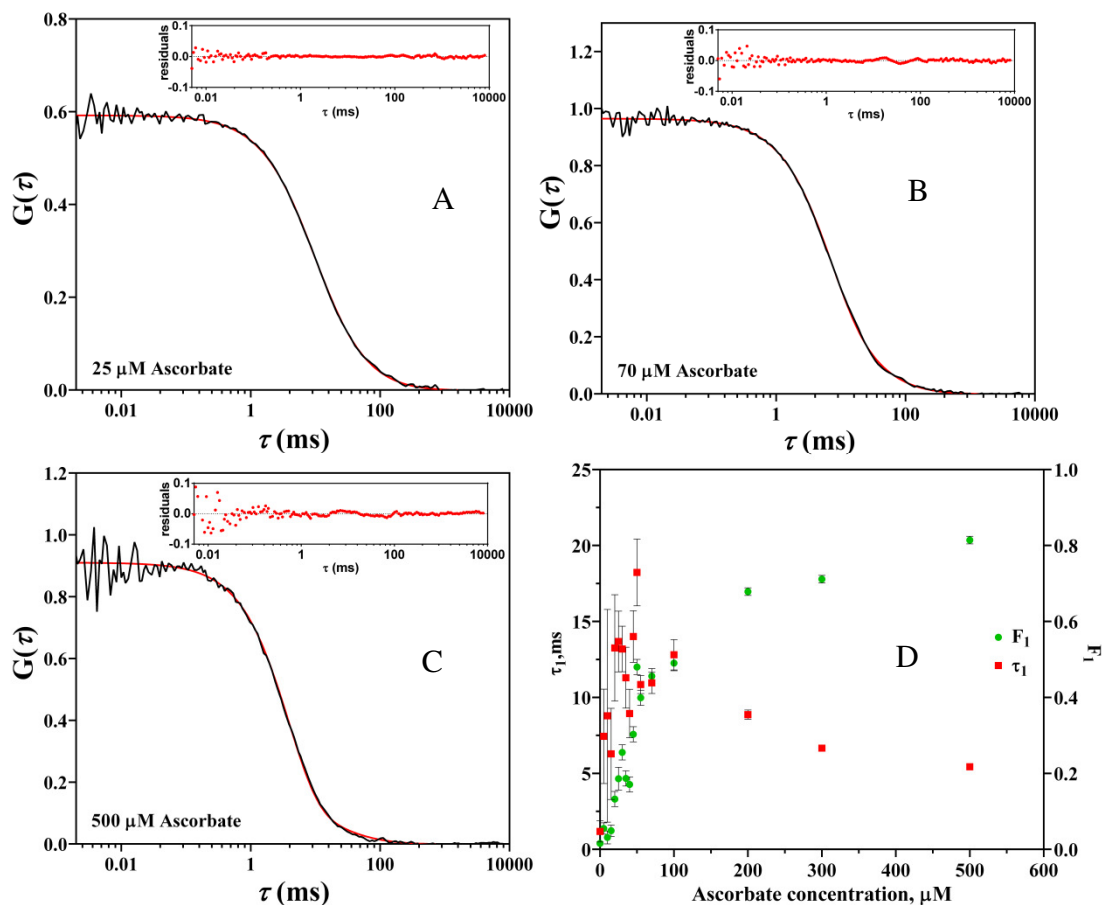


**Figure 3.10:** FCS curves and residual plots for N-terminally labeled ZnAz under reducing conditions (0-500  $\mu\text{M}$  ascorbate). The red lines are fits according to Eqn. 3.4 with  $G(\tau) = G(0) G_{\text{diff}}(\tau) G_I(\tau)$  and  $\tau_D = 12$  ms.

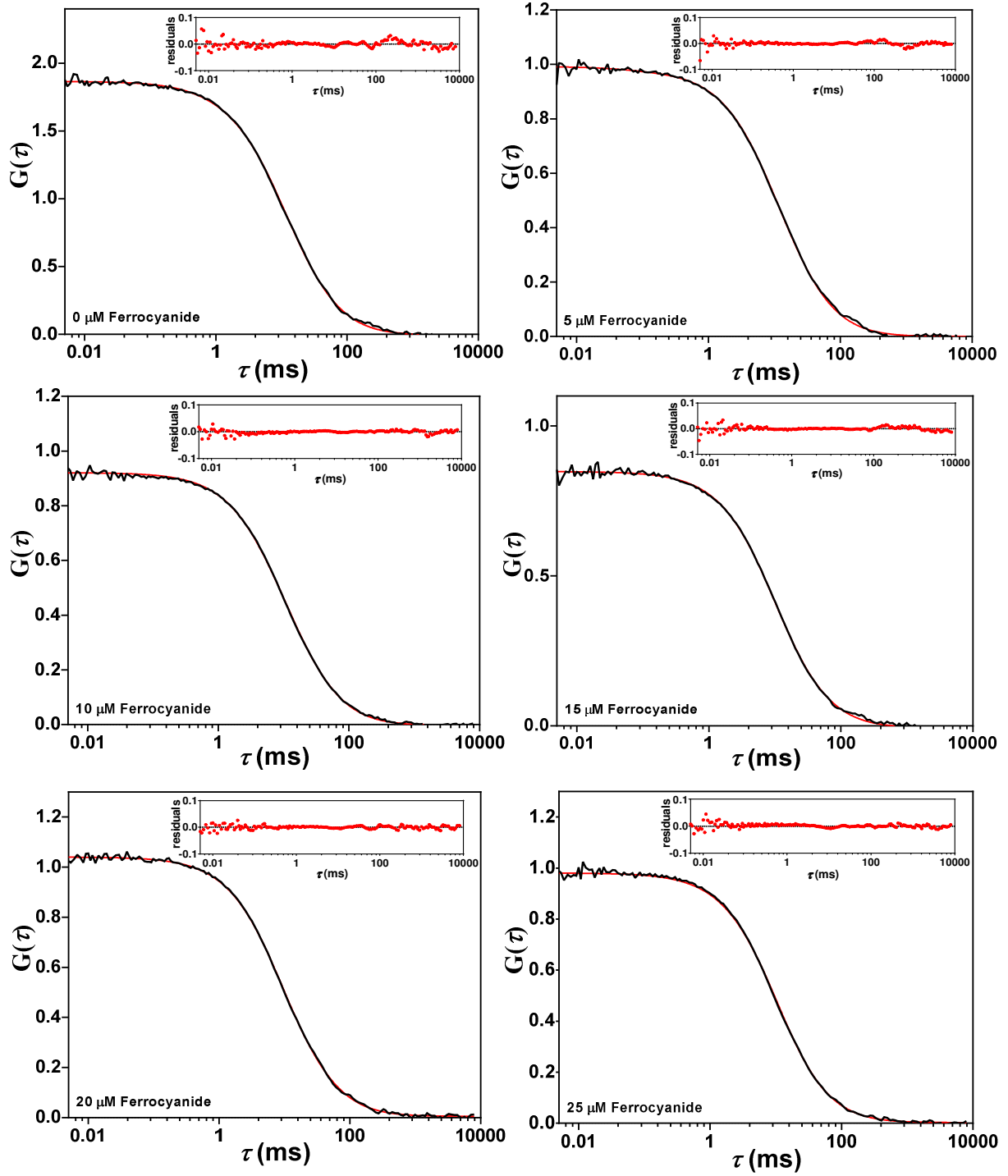
### 3.3.2.2 K122 labeled ZnAz (K122-ZnAz)

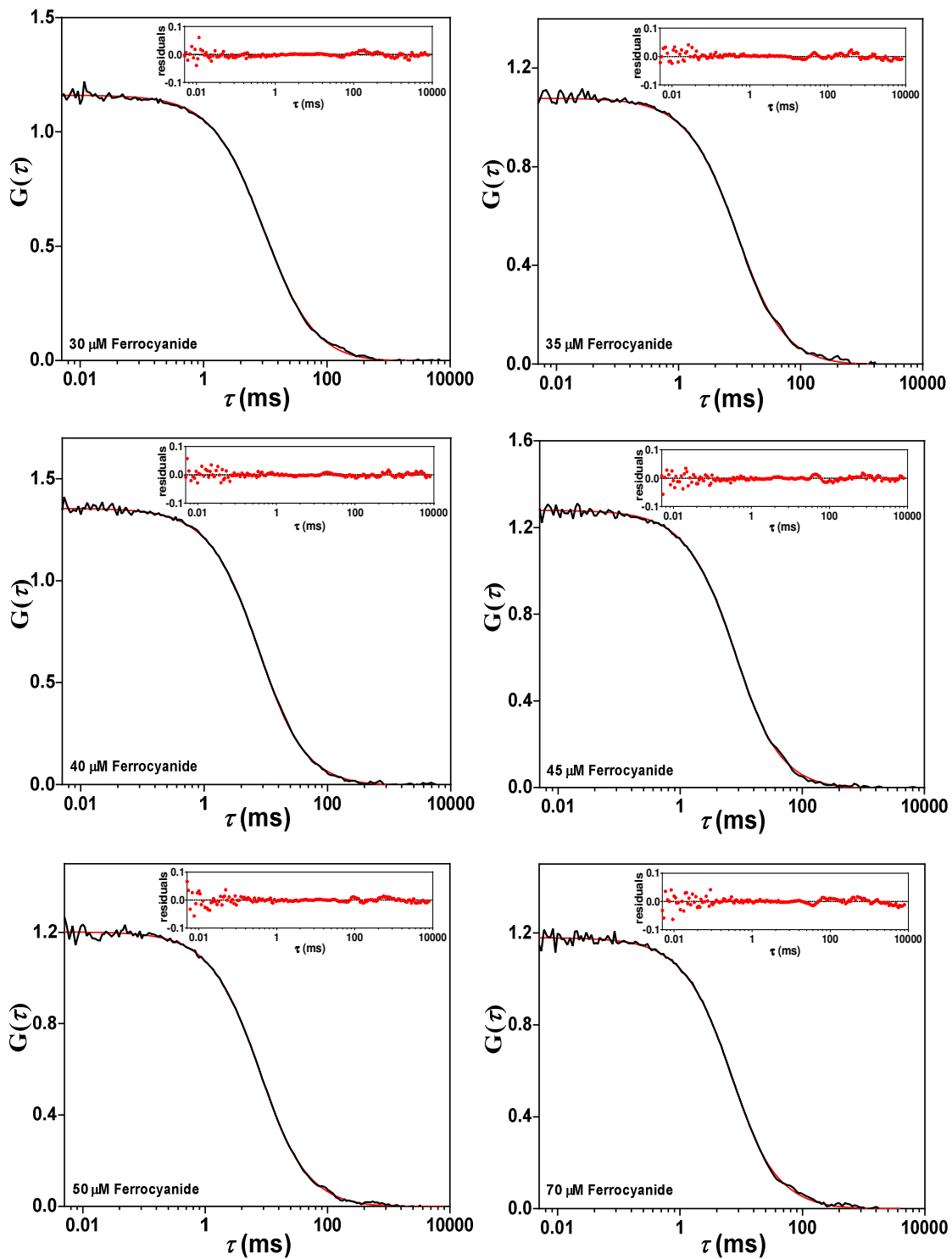
The experiments were repeated with ZnAz labeled at position 122. The results did not differ from what was observed for N-terminally labeled azurin. With hexacyanoferrate(III) as an oxidant, the autocorrelation functions could be well fit with a single diffusion term resulting in values for the diffusion correlation time between 12 and 14 ms with an average of  $12.8 \pm 0.5$  ms (Data presented in section 3.3.3). Under reducing conditions [hexacyanoferrate(II) or ascorbate] fitting with only a diffusion term resulted in values for  $\tau_D$  that strongly varied with reductant concentration, but inclusion of a blinking term and use of a constant  $\tau_D$  of 12 ms resulted in good

fits and values for  $\tau_1$  and  $F_1$  that, again, depended on reductant concentration. The best fit of all correlation curves with their residuals is displayed in Fig. 3.11 and 3.12.



**Figure 3.11:** Experimentally observed ACFs of Zn azurin labeled at the Lysine122 position with ATTO655 for samples containing 25 (A), 70 (B) and 500 (C)  $\mu\text{M}$  potassium hexacyanoferrate(II). The red lines are fits according to Eqn. 3.4 with  $G(\tau) = G(0)G_{\text{diff}}(\tau)G_1(\tau)$  and  $\tau_D = 12$  ms. The insets show the residuals of the fits. (D) Parameters obtained from the fits. The red squares and green circles show the values for  $\tau_1$  and  $F_1$ , and correspond with the left and right y-axis, respectively. Vertical bars denote 95% confidence intervals.





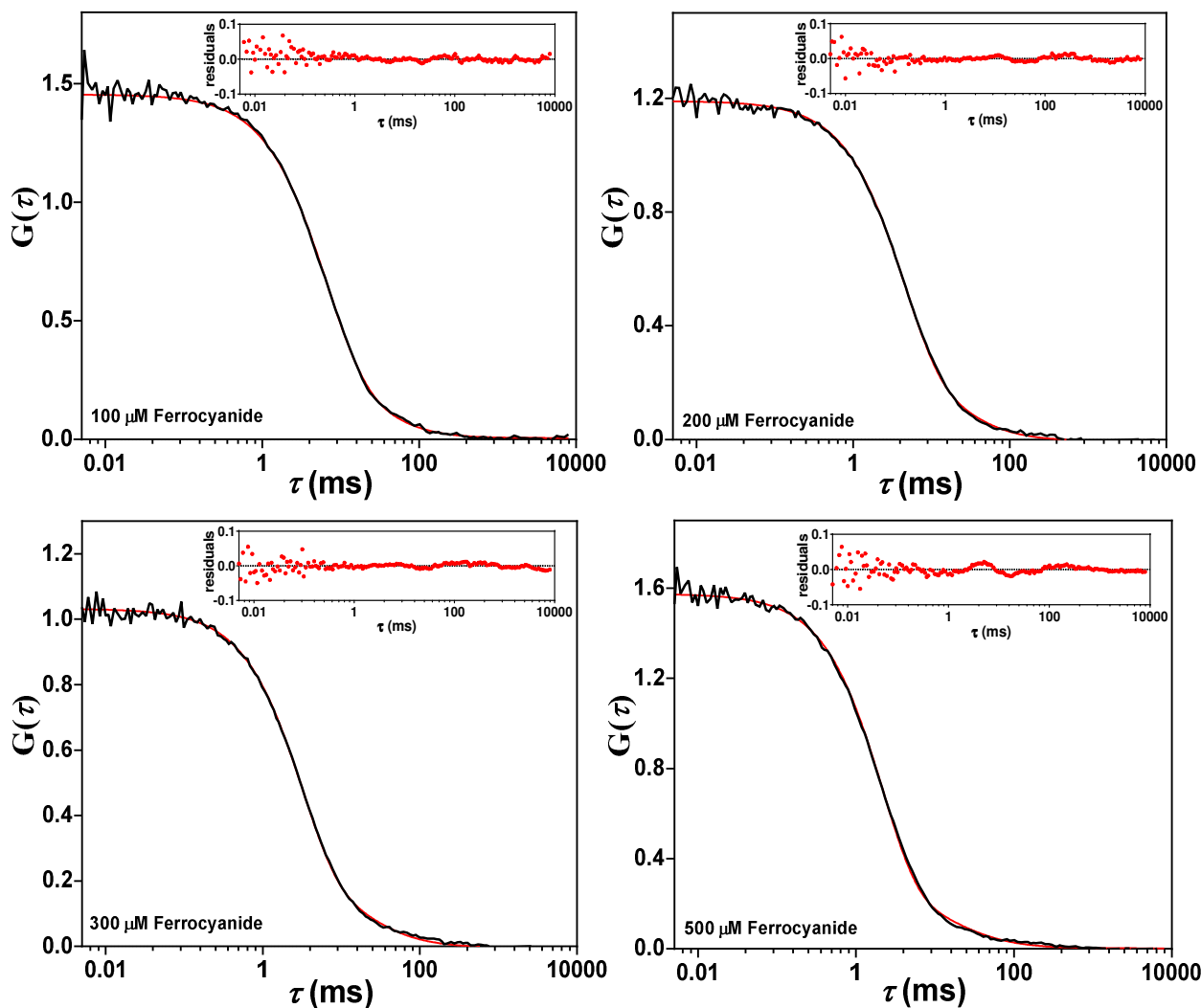


**Figure 3.12:** FCS curves and residual plots for K122 labeled ZnAz under reducing conditions [0-500  $\mu\text{M}$  potassium hexacyanoferrate (II)]. The red lines are fits according to Eqn. 3.4 with  $G(\tau) = G(0) G_{\text{diff}}(\tau) G_I(\tau)$  and  $\tau_D = 12$  ms.

### 3.4 Discussion

As ZnAz is an inactive species, only the reactions of the label with oxidants or reductants in the solution can be investigated utilizing FCS.

#### Redox kinetics

**Oxidizing conditions:** Under purely oxidizing conditions no redox kinetics could be noticed in the FCS curves of the labeled azurin (Nt-ZnAz and K122-ZnAz). The data obtained on the N-terminally labeled ZnAz provides a good example. Satisfactory fits of the autocorrelation traces could be obtained by using only a diffusion term in the expression for the ACF. An average  $\tau_D$  of



11.3  $\pm$ 0.6 ms was obtained. This value is a good agreement with the diffusion time of labeled ZnAz mentioned previously (12 $\pm$ 2 ms, page 76), considering the crudeness of the model used for the prediction. Clearly, at the hexacyanoferrate(III) concentrations used in this study, the label is not affected by the added oxidant. Moreover, in the FCS curves there is no sign of a photoinduced electron transfer (PET) reaction between the label and any amino side chains of the protein. Fluorescence switching experiments did not show any effect of oxidizing or reducing agents on the dye (Fig. 3.3B). The results obtained from FCS experiments, indicates that oxidizing conditions do not influence the label at the oxidant concentrations used for the single molecule experiments presented here. For Lys122 labeled ZnAz, the plot of  $\tau_D$  as a function of hexacyanoferrate(III) is shown in Fig. 3.13 F, and the measured FCS curves with their residual plots have also been displayed in the following Fig. 3.13 (A-E). As similar behaviour was observed for Lys122-labeled species under oxidizing condition, it has not been further discussed.

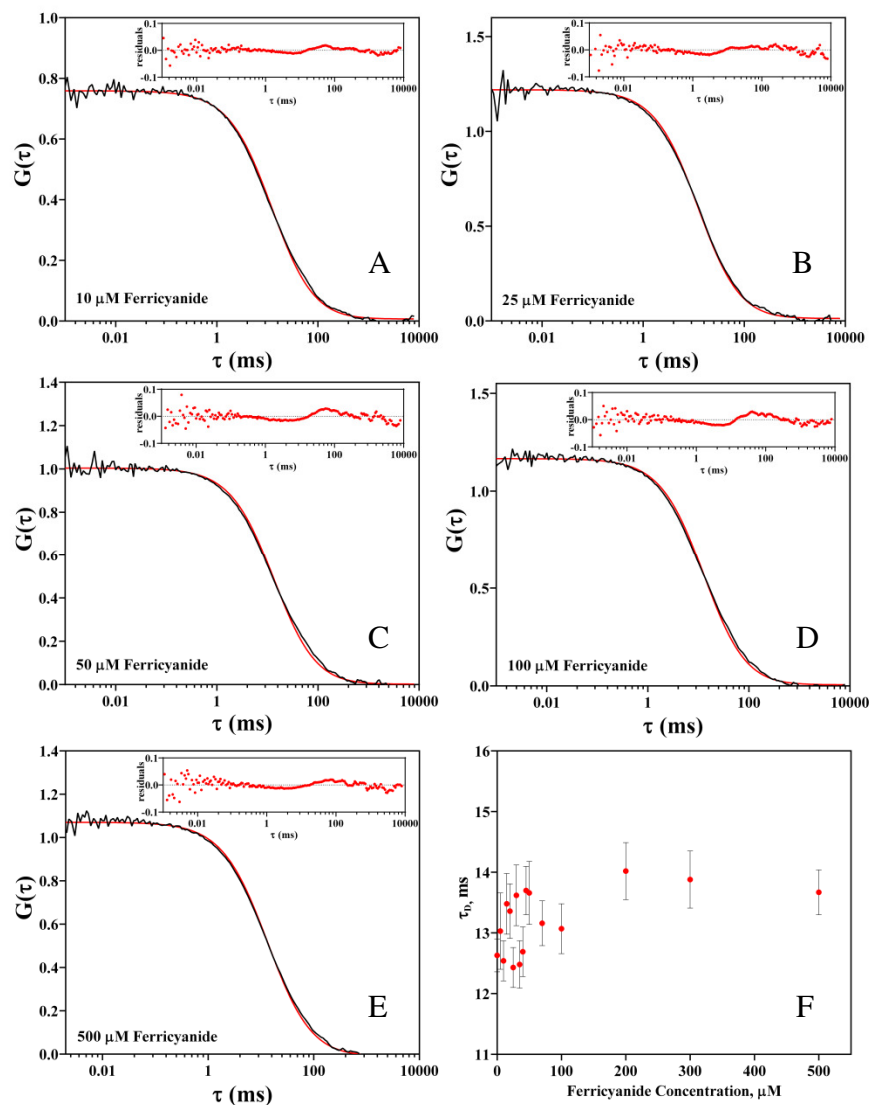


**Figure 3.13:** Experimentally observed ACFs of Zn azurin labeled at the Lysine122 position with ATTO655 for samples containing 10 (A), 25 (B), 50 (C), 100 (D) and 500 (E)  $\mu\text{M}$  potassium hexacyanoferrate(III). The red lines are fits according to Eqn. 3.1 with  $G(\tau) = G(0) G_{\text{diff}}(\tau)$ . The insets show the residuals of the fits. (F) Diffusion time derived from the fits for various concentrations of hexacyanoferrate(III). Vertical bars denote confidence intervals.

**Reducing conditions:** Under reducing conditions the situation is different for both Nt-ZnAzu and K122-ZnAzu. A blinking term,  $G_1(\tau)$ , had to be introduced in the expression for the correlation function to obtain satisfactory fits of the FCS curves (Eqn. 3.4). Few examples are displayed again for K122-ZnAzu under reducing conditions (Fig. 3.14: ascorbate). The variation in

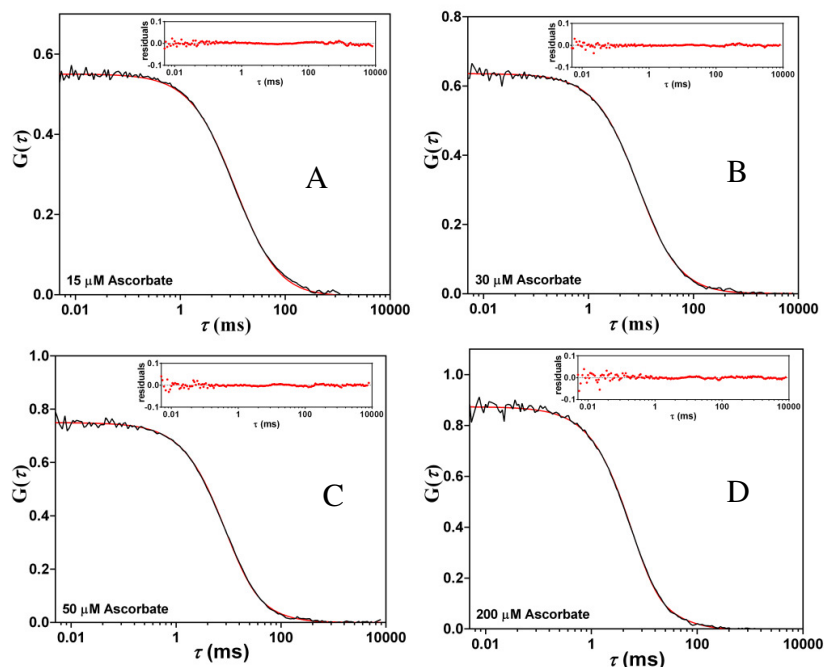
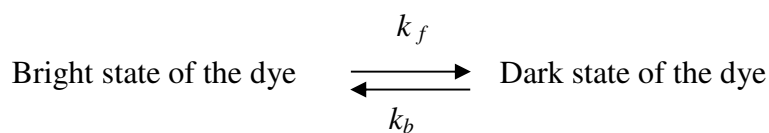


**Figure 3.14:** FCS curves and residual plots for K122 labeled ZnAzu under reducing conditions 15 (A), 30 (B), 50 (C) and 200 (D)  $\mu\text{M}$  ascorbate. The red lines are fits according to Eqn. 3.4 with  $G(\tau) = G(0) G_{diff}(\tau) G_I(\tau)$  with  $\tau_D = 12$  ms.

$F_1$  and  $\tau_1$  was analyzed by assuming that the label undergoes reversible transitions between bright and dark states with rate constants  $k_f$  for the transition from bright to dark and  $k_b$  for the reverse transition, i.e., the presence of ascorbate or hexacyanoferrate(II) induced blinking of ATTO655 in the solution. Expressions for  $F_1$  and  $\tau_1$  in terms of  $k_f$  and  $k_b$  are (Scheme 3.1)



$$F_1 = \frac{k_f}{k_f + k_b}$$

$$\tau_1 = (k_f + k_b)^{-1}$$

**Scheme 3.1:** Schematic representation of bright and dark states of the label. ATTO655 cycles between the bright and dark states under reducing conditions. The expressions of  $F_1$  and  $\tau_1$  as function of  $k_f$  and  $k_b$  are displayed.

The dependence of  $k_f = F_1/\tau_1$  and of  $k_b = (1-F_1)/\tau_1$  on reductant concentrations are shown in Fig. 3.15 and 3.16 for Nt-ZnAzu and K122-ZnAzu respectively. It is clear that  $k_f$  exhibits a linear dependence on reductant concentration; the corresponding reaction we ascribe to the one-electron reduction of the label by the reductant. The expression for  $k_f$  (25)(26);

$$k_f = k_r[R] \frac{k_{01}}{k_{10} + k_{01}} = k_r[R]f(I) \quad (3.6)$$

Here,  $k_r$  is the second-order rate constant for the reduction of the label,  $[R]$  is the concentration of reductant,  $k_{01} = \sigma I_{\text{exc}}$ , with  $\sigma$  the absorption cross section of the label at the wavelength of the laser and  $I_{\text{exc}}$  the laser power in terms of number of photons/sec  $\text{cm}^2$  and  $k_{10}$  is the decay rate of the excited state. The occurrence of the factor  $f(I)$  can be understood by considering that the optically excited label reacts with reductant in the solution on a timescale that is long compared with the excitation and fluorescence time scales ( $k_{01}^{-1}$  and  $k_{10}^{-1}$ ). The reaction can then be dealt with by a two-state scheme in which the reductant is in equilibrium with a pool of labels of which only the fraction in the excited state ( $f(I)$ ) is reactive. The slope of a graph of  $k_f$  vs.  $[R]$  (see Fig. 3.15 and 3.16 for Nt-ZnAzu and K122-ZnAzu respectively) provides a value of  $k_r f(I)$ . It amounts to  $7.8 \times 10^5 \text{ M}^{-1} \text{ s}^{-1}$  when hexacyanoferrate(II) and  $2.8 \times 10^5 \text{ M}^{-1} \text{ s}^{-1}$  when ascorbate was used as a reductant.

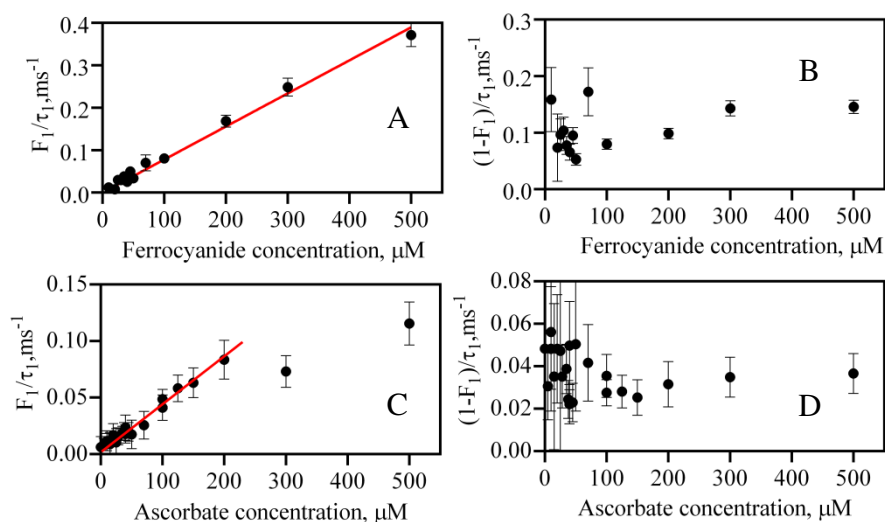


**Figure 3.15:** Plots of  $k_f = (F_1/\tau_1)$  and  $k_b = [(1-F_1)/\tau_1]$  against the reductant concentrations for N-terminally labeled ZnAzurin. The red lines are the fit and the vertical bars indicate 95% confidence intervals.

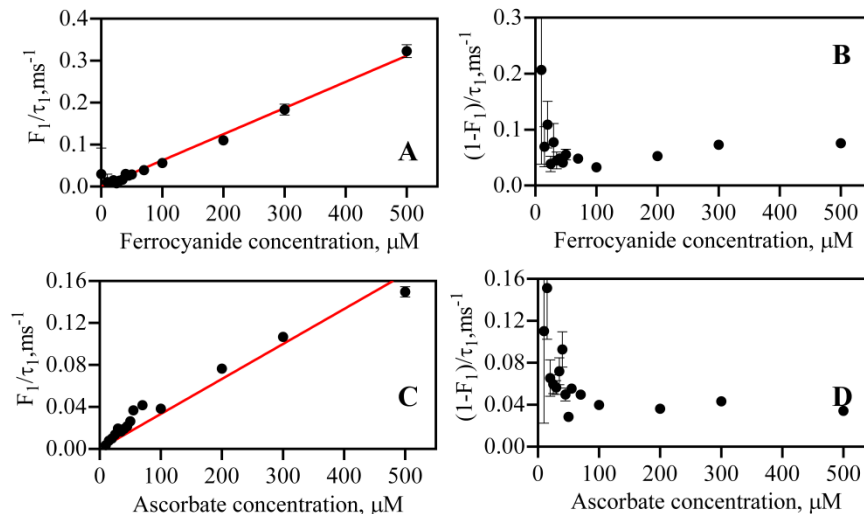


**Figure 3.16:** Variations of  $k_f (F_1/\tau_1)$  and  $k_b [(1-F_1)/\tau_1]$  as a function of reductant concentrations for Lys122 labeled ZnAzurin. The red lines are the fit and the vertical bars indicate 95% confidence intervals.

From the experimentally determined value of  $k_r f(I)$  a value of  $k_r$  can be extracted after an estimate of  $f(I)$  has been obtained. With a fluorescence lifetime of 2.7 ns (See Chapter 4, measured in sucrose solution), an incident light intensity of 4.3 kW/cm<sup>2</sup> at 636 nm and an absorbance cross-section of the label of  $1.3 \times 10^{-16}$  cm<sup>2</sup> (based on an estimated  $\epsilon_{636} = 8 \times 10^4$  M<sup>-1</sup>cm<sup>-1</sup>), one finds that  $\sigma I_{\text{exc}} = 1.80 \times 10^6$  s<sup>-1</sup> and  $f(I) = 4.8 \times 10^{-3}$ . Taking N-terminally labeled ZnAz reduced by hexacyanoferrate(II) as an example, with  $k_r f(I) = 7.8 \times 10^5$  M<sup>-1</sup>s<sup>-1</sup>, a value of  $k_r = 1.6 \times 10^8$  M<sup>-1</sup>s<sup>-1</sup> is obtained. Considering that the experiments were performed in 70% (w/v) (i.e. 57% w/w) sucrose solutions, this is of the order of a diffusion-controlled reaction rate. Table 3.2 represents the experimental values obtained for labeled ZnAzurin under oxidizing and reducing conditions. Table 3.3 displays the values of second order rate constants for this bimolecular interaction between the label and the redox chemicals in 70% (w/v) sucrose solution. The rates are smaller compared to diffusion controlled reaction in pure buffer ( $10^9$  M<sup>-1</sup>sec<sup>-1</sup>).

Intermolecular ET					
	Label at	$k_r f(I)^{(a)}, M^{-1} s^{-1}$	$k_r f(I)^{(b)}, M^{-1} s^{-1}$	$k_b^{(a)}, s^{-1}$	$k_b^{(b)}, s^{-1}$
ZnAzurin	N-terminus	$(7.8 \pm 0.2) \times 10^5$	$(2.8 \pm 0.2) \times 10^5$	$(6.0 \pm 0.4) \times 10^1$	$(4.0 \pm 0.2) \times 10^1$
	K122	$(6.2 \pm 0.3) \times 10^5$	$(3.3 \pm 0.1) \times 10^5$	$(10 \pm 0.9) \times 10^1$	$(7.5 \pm 0.8) \times 10^1$

**Table 3.2:** Experimental values of intermolecular ET rate constants: (a) Reductant: hexacyanoferrate(II) and (b) Reductant: ascorbate.

Label at	Reducing condition [Hexacyanoferrate(II)]	Reducing condition [Ascorbate]
<b>N-terminus</b>	$(1.6 \pm 0.04) \times 10^8$	$(5.8 \pm 0.4) \times 10^7$
<b>K122</b>	$(1.3 \pm 0.02) \times 10^8$	$(6.8 \pm 0.4) \times 10^7$

**Table 3.3:** Experimental values of second order rate constants ( $k_r$ ,  $M^{-1}sec^{-1}$ ) for the bimolecular reaction between the dye and the reductants.

In essence, such redox induced blinking is the result of the bimolecular reaction proceeding between the dye and the reductant in the sucrose solution. For labeled molecules in excited states, both oxidation and reduction reactions are possible: either an electron promoted to the LUMO is removed more easily so that the dark state has a lower oxidation potential than the ground state or the highest occupied molecular orbital when singly occupied, can accept an electron more easily than the ground state (Fig. 3.17). In the present case, the oxidant hexacyanoferrate(III) did not result in any blinking, but collisions of the excited fluorophore with electron donors e.g. ascorbate or hexacyanoferrate(II) easily led to the reduction, yielding radical ions. The radical ions stay in the stable dark states.

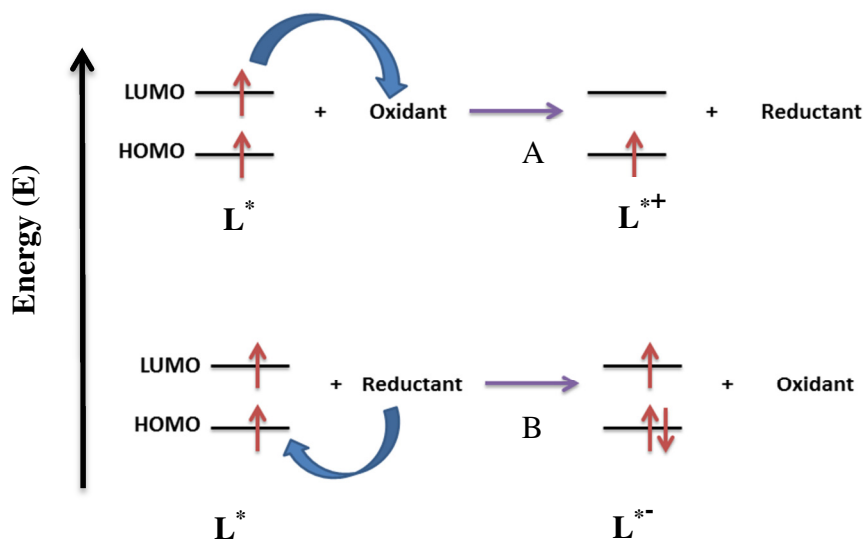
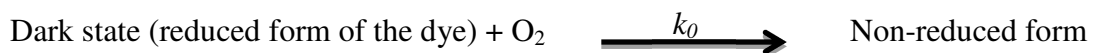


**Figure 3.17:** A simplified HOMO/LUMO energy level presentation of a labeled molecule.  $L^*$  represents the molecule in the excited state,  $L^{*+}$  represents the one electron oxidized state of the label and  $L^{*-}$  corresponds to the one electron reduced form of the label. (A): single electron removed from the LUMO by the oxidizing agent; (B): one electron is added to the HOMO of the label by the reductant.

There are non-absorbing fluorophores which are most likely long-lived radical ions. As for the oxidation of the reduced label back to the non-reduced form, the contribution of the blinking term  $G_1(\tau)$  to the autocorrelation function is small at low reductant concentrations and the spread in  $k_b$  (the back reaction) is relatively large (Fig. 3.15 B and D for Nt-ZnAz). These reactions are in microsecond up to millisecond time scale with concentration-dependent manner. It is clear that  $k_b$  does not vary systematically with the reductant concentration. Average values of  $k_b$  are listed in Table 3.2. That  $k_b$  appears to be constant is consistent with the idea that dissolved oxygen is responsible for the back oxidation of the label as oxygen is present in the solution in large excess and its concentration will not change appreciably over the duration of the experiment. When assuming that the reaction with oxygen is second order with rate  $k_o$ , one finds with  $k_b = 95 \text{ s}^{-1}$  (Fig. 3.15 B and Table 3.1) and  $[\text{O}_2] \approx 260 \text{ }\mu\text{M}$  (aerobic solution) that  $k_o = 3.6 \times 10^5 \text{ M}^{-1}\text{s}^{-1}$ . The diffusion controlled  $k_o$  can be well understood by  $k_d$  (see Chapter 2 for details). Reaction between the labeled protein and oxygen represents the bimolecular reaction between two reactants that is expected to take place with a diffusion-controlled rate constant  $k_d$  in most solvents. Since, the label is at the surface of the protein and flexible, it can move or rotate faster than the whole protein. Oxygen molecules rapidly diffuse and react with the labeled protein. In 57% w/w sucrose solution, the bimolecular reactions between them slow down.  $k_o$  is found to be one order of magnitude smaller than the predicted value of  $k_d$  for the present system ( $10^6 \text{ M}^{-1}\text{s}^{-1}$ ) in viscous solvent (see Chapter 2 for details), suggesting only fraction of the bimolecular encounters between the labeled protein and oxygen molecules give rise to successful oxidation of the reduced label. Reduced form of the dye is also known to have higher reduction potential than that of oxygen such that reaction with oxygen is insufficient(27). Similar behavior was observed for K122-labeled ZnAz (Fig. 3.16 B and Table 3.1).



### 3.5 Concluding remarks

In the present work a single-molecule based approach to the study of intermolecular electron-transfer processes in a labeled protein is presented. The time scale of intermolecular processes depends on the viscosity of the solution. Oxidizing conditions do not show any effect on the label, but reducing agents ascorbate and potassium hexacyanoferrate (II) affect markedly and the blinking processes are observed. The excited label does react with the redox active

components in the solution in a diffusion-controlled manner. Analysis of autocorrelation data produced rate constants for bimolecular reductive quenching of the excited dye by ascorbate and hexacyanoferrate(II). The diffusion rates were diminished by two orders of magnitude by increasing the viscosity.

### **References**

- (1) Goldsmith, R. H.; Tabares, L. C.; Kostrz, D.; Dennison, C.; Aartsma, T. J.; Canters, G. W.; Moerner, W. E. Redox cycling and kinetic analysis of single molecules of solution-phase nitrite reductase. *Proc. Natl. Acad. Sci. U. S. A.* **2011**, *108*, 17269–74.
- (2) Gustiananda, M.; Andreoni, A.; Tabares, L. C.; Tepper, A. W. J. W.; Fortunato, L.; Aartsma, T. J.; Canters, G. W. Sensitive detection of histamine using fluorescently labeled oxido-reductases. *Biosens. Bioelectron.* **2012**, *31*, 419–25.
- (3) Kuznetsova, S.; Zauner, G.; Aartsma, T. J.; Engelkamp, H.; Hatzakis, N.; Rowan, A. E.; Nolte, R. J. M.; Christianen, P. C. M.; Canters, G. W. The enzyme mechanism of nitrite reductase studied at single-molecule level. *Proc. Natl. Acad. Sci. U. S. A.* **2008**, *105*, 3250–3255.
- (4) Kuznetsova, S.; Zauner, G.; Schmauder, R.; Mayboroda, O. A.; Deelder, A. M.; Aartsma, T. J.; Canters, G. W. A Förster-resonance-energy transfer-based method for fluorescence detection of the protein redox state. *Anal. Biochem.* **2006**, *350*, 52–60.
- (5) Salverda, J. M.; Patil, A. V.; Mizzon, G.; Kuznetsova, S.; Zauner, G.; Akkilic, N.; Canters, G. W.; Davis, J. J.; Heering, H. A.; Aartsma, T. J. Fluorescent Cyclic Voltammetry of Immobilized Azurin: Direct Observation of Thermodynamic and Kinetic Heterogeneity. *Angew. Chemie Int. Ed.* **2010**, *49*, 5776–5779.
- (6) Patil, A. V.; Davis, J. J. Visualizing and tuning thermodynamic dispersion in metalloprotein monolayers. *J. Am. Chem. Soc.* **2010**, *132*, 16938–16944.
- (7) Schmauder, R.; Librizzi, F.; Canters, G. W.; Schmidt, T.; Aartsma, T. J. The oxidation state of a protein observed molecule-by-molecule. *Chemphyschem* **2005**, *6*, 1381–6.
- (8) Schmauder, R.; Alagaratnam, S.; Chan, C.; Schmidt, T.; Canters, G. W.; Aartsma, T. J.



- Sensitive detection of the redox state of copper proteins using fluorescence. *J. Biol. Inorg. Chem.* **2005**, *10*, 683–7.
- (9) Strianese, M.; Zauner, G.; Tepper, A. W. J. W.; Bubacco, L.; Breukink, E.; Aartsma, T. J.; Canters, G. W.; Tabares, L. C. A protein-based oxygen biosensor for high-throughput monitoring of cell growth and cell viability. *Anal. Biochem.* **2009**, *385*, 242–248.
- (10) Tabares, L. C.; Kostrz, D.; Elmalk, A.; Andreoni, A.; Dennison, C.; Aartsma, T. J.; Canters, G. W. Fluorescence lifetime analysis of nitrite reductase from *Alcaligenes xylooxidans* at the single-molecule level reveals the enzyme mechanism. *Chemistry* **2011**, *17*, 12015–9.
- (11) Zauner, G.; Lonardi, E.; Bubacco, L.; Aartsma, T. J.; Canters, G. W.; Tepper, A. W. J. W. Tryptophan-to-dye fluorescence energy transfer applied to oxygen sensing by using type-3 copper proteins. *Chem. - A Eur. J.* **2007**, *13*, 7085–7090.
- (12) Haustein, E.; Schwille, P. Ultrasensitive investigations of biological systems by fluorescence correlation spectroscopy. *Methods* **2003**, *29*, 153–166.
- (13) Haustein, E.; Schwille, P. Fluorescence correlation spectroscopy: novel variations of an established technique. *Annu. Rev. Biophys. Biomol. Struct.* **2007**, *36*, 151–69.
- (14) Krichevsky, O. Fluorescence correlation spectroscopy : the technique. *Rep.Prog.Phys* **2002**, *65*, 251.
- (15) Ha, T.; Tinnefeld, P. Photophysics of Fluorescence Probes for Single Molecule Biophysics and Super-Resolution Imaging. *Annu Rev Phys Chem* **2012**, *63*, 595–617.
- (16) Ha, T.; Tinnefeld, P. Photophysics of Fluorescent Probes for Single-Molecule Biophysics and Super-Resolution Imaging. *Annu. Rev. Phys. Chem.* **2012**, *63*, 595–617.
- (17) Stennett, E. M. S.; Ciuba, M. a; Levitus, M. Photophysical processes in single molecule organic fluorescent probes. *Chem. Soc. Rev.* **2014**, *43*, 1057–75.
- (18) Wilson, M. T.; Greenwood, C.; Brunori, M.; Antonini, E. Electron transfer between azurin and cytochrome c-551 from *Pseudomonas aeruginosa*. *Biochem. J.* **1975**, *145*, 449–457.

- (19) E. T. Adman and L. H. Jensen Structural Features of Azurin at 2.7 Å Resolution. *Isr. J. Chem.* **1981**, *21*, 8–12.
- (20) Van de Kamp, M.; Hali, F. C.; Rosato, N.; Agro, A. F.; Canters, G. W. Purification and characterization of a non-reconstitutable azurin, obtained by heterologous expression of the *Pseudomonas aeruginosa* *azu* gene in *Escherichia coli*. *Biochim. Biophys. Acta* **1990**, *1019*, 283–292.
- (21) Nar, H.; Huber, R.; Messerschmidt, A.; Filippou, A. C.; Barth, M.; Jaquinod, M.; van de Kamp, M.; Canters, G. W. Characterization and crystal structure of zinc azurin, a by-product of heterologous expression in *Escherichia coli* of *Pseudomonas aeruginosa* copper azurin. *Eur. J. Biochem.* **1992**, *205*, 1123–1129.
- (22) Van Amsterdam, I. M. C.; Ubbink, M.; Einsle, O.; Messerschmidt, A.; Merli, A.; Cavazzini, D.; Rossi, G. L.; Canters, G. W. Dramatic modulation of electron transfer in protein complexes by crosslinking. *Nat. Struct. Biol.* **2002**, *9*, 48–52.
- (23) Nicolardi, S.; Andreoni, A.; Tabares, L. C.; Van Der Burgt, Y. E. M.; Canters, G. W.; Deelder, A. M.; Hensbergen, P. J. Top-down FTICR MS for the identification of fluorescent labeling efficiency and specificity of the Cu-protein azurin. *Anal. Chem.* **2012**, *84*, 2512–20.
- (24) Nicolardi, S.; Andreoni, A.; Tabares, L. C.; van der Burgt, Y. E. M.; Canters, G. W.; Deelder, A. M.; Hensbergen, P. J. Top-down FTICR MS for the identification of fluorescent labeling efficiency and specificity of the Cu-protein azurin. *Anal. Chem.* **2012**, *84*, 2512–20.
- (25) Widengren, J.; Rigler, R.; Mets, U. Triplet-state monitoring by fluorescence correlation spectroscopy. *J. Fluoresc.* **1994**, *4*, 255–8.
- (26) Widengren, J.; Mets, U.; Rigler, R. Fluorescence correlation spectroscopy of triplet states in solution: a theoretical and experimental study. *J. Phys. Chem.* **1995**, *99*, 13368–13379.
- (27) Holleman AF *Lehrbuch der Anorganischen Chemie*; de Gruyter: New York, 1995.

## **Chapter 4**

### **Observation of intramolecular electron-transfer reactions by fluorescence correlation spectroscopy: Photoinduced electron-transfer reaction between the label and the copper center**

## **Abstract**

A detailed investigation of the products of the labeling reaction of *wt* Cu azurin with the fluorescent dye ATTO655 has been performed. Fluorescence correlation spectroscopy was performed to understand the behavior of the labeled products. In this work, we have tried to understand the photoinduced electron-transfer (PET) reaction using two species: one labeled at the N-terminus and another one labeled at Lys122 position. Intramolecular photoinduced electron-transfer (PET) to the metal is observed when a redox metal ion occupies the active site, and the label is attached close enough to the metal center (at Lys122) and occurred in microsecond time scale. Two different mechanisms are equally likely to be involved in the electron-transfer event. In N-terminally labeled protein, the label is far away from the metal center and there is no PET reaction.

## 4.1 Introduction

Inter- and intramolecular electron transfer (ET) reactions have been a subject of research over the past few decades and several experimental and computation methods have been employed to investigate these. Application of redox proteins especially azurin, nitrite reductase, cytochrome P450 has tremendously enhanced the progress of this field. Single-molecule techniques appear eminently suited for the study of such enzymes at single-molecule level(1)(2)(3)(4)(5)(6)(7). To monitor the working of these oxido-reductases in detail, a novel FRET-based technique, FluoRedox had been developed(8)(9)(10)(11)(12). FluoRedox technique has tremendously facilitated the detection of the redox state change due to the sensitivity of fluorescence detection. The technique used here depends on the labeling of the protein by dye molecules, the fluorescence of which overlaps spectrally with the absorption of the protein's redox center. When a change in the redox-state affects the absorption spectrum of the redox protein, the energy-transfer process between the dye and the metal center is affected and this leads to a change in the fluorescence intensity of the dye (see Chapter 1 for details).

In the studies reported so far it has been tacitly assumed that quenching of the dye fluorescence is brought about solely by FRET(13). However, the optically excited label may be deactivated by photo-induced electron transfer (PET) as well. Instances have been reported where van der Waals contact between dye label and amino acid side chains appears to promote PET(14)(15)(16)(17). Working along different lines, Gray and co-workers found that photo-excited Ru labels may transfer an electron across a protein at the sub-microsecond to millisecond time scale(18)(19)(20)(21). In this chapter, we investigate to what extent PET between dye label and redox center may occur in an oxido-reductase.

As the model system we have chosen the blue copper protein azurin labeled with ATTO655. The effect of the redox state of the Copper (Cu) on the PET reaction was explored by studying the labeled azurin in the oxidized and in the reduced form. The technique chosen to study the time dependence of the label emission is fluorescence correlation spectroscopy (FCS), a single-molecule technique that can be used to monitor diffusing fluorescent particles in dilute solutions. Probing small numbers of molecules at a time by FCS and statistical analysis of the data reveals dynamics otherwise obscured by ensemble averaging(22)(23)(24)(25). When combined with modern hard- and software, FCS allows for a time resolution in the ps range(26).

The intermolecular reaction between the label and the redox agents affects the FCS signal and has been discussed in the previous chapter. In the present study, we have investigated the intramolecular ET reaction between the label and copper center. Redox active components in solution like potassium hexacyanoferrate(II) and (III), which have been used in the present study, react with azurin by forming an encounter complex within which ET occurs on the time scale of 20-200 ms(27). This is much longer than the time an azurin molecule needs on average to traverse the confocal volume, which means that these reactions fall outside the observation window of the FCS experiments. The same is true when ascorbate is used as a reductant. Thus for the interpretation of FCS traces we need to consider the intramolecular ET between label and Cu and the intermolecular ET reactions between the label and the redox chemicals that were discussed in Chapter 3.

The results presented here provide detailed insight into the kinetics of the intra- and intermolecular PET reactions. Rate constants for the reactions were determined. The rate constants also demonstrate that the position of the label on the protein surface has to be selected carefully in order to get reliable information on the mechanistic behaviour of a labeled oxidoreductase.

## **4.2 Materials and Methods**

### **4.2.1 Chemicals and proteins**

Unless stated otherwise, chemicals were purchased from Sigma-Aldrich (Sigma-Aldrich Corp., St. Louis, USA) and used as received. Wild-type Cu-azurin from *Pseudomonas aeruginosa* were expressed and purified as previously described (Chapter 3 and ref. (28)). For the labeling of the protein with the dye ATTO655 (ATTO655 NHS ester, ATTO-TEC GmbH, Siegen, Germany) the supplier-provided protocol was used. Labeling resulted in a mixture of products that could be separated by ion exchange chromatography on a MonoQ column. The elution profile is shown in Fig. 4.1. Peaks 1-5 correspond with unlabeled azurin, azurin labeled at the N-terminus (Nt-CuAzu)(29), labeled at Lys122 (K122-CuAzu) (Fig. 4.2), Lys24 or Lys27 (not further investigated), and a doubly labeled species, respectively(29). For the experiments described in this study, N-terminally labeled and Lys122 labeled azurin were selected. They represent azurins

where the label is either far away from (29.1 Å) or relatively close to (18.5 Å) the Cu-site, respectively.

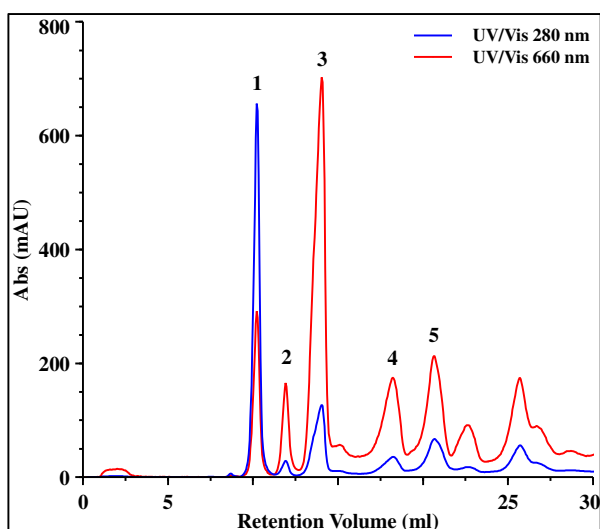


**Figure 4.1:** Chromatogram showing the separation of dye-labeled CuAzurin species. The peaks are labeled from 1 through 5 and correspond with unlabeled azurin (1), N-terminally labeled azurin (2), Lys122 labeled azurin (3), a mixture of differently labeled species (4), and a doubly labeled species (5), respectively.

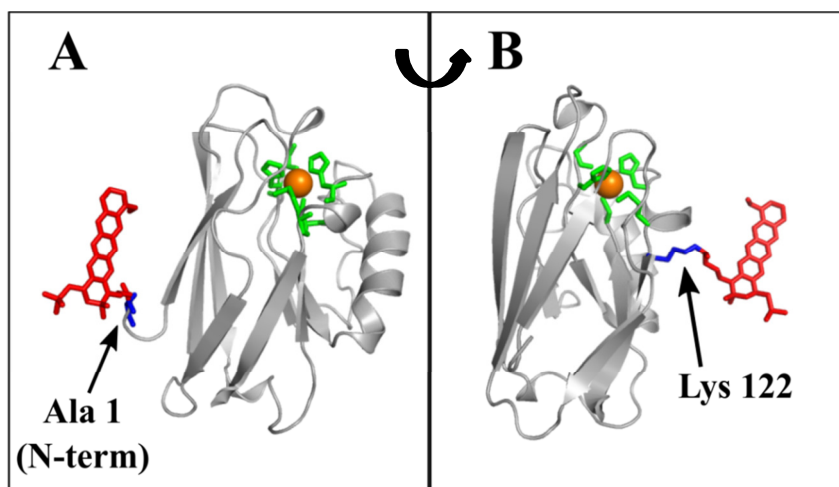


**Figure 4.2:** Depiction of azurin (gray) modified with ATTO655 (red) on the two positions studied in the present work. The Cu ion and the 5 residues coordinating it are depicted, respectively, as an orange sphere and green sticks. A) Label linked to the N-terminal residue Ala1 (blue). B) Label attached to the side chain of Lys122 (blue). The figures were prepared in silico by using the available crystal structure of azurin (1AZU)(30) and the molecular structure of the label ATTO655. The molecule in panel B has been rotated counterclockwise over  $90^{\circ}$  with respect to panel A around a vertical axis in the plane of the page.

#### **4.2.2 UV/Vis absorption and fluorescence spectroscopy**

All optical absorption and fluorescence experiments on bulk solutions were carried out at room temperature in 100 mM HEPES pH 7.0 under stirring. UV/Vis absorption spectra were recorded on a Cary 50 Spectrophotometer (Agilent Technologies, Santa Clara, CA, USA) at a speed of 400 nm/min with a bandwidth of 2 nm and an interval of 1 nm between data points. With the use of a Cary Eclipse Spectrophotometer (Agilent Technologies, Santa Clara, CA, USA), emission spectra of fluorescently labeled azurin samples were recorded in the 600 – 800 nm range by exciting the sample at 590 nm. Excitation and emission slits were set to 5 nm band-pass and suitable optical filters were automatically selected by the instrument to minimize second order diffraction effects of the monochromator. The concentration of labeled protein ranged from 50-100 nM and the total volume of the sample used was 100  $\mu$ l in a 3 windows, quartz glass ultra-micro cell for fluorescence measurements (HellmaAnalytics, Mullheim, Germany). The photomultiplier tube (PMT) voltage was adjusted during each experiment to avoid signal saturation. Redox switching was performed using sodium ascorbate and potassium hexacyanoferrate(III) as reducing and oxidizing agents respectively. The time traces of fluorescence switching for Nt-CuAzu and K122-CuAzu under redox conditions have been presented in Fig. 4.3. Details on the principles of fluorescence switching and “FluRedox” technique have been provided in Chapter 1.

#### **4.2.3 Sample preparation**

Details about the sample preparation have been provided in Chapter 3. Samples contained 57.0% sucrose (w/w) (viscosity 37.5 cP at 22<sup>0</sup>C)(31). The final sample concentrations of labeled protein were around 0.4-0.8 nM. Manipulation of the redox potential of the solution was achieved by employing hexacyanoferrate (III), hexacyanoferrate (II) or ascorbate.

#### **4.2.4 FCS setup**

The FCS calibration measurements were carried out at room temperature on our home-built confocal setup equipped with Axiovert 100 inverted microscope (Carl Zeiss, Germany) and a high numerical aperture (NA) water immersion objective (60x water, NA 1.2, Olympus UPLSAPO). Excitation at 639 nm was provided by a pulsed diode laser head (LDH-P-C-635-B, PicoQuant GmbH, Berlin, Germany) driven by a picosecond laser driver (LDH-800-B,



PicoQuant GmbH, Berlin, Germany). The fluorescence from the sample was collected by the water objective and spatially filtered using a 50  $\mu\text{m}$  pinhole. The fluorescence from the dye was

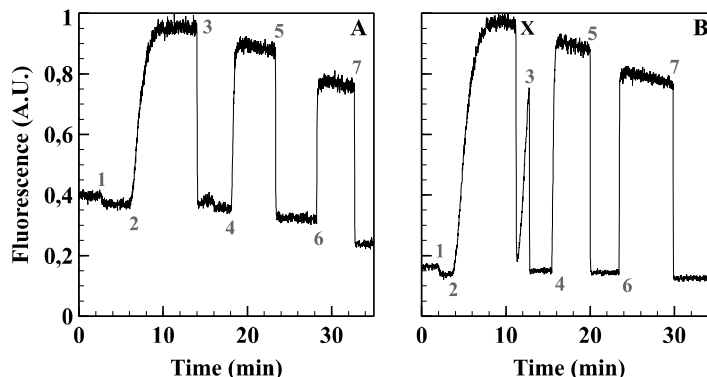


**Figure 4.3:** Fluorescence switching experiments on fluorescently labeled copper azurin. The black numbers mark the addition of oxidant to the samples, whereas the gray numbers indicate the addition of reductant. A: N-terminally labeled azurin. B: azurin labeled at Lys122. The time points 1, 3, 5, and 7 correspond to the addition of 0.05, 1, 6, and 18 mM (final concentrations) of potassium ferricyanide to the sample, respectively. The time points 2, 4, and 6 correspond to the addition of 0.25, 1.5, and 4.5 mM of sodium ascorbate (final concentrations), respectively. At time point 'X' in panel B the added amount of ferricyanide was too low to completely oxidize the azurin. The subsequent addition (time point 3) was sufficient to complete the oxidation.

passed through an emission filter (HQ 675/50m, Chroma Technology Corp., VT, USA), and focused onto a single-photon avalanche photodiode (SPCM-AQRH 14, Perkin Elmer Inc., USA). The signal from the diode was read out by using a TimeHarp200 counting board (PicoQuant GmbH, Berlin, Germany). The power used for the FCS measurements amounted to 20  $\mu\text{W}$ , as measured after the objective, corresponding to a specific power of  $\sim 7.0 \text{ kW/cm}^2$  at the sample. The acquisition of the data was performed in the Time-Tagged Time Resolved Single Photon Mode (t3r) using the software package SymPhoTime from PicoQuant, Germany and FCS experiments were performed with sample volume  $\sim 80\text{-}100 \mu\text{l}$ . A schematic diagram of the FCS setup has been displayed in Fig. 4.4.

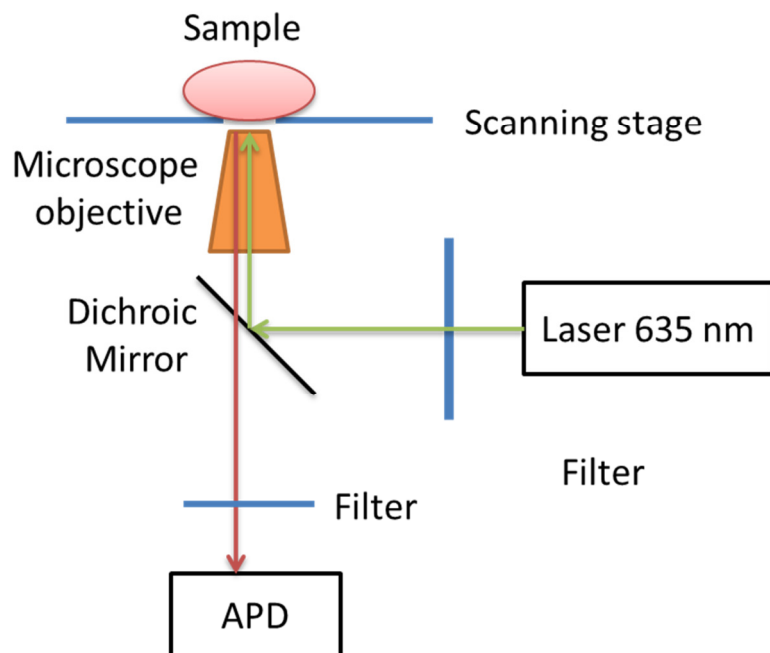


**Figure 4.4:** Schematic representation of the experimental setup. The laser light (excitation wavelength: 635 nm) is transmitted through the narrow-band filter and reflected from the dichroic mirror through the objective. The emission light is collected by the same objective, transmitted through the dichroic mirror and the emission filter, and then focused on the avalanche photodiode (APD).

#### 4.2.5 FCS data analysis

After acquisition of the data the time correlated single photon counting (TCSPC) histogram was built and fitting was performed after narrowing down the time window of the TCSPC decay. Based on the fitted values, the software generated a set of filter functions, which were subsequently used by the software to select the photons for the calculation of the autocorrelation function (ACF),  $G(\tau)$ . The functions were analyzed by fitting to the following equation:

$$G(\tau) = G(0) \cdot G_{diff}(\tau) \cdot G_1(\tau) \cdot G_2(\tau) \quad (4.1)$$

where  $G(0)$  is given by

$$G(0) = \frac{1}{\langle N \rangle} = \frac{1}{c \cdot V_{eff} \cdot N_A} \quad (4.2)$$

with  $\langle N \rangle$  the average number of particles in the probe volume,  $c$  the sample concentration,  $V_{eff}$  the effective probe volume, and  $N_A$  Avogadro's constant.  $V_{eff}$  amounted to 1.1-2.3 fL depending

on conditions (Chapter 2 for more details).

Equation (1) is composed of three terms: a diffusive term,  $G_{diff}(\tau)$  that describes the diffusion of molecules in solution due to Brownian motion, and two kinetic terms,  $G_1(\tau)$  and  $G_2(\tau)$ , that relate to zero-order reactions such as fluorophore blinking or monomolecular chemical reactions like deprotonation or electron transfer (ET).  $G_{diff}(\tau)$ ,  $G_1(\tau)$  and  $G_2(\tau)$  are given by

$$G_{diff}(\tau) = \left(1 + \frac{\tau}{\tau_D}\right)^{-1} \cdot \left(1 + \frac{\tau}{k^2 \tau_D}\right)^{-1/2} \quad (4.3)$$

$$G_1(\tau) = \frac{(1 - F_1 + F_1 e^{-\tau/\tau_1})}{(1 - F_1)} \quad (4.4)$$

$$G_2(\tau) = \frac{(1 - F_2 + F_2 e^{-\tau/\tau_2})}{(1 - F_2)} \quad (4.5)$$

where  $\tau_1$  and  $\tau_2$  are the decay times of two independent zero-order reactions, and  $F_1$  and  $F_2$  are the corresponding fractions of molecules in the dark state, respectively.

Specific cases, to be described below, required the inclusion of one or two zero-order reactions, *i.e.*,  $G_1(\tau)$  or both,  $G_1(\tau)$  and  $G_2(\tau)$ , in the fitting procedure to obtain a satisfactory fit.  $G_2(\tau)$ , or both  $G_1(\tau)$  and  $G_2(\tau)$ , were omitted when their inclusion in the fitting procedure gave no significant improvement of the fit. The fitting of the autocorrelation data was performed in GraphPad Prism 5 or 6.05 (GraphPad Inc., USA). The quality of the fits was judged by visual inspection of the residuals.

#### **4.2.6 Fluorescence lifetime data acquisition**

For the acquisition of fluorescence lifetime data the sample (~80  $\mu$ l) was deposited on a glass slide and covered with the cap of a polypropylene test tube to prevent evaporation of the solvent during the measurements. A new cap was used for each measurement to prevent sample cross-contamination. The focus was set at a distance of 20  $\mu$ m from the upper surface of the glass coverslip to prevent detection of fluorescence from surface-adsorbed molecules. The laser power for the measurements was adjusted by using a neutral density filter in front of the laser head and it was set at 20  $\mu$ W (7.0 kW/cm<sup>2</sup>, resolution of the setup ~300 nm), as measured at the

microscope objective. For power-dependence measurements, 6 different values of power were chosen ranging from 1 to 80  $\mu\text{W}$ , as measured after the microscope objective. For each experimental condition, time traces were recorded for durations varying from 5 to 10 minutes, depending on the conditions of the experiment. Sample concentration was kept around 1 nM in order to lower the probability of having more than one molecule at the time in the confocal volume. The raw data were stored as time-tagged time-resolved (t3r) data file and subsequently elaborated by using the SymPhoTime software package.

### 4.3 Results and discussion

#### 4.3.1. Lifetimes of labeled azurin

From the photon statistics, it is possible to extract information about the lifetimes of labeled Cu azurin under redox conditions. To estimate lifetimes, the decay curves could only be fitted with a double exponential function. The functions are given as

$$f = A_0 + A_1 \cdot \exp(-t/\tau_1) + A_2 \cdot \exp(-t/\tau_2) \quad (4.6)$$

where,  $A_1$ ,  $A_2$  and are the amplitudes and  $\tau_1$ ,  $\tau_2$  are the lifetimes of two processes present in solution and  $A_0$  represents a local background. In our experiments,  $\tau_1$  displayed the lifetime of the dye and was found to be in the order of few nanoseconds, which is significantly longer than the instrument response function which is in the order of ps. We compared the amplitudes of  $A_2$  and  $\tau_2$  with  $A_1$  and  $\tau_1$ . The contributions of  $A_2$  and  $\tau_2$  for a second process were found to be negligible compared to  $A_1$  and  $\tau_1$ .  $\tau_1$  is the major component of the excited molecule. The second process can be originated from other factors e.g. interaction between dye molecules, adsorption, different rates of molecular rotation (32)(33). Under oxidising condition, the lifetime ( $\tau_1$ ) of the labeled Cu azurin is 1.8 ns whereas the lifetime is increased to 2.7 ns under reducing conditions. The time correlated single-photon count (TCSPC) decay curves at oxidizing and reducing conditions have been displayed in Fig. 4.5.

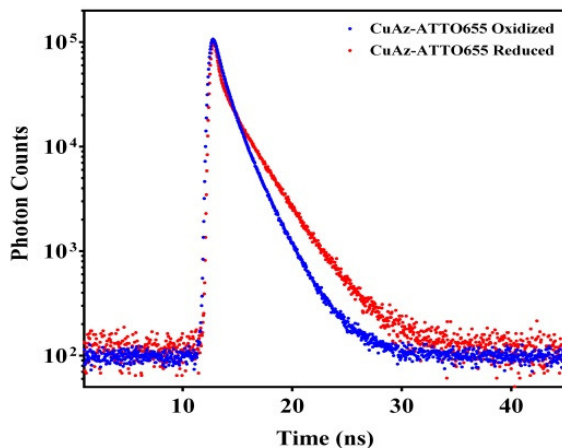


**Figure 4.5:** TCSPC decay of Cu azurin labeled with ATTO655 in sucrose in oxidizing and reducing conditions. It is possible to see the different slope of the lifetime decay when the protein is oxidized (blue) as compared to the reduced protein (red). The lifetime shortening is associated with FRET from the dye to the oxidized Cu center.

### 4.3.2 N-terminally labeled CuAz (Nt-CuAz)

#### 4.3.2.1 Oxidizing conditions

Fluorescence time traces of solutions of N-term-CuAz in 57% (w/w) sucrose were recorded in the presence of varying amounts (0-500  $\mu\text{M}$ ) of oxidant (potassium hexacyanoferrate (III)). 10-20 different concentrations of oxidant were analyzed. Examples of the experimentally observed autocorrelation functions have been provided for a few concentrations of hexacyanoferrate (III) (Fig. 4.6). Diffusion times are in the range of 10-12 ms. The diffusion times N-term-CuAz are in good agreement with  $\tau_D$  values of labeled ZnAzurin ( $12 \pm 2$  ms, page 45). It is also clear from Fig. 4.6 (A-E) that the label is not affected by the added oxidant.

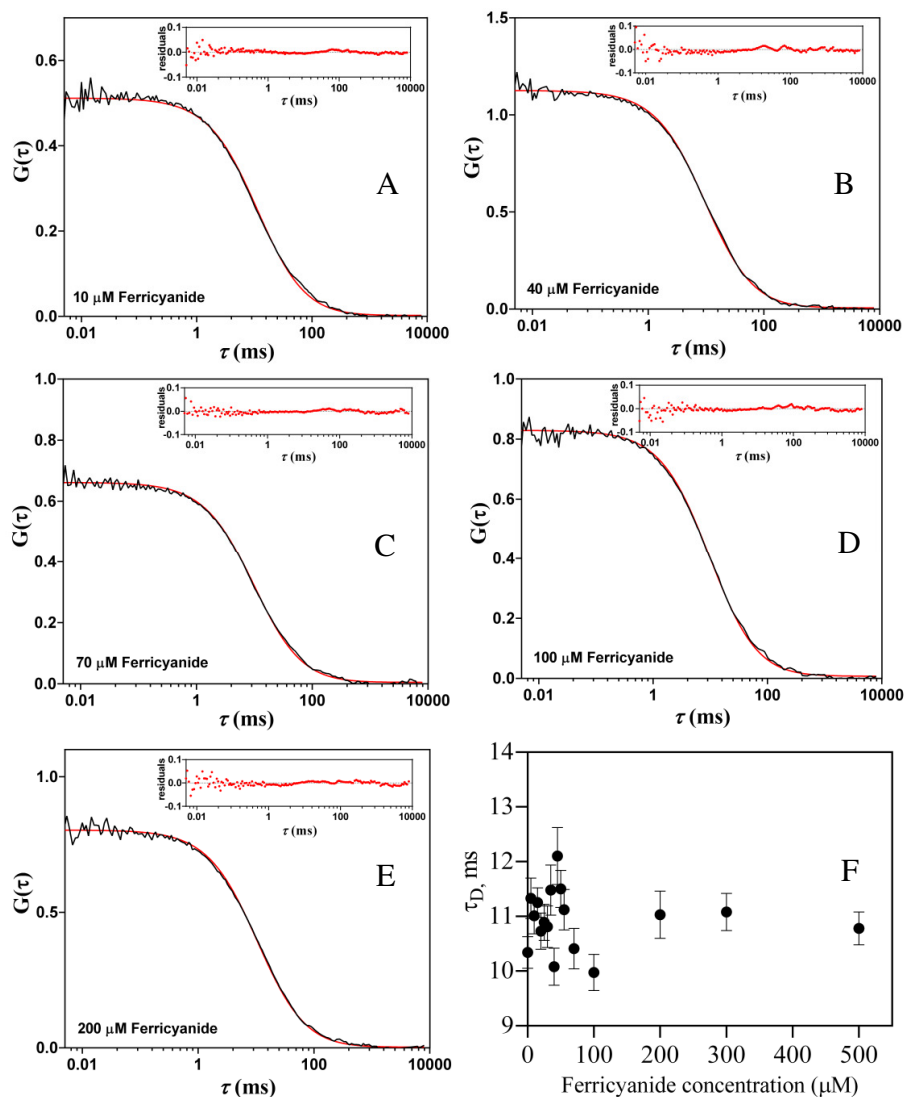


**Figure 4.6:** Experimentally observed ACFs of Cu azurin labeled at N-terminus with ATTO655 for samples containing 10 (A), 40 (B), 70 (C), 100 (D) and 200 (E) potassium hexacyanoferrate (III) (top to bottom). The red lines are fits according to Eqn. 3.1  $G(\tau) = G(0).G_{diff}(\tau)$ . The insets show the residuals of the fit. (F) Diffusion times derived from the fits for various concentrations of hexacyanoferrate (III).

#### 4.3.2.2 Reducing conditions

The observations are different when reducing conditions apply. The data obtained for N-term CuAzurin when titrated with potassium hexacyanoferrate (II) or sodium ascorbate were fitted with  $G(\tau) = G(0).G_{diff}(\tau)$ , but the residuals exhibited a noticeable non-random component. Similar to ZnAz,  $\tau_D$  varied strongly with reductant concentrations (Fig. 4.7). Hence, they were fit

with the Eqn. 3.4  $G(\tau) = G(0).G_{diff}(\tau).G_I(\tau)$  with diffusion time fixed at 12 ms. The values of  $F_I$  and  $\tau_I$  varied with reductant concentrations (Fig. 4.8).

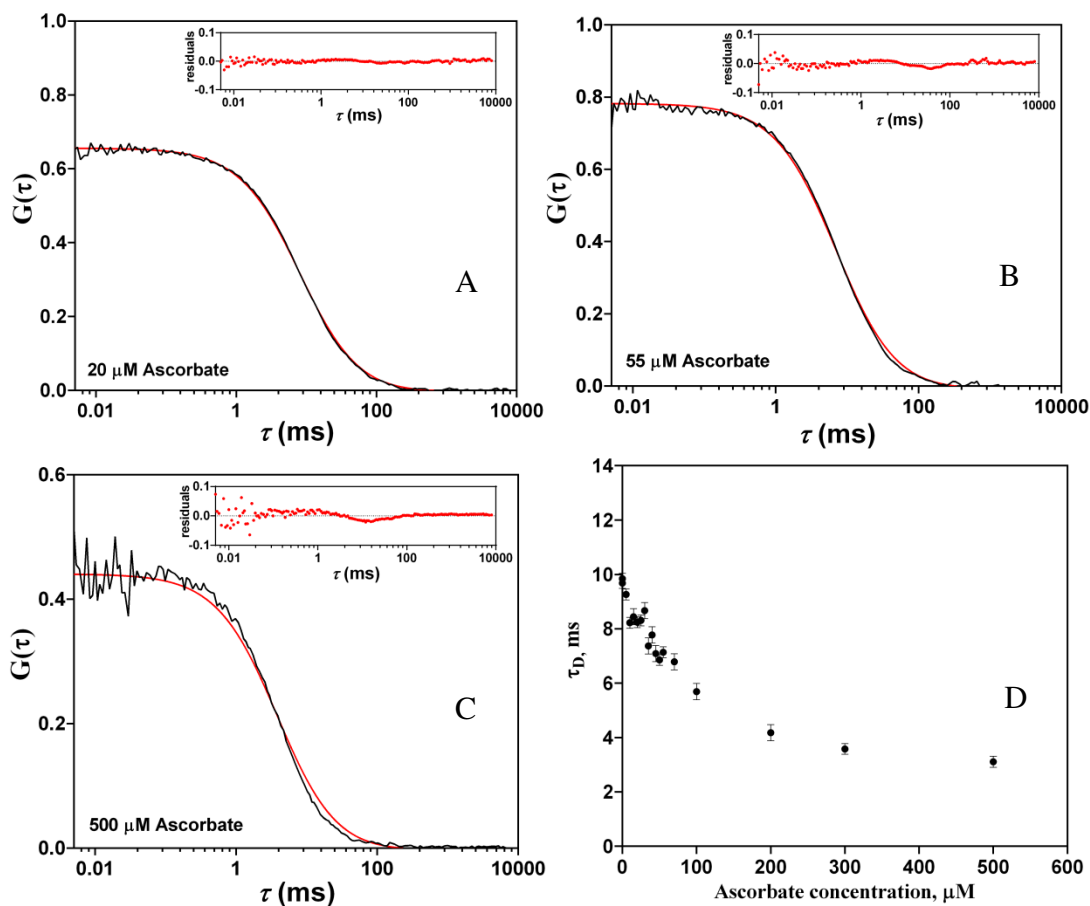


**Figure 4.7:** Experimentally observed ACFs of Cu azurin labeled at the N-terminus with ATTO655 for samples containing 20 (A), 55 (B) and 500 (C)  $\mu\text{M}$  ascorbate. The insets are the residuals of the fit. The red lines are fits according to Eqn. 3.1  $G(\tau) = G(0).G_{diff}(\tau)$ . (D) Diffusion times derived from the fits for various concentrations of ascorbate.

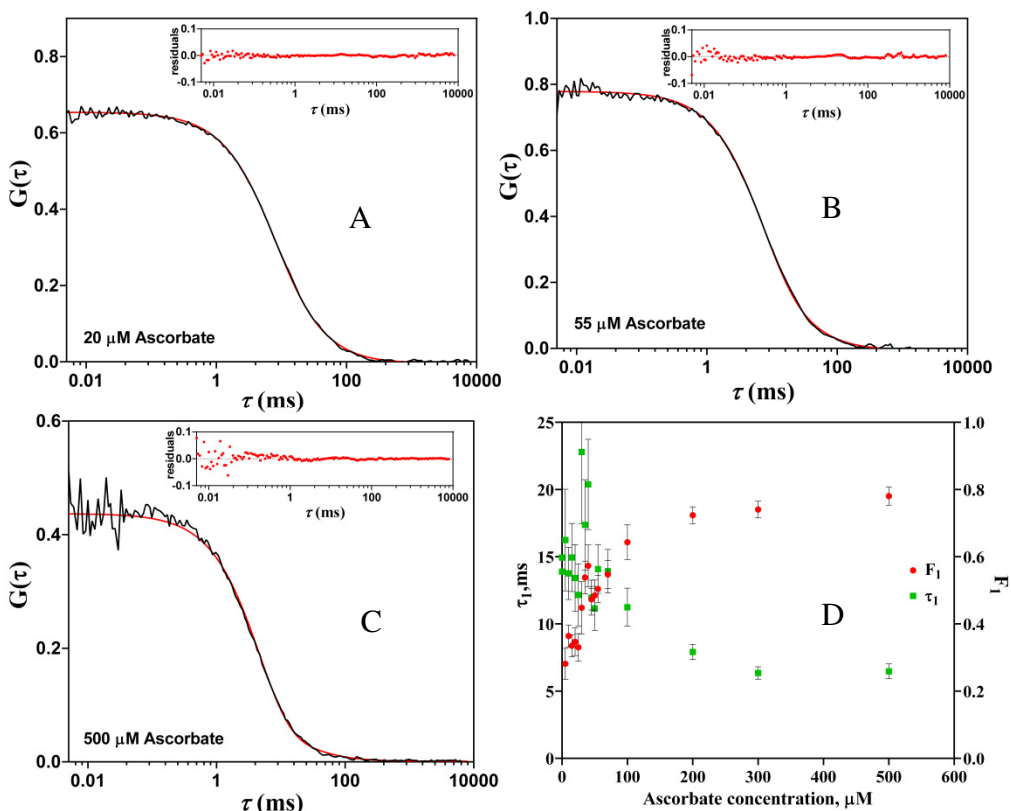
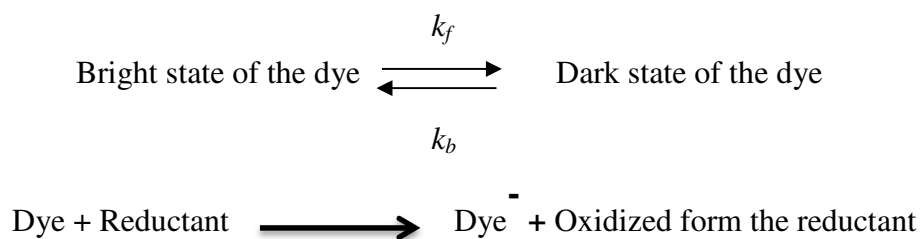


**Figure 4.8:** Experimentally observed ACFs of Cu azurin labeled at the N-terminus with ATTO655 for samples containing 20 (A), 55 (B) and 500 (C)  $\mu\text{M}$  ascorbate. The red lines are fits according to Eqn. 3.4  $G(\tau) = G(0) \cdot G_{\text{diff}}(\tau) \cdot G_1(\tau)$  with  $\tau_D = 12$  ms. The insets show the residuals of the fit. (D) Parameters obtained from the fits. The green squares and red dots show the values for  $\tau_1$  and  $F_1$ , and correspond with left and right y-axis, respectively. Vertical bars denote 95% confidence intervals.

It was clear again that the label undergoes transitions between a bright and a dark state in presence of reducing agents. Hence, the formalism which was discussed for ZnAz, was also applied for analyzing  $F_1$  and  $\tau_1$  for this species. The dependence of  $k_f = F_1/\tau_1$  and  $k_b = (1-F_1)/\tau_1$  on reductant concentrations is illustrated by Scheme 4.1.  $k_f$  will be linearly proportional to the reductant concentrations. The values of  $k_r f(I)$  and  $k_b$  (rate constant for the back oxidation of the label) are gathered in Table 4.1.





$$F_1 = \frac{k_f}{k_f + k_b} \qquad \tau_1 = (k_f + k_b)^{-1}$$

**Scheme 4.1:** Schematic representation of photoinduced processes of the label. The label ATTO655 cycles between the bright and dark states under reducing conditions. The expressions of  $F_1$  and  $\tau_1$  as function of  $k_f$  and  $k_b$  are displayed.

### 4.3.3 K122-CuAz

#### 4.3.3.1 Oxidizing conditions

When titrating K122-CuAz with hexacyanoferrate(III), the observed ACFs could not be fit adequately with the equation containing a single diffusion term (Fig. 4.9) and a two-term function with  $G_{diff}(\tau)$  and  $G_1(\tau)$  was needed to fit the data properly (Fig. 4.10). After fitting with two terms, we still observed inadequate fitting of ACFs for few concentrations of oxidants. Considering a third term  $G_2(\tau)$  in FCS equation could not make any improvement of the fitting of the ACFs.

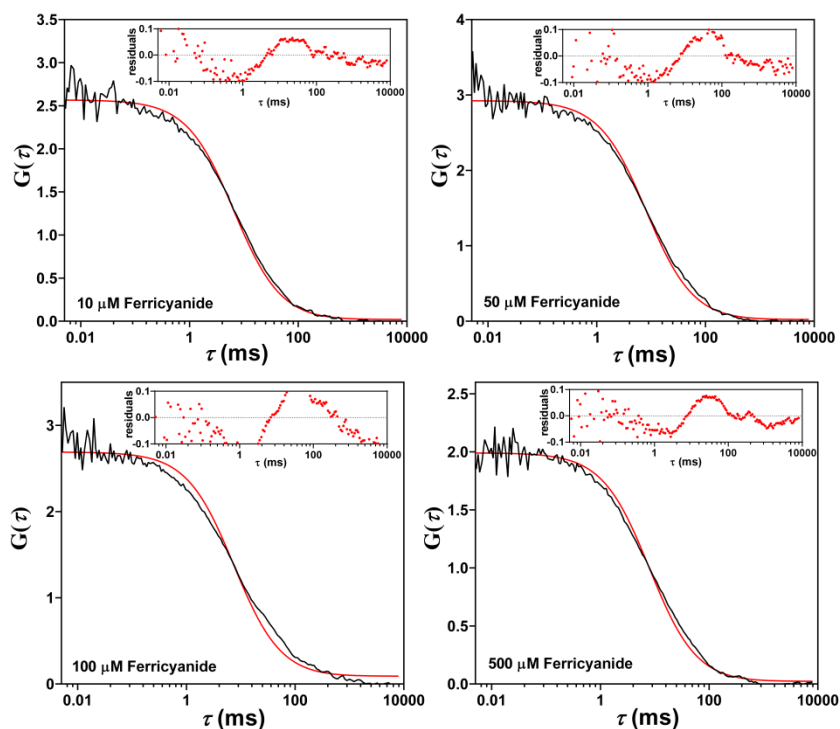


**Figure 4.9:** Examples of experimentally observed ACFs of Cu azurin labeled at K122 position with ATTO655. Data sets were obtained on samples containing 10, 50, 100 and 500  $\mu\text{M}$  hexacyanoferrate (III). The red lines are the fits according to Eqn. 3.1  $G(\tau) = G(0) \cdot G_{diff}(\tau)$ . The insets show the residuals of the fit.

It was clear, therefore, that next to the diffusion term ( $G_{diff}(\tau)$ ) only a one term ( $G_I(\tau)$ ) is needed to fit the experimental ACFs. After analysis, both  $F_I$  and  $\tau_I$  appeared independent of the ferricyanide concentration with  $F_I = 0.17$  and  $\tau_I = 1.1$  ms (Fig. 4.11). This blinking reaction was not observed in the case of the Zn containing protein and so the Cu center must be involved in this reaction. Moreover, the blinking is also absent in the N-terminally labeled CuAz, which must mean that the distance between the Cu and the label is a critical factor (29.1 Å for N-term-Az vs. 18.5 Å for K122-Az). These are strong indications that intramolecular ET from the excited label to the  $\text{Cu}^{2+}$  site, and back, is responsible for the observed blinking, according to Scheme 4.2.

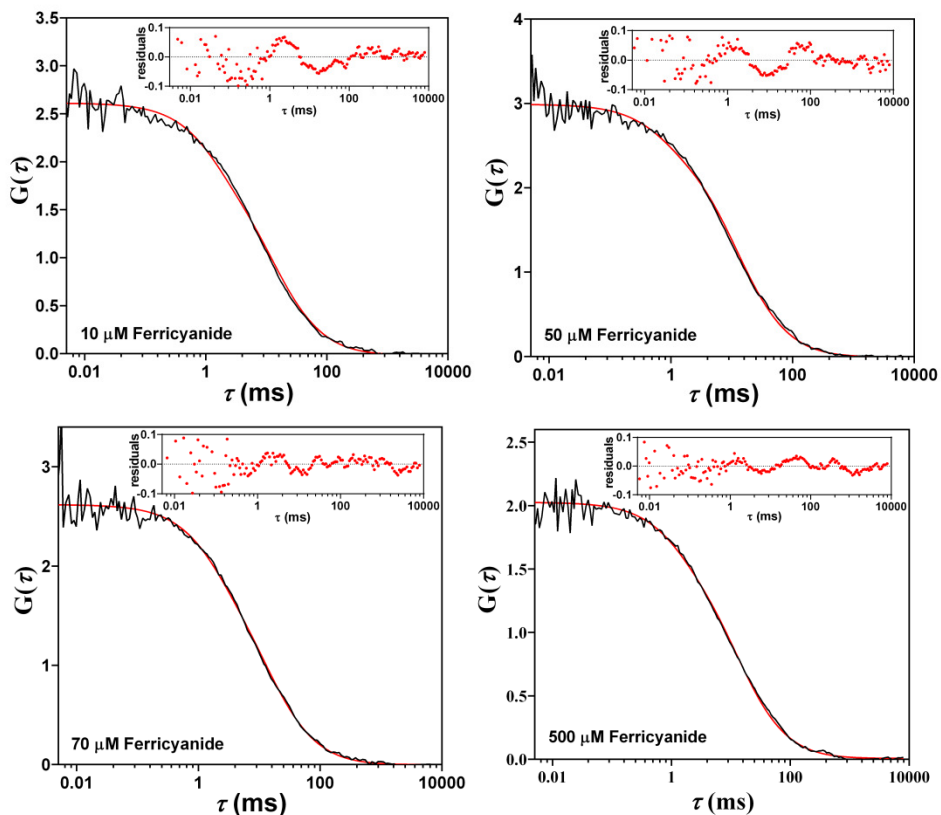
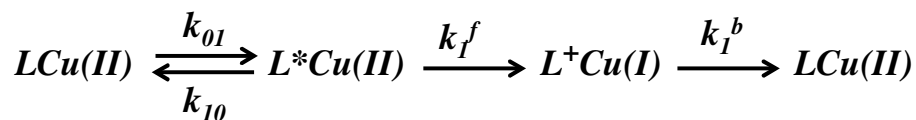


**Figure 4.10:** Examples of experimentally observed ACFs of Cu azurin labeled at K122 position with ATTO655. Data sets were obtained on samples containing 10, 50, 70 and 500  $\mu\text{M}$  hexacyanoferrate (III). The red lines are the fits according to Eqn. 3.4  $G(\tau) = G(0) \cdot G_{\text{diff}}(\tau) \cdot G_I(\tau)$  with  $\tau_D = 12$  ms. The insets show the residuals of the fit.



**Scheme 4.2:** Light induced ET reactions in oxidized CuAz.  $LCu$  symbolizes the labeled azurin molecule in which the Cu is in the reduced or oxidized form (Cu(I) or Cu(II), respectively) and the label, L, is excited or oxidized ( $L^*$  or  $L^+$ , respectively). The rates for intramolecular ET from  $L^*$  to Cu(II) and from Cu(I) to  $L^+$  are denoted by  $k_1^f$  and  $k_1^b$ .

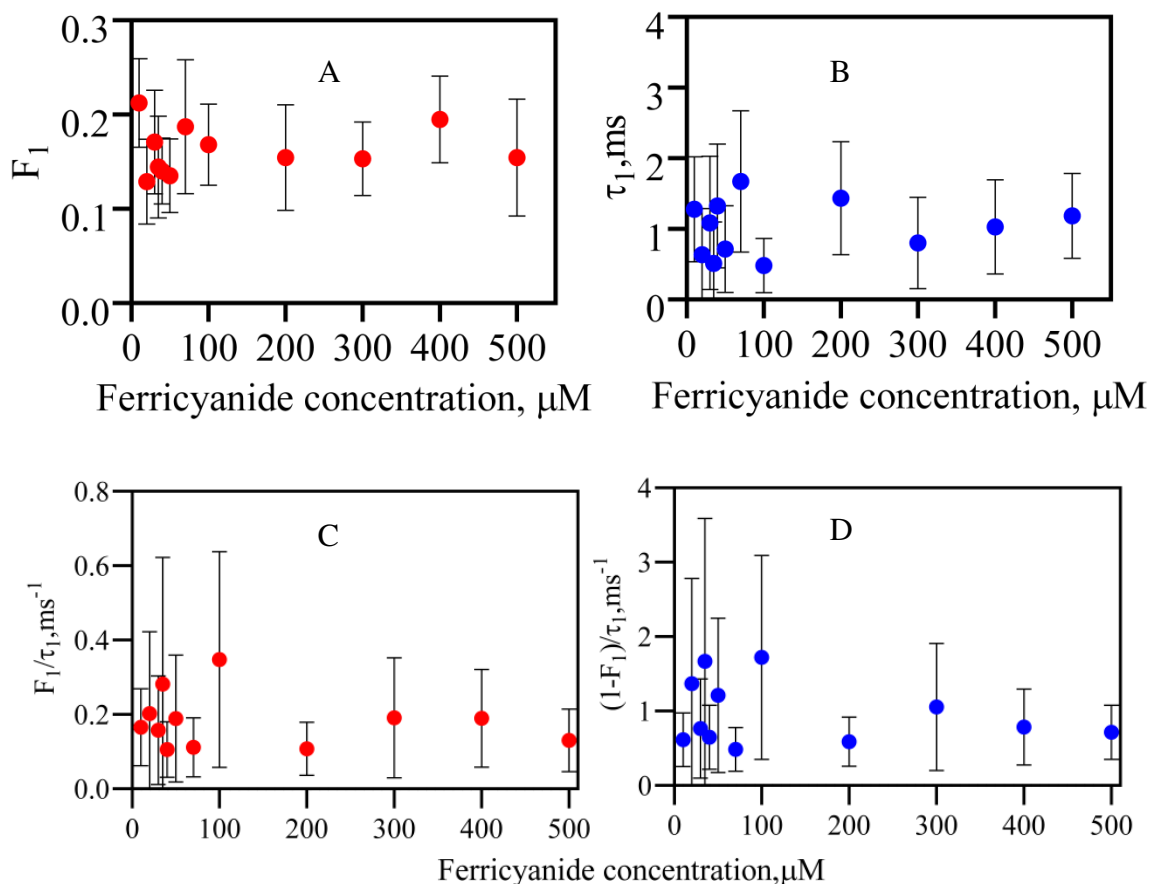


**Figure 4.11:** (A) and (B): Parameters ( $F_1$  and  $\tau_1$ ) obtained by fitting the ACFs of K122 labeled Cu azurin as a function of the concentration of added hexacyanoferrate (III). The equation used for the fits was  $G(\tau) = G(0).G_{diff}(\tau).G_1(\tau)$  with  $\tau_D = 12$  ms. The red and blue dots show the values for  $F_1$  and  $\tau_1$ . Vertical bars denote 95% confidence intervals. (C) and (D):  $F_1/\tau_1 = k^f$  and  $(1-F_1)/\tau_1 = k^b$  are plotted as a function of potassium hexacyanoferrate (III) concentrations. Vertical bars are the 95% confidence intervals. The ACFs were fitted the Eqn. 3.4  $G(\tau) = G(0).G_{diff}(\tau).G_1(\tau)$  with  $\tau_D = 12$  ms.

Consistent with the intramolecular character of the reaction, neither  $F_1$  nor  $\tau_1$  appears to depend on the concentration of oxidant (Fig. 4.11 A-B). Following the same formalism as applied for ZnAz (Chapter 3), one can obtain

$$F_1/\tau_1 = f(I) k_1^f \text{ and}$$

$$(1-F_1)/\tau_1 = k_1^b$$

In oxidized azurin the label fluorescence is partly quenched by the Cu center and the

fluorescence life time is shortened to 1.8 ns (Fig. 4.5). It leads to  $f(I) = 3.2 \times 10^{-3}$ . With  $F_1 = 0.17$  and  $\tau_1 = 1.1$  ms, one obtains  $k_1^f = 4.8 \times 10^4 \text{ s}^{-1}$  and  $k_1^b = 7.5 \times 10^2 \text{ s}^{-1}$ .

The rates can be used to extract a value for the reorganization energy of the ET reaction. Applying Marcus theory [see ref. (19)(34)(35)(36) and references contained therein] and assuming that the reorganization energies and the electronic coupling elements are the same for the forward and backward ET reactions one obtains

$$\ln(k_1^f / k_1^b) = [(\Delta G_b + \lambda)^2 - (\Delta G_f + \lambda)^2] / (4\lambda kT) \quad (4.7)$$

with  $\Delta G_f$  and  $\Delta G_b$  the driving forces for the forward and backward ET reactions, respectively, and  $\lambda$  the reorganization energy. The driving forces,  $\Delta G$  can be estimated with the Rehm-Weller equation(37)

$$\Delta G_f = eE_{D^+/D} - eE_{A/A^-} - \Delta G_{0,0} + (n_A - n_D - 1) \frac{e^2}{\epsilon d} \quad (4.8)$$

which describes the driving force  $\Delta G$  for the ET by a donor ( $D$ ) to an acceptor ( $A$ ) with  $E_{D^+/D}$  and  $E_{A/A^-}$  denoting the midpoint potentials of donor and acceptor, respectively. An analogous expression holds for  $\Delta G_b$ . Here, either the donor or the acceptor is optically excited with  $\Delta G_{0,0}$  denoting the energy of the corresponding optical  $0-0$  transition. In Eqn. (4.8),  $e$  denotes the electron charge,  $d$  the distance between donor and acceptor,  $\epsilon$  the dielectric constant and  $n_A$  and  $n_D$  the charges of acceptor and donor in units of  $|e|$ , respectively(37). For ATTO 655 the following values were used:  $E_{ATTO^+/ATTO} = 1.55$  V (vs NHE) and  $\Delta G_{0,0} = 1.86$  eV(17). The charges on label and Cu are  $n_{ATTO} = 0$ ,  $n_{Cu(II)} = 2$ . The midpoint potential of azurin at pH 7 is 0.31 V (vs NHE)(38)(39). This leads to driving forces of  $\Delta G_f = -0.476$  eV and  $\Delta G_b = -1.384$  eV for the reactions shown in *Scheme 4.2*. The values chosen for  $d$  and  $\epsilon$  were  $d = 10$  Å and  $\epsilon = 10$ , respectively (For our calculation, we set the distance ( $d$ ) between donor and acceptor at 10 Å, which is the distance between the copper and the aromatic part of the label when ATTO655 moiety is modelled as lying against the protein surface in the K122 labeled azurin. In this configuration, the effective  $\epsilon$  will be intermediate between that of pure protein ( $\epsilon = 4$ ) and that of water ( $\epsilon = 86$ ), and for the calculation purposes, we set  $\epsilon$  at 10). Insertion into Eqn. 4.7 and solving for  $\lambda$  leads to  $\lambda = 0.75$  eV. This value is slightly less than the theoretical value given by

the average of the known reorganization energies of ATTO655 and azurin (1.2 eV(40)(41) and 0.7(42) eV respectively).

### 4.3.3.2 Reducing conditions

Under reducing conditions an extra decay appeared in the ACF of K122-CuAz in the sub-millisecond time range. These curves could not be fitted with FCS equation containing two terms  $G_{diff}(\tau)$  and  $G_I(\tau)$  (Fig. 4.12). Only the use of a three-term correlation function (Eqn. (4.1)-(4.5),  $\tau_D$  fixed at 12 ms) resulted in satisfactory fits (Fig. 4.13). The amplitudes  $F_1$  and  $F_2$ , and the corresponding correlation times,  $\tau_1$  and  $\tau_2$  are presented in Fig. 4.14 (reductant: ascorbate), and Fig. 4.15 (reductant: hexacyanoferrate (II)) as a function of reductant concentrations.

As clear from Fig. 4.12 and 4.13, K122-labeled CuAz is involved in a reaction that occurs on a time scale of 10-100  $\mu$ s. Similar to the preceding case this reaction is ascribed to intramolecular ET, this time from the  $\text{Cu}^+$  site to the excited label and back (Scheme 4.3).

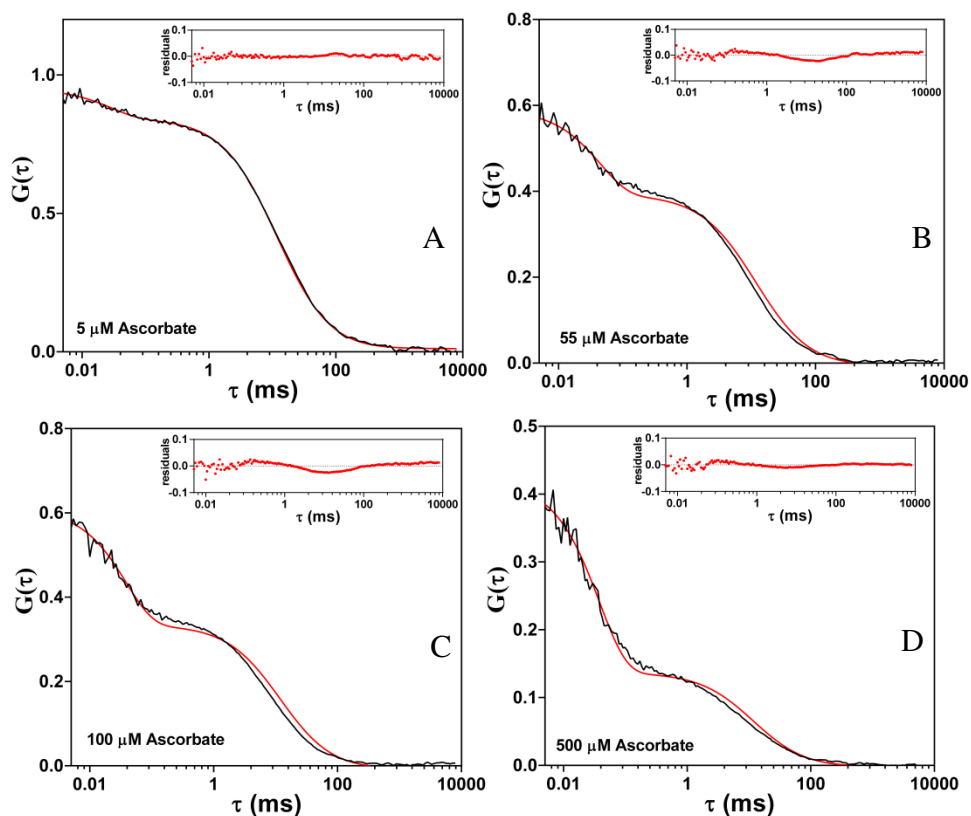


**Figure 4.12:** Experimentally obtained ACFs of Cu azurin labeled at K122 position with ATTO655 for samples containing 5 (A), 55 (B), 100 (C) and 500 (D)  $\mu$ M ascorbate. The red lines are fits according to Eqn. 3.4  $G(\tau) = G(0).G_{diff}(\tau).G_I(\tau)$  with  $\tau_D = 12$  ms. The residuals of the fits in the insets show unsatisfactory fitting of the ACFs.

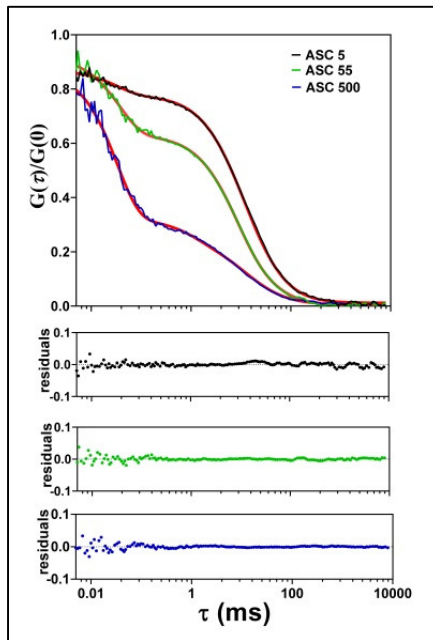


**Figure 4.13:** (A) ACFs of Cu azurin labeled at K122 with ATTO655 together with plots of the residuals (below). Samples contained 5 (black), 55 (green) and 500 (blue)  $\mu\text{M}$  of ascorbate. The lines represent the experimentally observed ACFs. The red lines are fits according to Eqn. 4.1 with  $G(\tau)/G(0) = G_{diff}(\tau) G_1(\tau) G_2(\tau)$  with  $\tau_D = 12$  ms.

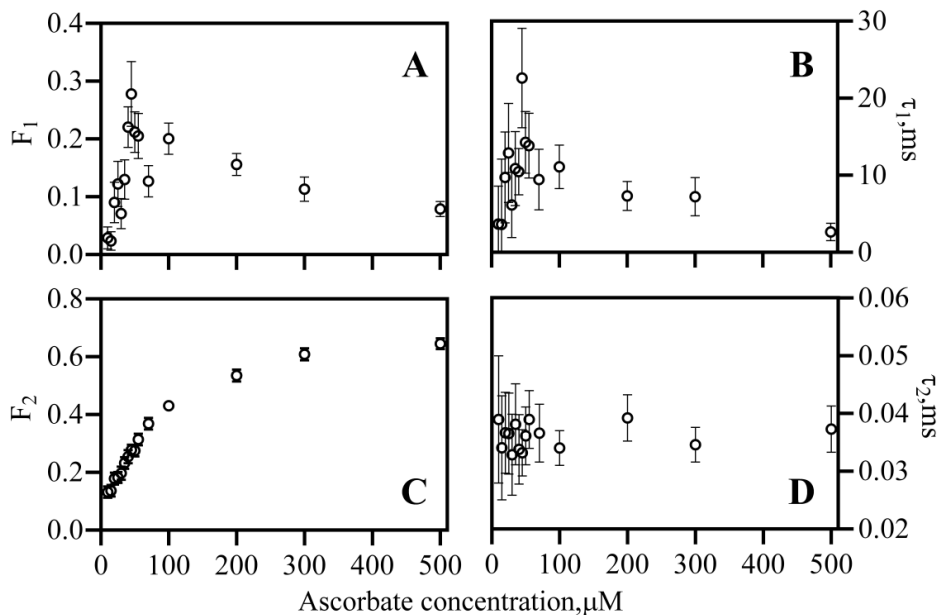


**Figure 4.14:** Parameters obtained from the fits of the ACFs of K122 labeled Cu azurin. The equation used was  $G(\tau) = G_{diff}(\tau) G_1(\tau) G_2(\tau)$  with  $\tau_D = 12$  ms. Shown are, as function of ascorbate concentration:  $F_1$  (A),  $\tau_1$  (B),  $F_2$  (C), and  $\tau_2$  (D).

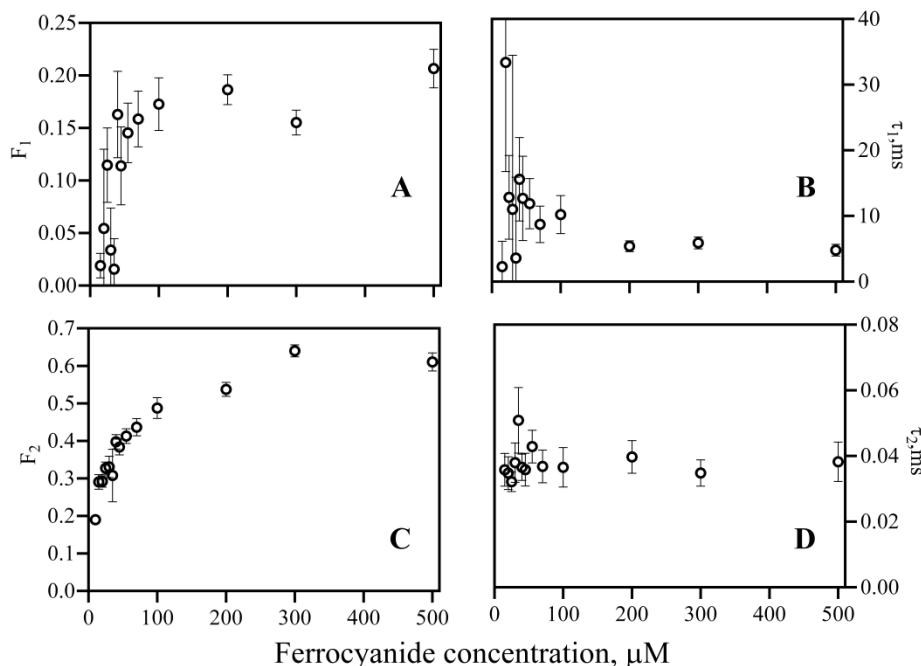
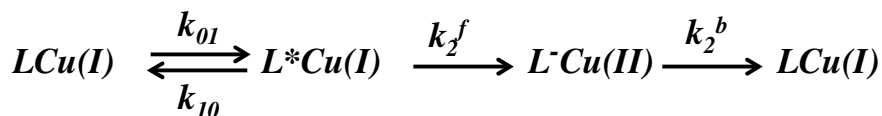


**Figure 4.15:** Parameters obtained from the fits of the ACFs of K122 labeled Cu azurin. The equation used was  $G(\tau) = G_{diff}(\tau) G_1(\tau) G_2(\tau)$  with  $\tau_D = 12$  ms. Shown are, as function of potassium hexacyanoferrate (II) concentration:  $F_1$  (A),  $\tau_1$  (B),  $F_2$  (C), and  $\tau_2$  (D).



**Scheme 4.3:** Light induced ET reactions in reduced CuAz. Symbols have the same meaning as in Scheme 2. The rates for intramolecular ET from Cu(I) to  $L^*$  and from  $L^-$  to Cu(II) to are denoted by  $k_2^f$  and  $k_2^b$ .

Again, consistent with the intramolecular character of the reaction,  $\tau_2$  appears independent from the reductant concentration. What seems at variance with this explanation is that the fraction of dark molecules  $F_2$ , increases with reductant concentration. We ascribe this to the oxygen present in the solution. Small amounts of reductant will be partly oxidized, which results in incomplete reduction of azurin. The ratio between reduced and oxidized protein will gradually shift towards reduced azurin as the amount of added reductant is increased. When the protein is oxidized, fluorescence from the label is reduced by FRET to the Cu site, whereas for reduced azurin the fluorescence of the label is not affected by FRET. Consequently, when both reduced and oxidized azurin are present in the solution, the expression for the ACF has to be slightly modified according to Eqn. (4.9) (The derivation of Eqn. 4.9 is shown in ‘Appendix’ of this



chapter)

$$G(\tau) \propto \frac{1}{\langle N \rangle} G_{diff}(\tau) G_1(\tau) (1 + \beta K e^{-\tau/\tau_2}) \quad (4.9)$$

with  $K = F_{2,red}/(1-F_{2,red})$  and  $\beta$  a numerical parameter between 0 and 1 depending on the ratio between the concentrations of oxidized and reduced azurin. For a 100% reduced or 100% oxidized solution  $\beta$  equals 1 or 0, respectively.

Eqn. (4.9) is similar to the equations (Eqn. 4.1-4.5) that were used to fit the data of K122-labeled CuAz except for the factor  $\beta$ . It is clear now why  $F_2$  as obtained from the fits is not constant. This is because the fit equation did not contain  $\beta$ , which depends on the redox potential of the solution. Since the experimental setup did not allow for control of the latter parameter, a detailed analysis of the data in Fig. 4.14C and 4.15C is not possible. However, assuming that at 500  $\mu$ M of reductant,  $\beta$  is close to its asymptotic value of 1, it follows that  $K = F_2/(1-F_2) = 1.5 \pm 0.3$  (Fig. 4.16). Applying the same analysis as before one obtains

$$F_2/\tau_2 = f(I) k_2^f \quad \text{and}$$

$$(1-F_2)/\tau_2 = k_2^b$$

With  $F_2 = 0.6$ ,  $\tau_2 = 30 \mu$ s and  $f(I) = 4.8 \times 10^{-3}$  one finds  $k_2^f = 4.2 \times 10^6 \text{ s}^{-1}$  and  $k_2^b = 1.3 \times 10^4 \text{ s}^{-1}$ .

Now, one might wonder why  $F_1$  is independent of oxidant concentration in Fig. 4.9 while the data for  $F_2$  in Fig. 4.14 and 4.15 show a pronounced curvature. The reason is that the midpoint potential of the hexacyanoferrate(II)/hexacyanoferrate(III) couple (430 mV vs NHE(43), pH 7.0, 100 mM ionic strength) is much higher than the azurin midpoint potential (270-330 mV vs. NHE depending on pH). Azurin will be readily oxidized when hexacyanoferrate (III) is added to the sample, and thus keeping the protein close to 100% oxidized is relatively simple and  $F_1$  will be constant. Keeping the protein reduced by employing hexacyanoferrate(II), on the other hand, requires a relatively large excess of reductant in order to lower the solution potential far enough. Even then, the oxygen in the sample will gradually raise the potential back, resulting in partial back oxidation of the reduced protein.

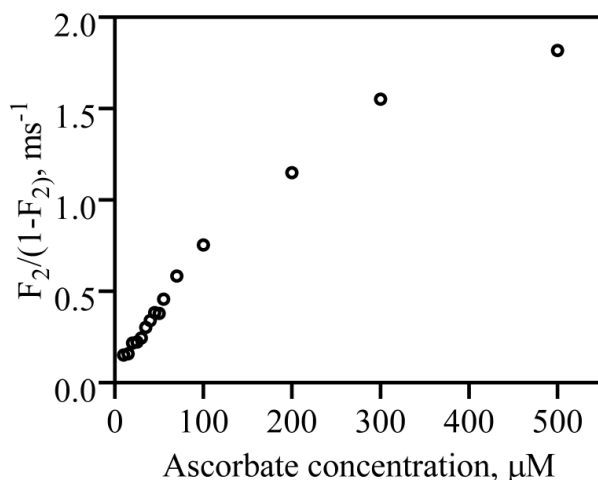


**Figure 4.16:** Plot of  $K = F_{2,red}/(1-F_{2,red})$  as a function of ascorbate concentrations. Kinetic parameters were obtained from the fitting of the ACFs for K122 labeled Cu azurin under reducing conditions (ascorbate). The equation used was  $G(\tau) = G_{diff}(\tau) G_I(\tau) G_2(\tau)$  with  $\tau_D = 12 \text{ ms}$ .

Thus,  $F_2$  will be constant only when a large excess of reductant is employed. As Fig. 4.14 or 4.15 demonstrates, this regime appears to be reached when the reductant concentration amounts to 0.5 mM or more. Again, from the forward and backward ET rates of  $k_2^f = 4.2 \times 10^6 \text{ s}^{-1}$  and  $k_2^b = 1.3 \times 10^4 \text{ s}^{-1}$  a value for the reorganization energy of the ET reaction can be extracted. The data obtained with ascorbate instead of hexacyanoferrate (II) were analyzed in a similar way. The resulting intramolecular ET rates are presented in Table 4.1. With  $E_{ATTO/ATTO^-} = -0.17 \text{ V}$  (vs NHE),  $n_{ATTO} = 0$  and  $n_{Cu(I)} = 1$  and the same values as above for the other parameters one obtains  $\Delta G_f = -1.67 \text{ eV}$ ,  $\Delta G_b = -0.19 \text{ eV}$  and  $\lambda = 1.16 \text{ eV}$ . The latter value is slightly higher than the theoretically expected value (0.95 eV).

Finally,  $G_I(\tau)$  is related to the reduction of the label by the reductant and  $F_1$  and  $\tau_1$  are analyzed as before, taking into account that only a fraction  $(1-F_2)$  of the labeled molecules is in the bright state. The analysis is presented in the Fig. 4.17 and data are gathered in Table 4.1. The observed rates ( $k_b$ ) are in good agreement with the back oxidation rates of labeled Zn-Azurin obtained previously under redox conditions (see Chapter 3, page 90-91), since the non-fluorescent (reduced) labeled molecules have the bimolecular reactions with oxygen in a diffusion-controlled manner.

Intermolecular ET	Label at	$k_f(I)^{(a)}, M^{-1}s^{-1}$	$k_f(I)^{(b)}, M^{-1}s^{-1}$	$k_b^{(a)}, s^{-1}$	$k_b^{(b)}, s^{-1}$
	CuAzurin	N-term	$(7.0 \pm 0.4) \times 10^5$	$(3.2 \pm 0.3) \times 10^5$	$(4.2 \pm 0.1) \times 10^1$
K122		$(4.2 \pm 0.3) \times 10^5$	$(2.0 \pm 0.3) \times 10^5$	$(9.7 \pm 0.9) \times 10^1$	$(5.6 \pm 0.6) \times 10^1$
Intramolecular ET	Label at	$k_1^f, s^{-1(c)}$	$k_1^b, s^{-1(c)}$	$k_2^f, s^{-1(d)}$	$k_2^b, s^{-1(d)}$
	CuAzurin	K122	$(4.8 \pm 0.3) \times 10^4$	$(0.7 \pm 0.1) \times 10^3$	$(3.3 \pm 0.7) \times 10^6$
-			-	(e) $(2.2 \pm 0.1) \times 10^6$	(e) $(1.4 \pm 0.1) \times 10^4$

**Table 4.1:** Experimental values of inter- and intramolecular ET rate constants. See text for further explanations.

(a) hexacyanoferrate (II),

(b) ascorbate,

(c) in presence of excess of hexacyanoferrate (III),

(d) in presence of excess of ascorbate and

(e) in presence of excess of hexacyanoferrate (II).

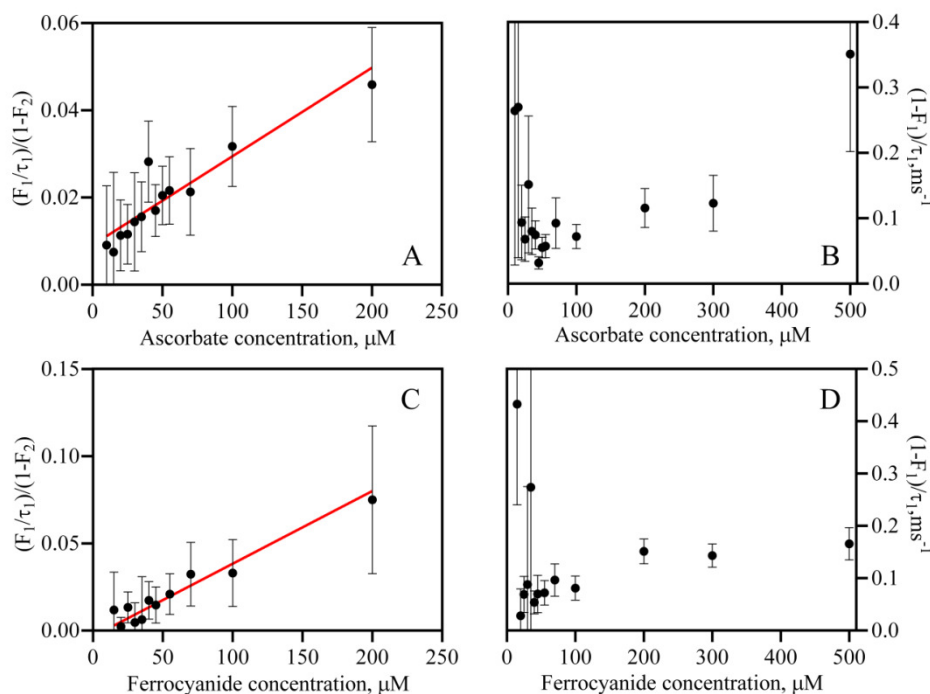


**Figure 4.17:** Analysis of the ACFs of K122-labeled Cu azurin. ACFs were fitted with Eqn. 4.1  $G(\tau) = G(0)G_{\text{diff}}(\tau)G_1(\tau)G_2(\tau)$  with  $\tau_D = 12$  ms. A. Parameters  $\tau_1$  and  $F_1$ , as obtained from the fits, correspond with  $G_1(\tau)$ . A and C:  $(F_1/\tau_1)/(1-F_2)$  ( $k_f$ ) as a function of the concentration of ascorbate (A) or hexacyanoferrate(II) (C); B and D:  $(1-F_1)/\tau_1$  ( $k_b$ ) as a function of the concentration of ascorbate (B) or hexacyanoferrate(II) (D). The red straight lines are least-squares fits to the data points.

#### 4.3.3.3 ET reactions in K122-Cu Azurin as a function of viscosity

FCS studies were performed on K122-labeled CuAzurin under 100  $\mu\text{M}$  ascorbate or potassium hexacyanoferrate (II) as a function of viscosity of the solution. The buffer was kept at 20 mM HEPES pH 7.0 and the sucrose concentration was varied from 0 – 70% (w/v) in the buffer. When using highly viscous solvent, diffusion of the labeled molecule will slow down to the millisecond time scale whereas the intramolecular ET reactions between the copper and the label would remain (Fig. 4.18). ET rates do not depend on the viscosity of the solvent.

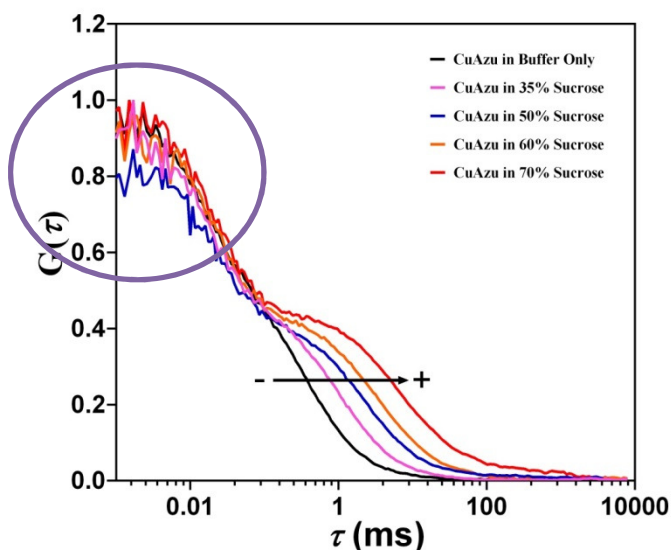


**Figure 4.18:** ACFs of K122 labeled Cu-Azurin measured in the presence of 100  $\mu\text{M}$  ascorbate at different concentration of sucrose solutions. The diffusion decay shifts toward longer times, whereas the decay in the sub-millisecond time range, attributed to the intramolecular electron-transfer reaction, does not shift when the viscosity is increased. The circled region represents the fraction of molecules associated with the intramolecular ET reaction.

#### 4.3.3.4 Light intensity dependence of ET reactions

Photoinduced electron transfer is supposed to be a monophotonic process. During the laser pulse, part of the ground-state molecules are pumped into the lowest excited-singlet state, and the kinetics among the thermally equilibrated lowest excited-singlet and triplet or dark states can be described by the Jablonski diagram of Chapter 1.

As mentioned earlier in this chapter, the power used for the FCS measurements is 20  $\mu\text{W}$ , as measured after the objective, corresponding to a specific power of  $\sim 4.3 \text{ kW/cm}^2$  at the sample.

In this study, to understand the effect of laser intensity on the photoinduced intramolecular electron transfer reaction in K122 labeled CuAzurin under reducing conditions, the laser power was varied from 1  $\mu\text{W}$  to 80  $\mu\text{W}$  (Fig. 4.19). Then, the ACFs were analyzed according to Eqn. 4.1 with  $G(\tau) = G_{diff}(\tau) G_1(\tau) G_2(\tau)$  with  $\tau_D = 12$  ms. Variation of  $F_1$ ,  $\tau_1$ ,  $F_2$ , and  $\tau_2$  as a function of laser power is shown in Fig. 4.20. Some qualitative statements can be made depending on the results.

Under redox conditions, these excited molecules react with ascorbate or hexacyanoferrate (II) and enter into dark states. These states have longer lifetimes than that of the excited dye. The process of pumping ground-state molecules into their excited states is directly related to the absorption of the ground-

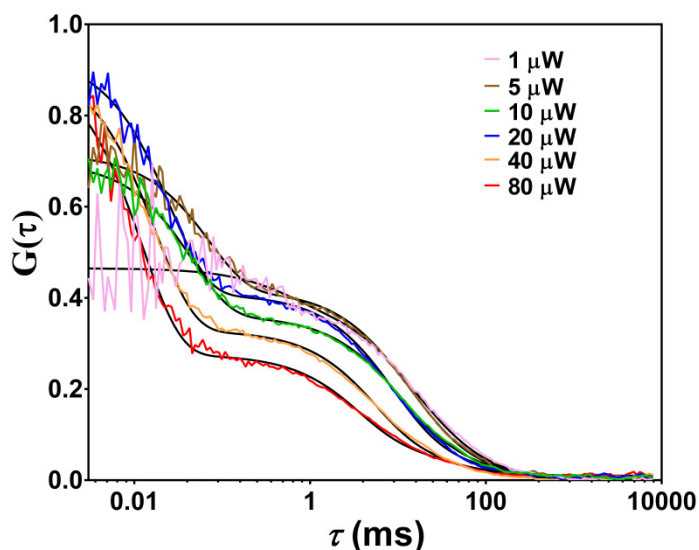


**Figure 4.19:** ACFs of K122 labeled Cu-azurin measured in the presence of 100  $\mu\text{M}$  ascorbate at different laser power in 70% (w/v) sucrose solution. For fitting, the equation used was  $G(\tau) = G_{diff}(\tau) G_1(\tau) G_2(\tau)$  with  $\tau_D = 12$  ms. The black lines are the fit according to the same equation.

state molecules, i.e. excitation of the labeled molecules by the pulsed laser. Under high excitation power, more molecules are excited and become available for the reaction with reducing agents. As a result, intramolecular ET between the reduced label and the copper center is observed. The fraction ( $F_2$ ) of labeled azurin associated with ET reaction becomes saturated at  $\sim 70\%$  (transitions into dark states for ET reactions) and  $\tau_2$  becomes 20-30  $\mu\text{sec}$  at higher laser power. At very low laser power (1 $\mu\text{W}$ ), either ET reaction is absent or it is negligible. Hence, the data

points with low  $\tau_1$  and  $\tau_2$  values at the lowest laser power are not present in Fig. 4.20 and Fig. 4.21. The fraction ( $F_1$ ) of molecules associated with blinking was found to be 0.2. The excitation power of the laser beam and the time scale of intramolecular reaction ( $\tau_2$ ) under reducing conditions are related in the following ways (Chapter 3 for details):

$$F_2/\tau_2 = f(I) k_2^f$$

$$\text{and } f(I) = \frac{k_{01}}{k_{10} + k_{01}}$$

where  $k_{01} = \sigma I_{\text{exc}}$ , with  $\sigma$  the absorption cross section of the label at the wavelength of the laser and  $I_{\text{exc}}$  the laser power in terms of number of photons/sec  $\text{cm}^2$  and  $k_{10}$  is the decay rate of the excited state. Increasing excitation intensities lead to a proportional increase in the emitted fluorescence intensity. The occurrence of the factor  $f(I)$  can be understood by considering that the optically excited label reacts with reductant in the solution on a timescale that is long compared with the excitation and fluorescence time scales ( $k_{01}^{-1}$  and  $k_{10}^{-1}$ ). For simplicity, a plot of  $\tau_2$  as a function of (1/laser power) is presented. It reports their linear relationship with a positive slope (Fig. 4.21).

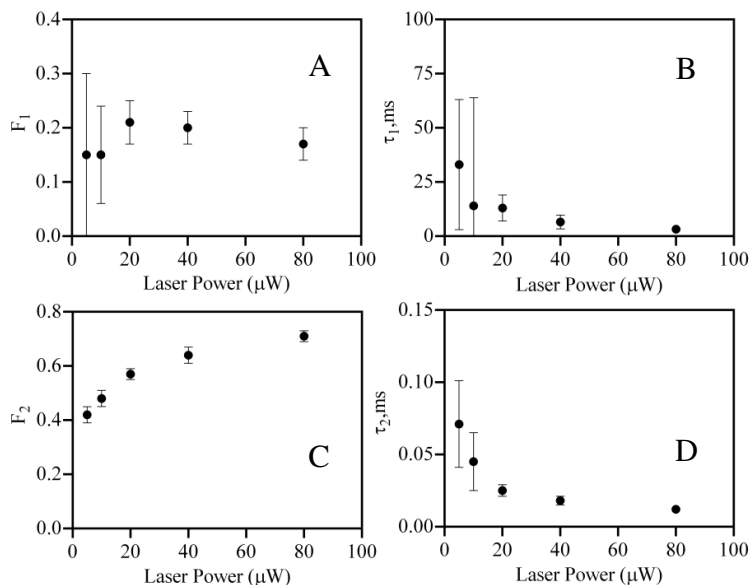


**Figure 4.20:** Parameters obtained from the fits of the ACFs of K122 labeled Cu-Azurin under reducing conditions as a function of laser intensities. The equation used was  $G(\tau) = G_{\text{diff}}(\tau) G_1(\tau) G_2(\tau)$  with  $\tau_D = 12$  ms. Shown are, as function of laser power:  $F_1$  (A),  $\tau_1$  (B),  $F_2$  (C), and  $\tau_2$  (D). Data obtained at 1  $\mu\text{W}$  laser power was neglected due to negligible ET rate.

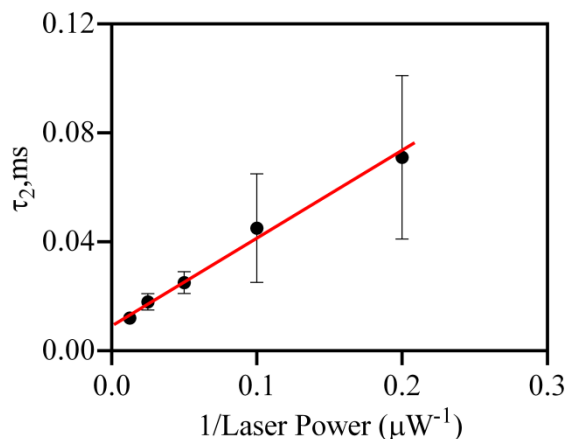


**Figure 4.21:** Plot of experimentally obtained intramolecular electron transfer time scales ( $\tau_2$ ) as a function of ( $1/\text{laser power}$ ) under reducing conditions ( $100 \mu\text{M}$  ascorbate) for K122-CuAzu in 70% (w/v) sucrose solution. Data obtained at  $1 \mu\text{W}$  laser power was neglected due to negligible ET rate.

#### 4.4 Concluding remarks

The first conclusion from the present work is that no PET reactions with amino acids in the protein are observed, but PET to the metal is observed when Cu occupies the active site, and the label is attached close enough to the metal center (at Lys122). It means that a judicious choice of the attachment point for the label on the protein surface can diminish the effect of PET reactions on the fluorescence time trace of a single molecule. The distance between label and active center will also affect the FRET and thereby the switching ratio ( $SR$ ), defined as:

$$SR = \frac{F_{red} - F_{ox}}{F_{red}}$$

Here  $F_{red}$  and  $F_{ox}$  are the emission intensities of the label when the protein is in the reduced (bright) and oxidized (dim) state, respectively. A high switching ratio is desirable when the label fluorescence is used to monitor the enzyme's activity. As the example of the present study shows, increasing the distance between Cu and the attachment point of the label from 18.5 to 29.1 Å abolishes PET, while it reduces the switching ratio only from ~86 to ~65% (Fig. 4.3).

Secondly, the excited label may react with redox-active components in the solution in a diffusion-controlled manner<sup>(44)(45)</sup>. In the case of ATTO655 the reactions occur when there are reductants present in solution. The diffusion rates were diminished by two orders of magnitude

by increasing the viscosity. In this way the intermolecular ET reactions between label and reductant could be singled out from the intramolecular events.

Analysis of the (intramolecular) PET reactions provided values of the driving forces and the reorganization energies for the ET reactions between label and Cu center. The electronic coupling matrix elements between label and center can now be calculated. Assuming a covalent pathway for ET and expressing the electronic coupling in terms of the number of equivalent C-C bonds between Cu and label, the Marcus equation can be written as(19)(36)(46)(47)(48)

$$k_{ET} = 3 \times 10^{13} e^{-\beta_0 \sigma_C \ell} e^{-\frac{(\Delta G_f + \lambda)^2}{4\lambda kT}} \quad (4.10)$$

with  $\beta_0$  an attenuation factor ( $0.7 \text{ \AA}^{-1}$ ),  $\ell$  the length of a C-C bond ( $1.4 \text{ \AA}$ ) and  $\sigma$  the number of equivalent C-C bonds in the path. Using the values of  $G_f$  and  $\lambda$  reported above one obtains a number of 12 or 17 equivalent bonds (Scheme 4.2 or 4.3, respectively). The actual number of bonds, depending on where the linker is considered to end and the fluorophore begins is between 13 to 17 bonds (Fig. 4.22).<sup>1</sup> A quantum-chemical calculation of the ground and excited state wave functions of the label, which might give more transparency on this point, is beyond the scope of the present work. The experimental data appear compatible with ET through a covalent pathway between Cu and label.

It is conceivable that instead of using a covalent pathway the electron jumps through space from the label to the protein and vice versa so that the electronic coupling will be sensitive to the motion of the label. In that case the ET rate may be expected to vary with the viscosity of the solution. In preliminary experiments where the viscosity was varied over almost two orders of magnitude the ET rate stayed constant within a factor of two (Fig. 4.18) compatible with the prevalence of a covalent pathway.

The electrostatic work term in Eqn. (4.8) contributes an amount of +144 meV (Scheme 2) or -288 meV (Scheme 3) to the driving force and eventually contributes an amount of 60 meV (Scheme 2) or -210 meV (Scheme 3) to  $\lambda$ . In both cases this gives a slightly better agreement

---

<sup>1</sup> The most direct pathway between Cu and label consists of Cu-S $\delta$ C $\gamma$ C $\beta$ C $\alpha$ (Met121)-C $\alpha$ C $\beta$ C $\gamma$ C $\delta$ C $\epsilon$ N $\eta$ (Lys122)(4C)-N<sub>het</sub>ATTO 655. These are 15 bonds, if we consider the Cu-S link as a bond and not as a through space jump.



with the expected value for  $\lambda$  (950 meV) than when the electrostatic term would have been neglected. The work term was evaluated by setting the distance between donor and acceptor at  $10\text{\AA}$ , which is the distance between Cu and the aromatic part of the label when the ATTO655 moiety is modelled as lying against the protein surface in the K122 labeled Azu variant. In this configuration the effective  $\epsilon$  will be intermediate between that of the pure protein ( $\epsilon = 4$ ) and that of water ( $\epsilon = 86$ )(49)(50). For obtaining an order of magnitude estimate of the possible effect of including the electrostatic work term in the calculations, the relative dielectric constant was set at 10. The numbers are only rough estimates but the calculation illustrates what effect the inclusion of the electrostatic work terms may have on the final outcome.

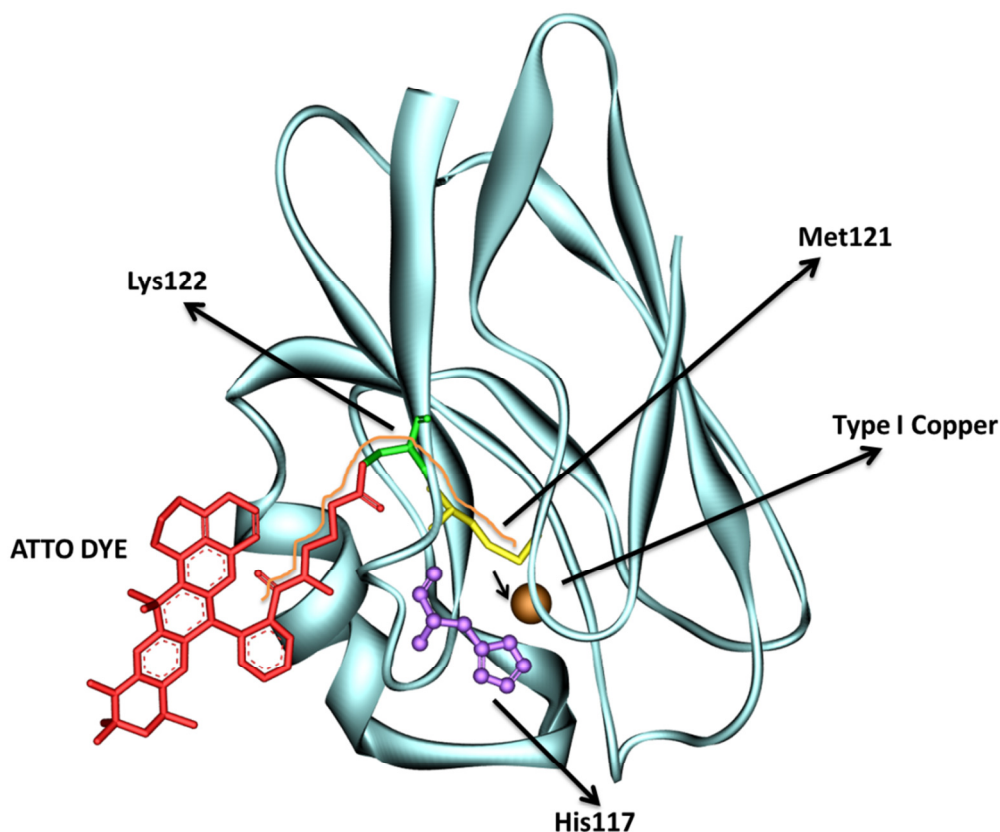


**Figure 4.22:** Close-up of azurin labeled at lys122 (green) with ATTO655 (red). Type I copper is shown as a brown sphere, Met121 is shown in yellow and a small arrow points to the space between the copper and Met121 amino acid. An orange curved line has been drawn to display the most direct pathway between Cu and label consisting of  $\text{Cu-S}\delta\text{C}\gamma\text{C}\beta\text{C}\alpha(\text{Met121})-\text{C}\alpha\text{C}\beta\text{C}\gamma\text{C}\delta\text{C}\epsilon\text{N}\eta(\text{Lys122})(4\text{C})-\text{N}_{\text{het}}\text{ATTO 655}$ . These are 15 bonds, if we consider the Cu-S link as a bond and not as a through space jump.

The overall conclusion of the present study is that in oxido-reductases photoinduced intramolecular ET between label and active center may occur and is not restricted to situations where the label is in Van-der-Waals contact with the redox center. This differs from instances where PET involving aromatic residues was studied and Van der Waals contact was considered a requirement for PET to occur(51)(52)(53)(54)(55)(56). The necessity for Van der Waals contact in these cases probably reflects the much lower driving force for ET due to the unfavorable midpoint potential of the aromatic residues. It is clear that for labeled oxido-reductases PET between dye and redox center can be avoided by making the distance between these large enough. The present work shows that simple thermodynamic considerations combined with ET calculations can provide a good estimate of the chances that PET may occur, and may help in designing experiments for single-molecule studies of oxido-reductases.

Although so far we have only dealt with proteins labeled via lysines or the N-terminus, the conclusions may be expected to apply equally well when (engineered) cysteines are used as anchoring points for labels.

## **References**

- (1) Chen, P.; Andoy, N. M. Single-molecule fluorescence studies from a bioinorganic perspective. *Inorganica Chim. Acta* **2008**, *361*, 809–819.
- (2) Chi, Q.; Farver, O.; Ulstrup, J. Long-range protein electron transfer observed at the single-molecule level : In situ mapping of redox-gated tunneling resonance. *Proc. Natl. Acad. Sci. U. S. A.* **2005**, 16203–16208.
- (3) Wang, Q.; Goldsmith, R. H.; Jiang, Y.; Bockenhauer, S. D.; Moerner, W. E. Probing single biomolecules in solution using the anti-Brownian electrokinetic (ABEL) trap. *Acc. Chem. Res.* **2012**, *45*, 1955–64.
- (4) Zhang, J.; Grubb, M.; Hansen, A. G. Electron transfer behaviour of biological macromolecules towards the single-molecule level. *1873*.
- (5) Zhang, J.; Chi, Q.; Hansen, A. G.; Jensen, P. S.; Salvatore, P.; Ulstrup, J. Interfacial electrochemical electron transfer in biology - towards the level of the single molecule. *FEBS Lett.* **2012**, *586*, 526–35.
- (6) Chung, Y.-H.; Lee, T.; Park, H. J.; Yun, W. S.; Min, J.; Choi, J.-W. Nanoscale biomemory composed of recombinant azurin on a nanogap electrode. *Nanotechnology* **2013**, *24*,

365301.

- (7) Artés, J. M.; López-Martínez, M.; Giraudet, A.; Díez-Pérez, I.; Sanz, F.; Gorostiza, P. Current-voltage characteristics and transition voltage spectroscopy of individual redox proteins. *J. Am. Chem. Soc.* **2012**, *134*, 20218–21.
- (8) Schmauder, R.; Librizzi, F.; Canters, G. W.; Schmidt, T.; Aartsma, T. J. The oxidation state of a protein observed molecule-by-molecule. *Chemphyschem* **2005**, *6*, 1381–6.
- (9) Kuznetsova, S.; Zauner, G.; Aartsma, T. J.; Engelkamp, H.; Hatzakis, N.; Rowan, A. E.; Nolte, R. J. M.; Christianen, P. C. M.; Canters, G. W. The enzyme mechanism of nitrite reductase studied at single-molecule level. *Proc. Natl. Acad. Sci. U. S. A.* **2008**, *105*, 3250–3255.
- (10) Tabares, L. C.; Kostrz, D.; Elmalk, A.; Andreoni, A.; Dennison, C.; Aartsma, T. J.; Canters, G. W. Fluorescence lifetime analysis of nitrite reductase from *Alcaligenes xylooxidans* at the single-molecule level reveals the enzyme mechanism. *Chemistry* **2011**, *17*, 12015–9.
- (11) Schmauder, R.; Alagaratnam, S.; Chan, C.; Schmidt, T.; Canters, G. W.; Aartsma, T. J. Sensitive detection of the redox state of copper proteins using fluorescence. *J. Biol. Inorg. Chem.* **2005**, *10*, 683–687.
- (12) Kuznetsova, S.; Zauner, G.; Schmauder, R.; Mayboroda, O. A.; Deelder, A. M.; Aartsma, T. J.; Canters, G. W. A Förster-resonance-energy transfer-based method for fluorescence detection of the protein redox state. *Anal. Biochem.* **2006**, *350*, 52–60.
- (13) Tabares, L.; Gupta, A.; Aartsma, T.; Canters, G. Tracking Electrons in Biological Macromolecules: From Ensemble to Single Molecule. *Molecules* **2014**, *19*, 11660–11678.
- (14) Doose, S.; Neuweiler, H.; Sauer, M. A close look at fluorescence quenching of organic dyes by tryptophan. *Chemphyschem* **2005**, *6*, 2277–85.
- (15) Michalet, X.; Weiss, S.; Jäger, M. Single-Molecule Fluorescence Studies of Protein Folding and Conformational Dynamics. *Chem. Rev.* **2006**, *106*, 1785–1813.
- (16) Furukawa, Y.; Ban, T.; Hamada, D.; Ishimori, K.; Goto, Y.; Morishima, I. Electron transfer reaction in a single protein molecule observed by total internal reflection fluorescence microscopy. *J. Am. Chem. Soc.* **2005**, *127*, 2098–2103.
- (17) Doose, S.; Neuweiler, H.; Sauer, M. Fluorescence quenching by photoinduced electron transfer: A reporter for conformational dynamics of macromolecules. *ChemPhysChem* **2009**, *10*, 1389–1398.
- (18) Gray, H. B.; Winkler, J. R. Electron tunneling through proteins. *Q. Rev. Biophys.* **2003**, *36*, 341–372.
- (19) Gray, H. B.; Winkler, J. R. Electron flow through metalloproteins. *Biochim. Biophys. Acta* **2010**, *1797*, 1563–72.
- (20) Winkler, J. R.; Gray, H. B. Long-range electron tunneling. *J. Am. Chem. Soc.* **2014**, *136*, 2930–2939.
- (21) Gray, H. B.; Winkler, J. R.; Wiedefeld, D. Effects of driving force on the rates of

- intramolecular and bimolecular electron-transfer reactions. *Coord. Chem. Rev.* **2000**, *200–202*, 875–886.
- (22) Haustein, E.; Schwille, P. Fluorescence correlation spectroscopy: novel variations of an established technique. *Annu. Rev. Biophys. Biomol. Struct.* **2007**, *36*, 151–69.
- (23) Ries, J.; Schwille, P. Fluorescence correlation spectroscopy. *BioEssays* **2012**, *34*, 361–368.
- (24) Haustein, E.; Schwille, P. Ultrasensitive investigations of biological systems by fluorescence correlation spectroscopy. *Methods* **2003**, *29*, 153–166.
- (25) Krichevsky, O. Fluorescence correlation spectroscopy : the technique. *Rep.Prog.Phys* **2002**, *65*, 251.
- (26) Felekyan, S.; Kühnemuth, R.; Kudryavtsev, V.; Sandhagen, C.; Becker, W.; Seidel, C. a M. Full correlation from picoseconds to seconds by time-resolved and time-correlated Single photon detection. *Rev. Sci. Instrum.* **2005**, *76*, 1–14.
- (27) Goldberg, M.; Pecht, I. Kinetics and equilibria of the electron transfer between azurin and the hexacyanoiron (II/III) couple. *Biochemistry* **1976**, *15*, 4197–4208.
- (28) Van de Kamp, M.; Hali, F. C.; Rosato, N.; Agro, A. F.; Canters, G. W. Purification and characterization of a non-reconstitutable azurin, obtained by heterologous expression of the *Pseudomonas aeruginosa* *azu* gene in *Escherichia coli*. *Biochim. Biophys. Acta* **1990**, *1019*, 283–292.
- (29) Nicolardi, S.; Andreoni, A.; Tabares, L. C.; van der Burgt, Y. E. M.; Canters, G. W.; Deelder, A. M.; Hensbergen, P. J. Top-down FTICR MS for the identification of fluorescent labeling efficiency and specificity of the Cu-protein azurin. *Anal. Chem.* **2012**, *84*, 2512–20.
- (30) E. T. Adman and L. H. Jensen Structural Features of Azurin at 2.7 Å Resolution. *Isr. J. Chem.* **1981**, *21*, 8–12.
- (31) Robert C. Weast, M. J. A. *CRC Handbook of Chemistry and Physics*; CRC Press, Inc, Boca Raton, Florida.
- (32) Lakowicz, J. R.; Gryczynski, I.; Laczko, G.; Gloyna, D. Picosescond fluorescence lifetime standards for frequency- and time-domain fluorescence. *J. Fluoresc.* **1991**, *1*, 87–93.
- (33) Lampert, R. A.; Chewter, L. A.; Phillips, D.; O'Connor, D. V; Roberts, A. J.; Meech, S. R. Standards for nanosecond fluorescence decay time measurements. *Anal. Chem.* **1983**, *55*, 68–73.
- (34) Marcus, R. a.; Sutin, N. Electron transfers in chemistry and biology. *Biochim. Biophys. Acta - Rev. Bioenerg.* **1985**, *811*, 265–322.
- (35) Newton, M. Electron transfer reactions in condensed phases. **1984**, *35*, 437–480.
- (36) Canters, G. W.; van de Kamp, M. Protein-mediated electron transfer. *Curr. Opin. Struct. Biol.* **1992**, *2*, 859–869.
- (37) Rehm, D.; Weller, A. Kinetics of fluorescence quenching by electron and hydrogen-atom

- transfer. *Isr. J. Chem.* **1970**, *8*, 259–271.
- (38) Van De Kamp, M.; Canters, G. W.; Andrew, C. R.; Sanders-Loehr, J.; Bender, C. J.; Peisach, J. Effect of lysine ionization on the structure and electrochemical behaviour of the Met44-->Lys mutant of the blue-copper protein azurin from *Pseudomonas aeruginosa*. *Fed. Eur. Biochem. Soc. J.* **1993**, *218*, 229–238.
- (39) Clair, C. S.; Ellis, W.; Gray, H. Spectroelectrochemistry of blue copper proteins: pH and temperature dependences of the reduction potentials of five azurins. *Inorganica Chim. Acta* **1992**, *191*, 149–155.
- (40) Zhu, R.; Li, X.; Zhao, X. S.; Yu, A. Photophysical properties of Atto655 dye in the presence of guanosine and tryptophan in aqueous solution. *J. Phys. Chem. B* **2011**, *115*, 5001–7.
- (41) Seidel, C. a. M.; Schulz, A.; Sauer, M. H. M. Nucleobase-Specific Quenching of Fluorescent Dyes. 1. Nucleobase One-Electron Redox Potentials and Their Correlation with Static and Dynamic Quenching Efficiencies. *J. Phys. Chem.* **1996**, *100*, 5541–5553.
- (42) Bellion, E. The Biological Chemistry of the Elements: The Inorganic Chemistry of Life (da Silva, J. J. R. Frausto; Williams, R. J. P.). *J. Chem. Educ.* **1992**, *69*, A326.
- (43) O'Reilly, J. E. Oxidation-reduction potential of the ferro-ferricyanide system in buffer solutions. *Biochim. Biophys. Acta* **1973**, *292*, 509–515.
- (44) Widengren, J.; Chmyrov, A.; Eggeling, C.; Löfdahl, P.-A.; Seidel, C. A. M. Strategies to improve photostabilities in ultrasensitive fluorescence spectroscopy. *J. Phys. Chem. A* **2007**, *111*, 429–440.
- (45) Vogelsang, J.; Kasper, R.; Steinhauer, C.; Person, B.; Heilemann, M.; Sauer, M.; Tinnefeld, P. A reducing and oxidizing system minimizes photobleaching and blinking of fluorescent dyes. *Angew. Chemie Int. Ed.* **2008**, *47*, 5465–5469.
- (46) Onuchic, J. N.; Beratan, D. N.; Winkler, J. R.; Gray, H. B. Pathway analysis of protein electron-transfer reactions. *Annu. Rev. Biophys. Biomol. Struct.* **1992**, *21*, 349–377.
- (47) Megan L. Jones, I. V. K.; Beraton, D. N. The nature of tunneling in pathway and average packing density models for protein-mediated electron transfer. **2002**, *106*, 2002–2006.
- (48) D. N. Beratan; J; J. N. Betts; N; Onuchic Protein Electron Transfer Rates set by the Bridging Secondary and Tertiary Structure. *Science (80- )*. **1991**, *7*, 1285–1288.
- (49) T. Simomson, C. L. B. Charge Screening and the Dielectric Constant of Proteins: Insights from Molecular Dynamics. *J. Am. Chem. Soc.* **1996**, *118*, 8452–8458.
- (50) C. G. Malmberg, A. A. M. Dielectric constant of water from 0° to 100 °C. *J. Res. Natl. Bur. Stand. (1934)*. **1956**, *56*, 1–8.
- (51) Tanaka, F.; Chosrowjan, H.; Taniguchi, S.; Mataga, N.; Sato, K.; Nishina, Y.; Shiga, K. Donor-acceptor distance-dependence of photoinduced electron-transfer rate in flavoproteins. *J. Phys. Chem. B* **2007**, *111*, 5694–9.
- (52) Porcal, G.; Bertolotti, S. G.; Previtali, C. M.; Encinas, M. V. Electron transfer quenching of singlet and triplet excited states of flavins and lumichrome by aromatic and aliphatic

- electron donors. *Phys. Chem. Chem. Phys.* **2003**, *5*, 4123.
- (53) Murakami, M.; Ohkubo, K.; Fukuzumi, S. Inter- And intramolecular photoinduced electron transfer of flavin derivatives with extremely small reorganization energies. *Chem. - A Eur. J.* **2010**, *16*, 7820–7832.
- (54) Kang, H.; Jouvét, C.; Dedonder-Lardeux, C.; Martrenchard, S.; Charrière, C.; Grégoire, G.; Desfrancois, C.; Schermann, J. P.; Barat, M.; Fayeton, J. a Photoinduced processes in protonated tryptamine. *J. Chem. Phys.* **2005**, *122*, 84307.
- (55) Grégoire, G.; Lucas, B.; Barat, M.; Fayeton, J. A.; Dedonder-Lardeux, C.; Jouvét, C. UV photoinduced dynamics in protonated aromatic amino acid. *Eur. Phys. J. D* **2009**, *51*, 109–116.
- (56) Jones, G.; Farahat, C. W. Photoinduced electron and hole transfer involving eosin conjugates of tryptophan derivatives. *Res. Chem. Intermed.* **1994**, *20*, 855–877.
- (57) Gupta, A.; Aartsma, T. J.; Canters, G. W. One at a time: Intramolecular electron-transfer kinetics in small laccase observed during turnover. *J. Am. Chem. Soc.* **2014**, *136*, 2707–2710.
- (58) Salverda, J. M.; Patil, A. V.; Mizzon, G.; Kuznetsova, S.; Zauner, G.; Akkilic, N.; Canters, G. W.; Davis, J. J.; Heering, H. A.; Aartsma, T. J. Fluorescent Cyclic Voltammetry of Immobilized Azurin: Direct Observation of Thermodynamic and Kinetic Heterogeneity. *Angew. Chemie Int. Ed.* **2010**, *49*, 5776–5779.

## Appendix

### *Autocorrelation function when the azurin in solution is only partly reduced in case of K122-Cu azurin*

When the azurin in a sample is only partly reduced the expression for the ACF has to be adapted from what is described by Eqns. 4.1 – 4.6 previously. This can be understood by realizing that a partly reduced sample contains reduced as well as oxidized azurin molecules and that these two species exhibit different brightness. In the oxidized form FRET quenches part of the fluorescence, while in the reduced azurin the fluorescence of the label is maximal. Consequently, the expression for the ACF has to be adapted.

When denoting the relative brightness of the label in the oxidized (Cu(II)Az) and the reduced (Cu(I)Az) azurin by  $\eta_{ox}$  and  $\eta_{red}$ , respectively, and the fractions of the azurin molecules in the oxidized and reduced form by  $\rho_{ox}$  and  $\rho_{red}$ , respectively, the expression for the ACF can be derived from the more general expression in (57)(58), and it becomes:

$$G(\tau) = \frac{\eta_{ox}^2 \rho_{ox} G_{ox}(\tau) + \eta_{red}^2 \rho_{red} G_{red}(\tau)}{(\eta_{ox} \rho_{ox} + \eta_{red} \rho_{red})^2} \quad (\text{A.1})$$

The ACFs for the oxidized and reduced particles,  $G_{ox}(\tau)$  and  $G_{red}(\tau)$ , respectively, each have the form of Eqn. (A.1). They are similar except for the part that corresponds with the intramolecular ET between  $\text{Cu}^+$  and the label and between the label and  $\text{Cu}^{2+}$ . Here we ignore the latter reaction. It occurs at a much longer time scale than the former reaction and the contribution to the ACF is small unless the degree of reduction is very low which is not the case considered here. Hence  $G_{2,ox} = 1$  whereas

$$G_{2,red}(\tau) = \frac{(1 - F_{2,red} + F_{2,red} e^{-\tau/\tau_2})}{(1 - F_{2,red})} \quad (\text{A.2})$$

The subscripts *ox* and *red* refer to the oxidized and reduced azurin molecules and the subscript 2 denotes the parts in the ACF that correspond with the ET reaction between label and Cu. After some rearrangement Eqn. A.1 becomes

$$G(\tau) = \frac{1}{\langle N \rangle} \alpha G_{diff}(\tau) G_1(\tau) (1 + \beta K e^{-\tau/\tau_2}) \quad (\text{A.3})$$

where,

$$K = \frac{F_{2,red}}{1 - F_{2,red}}$$

$$\alpha = \frac{\eta_{ox}^2 \rho_{ox} + \eta_{red}^2 \rho_{red}}{(\eta_{ox} \rho_{ox} + \eta_{red} \rho_{red})^2}$$

$$\beta^{-1} = 1 + \left(\frac{\eta_{ox}}{\eta_{red}}\right)^2 \frac{\rho_{ox}}{\rho_{red}}$$

The Eqn. (A.2) is similar to the Eqns. (4.1)-(4.6) that were used to fit the data of K122-labeled CuAz except for the factors  $\alpha$  and  $\beta$ . It is clear now why  $F_2$  did not come out as a constant from this fit since the fit equation did not contain the factor  $\beta$ . Also  $G(0)$  will vary with the degree of reduction when Eqns. (4.1)-(4.6) are used because of the factor  $\alpha$ . When the reduction proceeds,  $\rho_{ox}/\rho_{red}$  diminishes and  $\alpha$  and  $\beta$  will approach  $1/\rho_{red}$  and 1, respectively, and become constant. It is clear that both  $\alpha$  and  $\beta$  depend on the ratio between oxidized and reduced azurin, *i.e.*, on the redox potential of the solution.



## **Chapter 5**

### **Labeling and fluorescence correlation spectroscopic studies on Lys122Ser and Lys122Gln mutants of Copper Azurin**

## Abstract

A detailed investigation of the products of the labeling reaction of K122S and K122Q Cu azurin variants with the oxazine fluorophore ATTO655 has been performed. Fluorescence correlation spectroscopy was performed to understand the behavior of the labeled products under redox conditions. In this work, we have tried to understand the ET reaction using a specific species where the label is likely to be attached on a surface lysine and it reports sub-millisecond ET reaction under redox conditions. Slower ET rates in variants of azurin than the rates in *wt* Cu azurin reveal that these lysine residues must be at least 20 Å away from the copper center. Two different mechanisms are equally likely to be involved in the ET event.

## 5.1 Introduction

Biological electron transfer (ET) is observed for many processes in living cells and organisms. These processes include respiration, photosynthesis, immune response, solar-energy conversion and collagen synthesis. In most of these processes, electron transfer reactions take place with the help of redox proteins, with a certain prosthetic group, a metal ion or an organic molecule, which mostly determines the redox properties of the protein(1)(2)(3). We have chosen the prototype electron transfer (ET) protein, copper azurin from *Pseudomonas aeruginosa* for investigating ET reactions(4). Azurin is easily obtained by heterologous expression in *E. coli* bacteria in high yields(5), and the protein is very stable at room temperature(6)(7)(8)(9). It also has a rigid scaffold for the metal-binding site, the properties of which are fine-tuned by the surrounding protein matrix. Thus, azurin is among the most extensively studied redox enzymes. It serves as a donor or acceptor for several other proteins and substances in bacteria(10)(11)(12). A remarkable amount of information is available in the literature regarding its spectroscopic, structural and ET properties(13)(14)(15). Also many variants have been studied.

Recent advances in optical imaging techniques have established that it is possible to observe the dynamics of a protein at single-molecule level(16)(17)(18)(19). Analytical measurements at the single-molecule level using fluorescence techniques have become almost routine in many research laboratories in the past few years. Among these techniques, single-molecule fluorescence correlation spectroscopy (FCS) has proven to be valuable to investigate a range of processes such as ligand binding, protein folding, protonation and deprotonation (20)(21)(22)(23)(24)(25)(26)(27)(28). Ultimate goal in these investigations is the direct investigation of the molecular dynamics *in vivo*. In previous chapters, the inter- and intramolecular electron transfer processes were addressed by a FRET (Fluorescence resonance energy transfer)-FCS based approach.

Labeling oxidoreductases with a fluorescent dye has allowed the study of enzyme turnover at single-molecule level, provided Förster resonant energy transfer (FRET) occurs between the label and the active site(29)(30)(31)(32)(33). Our previous investigations on ATTO655 (oxazine dye) labeled azurin have revealed that it is possible to purify protein labeled at a specific position from a mixture that is obtained after performing a labeling reaction of the protein with a dye(34). In the case of azurin, we addressed the fluorescent behavior of those individual components at the single-molecule level (see Chapter 3 and 4 for details). That work

has enabled us to understand ET dynamics as a function of the position of the label on the protein surface. We have been able to monitor intramolecular ET dynamics in the microsecond region between the label attached at the K122 position of the protein surface and the metal center.

Interestingly, among all the lysine residues present in the protein (Lys 24, Lys27, Lys128, etc.) (Fig. 5.1), Lys122 was identified as the main reaction site during labeling with the NHS-ester of ATTO655(34). Subsequently, further questions arose relating to the microsecond ET process that emerged from the FCS curves of K122 labeled azurin. If single-molecule detection for ET dynamics is possible for K122 labeled Cu azurin, would it be possible to encounter the same decay in Cu azurin-ATTO655 bioconjugates where the reaction sites are other surface lysines of azurin (Lys24, Lys27, Lys128, etc.)? Will the time scale of intramolecular electron transfer in those cases be similar to our previous results?

In order to answer these questions, we have mutated the lysine residue at position 122 into a serine (K122S) and a glutamine (K122Q). In the present study, our strategy was to label the variants with ATTO655, to characterize the products of the labeling reaction and then study the properties of a specific species by means of FCS. Singly labeled azurin derivatives were separated from one another and purified by ion exchange chromatography. The redox properties of the solution containing the azurin-dye constructs were manipulated by using potassium hexacyanoferrate (III) and sodium ascorbate. The reaction rates of the photoinduced electron transfer from the Cu(I) ion to the label and for the back reaction from the label to the Cu(II) were obtained from FCS measurements. Analysis of the obtained rate constants for electron-transfer to or from the copper center revealed a good correlation between the time scale of ET and the length of the ET pathway.

## ***5.2 Materials and Methods***

### ***5.2.1 Chemicals***

Unless stated otherwise, all materials were purchased from Sigma-Aldrich Corp. St. Louis, USA and used as received.

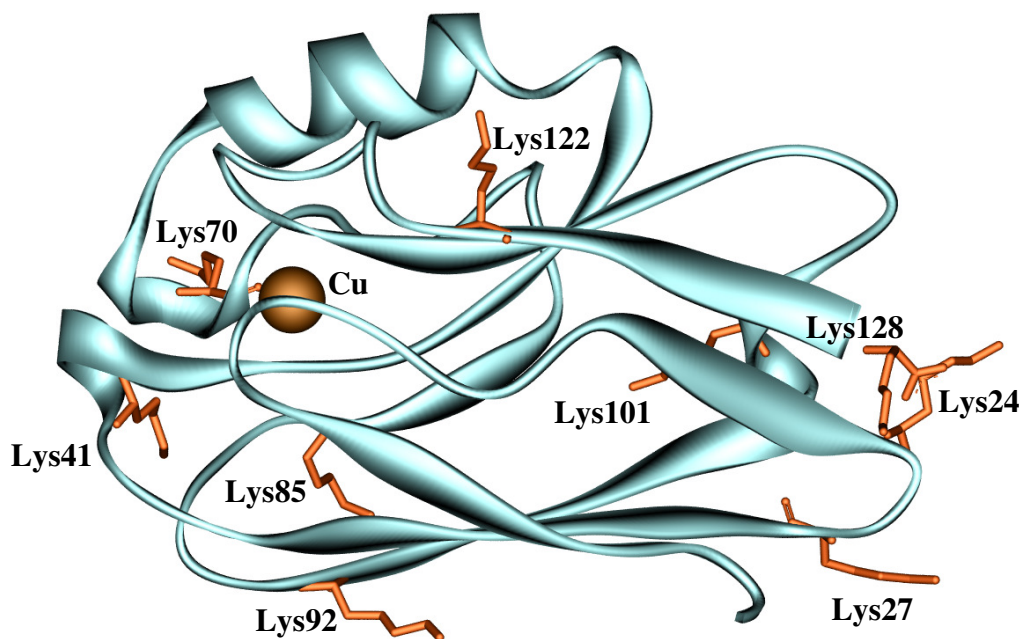


**Figure 5.1:** Cartoon representation of the structure of azurin with its surface lysine residues (PDB: 2AZU). The copper ion is displayed as a brown sphere. The lysine amino acids are represented by red sticks. The model of azurin was prepared by using the DS visualizer program (Accelrys Discovery Studio 2.0).

### 5.2.2 Site-directed mutagenesis and proteins

Lys122 to Ser (K122S) and Lys122 to Gln (K122Q) mutations were introduced into the azurin gene by site-directed mutagenesis (QuikChange Site-directed mutagenesis kit-Stratagene). The primers used for the respective mutations are given below; mutations are in bold and underlined. Primers were designed using the provided software of the QuikChange kit.

K122S_forward	5'-gtcagggtgcc <u>g</u> ctcatcagtgcgctatgacccg-3'
K122S_reverse	5'-cgggtcatagcgactgatga <u>g</u> cggcaccctgac-3'
K122Q_forward	5'-catagcgactgatg <u>ca</u> aggcaccctgaccc-3'
K122Q_reverse	5'-gggtcagggtgcctt <u>g</u> ctcatcagtgcgctatg-3'

Desired mutations were confirmed by DNA sequencing (BaseClear). The codon optimized gene was synthesized by Life Technologies and was cloned into pET28 vector. The expression and the

purification of the mutants were carried out as reported previously(5). The proteins were aliquoted and stored at -80 °C till further use. Models for the variants are displayed in Fig. 5.2. The absorption spectrum of *wt*-Cu Azurin, K122S, and K122Q variants are shown in Fig. 5.3.

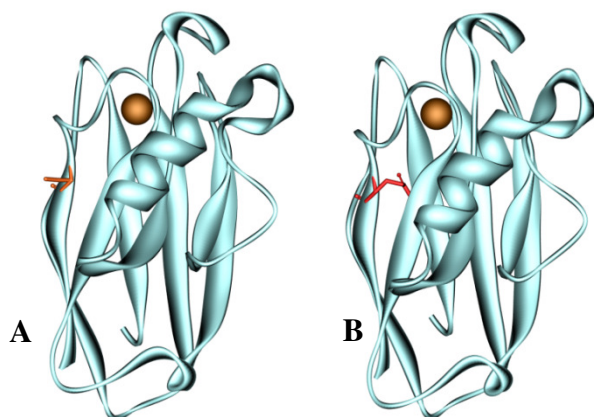


**Figure 5.2:** Models for K122S (A) and K122Q (B) variants. The Models were generated by using “WhatIf molecular modelling program”, Radboud University, The Netherlands (G. Vriend, *J. Mol. Graph.*, 1990, 8, 52-26). Visual rendering of the molecules was performed by using the DS visualizer program (Accelrys Discovery Studio 2.0). The copper ion is displayed as a brown sphere. Serine122 and Glutamine122 residues are presented as red sticks.

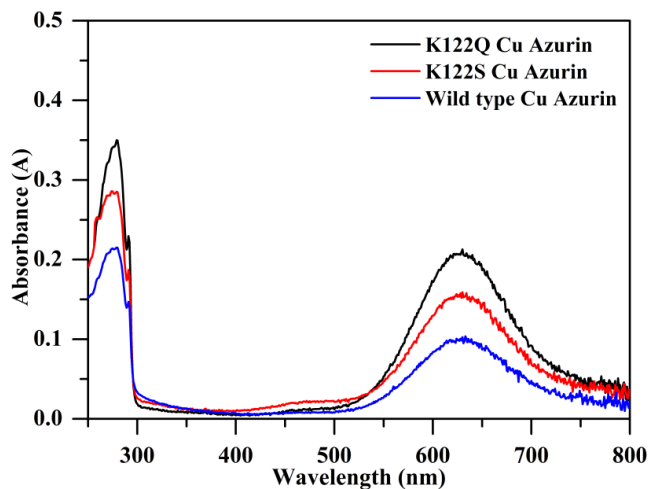


**Figure 5.3:** Absorption spectra of *wt* (20  $\mu$ M), K122S (30  $\mu$ M) and K122Q (35  $\mu$ M) Cu Azurin. The spectra were measured in 20 mM HEPES, pH 7.0 at room temperature.

### ***5.2.3 Protein labeling and chromatography of labeled species***

K122S and K122Q Cu-azurin from *Pseudomonas aeruginosa* were labeled using commercially available N-hydroxysuccinimidyl-ester (NHS) of ATTO655 dye (ATTO-TECH, GmbH, Germany). Elimination of the unreacted label from the labeling mixture and separation of the different labeled species using ion exchange chromatography were executed as previously reported(34). Labeling at pH 6.0 and pH 7.0 was performed using 20 mM HEPES. UV/Vis spectra were measured on a Cary50 UV/Vis (Varian Inc. Agilent Technologies, USA) spectrophotometer.

### ***5.2.4 Fluorescence switching in bulk***

Fluorescence spectroscopy experiments were carried out using a Cary Eclipse Spectrophotometer (Varian Inc. Agilent Technologies, USA). The experiments were performed in 20 mM HEPES, pH 7.0 at room temperature and the concentration of the labeled samples was 50-100 nM. The experiments were performed as previously described (See Chapter 3). Details on the measurement of the fluorescence switching ratio have been discussed in Chapter 1.

### ***5.2.5 Sample preparation for FCS experiments***

Samples were prepared as discussed in Chapter 2 and 3. They contained 57.0% sucrose (w/w) (viscosity 37.5 cP at 22<sup>0</sup>C)(35). All solutions were passed through a 0.22  $\mu$ m filter to avoid the presence of particulate. The final sample concentration of labeled protein was around 0.4-0.8 nM. Manipulation of the redox potential of the solution was established by employing potassium hexacyanoferrate (III) and sodium ascorbate as oxidizing and reducing agents, respectively.

### ***5.2.6 Fluorescence Correlation Spectroscopy setup and data acquisition***

FCS experiments were performed on a home-built confocal setup equipped for Time-Correlated Single-Photon Counting (TCSPC) measurements (See Chapter 2 for details). All experiments were performed at ambient temperature (22 °C). Excitation at 639 nm was provided by a pulsed diode laser head (LDH-P-C-635-B, 20 MHz rep rate, PicoQuant GmbH, Berlin, Germany) driven by a picosecond laser driver (LDH-800-B, PicoQuant GmbH, Berlin, Germany). The power used for the calibration and for the FCS measurements amounted to 20

$\mu\text{W}$ , as measured after the objective, corresponding to a specific power of  $\sim 4.3 \text{ kW/cm}^2$  at the sample.

For the acquisition of the FCS data, 80  $\mu\text{l}$  of the sample solution was deposited onto a glass slide (cover slips Nr. 1.5, thickness 0.16 - 0.19 mm, Gerhard Menzel GmbH, Germany) and covered with the cap of a polypropylene test tube to prevent evaporation of the solvent during the measurements. The focus was set at a distance of 20  $\mu\text{m}$  from the upper surface of the glass coverslip to prevent detection of fluorescence from surface-adsorbed molecules. Time traces were recorded with the SymPhoTime software package (PicoQuant GmbH, Berlin, Germany) for durations varying from 5 to 10 minutes. Raw data were stored as time-tagged time-resolved (t3r) data files and subsequently elaborated by using the SymPhoTime software package.

### 5.2.7 FCS data analysis

After acquisition of the data, the time-correlated single photon counting (TCSPC) histogram was built, and fitting was performed after narrowing down the time window of the TCSPC decay. The autocorrelation functions were analyzed by fitting to the following equation(26):

$$G(\tau) = G(0) \cdot G_{diff}(\tau) \cdot G_1(\tau) \cdot G_2(\tau) \quad (5.1)$$

where  $G(0)$  is given by

$$G(0) = \frac{1}{\langle N \rangle} = \frac{1}{c \cdot V_{eff} \cdot N_A} \quad (5.2)$$

$G_2(\tau)$ , or both  $G_1(\tau)$  and  $G_2(\tau)$ , were omitted when their inclusion in the fitting procedure gave no significant improvement of the fit. Fitting of the autocorrelation data was performed in GraphPad Prism 5 or 6.05 (GraphPad Inc., USA). The quality of the fits was judged by visual inspection of the residuals.



## 5.3 Results and discussion

### 5.3.1 Purification of labeled species and characterization

To isolate a homogeneous 100% singly labeled sample from the labeling solution, ion exchange chromatography (IEC) of the reaction mixture was performed following the protocol mentioned in(34). Fig. 5.4 shows the chromatogram of the labeling mixture of K122Q CuAzurin after reaction with ATTO655 dye. Each peak corresponds to a different species. The fractions were eluted under a gradient of 0 to 100 mM sodium chloride in 5 mM Tris pH 8.5 over 30 column volumes at a flow rate of 0.5 ml/min. The concentrations of the fractions were determined from the extinction coefficients  $\epsilon_{\text{Azurin}}^{280} = 9.8 \text{ mM}^{-1}\text{cm}^{-1}$  and  $\epsilon_{\text{dye}}^{663} = 125 \text{ mM}^{-1}\text{cm}^{-1}$  by UV/Vis spectrometry(36). K122S Cu azurin-ATTO655 displayed an elution profile similar to K122Q. The UV/Vis spectra of the various species are grouped in two panels in Fig. 5.5. In panel A the spectrum corresponding to fraction 1 is that of unlabeled reduced K122S Cu azurin. Fraction 1' (P1') and fraction 2 (P2) show a main peak around 663 nm and a shoulder at 618 nm. This pattern matches the spectrum of singly labeled azurin(37). Fractions 3 (P3) and 4 (P4) show a major peak at 615 nm and a less intense peak at 663 nm, reminiscent of H-type dimerization of ATTO dyes(38). Fractions 3-5 for both variants were not investigated further.

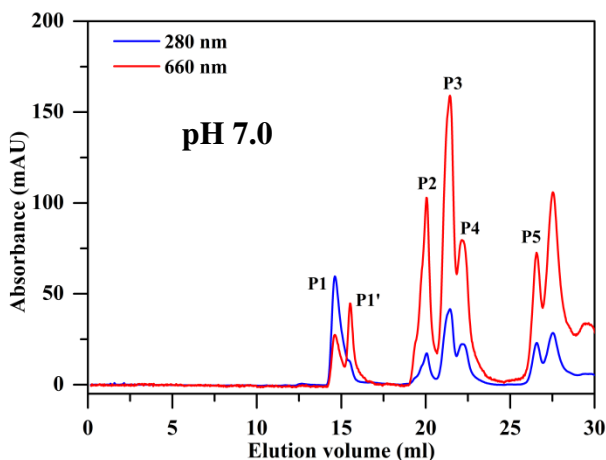


**Figure 5.4:** Elution profile of the reaction mixture after performing the labeling reaction for K122Q with the NHS ester of ATTO655 at 20 mM HEPES, pH 7.0. The elution was performed in 5 mM Tris buffer, pH 8.5 with a 0 to 100 mM NaCl gradient over 30 column volumes at a flow rate of 0.5 ml/min. Numerical tags are used to identify peaks. The chromatograms show the elution pattern when monitoring at two wavelengths: 280 nm (blue line), characteristic absorption of the protein; and 660 nm (red line), characteristic absorption of the label.

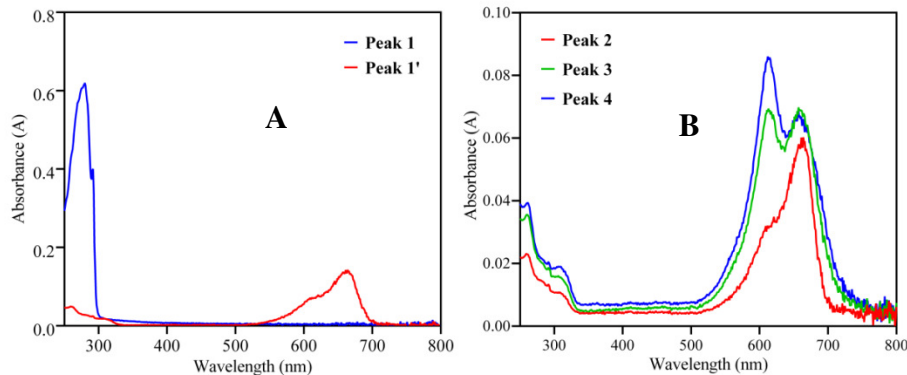


**Figure 5.5:** UV/Vis spectra of the fractions isolated during chromatographic separation from K122S Cu azurin-ATTO655 labeling mixture. The species are identified by the tag numbers used in Fig. 5.4.

### 5.3.2 Influence of the pH on the labeling reaction

To investigate the product distribution for these variants, we performed the labeling reactions at different pH values (6.0 and 7.0). In case of the K122S mutant (Fig. 5.6), when comparing the intensities of the first four fractions with one another, it is clear that when going from pH 6.0 to pH 7.0, fraction 1' and fraction 2 decrease and fraction 3 increases. As a general effect, an increase in pH increases slightly the yield of the labeling reaction. For both mutants, when comparing the relative intensities, the amount of fraction 1' was found to be lower than that of fraction 2 at pH 7.0. In the present case, fraction 1 is assigned to unlabeled reduced azurin as it shows no absorbance at 660 nm.

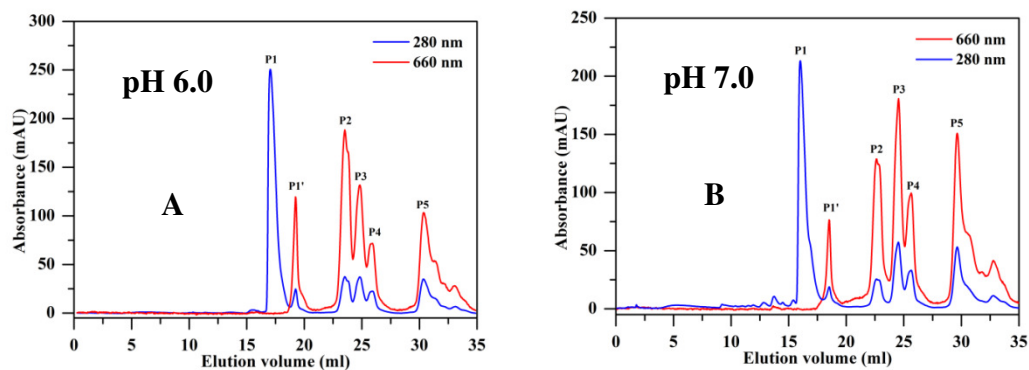


**Figure 5.6:** Elution profiles of the reaction mixtures for the K122S variant after performing the labeling reaction at different pHs as indicated in the top left corner of each panel. The conditions used for the separation are the same as indicated for Fig. 4. Numerical tags are used to identify peaks.

The  $pK_a$  values of lysine122 and the N-terminus are known (~ 7.0 and 8.0 respectively). But  $pK_a$ s of other surface lysines (Lys24, Lys27, Lys41, Lys128, etc.) are not available in the literature. It is expected that these lysine residues have  $pK_a$ s higher than the  $pK_a$  of K122(39). Increasing pH to 7.0 or higher makes those lysines available for labeling with dye. We choose fraction 1' and fraction 2 for further investigation.

### 5.3.3 Fluorescence switching experiments

For each species, the sample was excited at 660 nm, and the fluorescence emission was monitored at 685 nm after addition of redox agents (See Fig. 5.7). Upon addition of oxidant, the fluorescence drops, the magnitude of the drop depending on the initial redox state of the protein. Subsequent addition of reductant produces an increase of the fluorescence. This cycle was repeated, and the switching ratio was calculated for each fractions. Details about the calculation of the switching ratio have been discussed in Chapter 1. Table 5.1 presents the measured switching ratios.

N-hydroxysuccinimide (NHS) ester-mediated derivatization generally involves the reaction of the amine-reactive group with the primary amines of a protein or a biomolecule. We may expect that ATTO655 is not reactive towards a serine or glutamine residue at the 122 position of the protein. From experimentally obtained FRET efficiency or switching ratios and comparing the results with our previous work(34), it is tentatively proposed that the position of the label in fraction 1' is the N-terminus and that fraction 2 must contain a species where the label is attached to a lysine moiety close to the copper center. In the present work, further investigation was performed only on fraction 2.

<b>Fractions</b>	<b>Switching ratio</b>
fraction 1'	0.68
fraction 2	0.83

**Table 5.1:** Experimentally obtained switching ratios for fraction 1' and fraction 2.

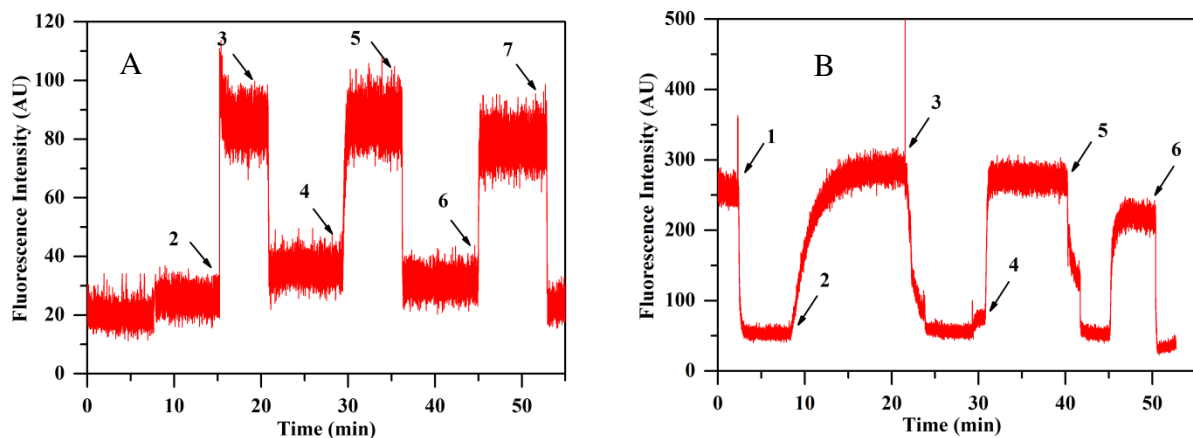


**Figure 5.7:** Fluorescence switching experiments on 50 nM of ATTO655 labeled K122S copper azurin in 20 mM HEPES, pH 7.0 at room temperature. The black numbers mark the addition of oxidant and reductant in the samples. A: fraction 1', B: fraction 2. The time points 1, 3, 5, and 7 correspond to the addition of 0.05, 1, 6, and 18 mM (final concentrations) of potassium ferricyanide to the sample, respectively. The time points 2, 4, and 6 correspond to the addition of 0.25, 1.5, and 4.5 mM of sodium ascorbate (final concentrations), respectively.

### 5.3.4 FCS experiments

FCS experiments were performed in 57% (w/w) sucrose solutions at room temperature (295 K) in 20 mM HEPES buffer pH 7.0. Redox conditions were controlled by the addition of potassium hexacyanoferrate (III) as oxidant and sodium ascorbate as reductant.

#### 5.3.4.1 K122Q CuAzurin-ATTO655, fraction 2, under oxidizing conditions

When titrating K122Q -CuAzu with hexacyanoferrate(III), the observed ACFs could not be fit adequately with the equation containing a single diffusion term (Fig. 5.8) and a two-term function with  $G_{diff}(\tau)$  and  $G_I(\tau)$  was used to fit the data (Fig. 5.9). Fitting with two terms still did not produce optimal fits (Fig. 5.9), but including a third term  $G_2(\tau)$  in the FCS equation did not markedly improve the plot of the residuals.

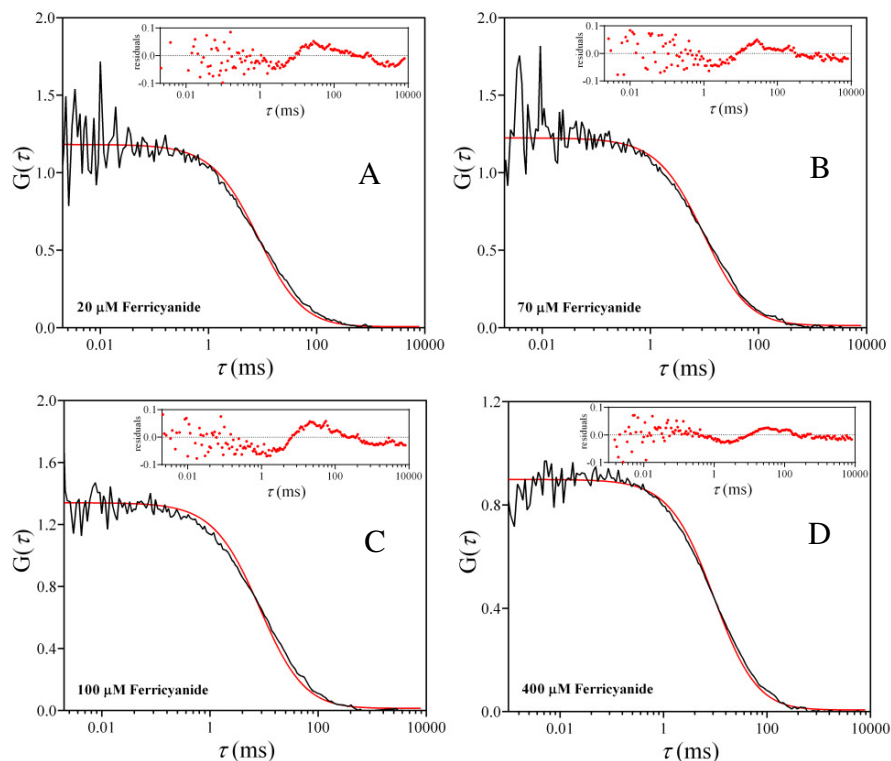


**Figure 5.8:** Experimentally obtained ACFs of fraction 2 from K122Q Cu azurin labeled with ATTO655 for samples containing 10 (A), 40 (B), 300 (C) and 500 (D)  $\mu\text{M}$  hexacyanoferrate (III). The red lines are fits according to Eqn. 3.1  $G(\tau) = G(0) \cdot G_{\text{diff}}(\tau)$ . The residuals of the fits in the insets show unsatisfactory fitting of the ACFs.

Thus, it is clear that next to the diffusion term a blinking term is needed to fit the experimental ACF. After analysis, both  $F_I$  and  $\tau_I$  ( $F_I$  is the fraction of molecules associated with the blinking reactions, and  $\tau_I$  is the relaxation time required for that reaction, see Chapter 4 for details) appeared independent of the ferricyanide concentration with  $F_I = 0.16$  and  $\tau_I = 0.68$  ms (Fig. 5.10). This blinking reaction was not observed in the case of the Zn containing *wt* azurin (See Chapter 3) and so the Cu center must be involved in this reaction (Scheme 5.1)

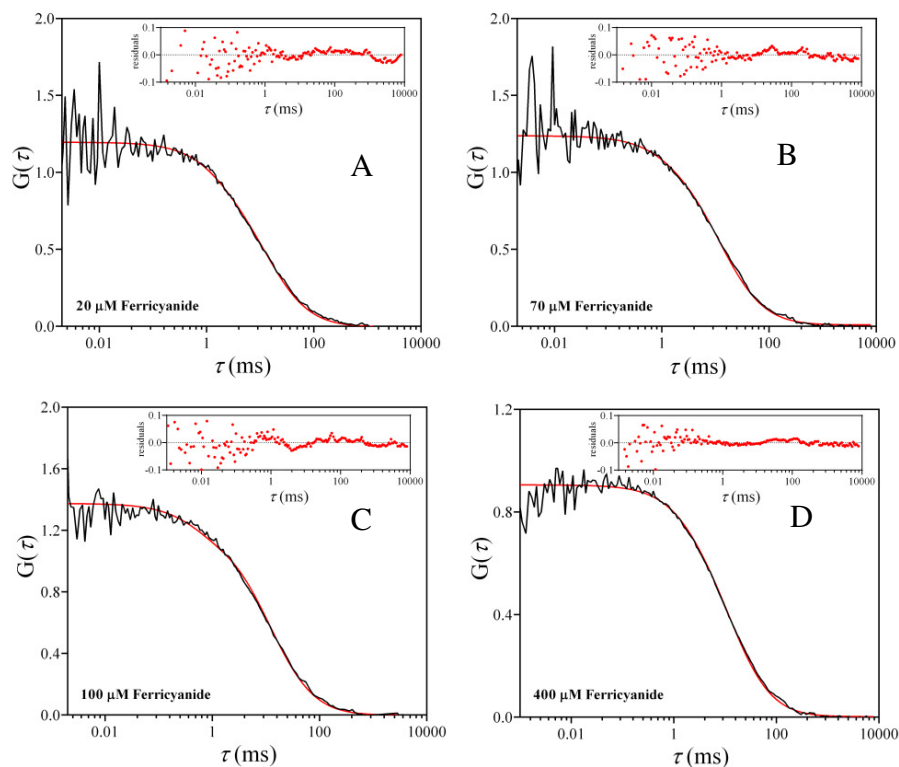
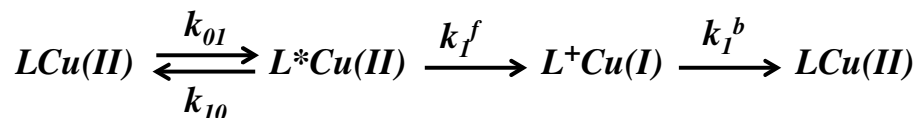


**Figure 5.9:** Experimentally obtained ACFs of fraction 2 from K122Q Cu azurin labeled with ATTO655 for samples containing 20 (A), 70 (B), 100 (C) and 400 (D)  $\mu\text{M}$  hexacyanoferrate (III). The red lines are fits according to Eqn. 3.4  $G(\tau) = G(0) \cdot G_{\text{diff}}(\tau) \cdot G_1(\tau)$  with  $\tau_D = 12$  ms.



**Scheme 5.1:** Light induced ET reactions in oxidized CuAz. LCu symbolizes the labeled azurin molecule in which the Cu is in the reduced or oxidized form (Cu(I) or Cu(II), respectively) and the label, L, is excited or oxidized ( $\text{L}^*$  or  $\text{L}^+$ , respectively). The rates for intramolecular ET from  $\text{L}^*$  to Cu(II) and from Cu(I) to  $\text{L}^+$  are denoted by  $k_1^f$  and  $k_1^b$ .

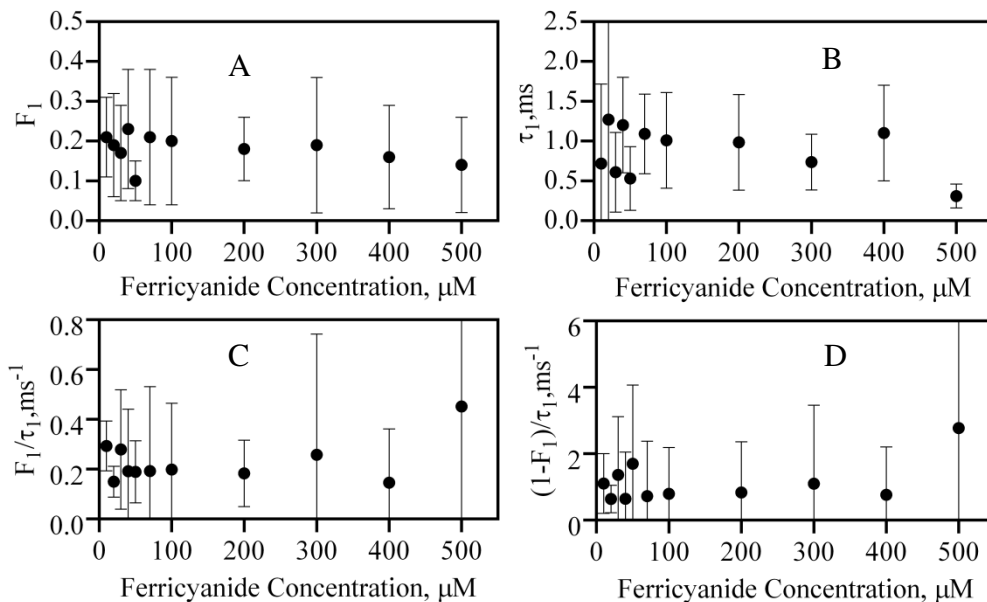


**Figure 5.10:** (A) and (B): Parameters ( $F_1$  and  $\tau_1$ ) obtained by fitting the ACFs of K122Q labeled Cu azurin as a function of the concentration of added hexacyanoferrate (III). The equation used for the fits was  $G(\tau) = G(0).G_{diff}(\tau).G_1(\tau)$  with  $\tau_D = 12$  ms. (C) and (D):  $(1-F_1)/\tau_1 = k^b$  and  $F_1/\tau_1 = k^f$  are plotted as a function of potassium hexacyanoferrate (III) concentration, respectively. Vertical bars denote 95% confidence intervals.

Consistent with the intramolecular character of the reaction, neither  $F_1$  nor  $\tau_1$  appears to depend on the concentration of oxidant (Fig. 5.10 A-B). Following the formalism discussed in Chapter 4, one obtains

$$F_1/\tau_1 = f(I) k_1^f \text{ and}$$

$$(1-F_1)/\tau_1 = k_1^b .$$

$k_1^f$  and  $k_1^b$  are the forward and backward ET rate constants under Scheme 5.1. In oxidized azurin the label fluorescence is partly quenched by the Cu center and the fluorescence life time is shortened to 1.8 ns (See Chapter 4 for details and Fig. 4.5). It leads to  $f(I) = 3.2 \times 10^{-3}$  where the factor  $f(I)$  can be understood by considering that the optically excited label reacts with oxidant in the solution (see Chapter 4 for details). With  $F_1 = 0.16$  and  $\tau_1 = 0.54$  ms, one obtains  $k_1^f =$

$6.1 \times 10^4 \text{ s}^{-1}$  and  $k_1^b = 1.2 \times 10^3 \text{ s}^{-1}$ . As before (see Chapter 4), these values can be used to obtain the reorganization energy for electron transfer.

With  $E_{ATTO+/ATTO} = 1.55 \text{ V}$  (vs NHE) and  $\Delta G_{0,0} = 1.86 \text{ eV}$ (40),  $n_{ATTO} = 0$ ,  $n_{Cu(II)}=2$  and a midpoint potential of azurin at pH 7 of  $0.31 \text{ V}$  (vs NHE)(41)(42), one obtains driving forces of  $\Delta G_f = -0.476 \text{ eV}$  and  $\Delta G_b = -1.384 \text{ eV}$  for the reactions shown in Scheme 5.1. This, finally leads (see details in Chapter 4) to  $\lambda$  (K122Q) =  $0.76 \text{ eV}$ .

#### 5.3.4.2 K122Q Cu Azurin-ATTO655, fraction 2, under reducing conditions

Fluorescence time traces were recorded of 0.5-1 nM solutions of fraction 2 of K122Q Cu Azu-ATTO655 in 57% w/w (i.e. 70% w/v) sucrose in the presence of varying amounts (0-500  $\mu\text{M}$ ) of ascorbate. For each time trace the autocorrelation function was calculated. It appears that application of  $G(\tau) = G(0) G_{diff}(\tau)$  and/or  $G(\tau) = G(0) G_{diff}(\tau) G_1(\tau)$  did not result in good fits: and the residuals exhibited a noticeable non-random component (Fig. 5.11). Then the ACFs were fit with an equation containing an additional term  $G_2(\tau)$  ( $G(\tau) = G(0) G_{diff}(\tau) G_1(\tau) G_2(\tau)$ ) (see Eqn. 5.1) with the diffusion correlation time fixed at  $\tau_D = 12 \text{ ms}$  (Fig. 5.12). Including the third term  $G_2(\tau)$  in the Eqn. 5.1 resulted in good fits.

The amplitudes  $F_1$  and  $F_2$ , and the corresponding correlation times,  $\tau_1$  and  $\tau_2$  are presented in Fig. 5.13. After fitting the ACFs, it was clear that K122Q-labeled CuAz-fraction 2 is involved in a reaction that occurs on a time scale of 400-500  $\mu\text{s}$ . Similar to our previous experiments on *wt* Cu azurin, this reaction is ascribed to intramolecular ET from the Cu(I) site to the excited label and back (Scheme 5.2). In case of K122Q variant, with  $F_2 = 0.23$ ,  $\tau_2 = 0.23 \text{ ms}$  and  $f(I) = 4.8 \times 10^{-3}$  under reducing conditions (lifetime of the dye is 2.7 ns under reducing conditions, See Chapter 4, Fig. 4.5), one finds  $k_2^f = 2.1 \times 10^5 \text{ s}^{-1}$  and  $k_2^b = 3.3 \times 10^3 \text{ s}^{-1}$ . Using these rates and  $E_{ATTO/ATTO-} = -0.17 \text{ V}$  (vs ~ NHE),  $n_{ATTO} = 0$  and  $n_{Cu(I)}=1$  (See Chapter 4), one obtains  $\lambda$  (K122Q) =  $1.08 \text{ eV}$ .



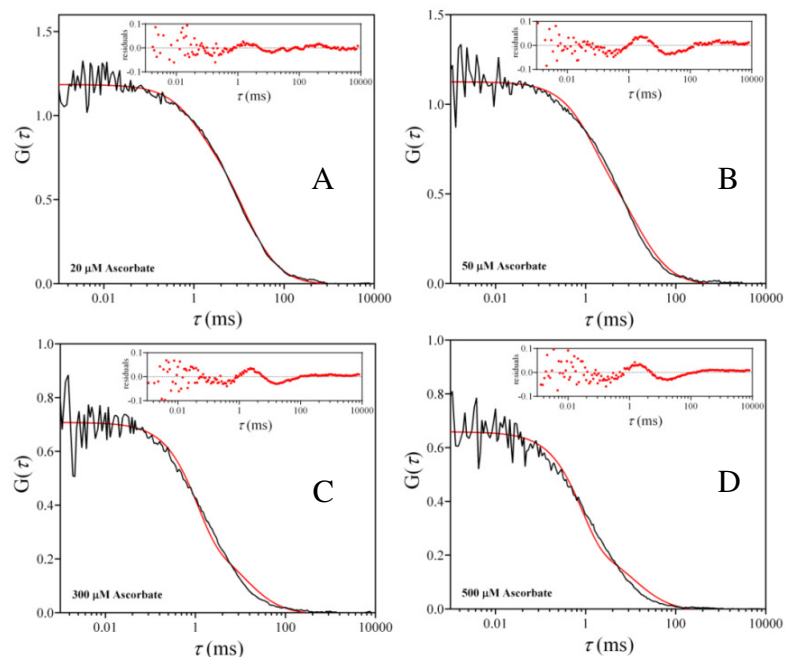


**Figure 5.11:** Experimentally obtained ACFs of K122Q Cu azurin labeled with ATTO655, fraction 2, for samples containing 20 (A), 50 (B), 300 (C) and 500 (D)  $\mu\text{M}$  ascorbate. The red lines are fits according to  $G(\tau) = G(0).G_{diff}(\tau).G_I(\tau)$  with  $\tau_D = 12$  ms. The residuals in the insets show unsatisfactory fitting of the ACFs.

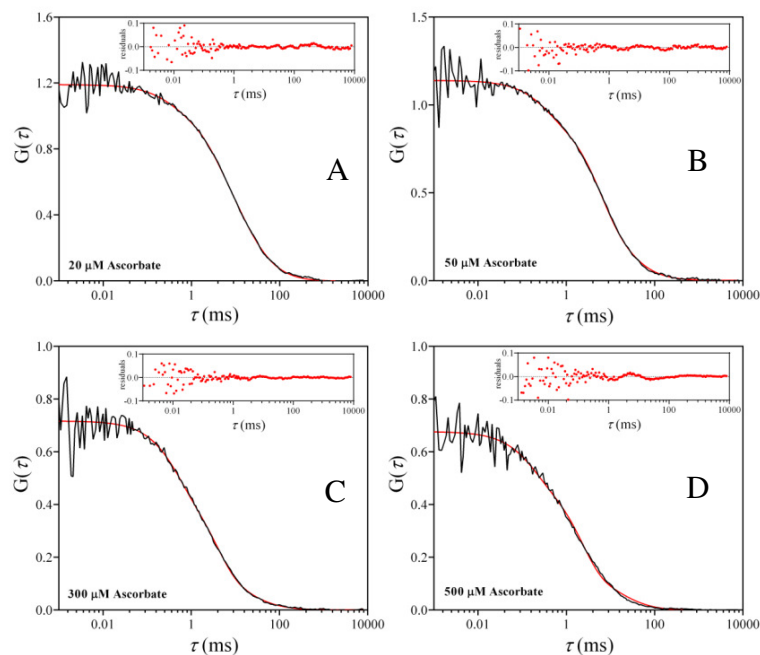


**Figure 5.12:** Experimentally obtained ACFs of K122Q Cu azurin labeled with ATTO655, fraction 2, for samples containing 20 (A), 50 (B), 300 (C) and 500 (D)  $\mu\text{M}$  ascorbate. The red lines are fits according to Eqn. 5.1  $G(\tau) = G(0).G_{diff}(\tau).G_I(\tau).G_2(\tau)$  with  $\tau_D = 12$  ms. The residuals in the insets show satisfactory fitting of the ACFs.

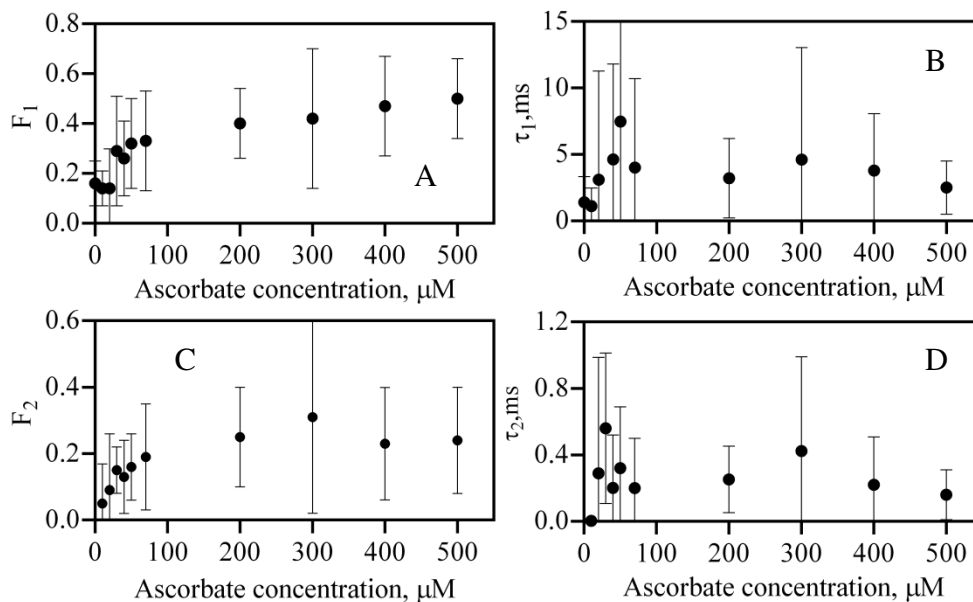
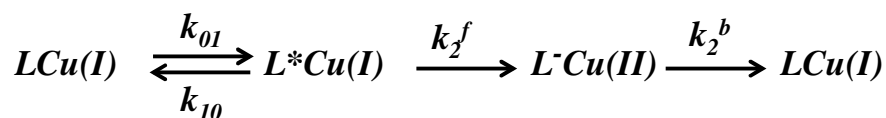


**Figure 5.13:** Parameters obtained from the fits of the ACFs of fraction 2 (K122Q Cu azurin-ATTO655). The equation used was  $G(\tau) = G_{diff}(\tau) G_1(\tau) G_2(\tau)$  with  $\tau_D = 12$  ms. Shown are, as a function of ascorbate concentration:  $F_1$  (A),  $\tau_1$  (B),  $F_2$  (C), and  $\tau_2$  (D).



**Scheme 5.2:** Light induced ET reactions in reduced CuAz. Symbols have the same meaning as in Scheme 2.

The rates for intramolecular ET from Cu(I) to  $L^*$  and from  $L^-$  to Cu(II) to are denoted by  $k_2^f$  and  $k_2^b$ .

$G_1(\tau)$  is related to the reduction of the label by the reductant and  $F_1$  and  $\tau_1$  are analysed as before (See Chapter 4 for details), taking into account that only a fraction  $(1-F_2)$  of the labeled molecules is in the bright state. From the experimentally determined value of  $k_r f(I)$  a value of  $k_r$  can be extracted after an estimate of  $f(I)$  has been obtained ( $k_r$  is the second order rate constant for the reduction of the dye, See Chapter 3 for details). Fluorescence lifetimes of the labeled variants were found to be similar to labeled *wt* copper azurin (1.8 ns and 2.7 ns under oxidizing and reducing conditions respectively). With a fluorescence lifetime of 2.7 ns (See Chapter 4), an incident light intensity of  $4.3 \text{ kW/cm}^2$  at 636 nm and an absorbance cross-section of the label of  $1.3 \times 10^{-16} \text{ cm}^2$  (based on an estimated  $\epsilon_{636} = 8 \times 10^4 \text{ M}^{-1} \text{ cm}^{-1}$ ), one finds that  $\sigma I_{exc} = 1.80 \times 10^6 \text{ s}^{-1}$

and  $f(I)=4.8\times 10^{-3}$ . Taking K122Q Cu azurin under reducing condition as an example, with  $k_r$   $f(I)=3.4\times 10^5 \text{ M}^{-1}\text{s}^{-1}$ , a value of  $k_r = 7\times 10^7 \text{ M}^{-1}\text{s}^{-1}$  is obtained. As discussed in Chapter 2, considering that the experiments were performed in 70% (w/v) sucrose solutions, this is of the order of a diffusion-controlled reaction rate. The analysis is presented in the Fig. 5.14 and data are gathered in Table 5.2.

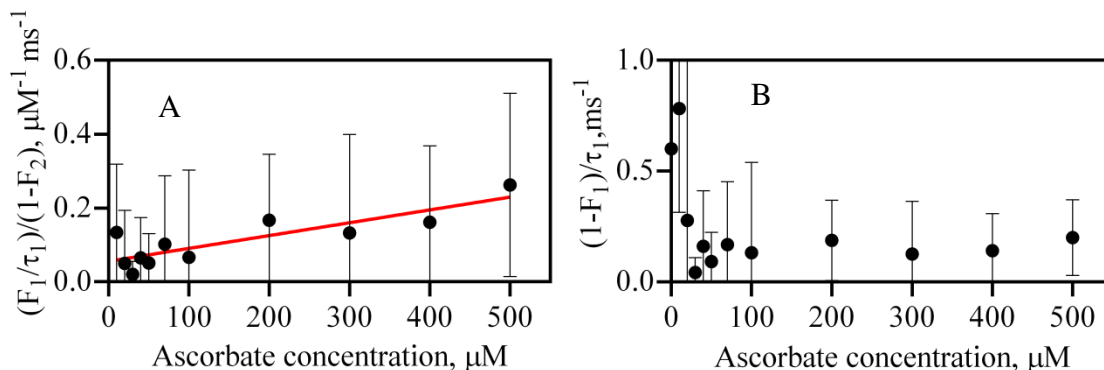


**Figure 5.14:** Analysis of the ACFs of labeled Cu azurin variant (K122Q-fraction 2). ACFs were fitted with the equation  $G(\tau) = G(0) G_{diff}(\tau) G_I(\tau) G_2(\tau)$  with  $\tau_D = 12 \text{ ms}$ . Parameters  $\tau_1$  and  $F_1$ , as obtained from the fits, correspond with  $G_I(\tau)$ . (A)  $(F_1/\tau_1)/(1-F_2)$  ( $=k_f$ ) as a function of the concentration of ascorbate for K122Q (B) and (B)  $(1-F_1)/\tau_1$  ( $=k_b$ ) as a function of the concentration of ascorbate for the same variant. The red straight line is least-squares fit to the data points.

$k_b$  appears to be constant, which is consistent with the idea that dissolved oxygen is responsible for the back oxidation of the label as oxygen is present in the solution in large excess and its concentration will not change appreciably over the duration of the experiment. This has been discussed in Chapter 3. Data for the variants are gathered in Table 5.2.

#### 5.3.4.3 K122S Cu Azurin-ATTO655, fraction 2, under oxidizing conditions

When titrating K122S -CuAzu with hexacyanoferrate(III), the observation was similar to K122Q. A two-term function with  $G_{diff}(\tau)$  and  $G_I(\tau)$  was needed to fit the data properly (Fig. 5.15). Fitting with two terms still did not produce optimal fits, but including a third term  $G_2(\tau)$  in the FCS equation did not markedly improve the plot of the residuals. The data is gathered in Fig. 5.16.

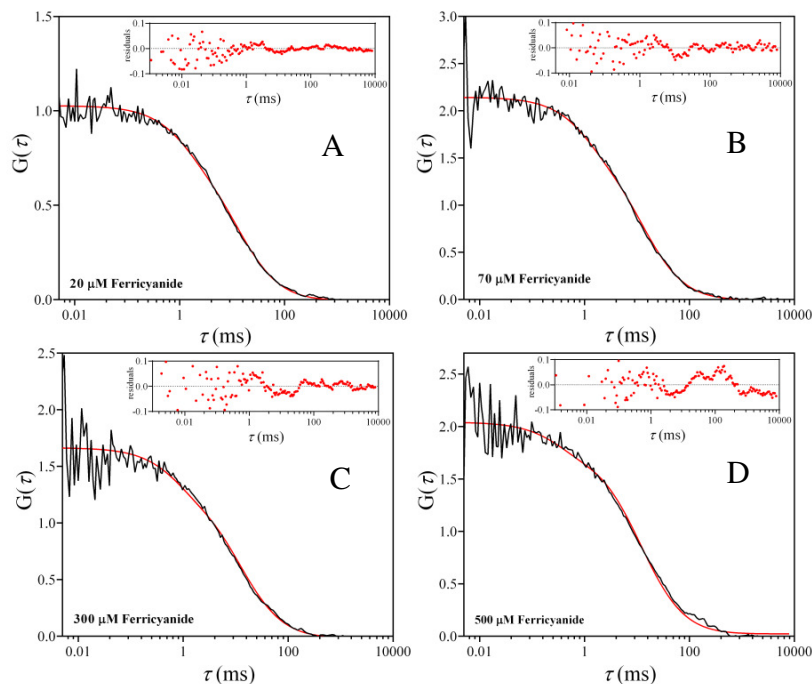


**Figure 5.15:** Experimentally obtained ACFs of fraction 2 (K122S Cu azurin labeled with ATTO655) for samples containing 20 (A), 70 (B), 300 (C) and 500 (D)  $\mu\text{M}$  hexacyanoferrate (III). The red lines are fits according to Eqn. 3.4  $G(\tau) = G(0).G_{diff}(\tau).G_I(\tau)$  with  $\tau_D = 12$  ms.

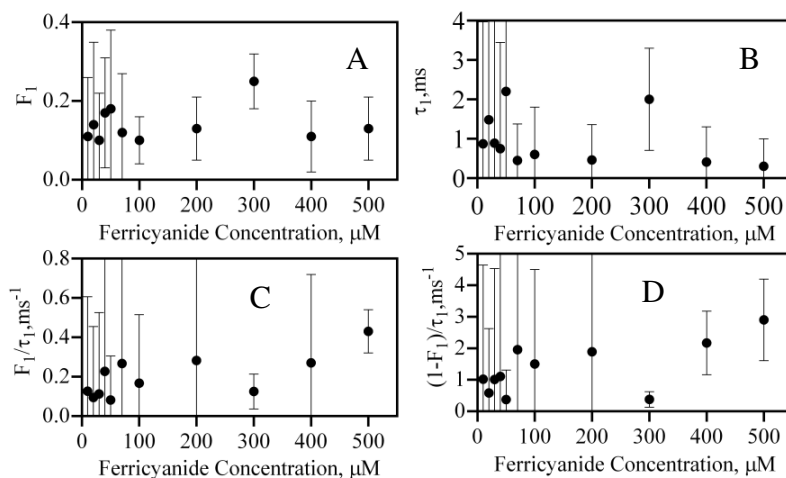


**Figure 5.16:** (A) and (B): Parameters ( $F_1$  and  $\tau_1$ ) obtained by fitting the ACFs of K122S labeled Cu azurin (fraction 2) as a function of the concentration of added hexacyanoferrate (III). The equation used for the fits was  $G(\tau) = G(0).G_{diff}(\tau).G_I(\tau)$  with  $\tau_D = 12$  ms. (C) and (D):  $F_1/\tau_1 = k^f$  and  $(1-F_1)/\tau_1 = k^b$  are plotted as a function of potassium hexacyanoferrate (III) concentrations, respectively. Vertical bars denote 95% confidence intervals.

Applying the same formalism as discussed in Chapter 4 and for K122Q under scheme 5.1, one

obtains  $k_1^f = 8 \times 10^4 \text{ s}^{-1}$  and  $k_1^b = 1.5 \times 10^3 \text{ s}^{-1}$ . As before (See Chapter 4), these values can be used to obtain the reorganization energy for electron transfer. We obtained driving forces of  $\Delta G_f = -0.476 \text{ eV}$  and  $\Delta G_b = -1.384 \text{ eV}$  for the reactions shown in Scheme 5.1. This, finally leads (See details in Chapter 4) to  $\lambda$  (K122S) = 0.75 eV.

#### 5.3.4.4 K122S Cu Azurin-ATTO655, fraction 2, under reducing conditions

The observations for K122S CuAzurin-ATTO655, fraction 2, were comparable to K122Q species 2. For each time trace the autocorrelation function was calculated. Application of  $G(\tau) = G(0) G_{diff}(\tau)$  and/ or  $G(\tau) = G(0) G_{diff}(\tau) G_I(\tau)$  produced fits with a noticeable non-random component (Fig. 5.17). Therefore, the ACFs were fit with an equation containing the additional term,  $G_2(\tau)$ , ( $G(\tau) = G(0) G_{diff}(\tau) G_I(\tau) G_2(\tau)$ ) (Eqn. 5.1) with the diffusion correlation time fixed at  $\tau_D = 12 \text{ ms}$  (Fig. 5.18). The amplitudes  $F_1$  and  $F_2$ , and the corresponding correlation times,  $\tau_1$  and  $\tau_2$ , are presented in Fig. 5.19. The same scheme 5.2 can be applied here.

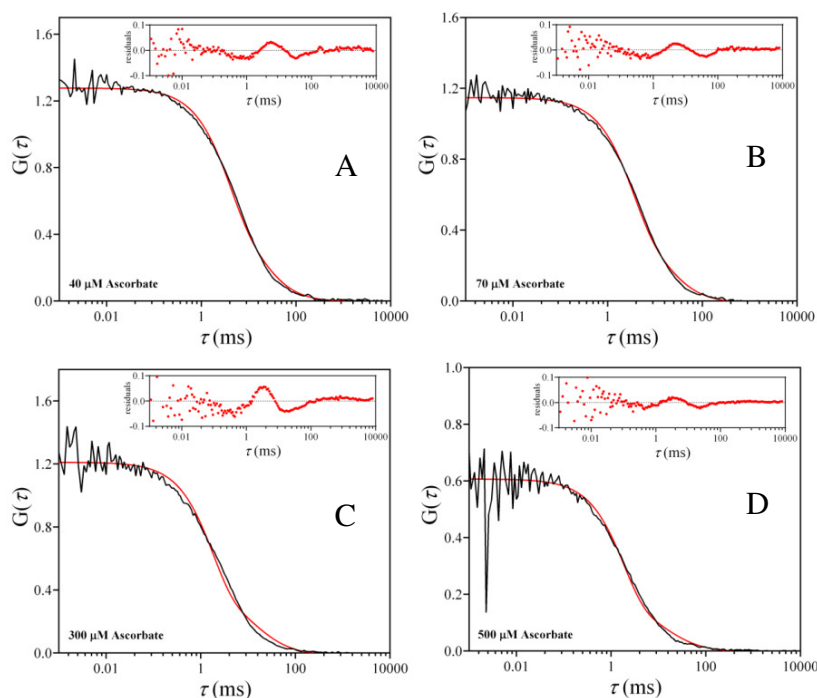


**Figure 5.17:** Experimentally obtained ACFs of species 2 from K122S Cu azurin labeled with ATTO655 for samples containing 40 (A), 70 (B), 300 (C) and 500 (D)  $\mu\text{M}$  ascorbate. The red lines are fits according to Eqn. 3.4  $G(\tau) = G(0) \cdot G_{diff}(\tau) \cdot G_I(\tau)$  with  $\tau_D = 12 \text{ ms}$ . The residuals of the fits in the insets show unsatisfactory fitting of the ACFs.

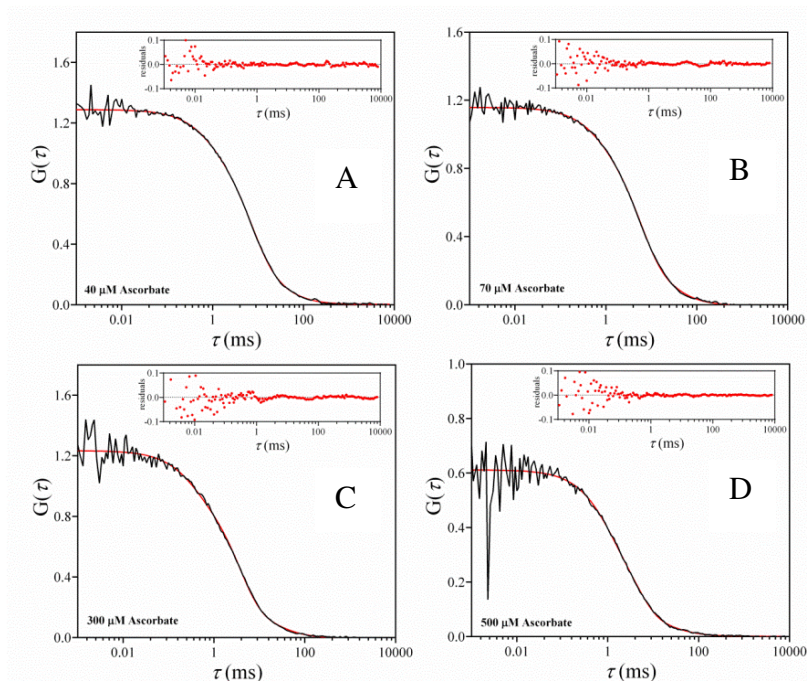


**Figure 5.18:** Experimentally obtained ACFs of fraction 2 from K122S Cu azurin labeled with ATTO655 for samples containing 40 (A), 70 (B), 300 (C) and 500 (D)  $\mu\text{M}$  ascorbate. The red lines are fits according to Eqn. 5.1  $G(\tau) = G(0).G_{diff}(\tau).G_1(\tau) G_2(\tau)$  with  $\tau_D = 12$  ms. The residuals of the fits (See insets) show satisfactory fitting of the ACFs.

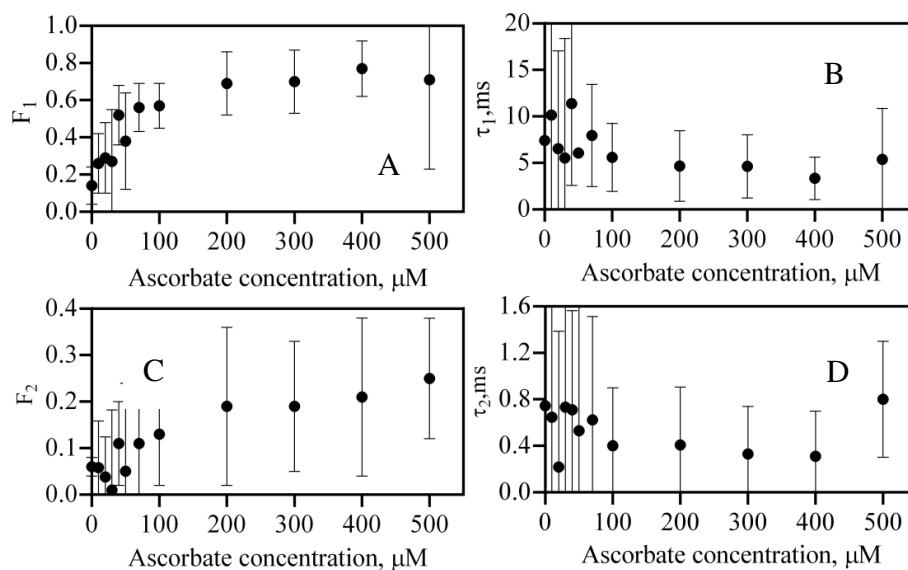


**Figure 5.19:** Parameters obtained from the fits of the ACFs of K122S Cu azurin-ATTO655, fraction 2. The equation used was  $G(\tau) = G_{diff}(\tau) G_1(\tau) G_2(\tau)$  with  $\tau_D = 12$  ms. Shown are, as function of ascorbate concentration:  $F_1$  (A),  $\tau_1$  (B),  $F_2$  (C), and  $\tau_2$  (D).

As discussed in Chapter 4, consistent with the intramolecular character of the reaction,  $\tau_2$  appears independent of the reductant concentration. The fraction of dark molecules  $F_2$ , increases with reductant concentration. The issue of dissolved oxygen in the solution has already been discussed in the previous chapter (see Chapter 4 for details). As seen from the analysis,  $F_2$ , as obtained from the fits, is not constant. Only with excess of ascorbate,  $F_2$  approaches a constant value. Applying the same formalism (Chapter 4) to find  $k_2^f$  and  $k_2^b$ , we find,

$$F_2/\tau_2 = f(I) k_2^f \text{ and}$$

$$(1-F_2)/\tau_2 = k_2^b$$

Applying the same formalism for the K122S variant (see Chapter 4), we find  $k_2^f = 1.1 \times 10^5 \text{ s}^{-1}$  and  $k_2^b = 1.8 \times 10^3 \text{ s}^{-1}$  with  $F_2 = 0.23$ ,  $\tau_2 = 0.45 \text{ ms}$ . The resulting intramolecular ET rates are presented in Table 5.2.

	$L^* \rightarrow Cu(II)$	$Cu(I) \rightarrow L^+$	$Cu(I) \rightarrow L^*$	$L^- \rightarrow Cu(II)$
<b>Sample</b>	$k_1^f, \text{s}^{-1}$ (a)	$k_1^b, \text{s}^{-1}$ (a)	$k_2^f, \text{s}^{-1}$ (b)	$k_2^b, \text{s}^{-1}$ (b)
K122Q Cu-azurin	$8.0 \times 10^4$	$1.5 \times 10^3$	$2.1 \times 10^5$	$3.3 \times 10^3$
K122S Cu-azurin	$6.1 \times 10^4$	$1.2 \times 10^3$	$1.1 \times 10^5$	$1.8 \times 10^3$
wt Cu azurin <sup>#</sup> labeled at K122	$4.8 \times 10^4$	$0.7 \times 10^3$	$3.3 \times 10^6$	$1.0 \times 10^4$

(#) see Chapter 4, page 120, Table 4.1

**Table 5.2:** Experimentally obtained intramolecular rate constants for K122Q and K122S-species 2 and K122 labeled wt Cu azurin.

(a) in presence of excess of hexacyanoferrate (III) and

(b) in presence of excess of ascorbate

Using those experimentally obtained forward and backward rate constants and  $E_{ATTO/ATTO} = -0.17 \text{ V}$  (vs NHE),  $n_{ATTO} = 0$  and  $n_{Cu(I)} = 1$  and the values used in chapter 4 for the other parameters, one obtains  $\lambda$  (K122S) = 1.05 eV under reducing conditions.

$F_1$  and  $\tau_1$  are analysed as before (Chapter 4 for details), taking into account that only a fraction

$(1-F_2)$  of the labeled molecules is in the bright state. Based on the value of  $f(I)$  we can again estimate  $k_r f(I)$ . The data for  $k_r f(I)$  and  $k_b$  have been gathered in Table 5.3.

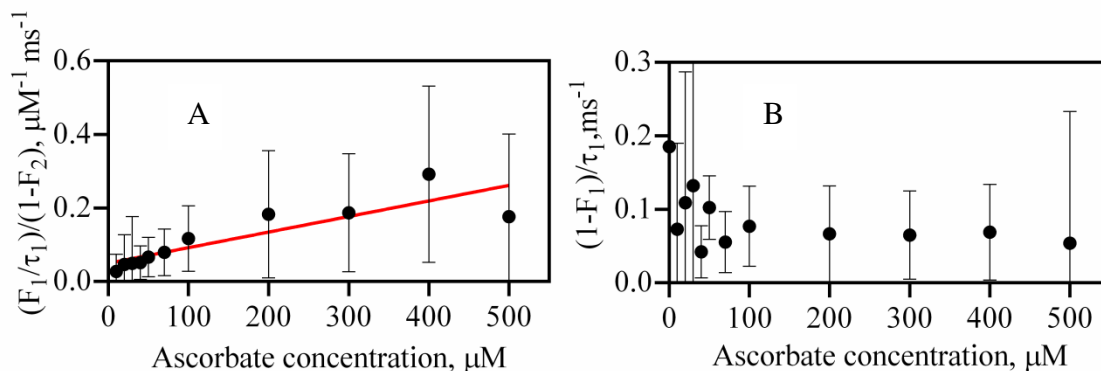


**Figure 5.20:** Analysis of the ACFs of labeled Cu azurin variant (K122S). ACFs were fitted with the equation  $G(\tau) = G(0) G_{diff}(\tau) G_1(\tau) G_2(\tau)$  with  $\tau_D = 12$  ms. Parameters  $\tau_1$  and  $F_1$ , as obtained from the fits, correspond with  $G_1(\tau)$ . (A)  $(F_1/\tau_1)/(1-F_2)$  ( $=k_f$ ) as a function of the concentration of ascorbate (B)  $(1-F_1)/\tau_1$  ( $=k_b$ ) as a function of the concentration of ascorbate for the same variants. The red straight line in (A) is a least-squares fit to the data points.

Species	$k_r f(I), M^{-1} s^{-1}$	$k_b, s^{-1}$
K122Q-species 2	$(3.4 \pm 0.7) \times 10^5$	$(9.6 \pm 4.0) \times 10^1$
K122S-species 2	$(4.2 \pm 0.8) \times 10^5$	$(6.6 \pm 1.5) \times 10^1$
wt Cu azurin labeled at K122 <sup>#</sup>	$(2.0 \pm 0.3) \times 10^5$	$(5.6 \pm 0.6) \times 10^1$
wt Cu azurin labeled at N-terminus <sup>#</sup>	$(3.2 \pm 0.3) \times 10^5$	$(3.5 \pm 0.2) \times 10^1$

(#) see Chapter 4, page 120, Table 4.1

**Table 5.3:** Experimental values of  $k_r f(I)$  and  $k_b$  for CuAzurin (wt and the variants) in presence of reducing agents (ascorbate). See text and Chapter 4 for further explanations.



<i>Species</i>	<i>Oxidizing condition(a)</i>	<i>Reducing condition(b)</i>
K122Q-species 2	0.76	1.08
K122S-species 2	0.75	1.05
Wt azurin labeled at K122 <sup>#</sup>	0.75	1.16

(#) see Chapter 4 for details

**Table 5.4:** Experimental values of reorganization energies (eV) for Cu Azurin (wt and the variants) in presence of redox agents (ascorbate). See text and Chapter 4 for further explanations.

(a) in presence of potassium hexacyanoferrate (III)

(b) in presence of ascorbate

#### 5.4 Comparison of fluorescence resonance energy transfer (FRET) and photoinduced electron-transfer (PET) reaction in Copper Azurin-ATTO655

In view of the increasing use of fluorescence labeling of biomolecules *in vivo* and *in vitro* the quenching of dye fluorescence in a labeled protein is an important subject. FRET and PET may occur simultaneously and it will be helpful to obtain an idea when PET may be expected to occur and when not. Whereas the FRET between ATTO655 and the Cu(II) center occurs on the nanosecond scale, the PET occurs on the microsecond-sub-millisecond scale, several orders of magnitude larger than FRET. With the experimental data ( $\Delta G$ ,  $\lambda$  for the wild type and the variants of azurin) in hand, we can calculate the dependence of the FRET and PET rates on the Cu-label distance in the azurin-ATTO655 system. Calculations of the two rates ( $k_{\text{FRET}}$  and  $k_{\text{ET}}$ ) have been performed over a distance from 0 to 80 Å of the Cu-label system.

Calculation of the rate of FRET ( $k_{\text{FRET}}$ ) was performed using the following equation:

$$k_{\text{FRET}} = \frac{1}{\tau_L} \left( \frac{R_0}{R} \right)^6 \quad (5.3)$$

where  $\tau_L$  is the lifetime of the fluorescent donor in the absence of the acceptor (ATTO655 in sucrose, 2.7 ns),  $R_0$  is the Förster radius of the ATTO655-azurin pair and  $R$  is the donor-acceptor distance. The so-called Förster radius is given by (43)

$$R_0 = 0.211[\kappa^2 n^{-4} Q_D J(\lambda)]^{1/6} \quad (5.4)$$

where  $R_0$  is the distance at which the transfer efficiency is at 50% of its maximum value,  $Q_D$  is the fluorescence quantum yield of the donor in absence of the acceptor,  $n$  is the refractive index of the sample,  $\kappa$  is the orientation factor for the dipolar interaction and  $J(\lambda)$  is the overlap integral which is given by (see Chapter 1, Eqn. 1.3)

$$J(\lambda) = \int_0^{\infty} I_b(\lambda) \varepsilon_a(\lambda) \lambda^4 d\lambda / \int_0^{\infty} I_b(\lambda) d\lambda$$

The spectral calculator in the Quick Fit 3.0 software was used to obtain the FRET radius between Oxidized copper azurin and ATTO655. A value of  $R_0$  of 37 Å was calculated for the donor-acceptor pair ATTO655-oxidized Cu Azurin, based on the absorption spectrum of the oxidized form of *wt* Cu Azurin and on the emission spectrum of ATTO655 measured experimentally(43)(44)(45).

Photoinduced electron transfer may occur next to FRET. For the calculation of the PET rates, two models are at our disposal: “Pathway model” and “Organic glass model”.

When structural information is available a pathway can be delineated along which ET may be effectuated. The most efficient pathway is usually the shortest one that can be constructed. It will contain mostly covalent bonds with an occasional through space jump or a step comprising a hydrogen bond. The formula to calculate the ET rate according to this “pathway model” has been discussed already in Chapter 4 and is reproduced here(46)(47)

$$k_{ET} = 3 \times 10^{13} e^{-\beta_0 \sigma_C \ell} e^{-\frac{(\Delta G_f + \lambda)^2}{4\lambda kT}} \quad (5.5)$$

where,  $\beta_0$  is the electron transfer attenuation factor (0.7, or 1.4 Å<sup>-1</sup>, *vide infra*),  $\ell$  is the length of a C-C bond (1.4 Å) and  $\sigma_C$  is the number of equivalent C-C bonds in the path,  $\Delta G$  is the driving force for the electron transfer reaction,  $\lambda$  is the reorganization energy of the electron donor-acceptor system,  $k$  is Boltzmann’s constant,  $T$  is the temperature in Kelvin.

In case, no detailed structural information on donor-acceptor pair is available or when donor and acceptor are not covalently linked, the “organic glass” model of Moser and Dutton may be applied according to which the ET through a protein can be linked to tunneling of

electron through an organic glass. The formula to calculate the ET rate according to this model is(48)(49):

$$\log k_{ET} = 13 - 0.6(R - 3.6) - (\Delta G + \lambda)^2/4\lambda kT \quad (5.6)$$

where,  $\Delta G$  is the driving force for the electron transfer reaction,  $\lambda$  is the reorganization energy of the electron donor-electron acceptor system,  $k$  is Boltzmann's constant,  $T$  is the temperature in Kelvin and  $R$  is the distance between donor and acceptor molecule. The coefficient "0.6" reflects the quantized nuclear term as provided by extensive studies in the photosynthetic reaction-centers. This pathway model might apply when the dye forms an association complex and an electron jumps directly from the dye to the copper center and vice versa.

The variation of PET and FRET rates over a distance from 0 to 80 Å for ATTO655 labeled Cu azurin is depicted in Fig. 5.21 when oxidizing conditions apply. Under reducing conditions, FRET between ATTO655 and the reduced Cu site in azurin does not occur, and it is likely that PET is the main event occurring upon excitation of the label. We have used the parameters that correspond with the case of CuAz-K122-ATTO655. The PET rates were calculated by using the experimentally obtained  $\Delta G_f$  (free energy change for the ET reaction from the label to the metal center),  $\Delta G_b$  (free energy change for the ET reaction from the label to the metal center) and  $\lambda$  (reorganization energy of ET reaction in wt CuAzurin-ATTO655) (Chapter 4 for details). Three different values of  $\beta_0$  were used for the calculation of PET.  $\beta_0 = 1.0 \text{ \AA}^{-1}$  reflects the situation encountered for the label on Lys122, where a clear through bond pathway is identifiable, whereas  $\beta_0 = 1.4 \text{ \AA}^{-1}$  is more suitable to model the situation where the label is on Ala1 and an electron most likely would have to travel to the copper center through a mixed pathway (through bond as well as through space hops) (Fig. 5.21).

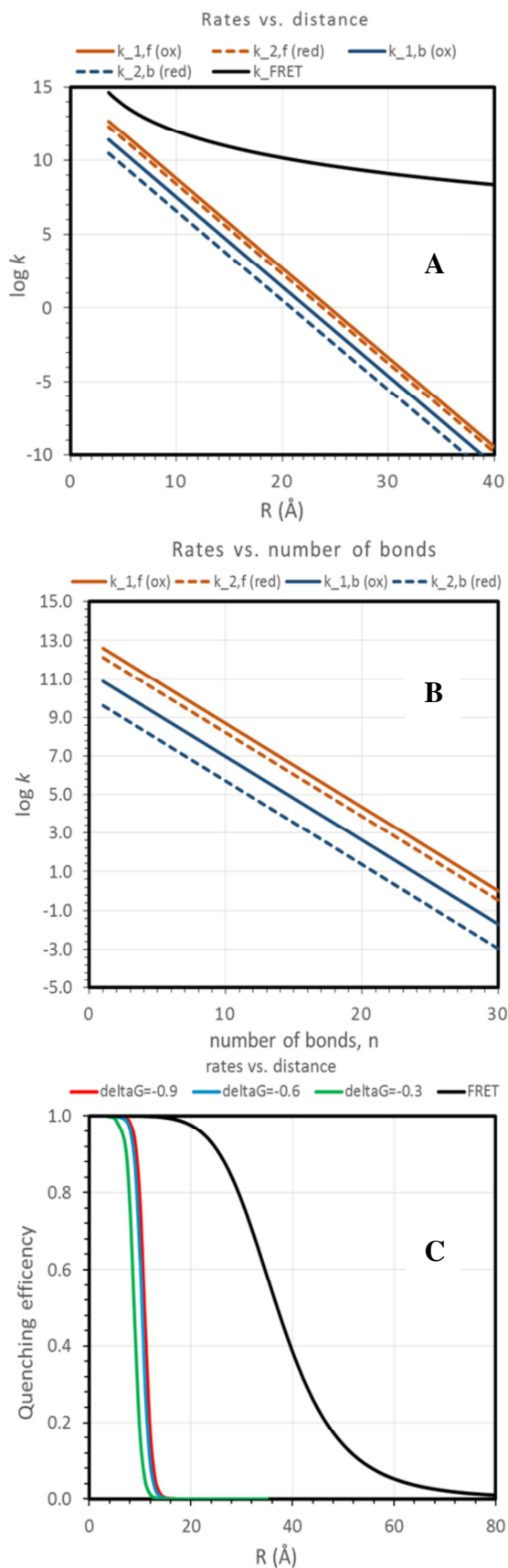


**Figure 5.21:** FRET and PET rates and quenching efficiencies for labeled azurin as a function of length parameters. (A). FRET (black) and PET quenching rates as a function of the distance  $R$  between Cu center and chromophore. The FRET rates were calculated with Eqn. 5.3 with a Förster radius  $R_0 = 37$  Å and life time of the dye in the absence of quenching of  $\tau = 2.7$  ns. PET rates were calculated from  $\log k_{ET} = 13 - 0.6(R - 3.6) - \frac{(\Delta G + \lambda)^2}{4\lambda kT}$  (49) with  $\lambda = 0.76$  eV, and  $\Delta G = -0.476$  ( $k_1^f$ , red solid line);  $\lambda = 1.16$  eV, and  $\Delta G = -1.67$  ( $k_2^f$ , red dashed line);  $\lambda = 0.76$  eV, and  $\Delta G = -1.384$  ( $k_1^b$ , blue solid line);  $\lambda = 1.16$  eV, and  $\Delta G = -0.19$  ( $k_2^b$ , blue dashed line)

(B). PET quenching rates as a function of the number of covalent bonds  $n$  between chromophore and Cu site. Rates were calculated from Eqn. 5.5(50)(51), with  $\beta_0 = 1$  per bond. Different lines refer to similar cases as in panel (A). (C). Quenching efficiency  $Q_E \equiv (F_0 - F)/F_0 = k/(k_0 + k)$  calculated as a function of distance between chromophore and Cu center. Here  $k_0 = 1/\tau_L$  and  $k$  is either the PET or the FRET rate. FRET rates were calculated as in panel (A). PET rates were calculated as in panel (A) with  $\lambda = 0.90$  eV and  $\Delta G = -0.9$ ,  $-0.6$  and  $-0.3$  eV (green, blue and red lines, respectively).

The data in panel (C) clearly show that quenching by PET is short ranged while FRET quenching extends over a much long range.

It is seen that PET may occur much more generally and may take place over large distances between the dye and the redox center in azurin. PET rates may slow down to  $10^3 \text{ s}^{-1}$  for pathways longer than  $19 \pm 3$  effective C-C bonds. In practice it means that when the label is more than  $18 \text{ \AA}$  away from the copper and attached more than 17 equivalent bonds away from the copper center, PET quenching can be ignored for the type of experiments described in this thesis. The FRET rate, on the other hand, shows a much shallower distance dependence.

### **5.5 Future prospects and concluding remarks**

In the present work a single-molecule based approach for the study of electron-transfer process within proteins was presented. In some of the isolated species an electron-transfer reaction between azurin and the attached ATTO655 is observed using FCS. In future, the position of the label in the variants will be established by mass spectrometry experiments. Improvements in the separation, as well as application of methods other than ion exchange chromatography will be useful for other proteins as well. A most important finding is the observation of ET reaction between the label and the metal center when the former is bound to surface lysines (Lys 24/Lys27/Lys128). Proximity of those lysines to the copper site makes it possible that either through-bond electron tunneling or back-folding of the label toward the surface of the protein allows transfer of electrons. As  $k_{ET}$  and  $\lambda$  have been determined experimentally and good estimates of  $\Delta G$  are available, the electronic couplings between the donor and the acceptor can be extracted and its value can be compared with predictions from currently prevailing models.

Overall, we see that it be possible to encounter intramolecular ET reaction in Cu azurin-ATTO655 bioconjugates where the reaction sites can be surface lysines of azurin (Lys24, Lys27, Lys128, etc.) other than Lys122 and the time scale of intramolecular electron-transfer in those cases might not be similar to our previous results obtained in *wt* azurin. In case of the variants, no extra decay was observed in autocorrelation curves for the electron-transfer reactions and the inverse of  $k_{ET}$  is found in the sub-millisecond time scale. As the ET parameters (driving forces, reorganization energies) were determined experimentally for a number of cases (*wt* Cu azurin, K122S and K122Q), the variation of the rates with distance was calculated with ET-models and it was our additional interest to see how these rates compare to FRET promoted deactivation of

the excited labels. The PET rates observed in fraction 2 of K122S and K122Q Cu-Azurin indicate that the label is likely to be attached to the one of the lysine residues e.g. Lys 24/Lys27/Lys128 which is  $\geq 20$  Å away from the copper center. Previously, PET was thought to occur only when donor and acceptor are in Van-der-Waal contact. We show here that PET still may occur over large distances in labeled oxido-reductases. Thus, our study provides insights on discovery and characterization of long-range photo-induced electron-transfer processes in dye labeled proteins.

### References

- (1) Holm, R. H.; Kennepohl, P.; Solomon, E. I. Structural and Functional Aspects of Metal Sites in Biology. *Chem. Rev.* **1996**, *96*, 2239–2314.
- (2) Thomson, A. J.; Gray, H. B. Bio-inorganic chemistry. *Curr. Opin. Chem. Biol.* **1998**, *2*, 155–158.
- (3) Marcus, R. a.; Sutin, N. Electron transfers in chemistry and biology. *Biochim. Biophys. Acta - Rev. Bioenerg.* **1985**, *811*, 265–322.
- (4) Kolczak, U., Dennison, C., Messerschmidt, A., and Canters, G. W. *Handbook of Metalloproteins*; 2001.
- (5) Van de Kamp, M.; Hali, F. C.; Rosato, N.; Agro, A. F.; Canters, G. W. Purification and characterization of a non-reconstitutable azurin, obtained by heterologous expression of the *Pseudomonas aeruginosa* *azu* gene in *Escherichia coli*. *Biochim. Biophys. Acta* **1990**, *1019*, 283–292.
- (6) Leckner, J.; Bonander, N.; Wittung-Stafshede, P.; Malmström, B. G.; Karlsson, B. G. The effect of the metal ion on the folding energetics of azurin: A comparison of the native, zinc and apoprotein. *Biochim. Biophys. Acta - Protein Struct. Mol. Enzymol.* **1997**, *1342*, 19–27.
- (7) Carmelo Rosa, Danilo Milardi, Domenico Grasso, Rita Guzzi, L. S. Thermodynamics of the thermal unfolding of azurin. *J. Phys. Chem.* **1995**, *99*, 14864–14870.
- (8) Engeseth, H. R.; McMillin, D. R. Studies of thermally induced denaturation of azurin and azurin derivatives by differential scanning calorimetry: evidence for copper selectivity. *Biochemistry* **1986**, *25*, 2448–2455.
- (9) Palm-Espling, M. E.; Niemiec, M. S.; Wittung-Stafshede, P. Role of metal in folding and stability of copper proteins in vitro. *Biochim. Biophys. Acta - Mol. Cell Res.* **2012**, *1823*, 1594–1603.
- (10) Kamp, M. Van De; Floris, R. Site-directed mutagenesis reveals that the hydrophobic patch of azurin mediates electron transfer. *J. Am. Chem. Soc.* **1990**, *112*, 907–908.

- (11) Vijgenboom, E.; Busch, J. E.; Canters, G. W. In vivo studies disprove an obligatory role of azurin in denitrification in *Pseudomonas aeruginosa* and show that azu expression is under control of rpoS and ANR. *Microbiology* **1997**, *143* ( Pt 9, 2853–2863.
- (12) Yamada, T.; Goto, M.; Punj, V.; Zaborina, O.; Kimbara, K.; Das Gupta, T. K.; Chakrabarty, a. M. The bacterial redox protein azurin induces apoptosis in J774 macrophages through complex formation and stabilization of the tumor suppressor protein p53. *Infect. Immun.* **2002**, *70*, 7054–7062.
- (13) Tobin, P. H.; Wilson, C. J. Examining photoinduced energy transfer in pseudomonas aeruginosa azurin. *J. Am. Chem. Soc.* **2014**, *136*, 1793–1802.
- (14) Farver, O.; Bonander, N.; Skov, L. K.; Pecht, I. The pH dependence of intramolecular electron transfer in azurins. *Inorganica Chim. Acta* **1996**, *243*, 127–133.
- (15) Jensen, P. S.; Chi, Q.; Zhang, J.; Ulstrup, J. Long-Range interfacial electrochemical electron transfer of *Pseudomonas aeruginosa* azurin-gold nanoparticle hybrid systems. *J. Phys. Chem. C* **2009**, *113*, 13993–14000.
- (16) Edman, L.; Mets, U.; Rigler, R. Conformational transitions monitored for single molecules in solution. *Proc. Natl. Acad. Sci. U. S. A.* **1996**, *93*, 6710–6715.
- (17) Chen, P.; Andoy, N. M. Single-molecule fluorescence studies from a bioinorganic perspective. *Inorganica Chim. Acta* **2008**, *361*, 809–819.
- (18) Wang, Q.; Goldsmith, R. H.; Jiang, Y.; Bockenbauer, S. D.; Moerner, W. E. Probing single biomolecules in solution using the anti-Brownian electrokinetic (ABEL) trap. *Acc. Chem. Res.* **2012**, *45*, 1955–64.
- (19) Mollova, E. T. Single-molecule fluorescence of nucleic acids. *Curr. Opin. Chem. Biol.* **2002**, *6*, 823–828.
- (20) Xie, X. S. Single-Molecule Approach to Enzymology. *Single Mol.* **2001**, *2*, 229–236.
- (21) Haustein, E.; Schwille, P. Ultrasensitive investigations of biological systems by fluorescence correlation spectroscopy. *Methods* **2003**, *29*, 153–166.
- (22) Chiantia, S.; Ries, J.; Schwille, P. Fluorescence correlation spectroscopy in membrane structure elucidation. *Biochim. Biophys. Acta* **2009**, *1788*, 225–233.
- (23) Kapusta, P.; Macháň, R.; Benda, A.; Hof, M. Fluorescence lifetime correlation spectroscopy (FLCS): Concepts, applications and outlook. *Int. J. Mol. Sci.* **2012**, *13*, 12890–12910.
- (24) Ries, J.; Schwille, P. Fluorescence correlation spectroscopy. *Bioessays* **2012**, *34*, 361–8.
- (25) Elson, E. L. Fluorescence correlation spectroscopy: Past, present, future. *Biophys. J.* **2011**, *101*, 2855–2870.
- (26) Krichevsky, O. Fluorescence correlation spectroscopy : the technique. *Rep.Prog.Phys* **2002**, *65*, 251.
- (27) Hess, S. T.; Huang, S.; Heikal, A. A.; Webb, W. W. Biological and chemical applications of fluorescence correlation spectroscopy: A review. *Biochemistry* **2002**, *41*, 697–705.

- (28) Magde, D.; Elson, E.; Webb, W. W. Thermodynamic fluctuations in a reacting system measurement by fluorescence correlation spectroscopy. *Phys. Rev. Lett.* **1972**, *29*, 705–708.
- (29) Schmauder, R.; Librizzi, F.; Canters, G. W.; Schmidt, T.; Aartsma, T. J. The oxidation state of a protein observed molecule-by-molecule. *Chemphyschem* **2005**, *6*, 1381–6.
- (30) Schmauder, R.; Alagaratnam, S.; Chan, C.; Schmidt, T.; Canters, G. W.; Aartsma, T. J. Sensitive detection of the redox state of copper proteins using fluorescence. *J. Biol. Inorg. Chem.* **2005**, *10*, 683–687.
- (31) Kuznetsova, S.; Zauner, G.; Schmauder, R.; Mayboroda, O. A.; Deelder, A. M.; Aartsma, T. J.; Canters, G. W. A Förster-resonance-energy transfer-based method for fluorescence detection of the protein redox state. *Anal. Biochem.* **2006**, *350*, 52–60.
- (32) Tabares, L.; Gupta, A.; Aartsma, T.; Canters, G. Tracking Electrons in Biological Macromolecules: From Ensemble to Single Molecule. *Molecules* **2014**, *19*, 11660–11678.
- (33) Goldsmith, R. H.; Tabares, L. C.; Kostrz, D.; Dennison, C.; Aartsma, T. J.; Canters, G. W.; Moerner, W. E. Redox cycling and kinetic analysis of single molecules of solution-phase nitrite reductase. *Proc. Natl. Acad. Sci. U. S. A.* **2011**, *108*, 17269–74.
- (34) Nicolardi, S.; Andreoni, A.; Tabares, L. C.; Van Der Burgt, Y. E. M.; Canters, G. W.; Deelder, A. M.; Hensbergen, P. J. Top-down FTICR MS for the identification of fluorescent labeling efficiency and specificity of the Cu-protein azurin. *Anal. Chem.* **2012**, *84*, 2512–20.
- (35) Robert C. Weast, M. J. A. *CRC Handbook of Chemistry and Physics*; CRC Press, Inc, Boca Raton, Florida.
- (36) Goldberg, M.; Pecht, I. Kinetics and equilibria of the electron transfer between azurin and the hexacyanoiron (II/III) couple. *Biochemistry* **1976**, *15*, 4197–4208.
- (37) Nicolardi, S.; Andreoni, A.; Tabares, L. C.; van der Burgt, Y. E. M.; Canters, G. W.; Deelder, A. M.; Hensbergen, P. J. Top-down FTICR MS for the identification of fluorescent labeling efficiency and specificity of the Cu-protein azurin. *Anal. Chem.* **2012**, *84*, 2512–20.
- (38) Gilani, A. G.; Moghadam, M.; Hosseini, S. E.; Zakerhamidi, M. S. A comparative study on the aggregate formation of two oxazine dyes in aqueous and aqueous urea solutions. *Spectrochim. Acta, Part A* **2011**, *83*, 100–105.
- (39) Monari, S.; Battistuzzi, G.; Dennison, C.; Borsari, M.; Ranieri, A.; Siwek, M. J.; Sola, M. Factors Affecting the Electron Transfer Properties of an Immobilized Cupredoxin. *J. Phys. Chem. C* **2010**, *114*, 22322–22329.
- (40) Doose, S.; Neuweiler, H.; Sauer, M. Fluorescence quenching by photoinduced electron transfer: a reporter for conformational dynamics of macromolecules. *Chemphyschem A Eur. J. Chem. Phys. Phys. Chem.* **2009**, *10*, 1389–1398.
- (41) Van de Kamp M1, Canters GW, Andrew CR, Sanders-Loehr J, Bender CJ, P. J. Effect of lysine ionization on the structure and electrochemical behaviour of the Met44-->Lys mutant of the blue-copper protein azurin from *Pseudomonas aeruginosa*. *Eur. J. Biochem.*



- 1993**, 218, 229–238.
- (42) Clair, C. S.; Ellis, W.; Gray, H. Spectroelectrochemistry of blue copper proteins: pH and temperature dependences of the reduction potentials of five azurins. *Inorganica Chim. Acta* **1992**, 191, 149–155.
- (43) Lakowicz, J. R. *Principles of Fluorescence Spectroscopy*; 2006.
- (44) L. Stryer Fluorescence energy-transfer as a spectroscopic ruler. *Annu. Rev. Biochem.* **1978**, 47, 819–846.
- (45) Jan Wolfgang Krieger and Jörg Langowski QuickFit 3.0: A data evaluation application for biophysics. **2015**.
- (46) Devault, D. Quantum mechanical tunnelling in biological systems. *Q. Rev. Biophys.* **1980**, 13, 387–564.
- (47) Marcus, R. A. Electron Transfer Reactions in Chemistry: Theory and Experiment. *Angew. Chemie Int. Ed. English* **1993**, 32, 1111–1121.
- (48) Moser, C. C.; Keske, J. M.; Warncke, K.; Farid, R. S.; Dutton, P. L. Nature of biological electron transfer. *Nature* **1992**, 355, 796–802.
- (49) Page, C. C.; Moser, C. C.; Chen, X.; Dutton, P. L. Natural engineering principles of electron tunnelling in biological oxidation-reduction. *Nature* **1999**, 402, 47–52.
- (50) Canters, G. W.; van de Kamp, M. Protein-mediated electron transfer. *Curr. Opin. Struct. Biol.* **1992**, 2, 859–869.
- (51) J N Onuchic, D N Beratan, J R Winkler, H. B. G. Pathway analysis of protein electron-transfer reactions. *Annu. Rev. Biophys. Biomol. Struct.* **1992**, 21, 349–377.

# **Chapter 6**

## **Outlook**

## ***6.1 Introduction***

In the present thesis, a series of single molecule FCS experiments on fluorescently labeled azurin was presented. The aim of those experiments was to gain broader understanding in electron transfer processes in oxido-reductases. The FRET based approach makes it possible to probe the redox state of absorbing cofactors inside a protein by attaching a fluorescent dye to its surface. The beauty in our method is that it can allow a more or less free choice of (redox) enzyme to be studied. Therefore, one way to continue research described here would be to investigate the electron transfer reactions within metalloprotein complexes and monitor protein-protein interactions. Other way could be to extend the investigation on the ET reactions of azurin labeled with different classes of fluorescent dyes e.g. ATTO647N or ALEXA647.

## ***6.2 Single molecule studies on azurin dimer***

To investigate protein-protein electron transfer reactions(1)(2)(3), cross-linking methods were developed previously to “freeze” these transient complexes(4)(5)(6). A successful example is azurin dimer that was structurally characterized by our group(7). This well characterized construct has been chosen to investigate protein-protein ET reactions. Depending on the redox states of the copper centers in the dimer, this dimer can exist in three different redox states: oxidized [Cu(II)-Cu(II)], reduced [Cu(I)-Cu(I)]and half oxidized [Cu(II)-Cu(I)]. When the dimer is half oxidized, intramolecular ET can happen between two copper centers in a dimer. This ET exchange can affect the fluorescence of the attached label. This reaction has been schematically presented in Fig. 6.1. The analysis of ACF of the dimer under redox conditions will eventually show the intramolecular ET rate (Fig. 6.2). The results will confirm the potential of FCS in solution to investigate intramolecular ET reactions in metalloproteins containing more than one redox center. Protein-protein interactions in the naturally occurring redox chains can be the ultimate application of this technique.

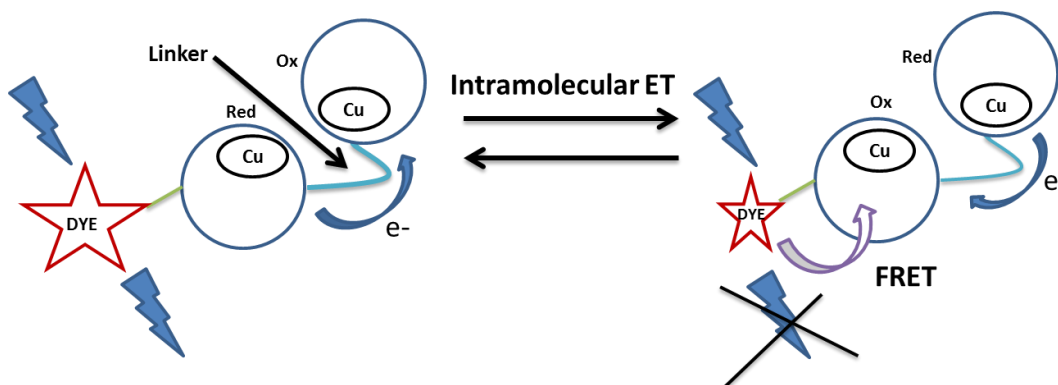


**Figure 6.1:** Schematic representation of the influence of the intramolecular ET reaction on the fluorescence emitted by the label attached to the half reduced/oxidized azurin dimer. Each monomer is depicted as a blue circle. Two monomers are connected by a light blue curved line representing BMME linker. On the left side: the dye is excited and its fluorescence is fully detected. On the right side: upon excitation, the fluorescence of the label is transferred to the oxidized copper due to FRET and the fluorescence intensity of the dye diminishes.

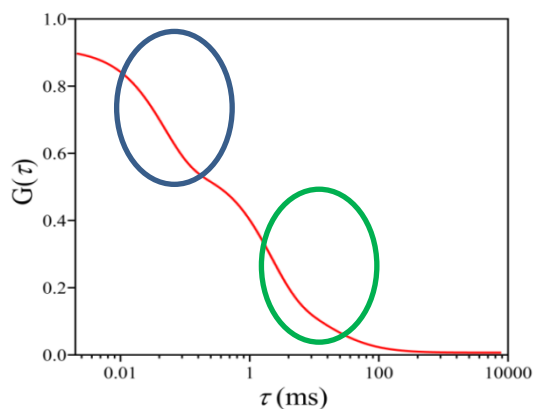


**Figure 6.2:** Example of an autocorrelation curve (red). The green circled region corresponds with the diffusion of the particle, the blue circled region corresponds with a reaction that is faster than diffusion. For azurin dimer, this blue circled region will represent the intramolecular ET reaction between two redox centers in the dimer.

### *Future plans*

(Cu-Cu) BMME azurin dimer can be used to test whether the combination of FRET-based detection of the redox state with FCS is suitable to measure ET rates. Our group has previously characterized electron self-exchange reaction of the BMME dimer by NMR(8). Experimentally (FCS) obtained ET rates can be used to compare with the value reported in literature. This technique can also be extended to study the ET reaction between proteins containing multiple redox centers at physiological conditions. Two redox partners can be labeled with two labels with different colors and by means of either spectral or lifetime characteristics the redox behavior of each center can be investigated. It is possible to co-localize the protein-complex and then cross-correlating the signals by FRET technology to reveal the kinetics of ET processes between two partners. Single molecule experiments will eventually extend our understanding on protein-protein ET transfer complexes and open up the possibilities of the development of biosensors based redox proteins as ET rate can be crucial parameter in such systems.

#### *6.3 Single molecule studies on azurin labeled with different classes of dyes*

Our previous investigations on ATTO655 (oxazine dye) labeled copper azurin revealed that it is possible to separate and characterize individual labeled component using chromatography and mass spectroscopy techniques from a biological sample which is heterogeneous after labeling. In the case of azurin, we addressed the fluorescent behavior of those individual components at single molecule level (See chapter 3, 4 and 5). That work has enabled us to understand ET dynamics as a function of the position of the label on the protein surface. Specifically, the ET processes between the label ATTO655 and the copper center of the labeled azurin were demonstrated using FCS. Under certain redox conditions, we have been able to monitor intramolecular ET dynamics in the microsecond region between the label and the metal center in azurin.

New insights emerged from the observation of intramolecular ET dynamics at single molecule level. Subsequently further questions have appeared from the microsecond ET process detected from FCS curves. If single molecule detection for ET dynamics is possible for ATTO655-azurin system, would it be possible to encounter the same in other fluorophores conjugated with the protein? Will the time scale of electron transfer be similar for any azurin-dye bioconjugate?

In order to answer these questions, two commonly used and commercially available red-absorbing fluorophores of different classes, ATTO647N (carbo-rhodamine) and ALEXA647 (cyanine) were selected for single molecule applications (Fig 6.3). In this study, our first strategy is to characterize the products of the labeling reactions for the aforementioned two different classes of dyes and then extend our investigation into the properties of a specific labeled species under redox conditions using FCS. Specifically, K122 labeled copper azurin will be chosen to monitor the intramolecular ET dynamics. The redox properties of the azurin-dye solution can be manipulated using potassium hexacyanoferrate (III) and potassium hexacyanoferrate (II) or sodium ascorbate as previously described (See chapter 3-5 for details).

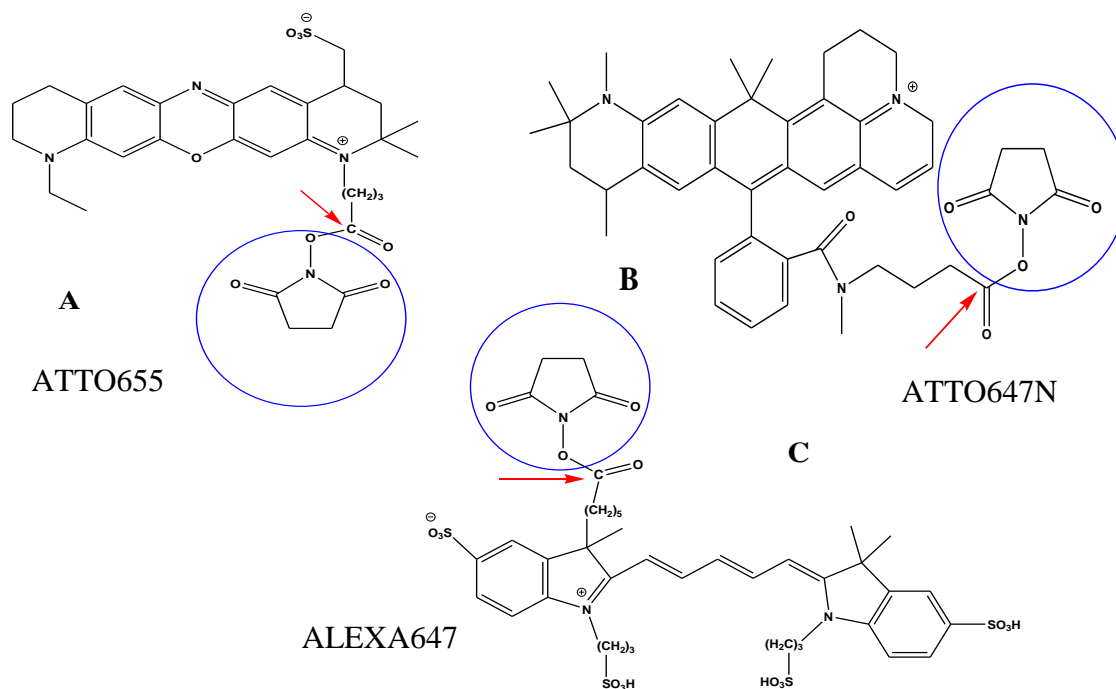


**Figure 6.3:** Chemical structures of three different classes of dyes: (A) ATTO 655 NHS (Oxazine class, overall charge on the dye = 0), (B) ATTO 647N NHS (Carbo-rhodamine group, overall charge on the dye = +1) and (C) ALEXA 647 NHS (Cyanine class, overall charge on the dye = -3). The blue circled region shows the NHS ester group of the individual dyes required for the labeling reaction with amino moieties on the protein surface. The red arrow shows the point of attachment of the protein with the dye.

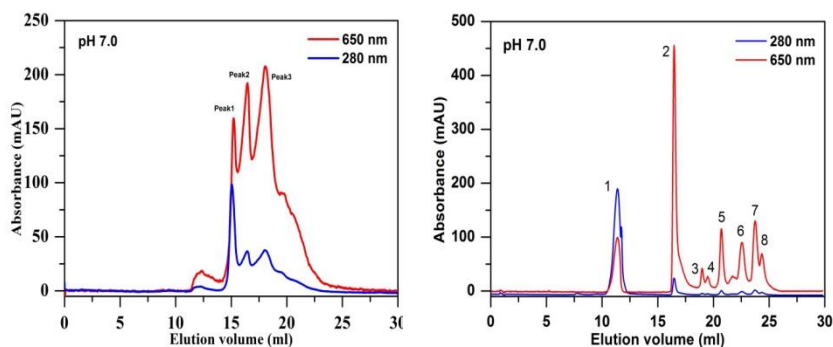


**Figure 6.4:** Anion exchange chromatography of the mixture obtained after labeling *wt* azurin with ATTO 647N (A) and ALEXA647 (B). The chromatogram shows the elution pattern with monitoring of two wavelengths: 280 nm (blue line), characteristic absorption of the protein; and 650 nm (red line), characteristic absorption of the label. The conditions used for the separations have been described in the main text.

Fluorescence switching experiments on the labeled species have suggested that fraction 3 of ATTO647N labeled Cu azurin and fraction 2 of ALEXA647 labeled Cu azurin contain the species where the label is attached to a lysine close to the copper center. Mass spectroscopic experiments confirmed the position (K122) of the label on the surface of azurin.

### *Future plans*

Using the K122 labeled species, FCS experiments can be used to investigate the intramolecular ET reactions in Cu azurin labeled with different dyes. In parallel, it is also possible to monitor the redox state changes of a labeled azurin molecule after surface confinement with single molecule resolution. In these cases, we can address the kinetics of ET process between the dye (ATTO655, ATTO647N or ALEXA647) and the copper center as well as the blinking rates under different redox conditions. It is a known fact that the problem of nonspecific interactions between the labeled protein and the solid support or the receptor often makes the biochemical screening process troublesome, especially with fluorescently labeled substrates that have charged or hydrophobic functional groups. Specially, the hydrophobic interactions occur between proteins and the dye molecules, which make specific interactions e.g. ET process hard to ascertain. This work will demonstrate how redox potential, charge and the

hydrophobicity/lipophilicity of the dyes can influence the inter- and intramolecular ET dynamics. The excitation conditions and local environment can also be varied to investigate the effect of those on ET dynamics. This work may help in designing experiments and choosing suitable dyes for single molecule studies in case of metalloproteins.

## References

- (1) Teixeira, V. H.; Baptista, A. M.; Soares, C. M. Modeling electron transfer thermodynamics in protein complexes: interaction between two cytochromes c(3). *Biophys. J.* **2004**, *86*, 2773–85.
- (2) Cardona, T.; Battchikova, N.; Zhang, P.; Stensjö, K.; Aro, E.-M.; Lindblad, P.; Magnuson, A. Electron transfer protein complexes in the thylakoid membranes of heterocysts from the cyanobacterium *Nostoc punctiforme*. *Biochim. Biophys. Acta* **2009**, *1787*, 252–63.
- (3) Bashir, Q.; Scanu, S.; Ubbink, M. Dynamics in electron transfer protein complexes. *FEBS J.* **2011**, *278*, 1391–1400.
- (4) Malatesta, F.; Antonini, G.; Nicoletti, F.; Giuffrè, A.; D'Itri, E.; Sarti, P.; Brunori, M. Probing the high-affinity site of beef heart cytochrome c oxidase by cross-linking. *Biochem. J.* **1996**, *315*, 909–916.
- (5) Hippler, M.; Drepper, F.; Haehnel, W.; Rochaix, J. D. The N-terminal domain of PsaF: precise recognition site for binding and fast electron transfer from cytochrome c6 and plastocyanin to photosystem I of *Chlamydomonas reinhardtii*. *Proc. Natl. Acad. Sci. U. S. A.* **1998**, *95*, 7339–44.
- (6) Qin, L.; Kostić, N. M. Importance of protein rearrangement in the electron-transfer reaction between the physiological partners cytochrome f and plastocyanin. *Biochemistry* **1993**, *32*, 6073–80.
- (7) van Amsterdam, I. M. C.; Ubbink, M.; Einsle, O.; Messerschmidt, A.; Merli, A.; Cavazzini, D.; Rossi, G. L.; Canters, G. W. Dramatic modulation of electron transfer in protein complexes by crosslinking. *Nat. Struct. Biol.* **2002**, *9*, 48–52.
- (8) van Amsterdam, I. M. C.; Ubbink, M.; Einsle, O.; Messerschmidt, A.; Merli, A.; Cavazzini, D.; Rossi, G. L.; Canters, G. W. Dramatic modulation of electron transfer in protein complexes by crosslinking. *Nat. Struct. Biol.* **2002**, *9*, 48–52.



*This page was intentionally left blank*

*This page was intentionally left blank*

# Summary

Biological processes such as photosynthesis, oxidative phosphorylation, respiration and much of the enzymatic catalysis occur via electron transfer (ET). In order to fulfil these tasks, a cell generally needs all its essential performers. Copper proteins are one of those major players, involved in a wide range of redox processes, predominantly in biological energy productions and metabolic processes. The last few decades have witnessed large efforts to understand ET mechanisms with cutting-edge experimental research combined with theories and molecular models of proteins. How ET flows through these proteins involving donor and acceptor and what determines the specificity is still a subject of debate. Azurin is a small blue copper protein that plays a role in ET processes in gram-negative bacteria. In this thesis, azurin has been chosen as the main redox protein because of its high stability and largely known structural, spectroscopic and mechanistic properties.

The availability of fluorescence based detection techniques has brought about a breakthrough in the optical studies of the properties of biomolecules e.g. enzyme mechanism, protein folding etc. To obtain detailed information on the ET reactions in proteins such as azurin, fluorescence correlation spectroscopy (FCS) has been used. This method can be easily applied to many other redox proteins and have potential applications in fluorescence based biosensors and molecular electronics. In the present thesis, a series of FCS experiments on ATTO655 labeled azurin was presented. The aim was to gain more insights in electron transfer processes.

In the introduction of **Chapter 1**, the general features of blue copper proteins and azurin are presented. Then an overview is given on the methods that are important to this thesis, e.g. fluorescence resonance energy transfer (FRET), fluredox principle, fluorescence correlation spectroscopy (FCS). This chapter also provides an outline on the theory of electron transfer.

**Chapter 2** describes the calibration of the experimental setup used for the investigation on ET reaction in azurin. ATTO655, a red-absorbing dye has been chosen to calibrate the setup. The main goal of this work was to precisely determine the three-dimensional parameters ( $k$  and  $r_0$ ) of the experimental setup. First an overview was given on the autocorrelation function (ACF), ' $D$ ' the diffusion coefficient of the molecule of interest, ' $\tau_D$ ' the residence time of the molecule in the probe volume, the three dimensional parameters ( $k$  and  $r_0$ ) and how they are related to each other by FCS equations. Then the calibration was performed using pure buffer and a 57.0% (w/w) sucrose solution containing different ATTO655 dye concentrations. Two approaches were undertaken to determine the effective volume of the setup. One way to determine the parameters was by plotting the average number of molecules in the probe volume as a function of the concentrations of the dye and the other way was by fitting of the obtained autocorrelation data with FCS equations. The first approach produced  $V_{eff} = 2.3 \pm 0.2$  fL in buffer and in 57% (w/w) sucrose solution it was  $2.9 \pm 0.1$  fL. The second method resulted  $V_{eff} = 2.1 \pm 0.5$  fL in buffer and  $V_{eff} = 1.3 \pm 0.2$  fL in 57% (w/w) sucrose solution. The experimentally obtained ' $k$ ' value in 57%

(w/w) sucrose solution was used for the fitting of the ACFs of labeled azurin samples (Chapter 3, 4 and 5). From the fits of the ACFs also  $\tau_D$  of the dye was determined. The average diffusion times for the dye was found to be  $0.10 \pm 0.01$  ms (in buffer) and  $2.9 \pm 0.3$  ms (in 57% w/w sucrose solution). Effective volume was also determined by imaging of sub-resolution gold nano-rods. The calculated volume was found to be similar to the values obtained with above two approaches using ATTO655. Next, we looked into the diffusion time scales of labeled proteins and the rates of the bimolecular reaction between the labeled azurin and redox agents. These bimolecular reactions have very small activation barriers and are diffusion controlled reactions with rates of  $k_d = 10^9$ - $10^{10}$   $M^{-1}s^{-1}$  in aqueous solution at room temperature. A rough estimate of the rate in sucrose solution was made using Smoluchowski's principle and it can reach values of  $10^6$   $M^{-1}s^{-1}$  in high viscous liquid. Then we briefly discussed the photoinduced processes of the dye using Jablonski diagram. At last, an overview was given on the thermodynamics of photoinduced electron transfer (PET) and a brief review was presented on the major contributions in understanding PET reactions in metalloproteins like azurin.

**Chapter 3** presents a detailed investigation of the products of the labeling reaction of Zinc azurin variants with the fluorescent dye ATTO655. First, we investigated the effects of viscosity on the translational diffusion times of labeled Zn-azurin in the absence of any redox chemicals. The diffusion time of the labeled molecule became larger with increase in sucrose concentration in the buffer [200  $\mu$ s in pure buffer (0% sucrose) and 12 ms in 57% (w/w) sucrose solution]. Then FCS experiments were performed to understand the behavior of the labeled products under redox conditions. We investigated the PET reactions using two species: one labeled at the N-terminus and another one labeled at Lys122 position. As Zn-azurin is inactive, only intermolecular ET reactions were observed between the label and the redox chemicals. Oxidizing agents had no effect on the autocorrelation functions of labeled Zn-azurin and could be fit with the FCS equation containing only diffusion term. But, the ACFs under reducing conditions could be fit with FCS equation containing diffusion and  $G_I(\tau)$  terms and the analysis showed that the forward reaction rate was linearly dependent on the reductant concentrations corresponding to the one-electron reduction of the label by the reductant e.g. sodium ascorbate, potassium hexacyanoferrate (II). It indicates that the reducing agents caused blinking of the dye. This bimolecular ET reaction rate between the label and the redox chemicals was found to be smaller  $\sim 10^7$ - $10^8$   $M^{-1}s^{-1}$  compared to diffusion-controlled reaction rates in pure buffer ( $10^9$   $M^{-1}s^{-1}$ ) supporting the fact that these reactions are slow in 57% (w/w) sucrose solution. The oxidation of the reduced label back to the non-reduced form appears to consistent with the idea that dissolved oxygen is responsible for the back oxidation of the label as oxygen is present in the sucrose solution in large excess and its concentration will not change appreciably over the duration of the experiment.

A detailed investigation of the products of the labeling reaction of wild type Cu-azurin with the fluorescent dye ATTO655 has been presented in **Chapter 4**. Fluorescence correlation spectroscopy was performed to understand the behavior of the labeled products under redox

conditions. In this work, we have also tried to understand the PET reaction using two species: one labeled at the N-terminus and another one labeled at Lys122 position. In the former, only blinking of the dye or intermolecular ET reaction was observed between the dye and reducing agents. Oxidizing chemicals had no effect. In Lys122 labeled Cu-azurin, a microsecond ET dynamics was observed under redox conditions and the reaction was found to be independent of redox concentrations. This reaction has been referred as intramolecular ET reaction between the dye and redox center. Two different mechanisms are believed to be involved in ET events. Applying Marcus theory of ET transfer and using the experimentally observed forward and backward rates, the values of reorganization energies under redox conditions were calculated. Using  $k_1^f = 4.8 \times 10^4 \text{ s}^{-1}$  and  $k_1^b = 7.5 \times 10^2 \text{ s}^{-1}$  under oxidizing conditions, one obtains  $\lambda = 0.75 \text{ eV}$ . Under reducing conditions,  $\lambda = 1.16 \text{ eV}$  was obtained using the experimental values  $k_2^f = 4.2 \times 10^6 \text{ s}^{-1}$  and  $k_2^b = 1.3 \times 10^4 \text{ s}^{-1}$ . The main conclusion from the present work is that no PET reactions with amino acids in the protein are observed, but PET to the metal is observed when Cu occupies the active site, and the label is attached close enough to the metal center (at Lys122). In the end, a covalent pathway model for ET reaction between Cu and label has been proposed to support the experimental data.

Similar to previous chapters 3 and 4, **Chapter 5** also represents a detailed investigation on photoinduced ET reactions in the labeled products of K122S and K122Q CuAzurin variants under redox conditions. In this work, we have tried to understand the ET reaction using a specific species where the label is assumed to be attached on a surface lysine. In case of these variants, no extra decay was observed in FCS curves and the time scale of ET reaction is sub-millisecond range. Slower ET rates revealed that the labeling position on the protein surface must be at least  $> 20 \text{ \AA}$  away from the copper center and the label is attached possibly to other lysine residues e.g. Lys 24/Lys27/Lys128 on the protein surface. Then, we calculated the reorganization energies of ET transfer under redox conditions for the labeled species using the experimentally obtained forward and backward rate constants and applying Marcus theory. In this chapter, we have also shown how the rate of PET between label and redox site may vary with the position of the label on the protein surface. As the ET parameters (driving forces, reorganization energies) have been determined experimentally for a number of cases the variation of the rates with distance were calculated and it became of interest to see how these rates compare to FRET promoted deactivation of the excited labels. Our calculation showed that inverse PET rate reaches the millisecond range for Cu-label distances between 15-20  $\text{\AA}$ , depending on driving force and reorganization energy, whereas the FRET rate showed a much shallower distance dependence. As no detailed structural information is available for the positions of the labels in K122S and K122Q-ATTO655 labeled species, we proposed the “organic glass” model of Moser and Dutton to calculate the ET rate through a protein.

# Samenvatting

Biologische processen zoals fotosynthese, oxidatieve fosforylering en ademhaling geschieden via elektronenoverdracht (ET). Om deze functies uit te kunnen voeren heeft een cel, over het algemeen, een aantal onmisbare componenten nodig. Kopereiwitten behoren tot deze hoofdrolspelers. Ze zijn bij een hele reeks redoxprocessen betrokken, voornamelijk bij de biologische energieproductie en de metabole processen. De laatste decennia zijn wij getuige geweest van grote inspanningen om de electronoverdrachtmechanismen te begrijpen. Baanbrekend onderzoek betrof de theorie en moleculaire modellen van eiwitten. Hoe ET, met behulp van donor en acceptor, in deze eiwitten verloopt en wat de specificiteit bepaalt: deze vragen zijn tot op heden onderwerp van discussie. Azurine is een klein blauw kopereiwit dat bij ET-processen in Gramnegatieve bacteriën een belangrijke rol speelt. In dit proefschrift werd azurine gekozen vanwege zijn hoge stabiliteit en vooral vanwege zijn bekende structurele, spectroscopische en mechanische eigenschappen.

De beschikbaarheid van detectietechnieken die op fluorescentie gebaseerd zijn, heeft geleid tot een doorbraak in de optische studies van de eigenschappen van biomoleculen zoals enzymmechanisme, eiwitvouwing enz. Fluorescentie correlatiespectroscopie (FCS) is toegepast om gedetailleerde informatie over ET reacties in azurine te verkrijgen. Deze methode kan ook op andere redox-eiwitten gemakkelijk worden toegepast. Tevens heeft deze methode ook potentiële toepassingen voor het onderzoek van biosensoren die op fluorescentie berusten, maar ook in moleculaire elektronica. In het huidige proefschrift wordt een aantal FCS experimenten met ATTO655-gelabeld azurine beschreven. Het doel hiervan was om meer inzicht te krijgen in de elektronoverdrachtprocessen.

In de inleiding (**Hoofdstuk 1**) worden de kenmerken van blauwe kopereiwitten in het algemeen, en van azurine in het bijzonder, gepresenteerd. Vervolgens wordt er een overzicht van de methoden gegeven die voor dit proefschrift relevant zijn. Voorbeelden van die methoden zijn: fluorescentie resonantie-energieoverdracht (FRET), fluredox principe, fluorescentie correlatiespectroscopie (FCS). Dit hoofdstuk bevat ook een overzicht van de theorie over elektronoverdracht.

In **Hoofdstuk 2** wordt de kalibratie van de experimentele opstelling beschreven, die gebruikt werd om de elektronoverdracht in azurine te bestuderen. ATTO655, een rood-absorberend label, werd gekozen voor het kalibreren van de opstelling. De belangrijkste doelstelling van dit werk was de nauwkeurige bepaling van de driedimensionale parameters ( $k$  en  $r_0$ ) van de experimentele opstelling. Eerst wordt een overzicht gegeven van de autocorrelatiefunctie (ACF), ' $D$ ' de diffusie coëfficiënt van het onderzochte molecuul, ' $\tau_D$ ' de verblijftijd van het molecuul in het onderzochte volume, de drie dimensionele parameters ( $k$  en  $r_0$ ) en hoe ze door FCS vergelijkingen aan elkaar zijn gerelateerd. Vervolgens wordt de kalibratie uitgevoerd in zuivere buffer en in een 57% (w/w) sacharoseoplossing die verschillende

concentraties van ATTO655 label bevat. Twee benaderingen werden gehanteerd om het werkelijke volume van de opstelling te bepalen. De eerste benadering was het gemiddelde aantal moleculen in het onderzochte volume uit te zetten als een functie van de concentraties van de label en de andere benadering was de verkregen gegevens uit de autocorrelatie te fitten met de FCS vergelijkingen. De eerste benadering leverde  $V_{eff} = 2.3 \pm 0.2$  fL in buffer en  $2.9 \pm 0.1$  fL in 57% (w/w) sucroseoplossing. De uitkomst bij de tweede benadering was  $V_{eff} = 2.1 \pm 0.5$  fL in buffer en  $V_{eff} = 1.3 \pm 0.2$  fL in 57% (w/w) sacharoseoplossing. De experimenteel verkregen ‘ $k$ ’ waarde in 57% (w/w) sacharoseoplossing werd gebruikt bij de fitting van de ACFs van gelabelde azurine samples (hoofdstuk 3, 4 en 5). Op basis van de fittings van ACFs werd  $\tau_D$  van het label bepaald. De gemiddelde diffusietijd van het label was  $0.10 \pm 0.01$  ms in buffer en  $2.9 \pm 0.3$  ms in 57% w/w sucrose oplossing. Het effectieve volume werd ook bepaald door afbeelding van nanostaafjes van goud. Het berekende volume bleek vergelijkbaar te zijn met de waarden van de twee bovengenoemde benaderingen. We hebben vervolgens gekeken naar de diffusietijd van gelabelde eiwitten en de snelheid van de bimoleculaire reactie tussen het gelabelde azurine en redox middelen. Deze bimoleculaire reacties hebben een zeer kleine activeringsbarrière en ze zijn door diffusie gecontroleerd met snelheden van  $k_d = 10^9 - 10^{10} \text{ M}^{-1}\text{s}^{-1}$  in waterige oplossing bij kamertemperatuur. Een ruwe schatting van de snelheid in een sacharoseoplossing werd gemaakt met behulp van Smoluchowski’s principe. Deze kan de waarden van  $10^6 \text{ M}^{-1}\text{s}^{-1}$  in hoge viskeuze vloeistof bereiken. Vervolgens hebben we met behulp van een Jablonski diagram de fotogeïnduceerde processen van het label besproken. Uiteindelijk kon een overzicht gegeven worden van de thermodynamica van de fotogeïnduceerde elektronoverdracht (PET) en ook van de belangrijke bijdragen in het begrijpen van PET reacties in metaaleiwitten zoals azurine.

**Hoofdstuk 3** beschrijft een uitgebreid onderzoek van de producten van de labelingsreactie van zink-azurine met het fluorescerende label ATTO655. Eerst hebben we het effect van viscositeit op de translationele diffusietijden van gelabelde Zn-azurine in afwezigheid van redoxchemicaliën onderzocht. De diffusietijd van het gelabelde molecuul nam toe naarmate de sucrose concentratie in de buffer hoger werd [200  $\mu\text{sec}$  in zuivere buffer (0% sucrose) en  $12 \pm 2$  ms in 57% (w/w) sucrose-oplossing]. Daarna werden FCS experimenten uitgevoerd om het gedrag van de gelabelde producten onder variërende redoxomstandigheden te begrijpen. We hebben de PET reacties onderzocht met behulp van twee varianten: de ene was gelabeld aan de N-terminus en de andere op de Lys122 positie. Omdat Zn-azurine redoxinactief is, werden er alleen intermoleculaire ET reacties tussen de label en de redox-chemicaliën waargenomen. Oxiderende middelen hadden geen effect op de autocorrelatiefuncties van gelabeld Zn-azurine en ze konden worden gefit met de FCS vergelijking die de diffusie-term als enige component bevat. Maar de ACFs onder reducerende omstandigheden konden gefit worden met een FCS vergelijking die een diffusie-term bevat en een  $G_I(\tau)$  term. De analyse van deze resultaten toonde aan dat de voorwaartse reactiesnelheid lineair afhankelijk was van de reducerende concentraties overeenkomstig de één-electron reductie van het label door de reductant [natrium ascorbaat of kaliumhexacyanoferraat (II)]. Dit geeft aan dat reducerende verbindingen de “blinking” van het label veroorzaakten. De bimoleculaire ET reactiesnelheid tussen de label en de redox-

chemicaliën was  $10^7$ - $10^8$   $M^{-1}s^{-1}$ , kleiner dan de diffusie-gecontroleerde reactiesnelheden in pure buffer ( $10^9$   $M^{-1}s^{-1}$ ). Dit onderbouwt de conclusie dat reacties in 57% (w/w) sucrose-oplossing langzaam verlopen. De oxidatie van het gereduceerde label terug naar de niet-gereduceerde vorm lijkt in overeenstemming te zijn met het idee dat opgeloste zuurstof verantwoordelijk is voor de reoxidatie van de label omdat zuurstof in de sucrose oplossing in grote overmaat aanwezig is en de zuurstofconcentratie in de loop van het experiment niet aanzienlijk verandert.

Een gedetailleerd onderzoek van de uitkomsten van de labelingsreactie van wild type Cu-azurine met het fluorescerende label ATTO655 wordt in **Hoofdstuk 4** beschreven. Fluorescentie correlatiespectroscopie werd uitgevoerd om het gedrag van de gelabelde producten onder variërende redoxomstandigheden te begrijpen. In deze studie hebben we ook geprobeerd twee varianten te gebruiken om de PET reacties te begrijpen: één was gelabeld aan de N-terminus en een andere op de Lys122 positie. In het eerste geval werd alleen de “blinking” van het label of de intermoleculaire ET reactie tussen de label en de reducerende middelen waargenomen. Oxiderende chemicaliën hadden geen effect. In Cu-azurine die op Lys122 gelabeld werd, hebben wij ET dynamics waargenomen op microseconde tijdschaal en de reactie bleek onafhankelijk van redox concentraties te zijn. Deze reactie werd aangemerkt als intramoleculaire ET reactie tussen de label en het redox-centrum. Er wordt verondersteld dat twee verschillende mechanismen bij ET betrokken zijn. Door de theorie van Marcus over ET-overdracht toe te passen en door middel van de experimenteel waargenomen voorwaartse en achterwaartse snelheden, werden de waarden van de reorganisatie-energie berekend. Met behulp van  $k_1^f = 4.8 \times 10^4$   $s^{-1}$  en  $k_1^b = 7.5 \times 10^2$   $s^{-1}$  onder oxiderende omstandigheden, verkrijgt men  $\lambda = 0.75$  eV. Onder reducerende omstandigheden werd  $\lambda = 1.16$  eV verkregen met behulp van de experimentele waarden  $k_2^f = 4.2 \times 10^6$   $s^{-1}$  en  $k_2^b = 1.3 \times 10^4$   $s^{-1}$ . De belangrijkste conclusie uit het huidige werk is dat er geen PET reacties met aminozuren in het eiwit worden waargenomen, maar PET naar het metaal wordt wel waargenomen als Cu de actieve site bezet en als het label dichtbij het metaalcentrum (op Lys122) is. Als laatste werd er een covalent routemodel voor de ET reactie tussen Cu en label voorgesteld ter ondersteuning van de experimentele gegevens.

Ook **hoofdstuk 5** beschrijft een uitgebreid onderzoek naar fotogeïnduceerde ET reacties in de gelabelde producten van K122S en K122Q Cu-azurine varianten onder redox omstandigheden. Hier hebben we geprobeerd de ET reactie te begrijpen door gebruik te maken van een specifieke mutant waarbij het label wordt verondersteld gebonden te zijn aan het Lysine-oppervlak. In het geval van deze varianten, werd er geen extra verval in de FCS curven waargenomen. De lage ET snelheden toonden aan dat de labelingspositie op het oppervlak van het eiwit op minimaal 20 Å afstand van het kopercenter moest zijn. Dit geeft ook aan dat het label op het oppervlak van het eiwit waarschijnlijk op andere lysine residuen bijv. Lys 24/Lys27/Lys128 gebonden is. Met behulp van Marcus theorie over ET-overdracht en door middel van de experimenteel waargenomen voorwaartse en achterwaartse snelheden, werden de waarden van de reorganisatie-energie berekend. In dit hoofdstuk is tevens aangegeven hoe de snelheid van PET tussen label en



redox site, afhankelijk van de positie van de label op het oppervlak van het eiwit, kan variëren. Aangezien de ET parameters (drijvende kracht, reorganisatie-energie) experimenteel werden bepaald, werden voor een aantal gevallen de variatie van de snelheden berekend. Het is nu van belang om te zien hoe deze snelheden met de deactivering van de geëxciteerde labels door FRET kunnen worden vergeleken. Onze berekening laat zien dat de PET snelheid, afhankelijk van drijvende kracht en reorganisatie-energie, de millisecondeschaal bereikt bij Cu-label afstanden tussen 15-20 Å, terwijl de FRET snelheid een veel minder geprononceerde afstandsafhankelijkheid vertoont. Omdat er geen gedetailleerde structurele informatie beschikbaar is voor de posities van de labels in K122S en K122Q-ATTO655 gelabeld species, hebben wij het model van een "organic glass" van Moser en Dutton voorgesteld voor de berekening van de ET-snelheid in het eiwit.

*This page was intentionally left blank*

## Curriculum Vitae

Saptaswa Sen was born in Kolkata (formerly known as Calcutta), West Bengal, India, on May 18, 1984. He obtained his Bachelor degree in Chemistry at Jadavpur University, Kolkata in July 2005. He continued to pursue his Master program in Inorganic Chemistry at the same university. He completed his master degree in August 2007 with a thesis entitled “Catalytic studies on small organic molecules with Manganese-Salen complexes: synthesis, characterization and catalysis”, under the supervision of Prof. Dr. Subratanath Koner. From May 2008-October 2011 he worked as full time junior and senior research fellow in the Chemical Science department of Tata Institute of Fundamental Research, Mumbai, India. In that period, he was supervised by Prof. Dr. Shyamalava Mazumdar and he worked in an Indo-French project in collaboration of Prof. Dr. Juan C. Fontecilla-Camps (Institute of Biological Sciences, Grenoble, France). In Mumbai, his research was focused on the development of a potential biocatalyst for the degradation of pesticides. His work was published in the Indian Journal of Chemistry (International Year of Chemistry Issue) and in a book entitled “Iron containing enzymes: Versatile Catalysts of Hydroxylation Reactions in Nature”.

In November 2011, he came to The Netherlands to join the group of Prof. G.W.Canters and Prof. T.J.Aartsma at the Leiden Institute of Physics and to work on a project funded by NWO (Netherlands Organization for Scientific Research). The research was aimed at the investigation of photoinduced electron transfer reaction in a labeled metalloprotein by means of single molecule fluorescence spectroscopy, particularly fluorescence correlation spectroscopy (FCS). The results obtained are presented in this thesis. His work was presented at the international conference in Bioinorganic Chemistry (ICBIC 16, 2013) at Grenoble, France, the Dutch Meetings on Protein Chemistry and Biophysics Conferences (Veldhoven, 2012-2015) and several other national meetings. Oral presentation was given at the Chains Chemistry Conference (Veldhoven, 2015).

*This page was intentionally left blank*

## List of Publications

1. Alessio Andreoni, Saptaswa Sen, Thijs J. Aartsma and Gerard W. Canters, Fluorescence correlation spectroscopy of labeled azurin reveals photo-induced electron-transfer between label and Cu center. [Manuscript submitted to “Proceedings of the National Academy of Sciences of the United States of America”].
2. Saptaswa Sen, Soumen Kanti Manna and Shyamalava Mazumdar, Oxidation of unnatural substrates by engineered cytochrome P450<sub>cam</sub>, in “Iron-Containing Enzymes: Versatile Catalysts of Hydroxylation Reactions in Nature”, Royal Society of Chemistry Publishing, Cambridge UK; Editors: Dr. Samuel de Visser and Dr. Devesh Kumar, Chapter 10, 330 (2011).
3. Saptaswa Sen, Soumen Kanti Manna and Shyamalava Mazumdar, Interaction of gammaxene with site-specific mutants of Cytochrome P450<sub>cam</sub>, Indian Journal of Chemistry (Special issue on Bioinorganic Chemistry), 50A, 438 (2011).

*This page was intentionally left blank*

## Acknowledgements

It is a genuine pleasure to express my deep sense of thanks and gratitude to my mentors, philosophers and guides, Prof. Canters and Prof. Aartsma. Their continuous support has helped for completing my work. I also would like to acknowledge my previous mentors from India, Prof. Dr. Shyamalava Mazumdar, Prof. Dr. Samaresh Bhattacharya and Prof. Dr. Subratanath Koner for their continuous support personally as well professionally.

I would like to express my sincere thanks to Dr. Alessio Andreoni especially for all useful discussions, help in developing or fixing the confocal laser setup and giving me the algorithm for data analysis when I joined the lab. He is the person who introduced me to the world of single molecule spectroscopy at the very beginning of my PhD. I learned a lot from his experiences, suggestions and how to work with different tricks effectively in a protein biochemistry/biophysics laboratory.

Special thanks to Marija and Manas with whom I shared my PhD life. They have patiently listened to all my thesis-related complaints and other personal issues. Thanks to other people of the Molecular Biophysics group with whom I worked: Dr. Namik Akkiliç, Dr. Muhammad Kamran, Dr. Mihaela Apetri, Biswajit and Dr. Ankur Gupta. I am also very happy that I could get help in purifying enzymes from Anneloes Blok from Chemistry department and Lionel Ndamba as well as Marcel Winter from our Biophysics laboratory. No research can be possible without wonderful colleagues and friends who have been my company in many occasions inside or outside the lab: Pravin, Aquiles, Faezeh, Enrico, Gabriele, Lena, Wietske, Sara, Olga, Pavel, Kirsten, Artur, Wim, Martin, Nemanja, Dominique, Stefano, Jeremie, Maria, Neli, Donny. Naming all of you goes beyond the aim of this page. I also thank Yvonne Kerkhof, Margareth van Hoorn and Barry Cats for their assistance and for making life easier.

Life in Leiden would have been very difficult without my Indian friends who are in touch even if they are far away: Abhishek, Satrajit, Joyee, Moumita, Sourav, Jayashree and Piyali. They have been the listeners of all my problems during PhD tenure. Indirectly they have contributed too and much more than one could think. Big thanks to my parents (especially to my mother) and family for their encouragement and continuous support throughout this long journey and for believing in me.

Saptaswa Sen

*This page was intentionally left blank*



*This page was intentionally left blank*